Spectroscopic Characterisation of Purine Nucleotides and their Interaction with Proteins

A thesis submitted to the University of Manchester for the degree of

Doctor of Philosophy

in the Faculty of Science and Engineering

2018

Omer Asad Azher

School of Chemistry

Table of contents

Table of Contents

Word count: 45.084

List of Figures

List of Tables

Abstract

The University of Manchester

Omer Azher

Doctor of philosophy

Spectroscopic Characterisation of Purine Nucleotides and their Interaction with Proteins

2018

Phosphorylation of adenosine or guanosine diphosphates to form ATP or GTP is one of the most important biochemical reactions. One of the enzymes that makes ATP *in vivo* is phosphoglycerate kinase (PGK), which transfers a phosphoryl group from 1,3-bisphosphoglycerate (1,3-BPG) to ADP, generating ATP and 3-phosphoglycerate (3-PG). PGK is a promiscuous enzyme and will also phosphorylate GDP. Both reactions require the binding of magnesium ions to the nucleotides. The binding of substrates and magnesium ions results in substantial conformational changes in the enzyme and the substrates, but these processes are not fully understood. Also, the dynamic behaviour of nucleotide-Mg complexes and the mode of coordination in aqueous phase remain elusive. Therefore, this thesis aimed to use Raman spectroscopy and Density Functional Theory (DFT) to characterise the common adenosine and guanosine nucleotides and identify the frequencies of the vibrational modes associated strongly with their phosphate groups. The study investigated the influence of magnesium binding on the spectral profile of adenosine and guanosine mono-, di-and tri-phosphates in aqueous solution at different pH values. These studies were supported by ^{31}P NMR measurements under identical conditions. These results identified marker bands for adenosine and guanosine mono-, di-and tri-phosphates. In the absence of the enzyme, magnesium ions was found to coordinate both α- and β-phosphate groups of 5'-adenosine and guanosine diphosphates, and the β- and γ-phosphate groups of 5'-adenosine and guanosine triphosphates at pH 7.0. The results also indicated that acidification does not substantially alter the coordination of magnesium ions or the phosphate binding sites but does measurably affect the vibrational modes associated with the phosphate groups in adenosine and guanosine mono-, di-and tri- phosphates. The study further applies Raman spectroscopy to explore the spectral profile of the human PGK (hPGK) in its open conformation and when closed in the presence of transition state analogues. The influence of conformational changes, isotopic substitution with ^{15}N, and substrate binding on the Amide I and Amide III regions of the enzyme were investigated. Changes in the PGK spectral profile upon binding to ADP and 3-PG were observed and attributed to the contribution of some α-helices of hPGK. In the closed conformation of hPGK, both β-sheets and α-helices of Amide I and III regions are involved. The study also suggested that Raman vibrations identified at 1030-1070 cm^{-1} in hPGK-ADP complex could arise from ADP vibrations. The results also highlighted the role of hydrogen bonding in stabilizing the enzyme during its catalytic cycle.

Declaration

No portion of the work referred to in this thesis has been submitted in support of an application for another degree or qualification of this or any other university or other institute of learning.

Copyrights Statement

Dedication

I dedicated my PhD thesis to my lovely parents, my precious wife and my sweet kids,

Acknowledgment

First and foremost, I would like to thank my Lord for providing me with endless blessings, strength and support to accomplish this work.

I would like to express my great appreciation to my supervisor, Professor Jonathan Waltho for his constant guidance, support and encouragement throughout the years of my PhD project. During my work, I benefited from his careful step by step planning and valuable feedback of various topics in my thesis.

I would like also to offer my special thanks to Professor Ewan Blanch for his continuous support and advice during the data interpretation process.

The contribution of Dr Shaun Mutter and Alex Wilson in the field of computational analysis is greatly appreciated. I wish to acknowledge the help of Dr Matt Cliff, Dr Derren Heyes and Zhalgas Serimbetov. Special thanks should be given all staff and students who provided me with their help and advice during the many years of this work.

My grateful thanks extended to the Ministry of Higher Education in Saudi Arabia for providing me with this sponsorship to study at The University of Manchester.

Finally, I wish to thanks my parents for their constant support and my family for their help and patience throughout the years of my study.

Abbreviations and Acronyms

A	Adenine
ADA	Adenosine deaminase
ADP	Adenosine diphosphate
AFP	α-fetoprotein
AMPDA	Adenylate deaminase
AMP	Adenosine monophosphate
Ala	Alanine
AMPK	AMP-activated protein kinase
Arg	Arginine
Asn	Aspartate
ATP	Adenosine triphosphate
C	Cytosine
cAMP	Cyclic adenosine monophosphate
cCMP	cytidine 3,5-cyclic monophosphate
CDP	Cytidine diphosphate
CEA	Carcinoembryonic antigen
cGMP	Guanosine 3', 5’ -cyclic monophosphate
CID	Circular intensity difference
cIMP	Inosine 3,5-cyclic monophosphate
CMV	Cytomegalovirus
cUMP	Uridine 3,5 cyclic monophosphate
EOM	Electro-optic modulator
FAD	Flavin adenine dinucleotide
FDA	Food and Drug Administration
FMN	Riboflavin 5’-monophosphate
G	Guanine
GDP	Guanosine diphosphate
Glu	Glutamic acid
Gly	Glycine
GMP	Guanosine monophosphate

GPCR	G-protein-coupled receptor
GTP	Guanosine triphosphate
HBV	Hepatitis B virus
HIV	Human immunodeficiency virus
ICP-ROA	Incident circular polarisation
IDP	Inosine diphosphate
Ile	Isoleucine
IMP	Inosine monophosphate
IR	Infrared
IRMPD	Infrared multiple photon dissociation spectroscopy
ITP	Inosine triphosphate
Leu	Leucine
Lys	Lysine
NAD	Nicotine amide adenine dinucleotide
NMR	Nuclear magnetic resonance
PGK	Phosphoglycerate kinase
PKA	cAMP-dependent protein kinase A
PKG	cGMP-dependent protein kinase G
PMEA	9-[2-(Phosphonomethoxy) ethyl] adenine
PRPP	Phospho-ribose pyrophosphate
ROA	Raman optical activity
SCP-ROA	Scattered circular polarisation
SERS	Surface enhance Raman scattering
T	Thymine
Thr	Threonine
U	Uracil

Abbreviations and Acronyms

1,3-BPG	1,3-bisphosphoglycerate
3-PG	3-phosphoglycerate

Preface

The transfer of a phosphoryl group from the nucleotide to a target substrate via the action of a kinase enzyme is one of the important metabolic reactions. During phosphorylation, the binding of the magnesium ions to the enzyme bound nucleotide results in significant conformational alterations in the nucleotides, enzymes or substrates. The application of the Raman spectroscopy as a sensitive tool to characterise various biological molecules and investigate their dynamic behaviour and interaction in aqueous solution has gained an increasing interest over the last years. This study aims to combine Raman spectroscopy and Density Functional Theory (DFT) in order to characterise purine nucleotides (adenosine and guanosine) and their phosphate derivatives in aqueous solution. The Raman and DFT results of the preliminary experiments directed further investigations towards understanding the impact of magnesium ions and pH on the spectral profile of adenosine/guanosine mono-, di-and tri- phosphate in aqueous solution. These studies into the effects of Mg^{2+} and pH are supported by ^{31}P NMR measurements. This study, to our knowledge, is the first to report the Raman spectrum of hPGK in its open and closed conformation in aqueous environment and the spectral changes associated with its amide I and amide III regions during the open and closed states of the enzyme.

This thesis is composed of five chapters; the first chapter introduces the structure, synthesis and functions of the most common nucleotides, followed by a description of nucleotide binding proteins. The chapter then includes a detailed explanation of the structure and function of the enzyme phosphoglycerate kinase, followed by a description of Raman and ROA spectroscopies, before reviewing their role in studying different nucleotides and proteins. The first chapter ends by reporting the overall aims of the study. Chapters two, three and four contain the three experimentally-based studies conducted for adenosines, for guanosines and for PGK, respectively, and a section is provided at the beginning of each chapter to accredit the contributions of collaborators in accomplishing this work. Finally, chapter five describes the overall conclusion and recommendations for future work.

The application of Raman spectroscopy, DFT and NMR, in addition to other techniques used during this study has improved my theoretical knowledge and equipped me with different practical and analytical skills that will have a great impact on my academic and professional career in the near future. The outcomes of this study can contribute, to some extent, to expanding our understanding of the structural features of nucleotides and the conformations of their associated proteins. The use of the Raman

spectroscopy, and the averaged atom displacements approach from DFT, can provide a powerful diagnostic tool that can be further applied in biological and pharmaceutical studies to gain insights into the dynamic characteristics of various nucleotides and their interactions with other cellular molecules.

Omer Azher

Chapter 1: Introduction

1.1 Nucleotides

Nucleotides are organic compounds made up of furanose ring attached to purine or pyrimidine bases and a phosphate group(s). These substances are the basic monomers for deoxyribonucleic acid (DNA) and ribonucleic acid (RNA). Nucleotides are also involved in a variety of biological processes, such as energy production in the form of adenosine tri-phosphate (ATP), signal transduction, neurotransmission and regulation of different metabolic pathways (Moss *et al*., 1995; Sperlagh and Vizi, 2011; Brito-Arias, 2016)

1.1.1 Structure

A single nucleotide is composed of a heterocyclic nitrogenous base, a pentose sugar ring (β-D-ribofuranose) and mono-, di-, or tri-phosphate group(s) (PO_3^{-2}). Nucleosides are structurally comparable to nucleotides but their sugar ring attached only to the nitrogenous base, i.e., the molecule dose not bind to any phosphate moieties. The majority of the nitrogenous bases can be classified into two groups: purines and pyrimidine (Table 1.1). The former primarily includes adenine (A) and guanine (G), while the later encompasses cytosine (C), thymine (T) and uracil (U) (Blackburn *et al*., 2006). Purine bases differ from pyrimidine ones due to the presence of an imidazole ring fused with the 6-membered heterocycle of the nitrogenous base (Figure 1.1). This structural difference between purine and pyrimidine bases causes their corresponding nucleotides and cyclic nucleotides to differ in their binding affinities for target proteins (Beste-Kerstin and Seifert, 2013; Seifert, 2014).

Table 1.1. List of common bases and their nucleoside and nucleotide nomenclatures. The majority of nucleotides can be grouped into purine and pyrimidine nucleotides. Purine nucleotides include adenosines and guanosines while pyrimidine nucleotides include cytosine, thymine and uracil.

Base	**Nucleoside**	**Nucleotide**
Purines	Adenosine	Adenylate
	Guanosine	Guanylate
Pyrimidines	Cytidine	Cytidylate
	Thymidine	Thymidylate
	Uridine	Uridylate

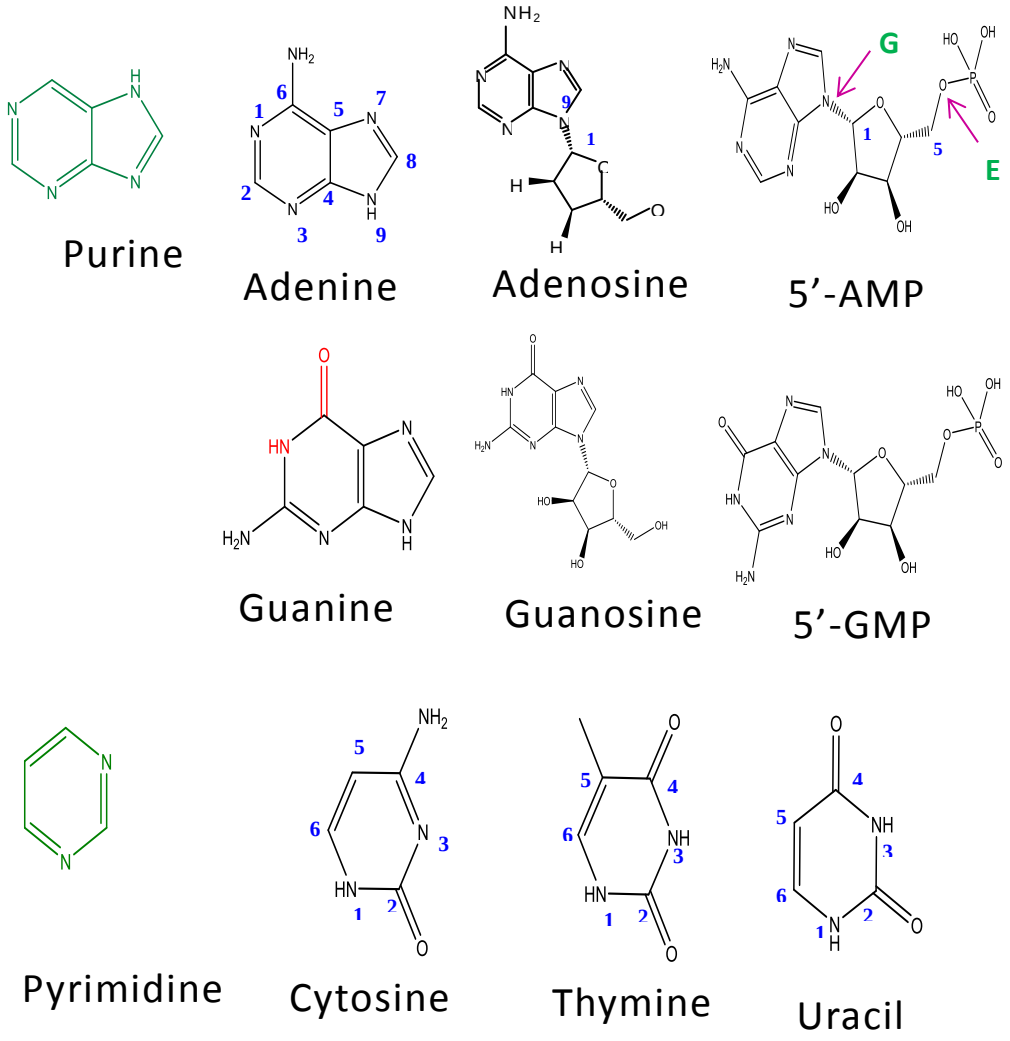

Figure 1.1 The chemical structure of purine (top) and pyrimidine (bottom) nucleotides. Purine nucleotides include adenine and guanine and pyrimidine nucleotides include cytosine, thymine and uracil bases. C1' of the ribose sugar binds to the nucleobase via β-glycosidic bond (G).C5' of the ribose binds to the phosphate group(s) forming ester bond (E). 5'-AMP: 5'-adenosine monophosphate and 5'-GMP: 5'-guanosine monophosphate.

Each nucleotide binds by N9 of its purine or N1 of its pyrimidine to (C1') of the ribose ring forming a β-glycosidic bond. The pentose sugar is a 5-membered ring exists in nature in a D-form configuration forming D-ribose, (in nucleosides, nucleotides and RNA), and 2-deoxy-D-ribose, (in deoxynucleosides, deoxynucleotides and DNA). In the phosphate containing nucleotides, the ribose sugar is attached via its (C5') to mono-, di- or tri-phosphate groups forming Ester bond (Figure 1.1). Another form of nucleotides is referred to as the cyclic nucleotide that can be defined as a monophosphate nucleotide in which the ribose sugar binds to the phosphate group by cyclic bonds. The most common naturally occurring cyclic nucleotides are adenosine 3',5'-cyclic monophosphate (cAMP) and guanosine 3,5-cyclic monophosphate (cGMP) (Figure 1.2).

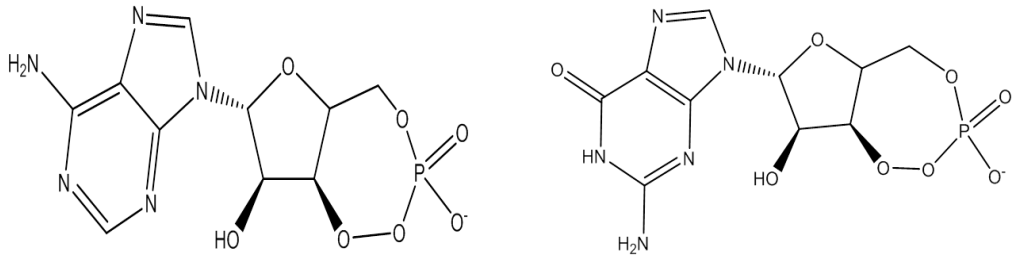

Figure 1.2 Structure of adenosine 3',5'-cyclic monophosphate (cAMP) and guanosine 3',5'-cyclic monophosphate (cGMP).

In addition to the purine and pyrimidine bases listed in Table 1, a number of different modified forms of nucleobases are existed naturally, e.g., 5-methylcytosine in DNA, mono-, di-N-methylated adenine/guanine in RNA, hypoxanthine and xanthine. These modified bases play an important role in many cellular activities, such as DNA repair, transcription, replication, oligonucleotides recognition and gene expression (Corvetta *et al*., 1991; Farias and Castro, 2014).

1.1.2 Conformations

Nucleosides and nucleotides can exist in distinct conformations in solution. Knowing the prevalent conformational structure will provide further information about the interaction of nucleobases with various molecules and will also aid in understanding the dynamic behaviour of DNA and RNAs during different genetic processes. Therefore, many studies have been conducted to investigate the variable conformers adopted by nucleoside and nucleotide molecules (Davies, 1978; Rosemeyer *et al.*, 1990; Plavec *et al.*, 1993). The conformational structures of most nucleosides and nucleotides can be described by the type of their sugar pucker and the torsion angles (χ) and (γ).

Sugar pucker: The ribose ring in nucleosides and nucleotides is non-planar therefore; it can adopt different structural conformations that often referred to as sugar puckering (Voet and Voet, 2011). The ribose conformers are mainly determined by the displacement of C2' and C3' atoms from the plain of the ring, i.e., the C2'-endo indicates that the displacement of the C2' is above the median plain and the opposite for the exo-conformation. Sugar puckers can be also defined by the ribose five torsion angles (V_0, V_1, V_2, V_3 and V_4) located on C1', C2', C3', C4', and C5', respectively. These angles can be combined to form what is referred to as pseudorotation angle (P) which can determine the ribose conformation by a unique P-value. C2'-endo conformation can be represented by the P-value of 144-180°, and is known as south (S) while C3-endo orientation can be defined by the P-value of 0-36°, and is known as north (N) (Figure 1.3) (Altona and Sundaralingam, 1972; Evich *et al.*, 2017).

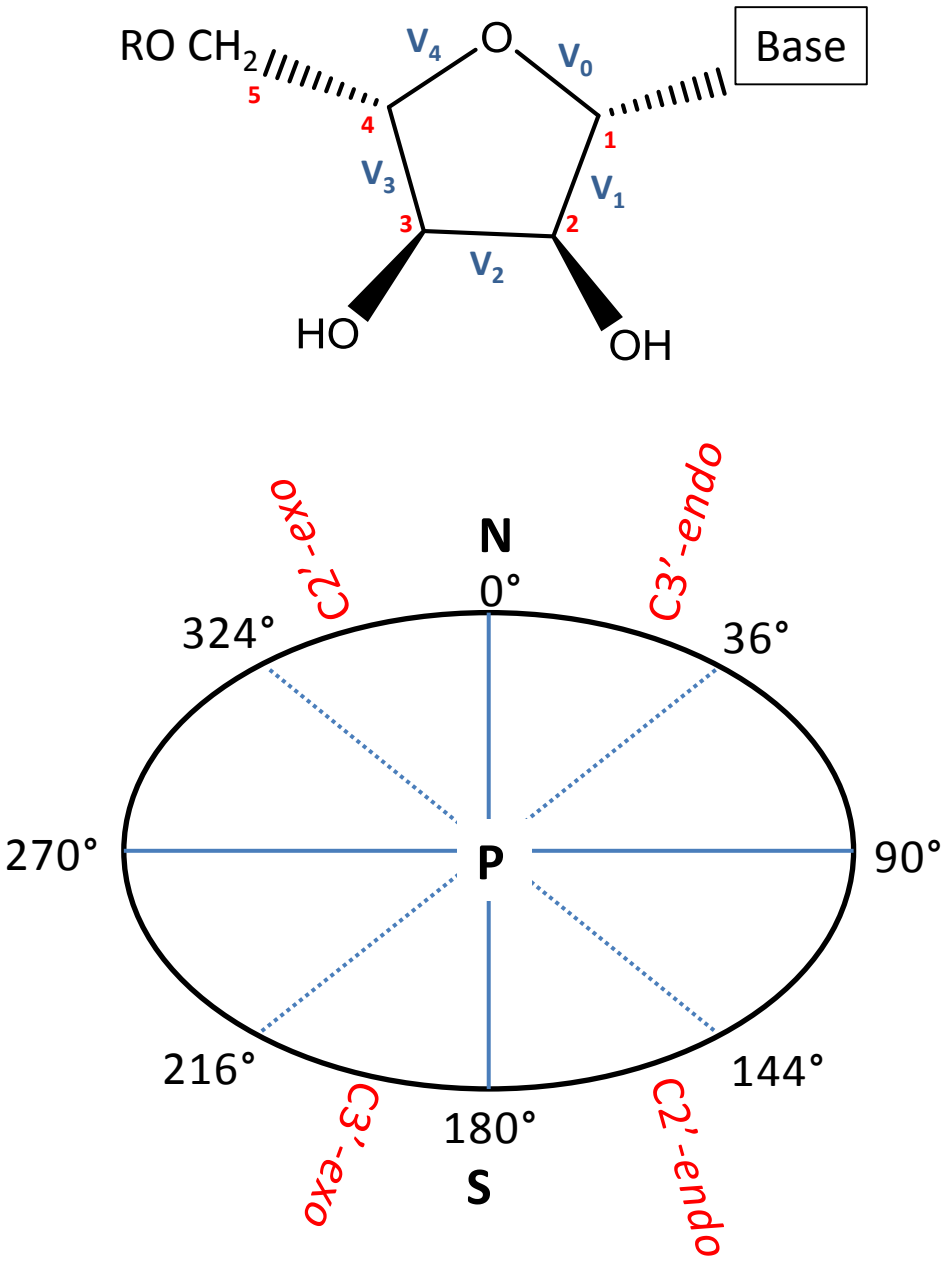

Figure 1.3.The five endocyclic torsion angels (V_0, V_1, V_2, V_3 and V_4) of the sugar ring. Numbers in red represent the position of the carbon atoms in the ring (top). The sugar pseudorotation cycle represents the angle P. The most common sugar puckers are *C2'*-endo *and* C3'-endo can be defined based on the values of the P angel. *C2'*-endo conformation presented in the south region at P= 144-180° and C3'-endo conformation found in the north region at P= 0-36° (bottom).

The majority of mono-phosphate nucleotides usually prefer two types of sugar puckers: S, C2'–endo and N, C3'-endo (Roy *et al.*, 2016); the former conformation is mainly found in DNA while the latter appears in RNA. Each of these sugar pucker conformations will change the distance between the attached phosphate groups (Figure 1.4).On the one hand, in the S,C2'-endo pucker, the two phosphate groups will be apart by ~7 Å allowing an extended twist of the nucleotides that form DNA. On the other hand, the N, C3'-endo pucker provide shorter distance of, ~5.8 Å between the adjacent phosphate molecules which in turn leads to a smaller twist angle as observed in RNA (Rich, 2003;Williams *et al.*, 2009). In addition to their role in shaping the helical structure of the different forms of DNA, sugar puckers can provide further information about the structural alterations associated with the secondary structure of some RNAs during their excited states (Clay *et al.*, 2017)

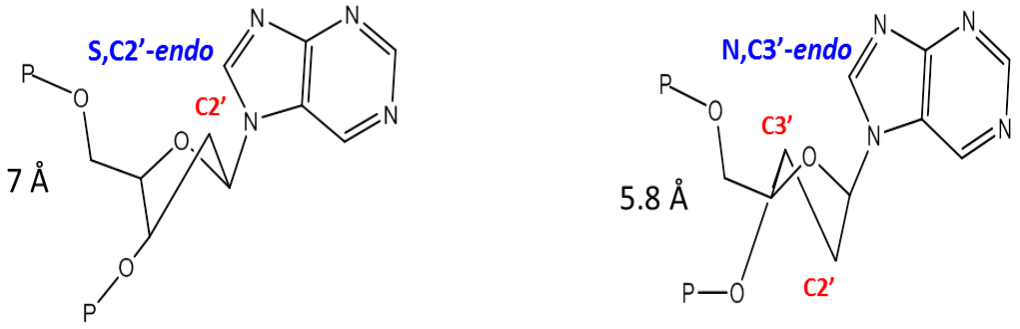

Figure 1.4. The two major types of sugar puckers in DNA and in RNA: S, C2'-endo pucker (left) is found mainly in DNA and separates the two phosphate atoms by 7 Å. The N, C3'-endo pucker (right) found in RNA and separates the two phosphates by 5.8 Å. ADP: adenosine diphosphate, P: (PO_3^{2-}).

Torsion Angle chi (χ): The orientation of the nucleotide's nitrogenous base with respect to its ribose sugar about the β-N-glycosidic bond (C1'-N9') is determined by the torsion angle (χ) (Figure 1.5).As a result, nucleotides can have two conformations: Syn- and Anti-; the latter is being the most common one for free nucleotides in liquid and solid phase as well as for

the nucleotides that form DNA and RNA molecules (Murthy *et al*., 1999; Sigel and Griesser, 2005; Sokoloski *et al*., 2011).

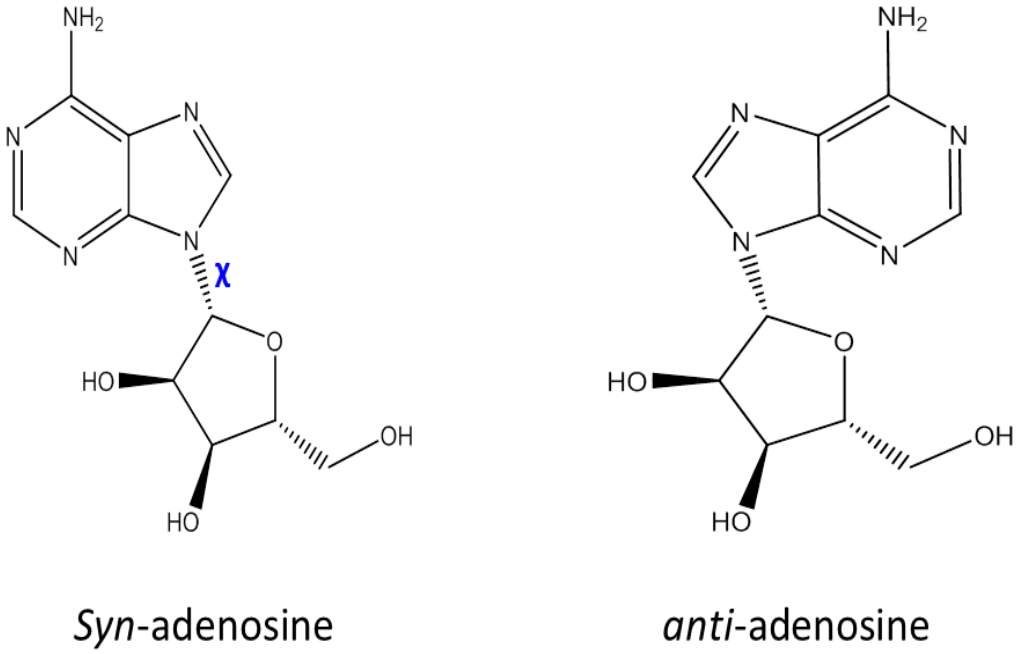

Figure 1.5 The adenosine nucleotide molecule in *Syn*- and *anti*- conformations around the torsion angle chi (χ).

Torsion Angle gamma (γ): The steric position of the 5'-OH group, relative to the ribose ring (C4'-C5'), is determined by the torsion angle (γ) (Figure 1.6). The structural conformations of the polynucleotides in DNA and RNA can be described by studying the possible orientations of the backbone torsion angles α, β, γ, δ, ε, and ζ (Blackburn *et al*., 2006). The degree of the orientation of these angles can be described using the terms gauche + (g+) = ~ 60°, gauche - (g-) = ~ -60° and trans (t) = ~180° (Neidle, 2002). In addition, the Klyne-Prelog system can be applied for DNA and RNA structures to describe the different orientations of the backbone torsion angles around a specific degree, for example, angles aggregated around 0° are referred to syn(s) while angles aggregated about 180° are referred to anti (a). The term synclinal (±sc) is used to describe the angles clustered around ± 60°, and anticlinal (±ac) is used for the

angles observed around ±120° (Eric and Dennis, 2005). The degree of the rotation of the backbone torsion angles is restricted and correlated to the structural conformation of the bonded molecules, such as the type of the ribose sugar pucker and the glycosidic angle (χ) (Neidle, 2008).

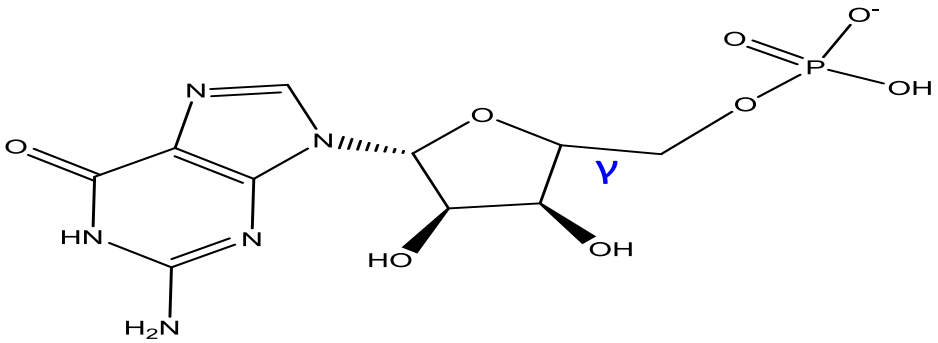

Figure 1.6 The torsion angle gamma (γ) in guanosine 5'-monophosphate (GMP) molecule determines the conformation of the phosphate group relative to the ribose ring.

1.1.3 Physical Characteristics

The dynamic behaviour of nucleotides and their chemical interactions with other molecules in physiological environment depend largely on their physical properties, such as the ability to form hydrogen bonds, the degree of ionisation and tautomerism (Blackburn *et al.*, 2006).

Hydrogen bonding (H-bonds): The formation of hydrogen bonds is critical for a variety of nucleotide interactions, such as base pairing in DNA and RNA molecules (Figure 1.7). The tendency of the nucleotides to establish hydrogen bonds depends on the ability of their constituent atoms to act as hydrogen donors or acceptors. This in turn depends on the charge densities of the constituent atoms. For instance, the charge density of the hydrogen atom in the NH group of the nitrogenous bases of adenine, guanine and cytosine is + 0.22 e, therefore, this hydrogen can act as an electron donor during the bond formation. Whereas, both oxygen and nitrogen atoms in

the nucleotide base are considered as electron acceptors as they possess a charge density of - 0.2 e (Saenger, 1984).

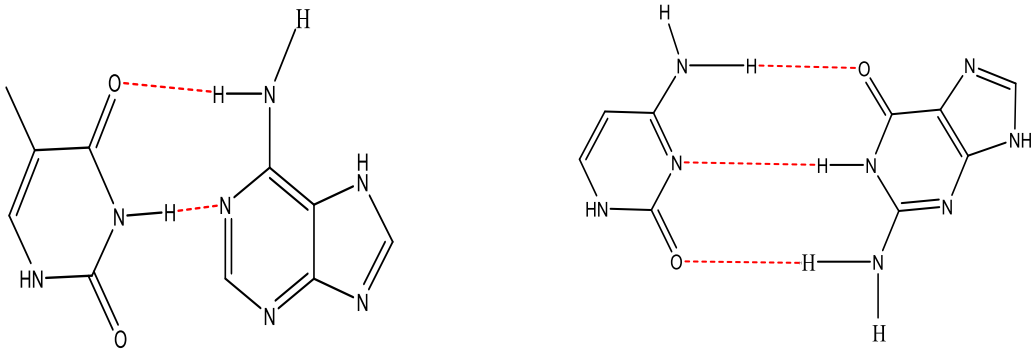

Figure 1.7 The formation of H-bonds (red dashed line) is important for the interaction between adenine (A)-thymine (T) and guanine (G) - cytosine (C) bases.

Ionisation: The dissociation constant (pK_a) is an important parameter for understanding the ionisation of nucleotides and their binding sites available for interaction with other metals or molecules. The pK_a values of nucleotides are usually determined experimentally using spectrometric titration methods (Roger and Fiona, 2010). At physiological pH, most of the nucleotide's nitrogenous bases are neutral; therefore, they have no tendency to act as acids or bases. Similar behaviour was also observed for the ribose sugar which has a pK_a value of ~ 13.0 (Velikyan *et al*., 2001).

Table 1.2. pK_a values for the nitrogenous bases and the phosphate groups of nucleotides.N: refers to the cyclic nitrogen atom and the assigned number represents its position (Blackburn *et al*., 2006; Shabarova and Bogdanov, 2007; Gollnest *et al*., 2016).

Base	5'-Nucleotide	Phosphate Residues	
		(pK_1)	**(pK_2)**
Adenine (N1')	3.7	0.9	6.0
Guanine (N1')	9.4	0.7	6.3
Cytosine (N3')	4.6	0.8	6.3
Thymine (N3')	10.0	1.6	6.5
Uracil (N3')	9.5	1.0	6.4

The phosphate groups in nucleotides act as dibasic molecules, and thus they exhibit two stages of proton loss (Figure 1.8). The pK_a values of the phosphate groups of different nucleotides are illustrated in Table 1.2. The pK_a values of the two stage of ionisation are ~1.0 for (pKa_1) and ~ 6.3 for (pKa_2). Therefore, the phosphate groups of all nucleotides are deprotonated (negatively charged) at physiological pH (~ 7).

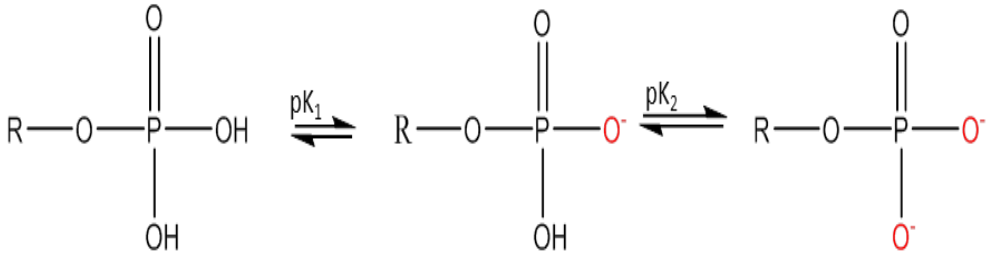

Figure 1.8 Ionization of the dibasic phosphate molecule in nucleotides showing the two steps of proton loss.

Adenine (A), like cytosine (C), each is composed of an amino group and display weak basic characteristics in alkaline solution, i.e., both (A) and (C) can accept a proton but the site for the proton attachment is the cyclic nitrogen atom instead of the amino group. By contrast, thymine (T) and

uracil (U) possess acidic properties as they can lose a proton easily during their tautomeric hydroxyl forms. However, guanine exhibits both acidic and basic features, depending on the surrounding medium. As in (A) and (C), the acceptance of the proton in guanosine occurs via the cyclic nitrogen and the tautomeric hydroxyl form facilitates the proton loss in alkaline media (Shabarova and Bogdanov, 2007).

For oligo- and poly nucleotides, the strength of the base pairing commonly investigated in terms of the differences in the pK_a (Δ pK_a) values between the hydrogen donor (d) and the acceptor (a) (Chen *et al*., 1998). Thus, the lower the value of (Δ pK_a) is between (d) and (a) of the base pairs, the stronger the H-bonds and vice versa. The guanosine (g)-cytosine (c) binding reflected lower (Δ pK_a) and, as a result, a stronger H-bonds compared to adenine (A) or Uracil (U) and Thymine (T) (Acharya *et al*., 2004).

Tautomerism: The nitrogenous bases of nucleotides have the ability to change the position of the proton in their cyclic structure leading to the rearrangements of the bonds and the formation of different tautomers (Figure 1.9).The dominant tautomers for nucleotides at physiological pH are keto and amino forms (Purrello *et al*., 1993). The formation of keto and amino tautomeric structures by nucleobases is an important process as it promotes the formation of H-bonds between the complementarily base pairs: adenine (A)-Thymine (T) and guanine (G)-cytosine(C). In some cases, rare tautomers, such as enol and imino structures can be formed by nucleotides and cause mismatched base pairing which can lead to the formation of different mutations (Singh *et al*., 2015). The ability of some tautomeric forms of nucleotides to cause mutations has been exploited by different studies to develop an antiviral therapeutic strategy, which uses tautomeric nucleoside analogues to increase the mutation rates of certain viruses and enhance lethal mutagenesis (Mullins *et al*., 2011; Li *et al*., 2014; Vivet-Boudou *et al*., 2015).

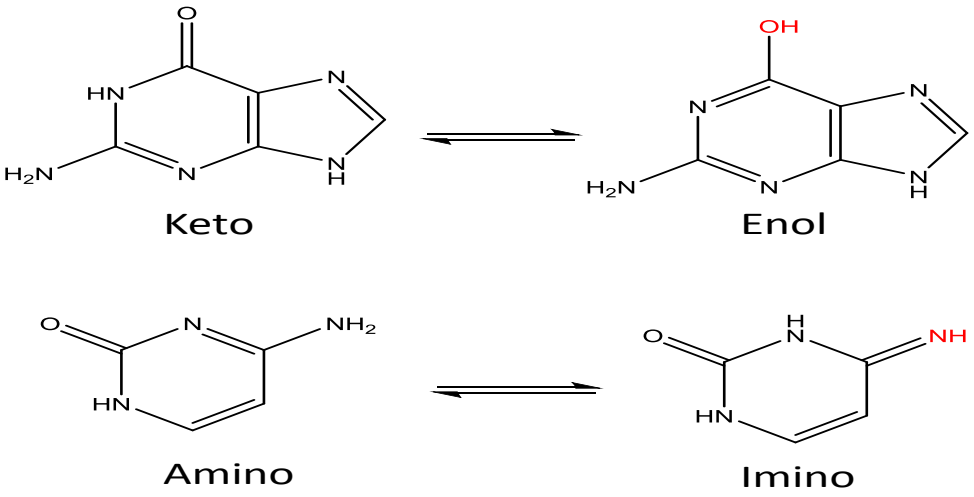

Figure 1.9.Nitrogenous base of nucleotides can rearrange the protons in the heterocycle that result in forming multiple tautomers. Common tautomers include Keto-enol tautomers for guanine (top) and amino and imino tautomers for cytosine (bottom).

1.2 Nucleotides synthesis

1.2.1 *In vivo* synthesis

The majority of the dietary polynucleotides are converted into mononucleotides and their bases are then oxidised resulting in uric acid that is excreted by the renal system. Therefore, most of the ingested nucleotides are not used for the synthesis of purine or pyrimidine bases (Robert *et al.*, 2003). Therefore, purine and pyrimidine precursors are obtained from various cellular metabolic intermediates, such as glutamate, aspartate, formate, glycine and bicarbonate. The synthesis of purine and pyrimidine nucleotides occurs via two major pathways: de novo and salvage pathways.

The de novo pathway consumes considerable amount of energy in the form of ATP compared to the salvage route which requires less energy as it utilises the preformed nitrogenous bases in the body to produce nucleotides. During the de novo synthesis of purine and pyrimidine nucleotides, metabolic substances, such as aspartate, glutamate and ribose-5-phosphate in addition to CO_2 and NH_3 molecules are used as precursors to establish the reaction. The de novo biosynthesis of purine nucleotide starts by converting ribose 5-phosphate, through a series of enzymatic reactions, into inosine monophosphate that is further converted to adenosine and guanosine monophosphates (Nelson *et al.*, 2008; Zhao *et al.*, 2013) (Figure 1.10). The de novo synthesis of pyrimidine nucleotides utilises glutamine, aspartic acid and CO_2 as precursors for the pyrimidine base (Figure 1.11). The reaction of carbamoyl phosphate with aspartic acid produces uracil monophosphate (UMP) as the first pyrimidine nucleotide. UMP then acts as a precursor for the formation of cytosine triphosphate (CTP) and thymine monophosphate (TMP).

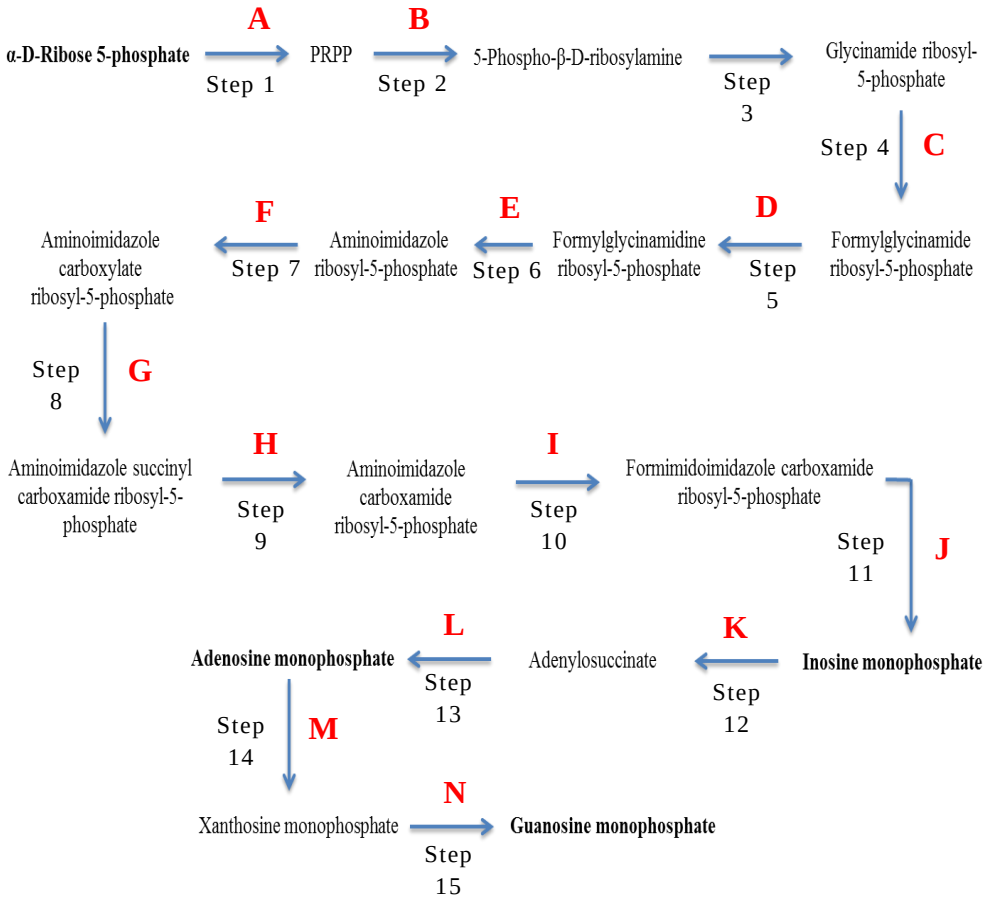

Figure 1.10. *De novo* biosynthesis of purine nucleotides. α-D-Ribose 5-phosphate is the precursor for the *de novo* synthesis of purines. This pathway involves series of enzyme catalysed reactions that resulted in forming inosine, adenosine and guanosine monophosphates. A refers to: phospho-ribose pyrophosphate (PRPP) synthase, B refers to: PRPP glutamyl amidotransferase, C refers to: formyltransferase D refers to: formylglycinamidine ribosyl-5-phosphate synthetase, E refers to: aminoimidazole ribosyl-5-phosphate synthetase, F refers to: aminoimidazole ribosyl-5-phosphate carboxylase, G refers to: aminoimidazole succinyl carboxamide ribosyl-5-phosphate synthetase, H refers to: adenylosuccinase, I refers to: formyltransferase, J refers to: inosine monophosphate cyclohydrolase, K refers to: adenylosuccinate synthase, L refers to: adenylosuccinase, M refers to: inosine monophosphate dehydrogenase, and N refers to: transamidinase. The diagram is adopted from (Robert *et al*. 2003).

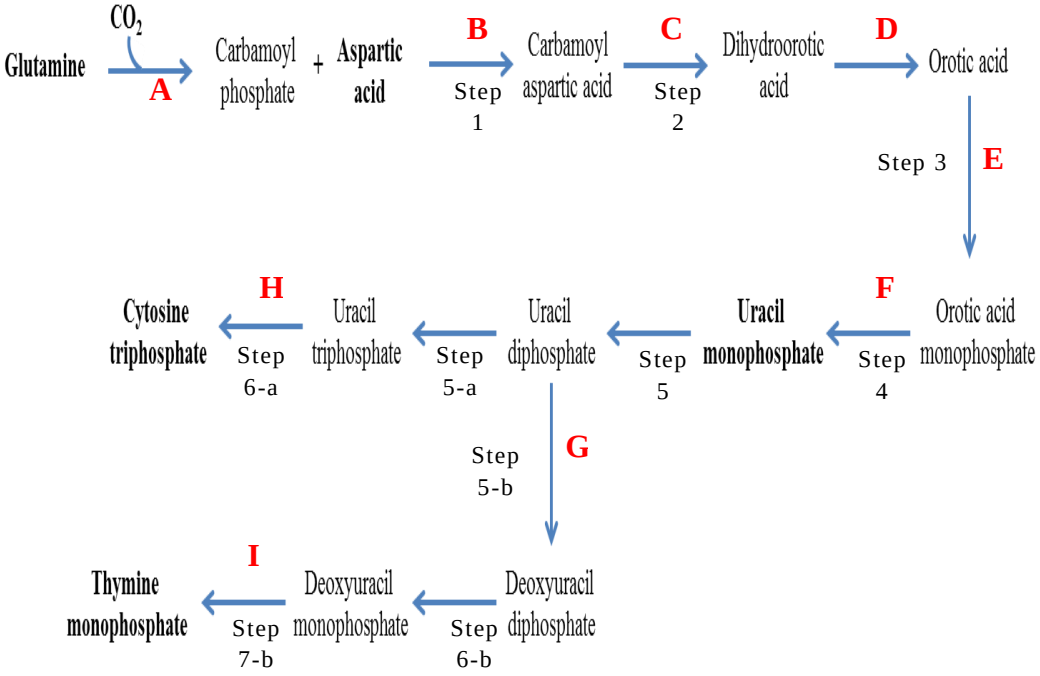

Figure 1.11 The *de novo* biosynthesis of pyrimidine nucleotides. Glutamine, aspartic acid and CO_2 act as precursors for the de novo synthesis of pyrimidines. The reaction results in the formation of uracil monophosphate, cytosine triphosphate and thymine monophosphate A refers to: carbamoyl phosphate synthase II, B refers to: aspartate transcarbamoylase, C refers to: dihydroorotase, D refers to: dihydrooretate dehydrogenase, E refers to: orotate phosphoribosyl transferase, F refers to: orotidylic acid decarboxylase, G refers to: ribonucleotide reductase, H refers to: cytosine triphosphate synthase, I refers to: thymidylate synthase. The diagram is adopted from (Robert *et al.*, 2003).

In the salvage rout, metabolic end products that may result from the cellular degradation of RNA and DNA, such as hypoxanthine, guanine and adenine, can be recycled and used as precursors for the synthesis of new nucleotides. During this pathway, hypoxanthine reacts with phospho-ribose pyrophosphate (PRPP) to produce inosine monophosphate (IMP). This reaction is catalysed by hypoxanthine phosphoribosyl transferase. Similarly, adenosine monophosphate (AMP) and guanosine monophosphate (GMP) can be synthesised via the reaction of (PRPP) with adenine and guanine bases, respectively. The enzymes involved herein are adenine phosphoribosyl transferase for (AMP) and guanine phosphoribosyl transferase for (GMP) (Lane and Fan, 2015).

1.3 Functions of Nucleotides

Nucleotides are the building blocks for DNA and RNA; they are bound to each other via the Ester bond (between C5' of one ribose ring and C3' of the other one) that forms the backbone of nucleic acids. Free nucleotides play an important role in a variety of physiological functions, such as energy production, enzyme cofactors, second messengers and allosteric modulation. Thus, the cellular concentration of free nucleotides is maintained at certain levels (~1µmol/g) to ensure their availability in sufficient amounts to be used in various biological processes (Traut, 1994).

Energy production: Nucleotides serve as a high energy transfer compounds. Adenosine 5-triphosphate ATP is considered as the most important nucleotide involved in phosphorylation reactions. The α-phosphate group in the ATP molecule is attached to the C5' of the sugar ring forming phosphate Ester bond and both β- and γ-phosphate groups bind to their α-analogue via a phosphoanhydride linkage. At physiological pH, all the phosphate groups of ATP nucleotide exist in anionic forms resulting in high negative charge density of the molecule and increasing the electrostatic repulsion between the three phosphate moieties. The breakdown (hydrolysis) of ATP, under the influence of enzymes,

neutralises the electrostatic repulsion between the phosphate groups and lowers the energy of the molecule. During hydrolysis, the released orthophosphate is stabilised by forming multiple resonance structures (Figure 1.12), and the product of adenosine diphosphate (ADP) is rapidly ionised releasing H^+ to the aqueous medium (Nelson *et al*., 2008)

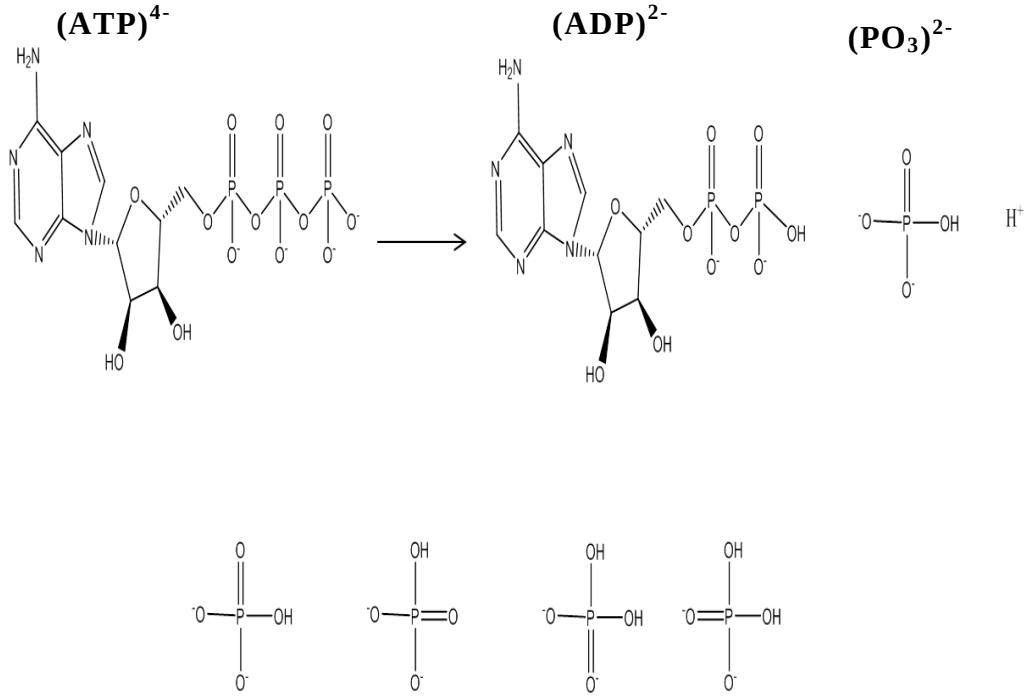

Figure 1.12. Enzymatic ATP hydrolysis forming ADP and orthophosphate (top). The breakdown of ATP reduces the high electrostatic repulsion between the oxygen anions of the triphosphates. The released orthophosphate is stabilised by adopting different possible resonance forms (bottom).

Enzyme cofactors: Nucleotides are considered as essential subunits of various cofactors including the, most common nicotinamide adenine dinucleotide (NAD) and flavin adenine dinucleotide (FAD). Both NAD and FAD function as oxidising and reducing agents in a variety of biochemical pathways. For the synthesis of NAD, each ATP provides an AMP molecule which reacts with nicotinate ribonucleotide in order to produce desamino-NAD+ that then receives an amino group from glutamine to form NAD^+ (Figure 1.13). For the synthesis of FAD, two ATP molecules are required:

One ATP molecule phosphorylates riboflavin to produce riboflavin 5'-monophosphate (FMN) and the other ATP donates an AMP molecule to FMN yielding FAD and two inorganic phosphates (Jeremy *et al*., 2015).

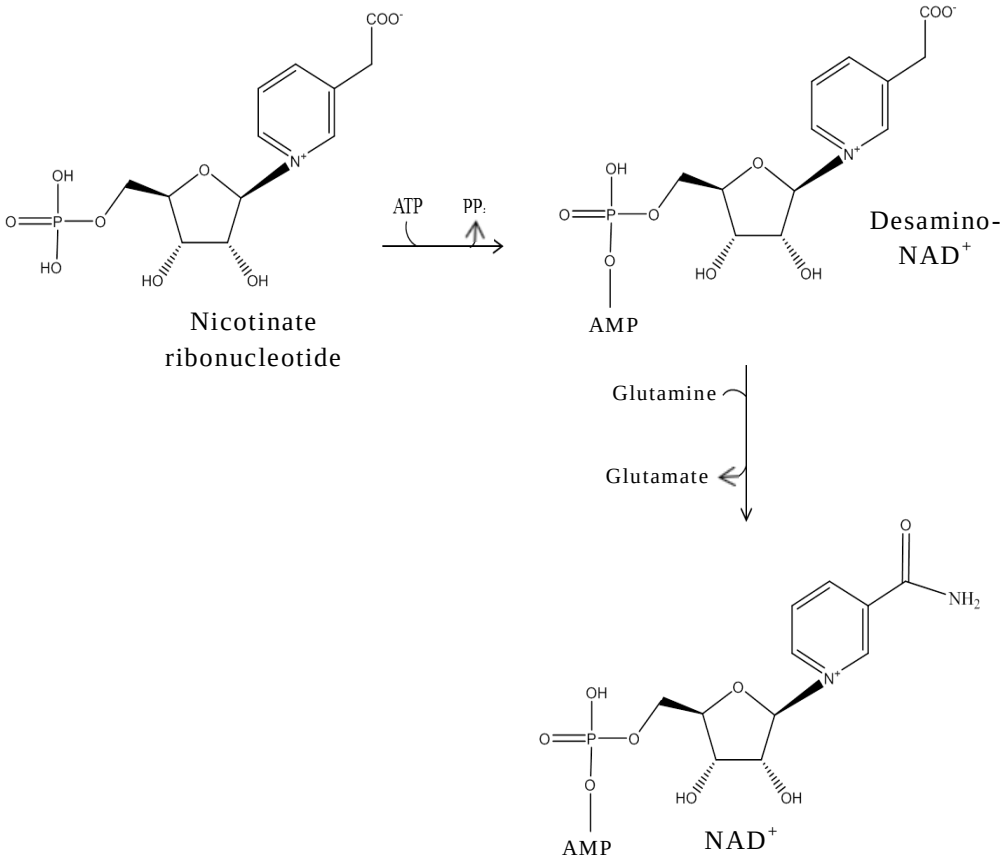

Figure 1.13. The role of ATP in the biosynthesis of NAD. AMP, transferred from ATP and reacts with nicotinate ribonucleotide to form desamino-NAD^+ which is further converted to NAD^+ after the addition of an amino group from glutamine.

Second messengers: Many cyclic nucleotides act as second messengers, in which they bind to signalling proteins during signal transduction and regulate their activity (Alberts *et al*., 2008). Cyclic 3',5'-adenosine monophosphate (cAMP) is the first second messenger to be discovered, which with guanosine 3',5'-cyclic monophosphate (cGMP) constitutes the most common second messengers (Hengge *et al*., 2016). Different cyclic nucleotides have been also reported as second messengers, such as cytidine

3,5-cyclic monophosphate (cCMP), uridine 3,5 cyclic monophosphate (cUMP) and inosine 3,5-cyclic monophosphate (cIMP) (Seifert, 2015).

During cAMP-dependant signal transduction, a hormone binds to a specific receptor on the cell membrane. This binding causes the G protein to replace its bound GDP with GTP. The GTP-bound G protein becomes active and stimulates adenylyl cyclase to convert ATP to cAMP. Once cAMP is produced, it activates a protein kinase which in turn phosphorylates next protein kinase, and so on. This phosphorylation cascade stimulates different hormones, such as adrenaline, adrenocorticotropic hormone, luteinising hormone, etc. (Alberts *et al.*, 2008) (Figure 1.14).

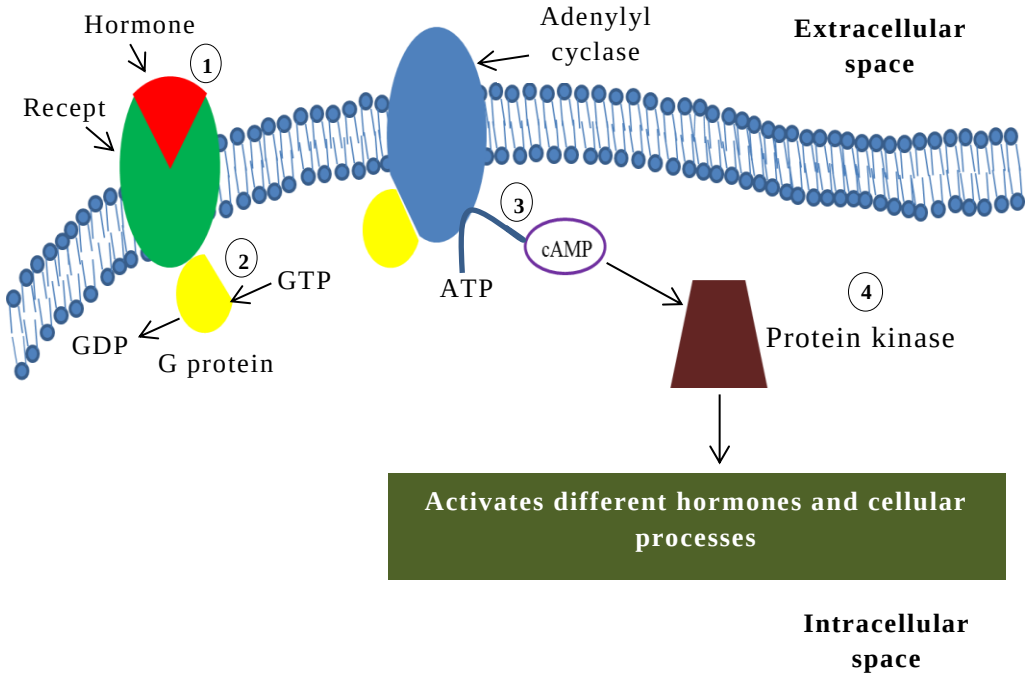

Figure 1.14. General scheme for the role of cAMP in signal transduction. 1-The binding of a hormone to target receptor activates G protein. 2- Activated G protein exchanges GDP for GTP and undergoes conformational changes resulted in the activation of Adenylyl cyclase. 3- Activated adenylyl cyclase converts ATP to cAMP which activates protein kinases and initiates a phosphorylation cascade.

Allosteric modulators: Several nucleotides can regulate the activity of certain enzymes by binding to specific sites and exert a conformational changes leading to the activation or inhibition of that enzyme (Ahalawat and Murarka, 2017). For example, AMP-activated protein kinase (AMPK) is a key enzyme in controlling multiple homeostatic pathways, such as cellular growth, reprogramming and autophagy (Mihaylova and Shaw, 2011). The binding of ATP to the γ-subunit of AMPK causes structural modification to different part of the enzyme and finally inhibiting its function (Ahalawat and Murarka, 2017). Guanosine triphosphate (GTP) also plays an inhibitory role when binds to cytidine 5-triphosphate synthase (CTPs), an enzyme involved in nucleotide metabolism. However, the mechanism of conformational changes induced by GTP to CTPs remains unclear (Lunn *et al*., 2008). In addition to the allosteric effects of ATP and GTP, pyrimidine nucleotides, for example cytosine tri-phosphate (CTP) has been reported as allosteric inhibitor for different enzymes, such as aspartate transcarbamoylase, extracted from *Escherichia coli*, and IspD (An enzyme involved in the third step of the non-mevalonate pathway for the synthesis of isoprenoids) (Wild *et al*., 1989; Kunfermann *et al*., 2014).

In addition to the participation of nucleotides in various biochemical processes, the use of nucleotides as dietary supplements has been demonstrated to enhance numerous body functions; animal studies revealed that supplementary nucleotides can improve cellular metabolism, increase mitochondrial DNA synthesis and restore nitrogen balance of the liver (Jin *et al*., 1996). The supplementation of monophosphate nucleotides has been reported to stimulate the concentrations of the unsaturated fatty acids and support the growth and maturation of the intestinal cells in rodents (Uauy *et al*., 1990; Bueno *et al*., 1994). There is accumulated body of evidence that support the beneficial role of supplementary nucleotides in enhancing various function of the immune system in human adults and infants (Carver *et al*., 1991; Navarro *et al*., 1996; Hess and Greenberg, 2012).

The chemical synthesis and modification of different nucleosides and nucleotides resulted in the formation of nucleoside/nucleotide analogues (See section 1.2.2.), which have been in use for 50 years as therapeutic

agents for the treatment of various disorders (most commonly viral infections and cancer) (Jordheim *et al*., 2013). Several viral infections, such as human immunodeficiency virus (HIV), hepatitis B virus (HBV), cytomegalovirus (CMV) and varicella zoster virus have been treated by nucleoside analogues. The mechanism of action of many antiviral nucleoside analogues, such as vidarabine, entecavir and telbivudine, depends on inhibiting the replication of viral DNA leading to the suppression of the target virus (Wishart *et al*., 2018). For the treatment of tumor, about 15 nucleoside analogues have been licenced by Food and Drug Administration (FDA) as chemotherapeutic agents (Shelton *et al*., 2016). The antitumor activity of many nucleoside analogues stems from their ability to interfere with the synthesis of cellular DNA and as a result suppressing the growth of the cancerous cells. Examples include capecitabine, for the treatment of breast and colorectal tumours, and fluorouracil, for gastric and cervical neoplasms (Walko and Lindley, 2005).

1.4 Nucleotide-binding proteins

The binding of many proteins to nucleotides is essential to perform their biological activities. Common examples of nucleotide binding proteins include kinases that usually bind to ATP/GTP, and G-proteins, that usually bind to GTP, and cyclic nucleotide-dependant protein kinases, that involve cAMP-dependent protein kinase A (PKA) and cGMP-dependent protein kinase G (PKG) (Scott, 1991; Xiao and Wang, 2016).

Kinases: The enzymes that catalyse the transfer of a terminal phosphate group from a nucleoside triphosphate (usually ATP or GTP) to another nucleoside, molecule or protein are described as kinases (Matte *et al*., 1998). Protein kinases are one of the common protein families in human cells with more than 500 protein been discovered (Manning *et al*., 2002). Kinases exert a fundamental role in a variety of cellular functions, for example regulation of some metabolic pathways, gene expression and signal transduction (Ventura and Maioli, 2001). Examples of kinases involved in different metabolic reactions include phosphoglycerate kinase

(PGK), phosphofructokinase and phosphoenolpyruvate carboxykinase. During phosphorylation, the binding of the kinase to its substrates resulted in conformational changes of the enzyme to adopt the correct geometry for its catalytic activity (Huse and Kuriyan, 2002).

The binding of ATP or GTP to magnesium is essential in many kinases as it leads to the coordination of β-, γ- or α-,β-, γ-phosphate groups of the nucleoside (Auerbach *et al.*, 1997). In some kinases, such as phosphoenolpyruvate carboxykinase, the binding of the divalent cation adapts the β- and γ-phosphate groups in high energy orientation (eclipsed conformation) increasing the electrostatic repulsion and decreasing the activation energy of the reaction. The magnesium cation can also facilitate the catalysis by sterically align the γ-phosphate group with the second substrate (Delbaere *et al.*, 2004). Many kinases adopt a dissociative transition state, i.e., the transfer of the terminal phosphate from ATP/GTP to the other substrate requires breaking the phosphoanhydride bond between γ- and β- phosphates followed by the binding of the released phosphate to the nucleophilic group of the other substrate (Wang and Cole, 2014).

G proteins: The guanine nucleotide binding proteins (G-proteins) and G-protein-coupled receptors (GPCRs) comprise a diverse family of proteins which play a pivotal role in signal transduction of eukaryotes. The number of discovered GPCRs in human cells exceeded 700 proteins. The G protein dependant signalling pathways control various physiological and cellular processes, such as hormonal regulation, neurotransmission and cell growth (Kroeze *et al.*, 2003). G-proteins signalling cascade is also essential for different human senses, such as hearing, taste and smell to perform their functions (Alberts *et al.*, 2008). G proteins are classified into two main groups: heterotrimeric G proteins and small G proteins. The former is composed of three subunits α, β, and γ which are attached with their GPCRs (Oldham and Hamm, 2008). The small G-proteins are monomeric polypeptides with five α-helices, six β-sheets and five loops (Paduch *et al.*, 2001). The mechanism of action of the G proteins depends largely on the ability of their α-subunits (Gα) to hydrolyse GTP following the binding of

specific substrate to the GPCR. In the inactive state, GDP is bound to Gα which is attached to Gβγ subunits. However, the activation of the GPCR causes conformational changes to the attached Gα subunit and as a result; the structure of the Gα subunit is modified. The activated Gα catalyses the exchange of GDP with GTP and as a result, GTP bound-Gα subunit dissociates from Gβγ subunits. The binding of Mg^{2+} to Gα is critical to change the conformation of the subunit and to facilitate its dissociation (Tuteja, 2009). The separated dimer has now been documented as being able to activate various molecules in the signalling cascade (Birnbaumer and Zurita, 2010; Sprang, 2016).

Cyclic nucleotide-dependant protein kinases: Cyclic purine nucleotides (cAMP and cGMP) are important cellular mediators that are required for triggering signal transduction cascades. PKA and PKG are the most important receptors activated by cAMP and cGMP respectively. PKA is a tetramer consisting of two catalytic subunits and two regulatory subunits. The binding of cAMP molecules to the regulatory subunits causes conformational changes of the focal enzyme which leads to the separation of the catalytic subunits and the concomitant phosphorylation of the target molecules (Taylor *et al*., 2008). The cGMP- dependant protein kinase (PKG) is a receptor protein which plays a central role in the control of cardiovascular and neural activities, such as smooth muscle contractions, platelet functions, learning and memory activities. PKG is a dimer enzyme exists in two types PKG I and II, which displayed N-terminal regulatory domain (R) and C-terminal catalytic domain (C) (Qin *et al*., 2015; Kim *et al*., 2016). The binding of cGMP to PKG exerted conformational changes to the receptor which resulted in a movement of the catalytic domains. Unlike PKA, the catalytic subunits perform their function while remained attached to the regulatory ones (Pinkse *et al*., 2009).

1.4.1 Phosphoglycerate kinase (PGK)

1.4.1.1 Overview

PGK is one of the glycolytic enzymes that catalyses the formation of ATP by converting 1,3-bisphosphoglycerate (1,3-BPG) to 3-phosphoglycerate (3-PG) (Figure 1.15). In humans, two PGK isozymes are identified: PGK-1 that is, expressed in all somatic cells and PGK-2 that is, distributed in testicular cells (spermatozoa). PGK-1 is a monomeric enzyme with a molecular weight of ~45 kDa and 417 amino acid residues PGK-1 gene is located on the X chromosome and spans 23kb (Huang *et al*., 1980; Tietz *et al*., 2006).

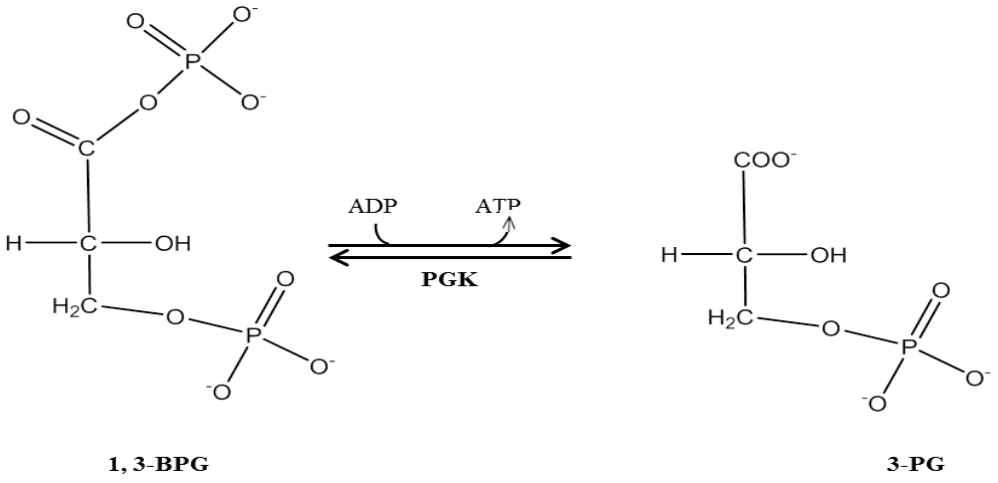

Figure 1.15. PGK catalyses the reversible conversion of 1,3-bisphosphoglycerate (1,3-BPG) to 3-phosphoglycerate (3PG).

1.4.1.2 Functions

In addition to the metabolic function of PGK in glycolysis, the enzyme is also involved in stimulating cellular DNA replication and viral mRNA transcription (Ogino *et al.*, 1999). PGK regulates the expression of urokinase-type plasminogen activator receptor (uPAR); a cell membrane protein that stimulates the lysis of extracellular matrices and is observed in high levels in different tumors. The overexpression of PGK-1has been reported to decrease the uPAR levels in tumor cells and prevent its migration in patients with lung cancer (Shetty *et al.*, 2005; Mauro *et al.*, 2017). An earlier study emphasised the critical role for PGK-2 for the activity of the sperms, as observed in mice with knocked out PGK-2 gene which reflected severe decrease in sperm motility and ATP concentrations (Danshina *et al.*, 2010).

1.4.1.3 Structure

The crystal structure of PGK was first prepared from two different sources: dried baker's yeast by Watson *et al*, (1971) and horse muscle by Blake *et al*, (1974) (Watson *et al.*, 1971; Blake and Evans, 1974). PGK enzyme is a monomeric polypeptide composed of two similar and equal size domains (N-terminal and C-terminal) joined by α-helix. The core of each domain is composed of six β-pleated sheets encircled by multiple α-helices (Blake and Rice, 1981) (Figure 1.16). Each one of the PGK substrates binds to specific domain i.e., 1,3-BPG/3-PG binds to the N-domain (which is composed of residues: Asp20, Asn22, Arg35, His58, Arg61, Arg112, Gly141, Arg145, Gly362, Gly363, and Ala364) and the magnesium-nucleotide complex binds to the C-domain (which contains the residues: Ser191, Lys196, Ile282, Leu283, Asn306, Glu313, Gly340, and Thr342). For the open (inactive) form of the PGK, the distance between the two substrates is about 12-15 Å but this distance decreased in the closed (active) form of the enzyme (Figure 1.17) (Balog *et al.*, 2007).

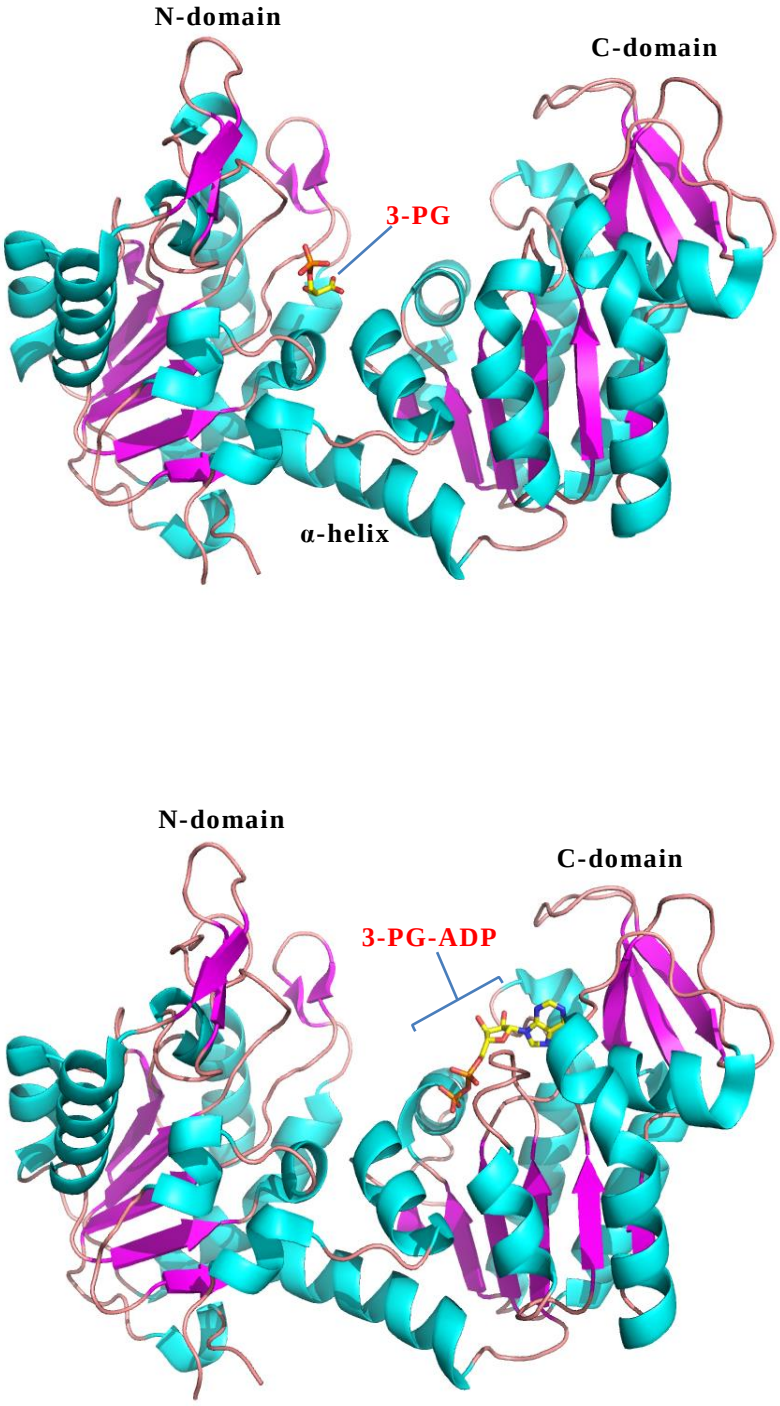

Figure 1.16. The structure of human PGK with its N- and C-domains. The secondary structure of the enzyme is composed of six β-sheets (arrows) located in the core of each domain and surrounded by multiple α-helices. (top): open conformation of human PGK-3PG complex. (bottom): open conformation of human PGK-ADP-3PG complex. This illustration was adopted from (Zerrad *et al.*, 2011).

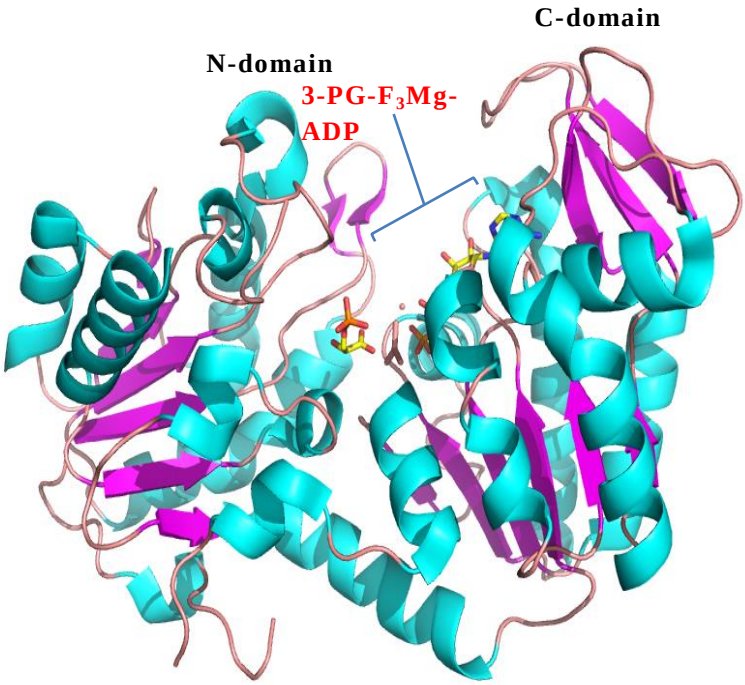

Figure 1.17. The structure of closed conformation of human PGK-3-PG-F_3Mg-ADP. In this conformation, the N- and C-domains come close to each other to facilitate the transfer of the phosphate group from the nucleotide to the 3-PG in order to form (1,3-BPG). This illustration was adopted from (Cliff *et al.*, 2010).

1.4.1.4 Open/closed conformation

The substrate-free form of the PGK enzyme exists in an (inactive) open conformation which has been identified from the unligated PGK crystals obtained from different bacteria (Lee *et al*., 2006; Zheng *et al*., 2012). However, upon binding of the PGK substrates to their correspondent domains, the enzyme undergoes substantial conformational changes and, as a result, the PGK domains come close to each other and the enzyme adopted a closed (active) conformation in which the distance between the PGK substrates reduced to be below 4.4 Å compared to 5.0 Å in the open form of the enzyme (Auerbach *et al*., 1997). The decrease in the distance between the PGK substrates in the closed form can facilitate the transfer of the phosphate group from the nucleotide to the 3-PG (Zheng *et al*., 2012) (Figure 1.17).

The switch from the open to the closed form of the PGK occurs via the movement of the N- and C-domains. This movement is known as hinge bending motion (Palmai *et al*., 2009). The first experimental evidence of the hinge bending motion came from the crystal structure of substrate-bound form of the Trypanosoma brucei (T.brucei) PGK enzyme in the closed conformation. The closed structure of the T.brucei PGK showed a domain rotation by 32° compared to the open conformation of the horse PGK (Bernstein *et al*., 1997). A study conducted by Kumar *et al*, (1999) reported the formation of an interdomain salt bridge between Arg62 and Asp200 of the Thermotoga maritima (Tm) PGK crystal which may maintain the closed conformation of the enzyme (Kumar *et al*., 1999). This can also indicate the strong interaction between the N- and C-domains of the closed form of the TmPGK beside the involvement of Lys197 in stabilising the phosphate group of the adenylyl-imido diphosphate analogue during the transition sate of the enzyme.

The transition state of the human PGK has been studied using transition state analogues, such as aluminium tetrafluoride (AlF^{4-}) and magnesium trifluoride (F_3Mg) to investigate the electrostatic environment of the PGK enzyme during its catalytic cycle. These findings indicate that the

transition state of the enzyme is dominated by charge neutralisation which is considered as a key feature for the transfer of the phosphate group between the two substrates (Cliff *et al*., 2010). Similar approach has been used later to study different enzyme –substrate interactions (Lallemand *et al*., 2011).

In addition to the involvement of the N- and C-domains in the hinge bending motion of the PGK enzyme, some studies proposed the participation of the α-helix, which connects the two domains (Figure 1.16), in establishing the motion of these domains. Vaidehi and Goddard (2000) applied molecular modelling simulation method (Hierarchical Newton-Euler Inverse Mass Operator) and suggested that the α-helix (Helix 7) exhibits a piston-like motion that aids the PGK to switch from the open to the closed conformation (Vaidehi and Goddard, 2000).

1.4.1.5 Substrate binding and hinge bending motion

Ligand-free and liganded PGK display two distinct structural conformations; therefore, different studies advocated that the role of substrate-binding in changing the conformation of protein can occur either by destabilising the interdomain region of the open conformation to facilitate the closure of the N- and C-termini which, decreases the free energy between the open and closed forms, or by utilising the free energy, resulting from the binding of substrates, via the initiation of the hinge bending motion (Adams and Pain, 1986; Blake, 1997; Varga *et al*., 2009). The stimulation of the hinge bending motion and the formation of the closed conformation of the enzyme is believed to occur only after the binding of both substrates (nucleotide and 1,3-BPG) (Zecchinon *et al*., 2005). By contrast, a study conducted by Gabba *et al*, (2014) suggested that the open conformation of the PGK enzyme exhibited various dynamic conformations. This dynamic behaviour is an intrinsic property of the enzyme and the binding of the substrates is not essential to initiate these conformations. However, the role of the substrates is to induce minor structural changes and restrict specific motions to enable the formation of the closed conformation (Gabba *et al*., 2014). From the previous studies we

can conclude the important role of substrate binding in providing the suitable energy and electrostatic environment to change the conformation of the enzyme and facilitate the phosphoryl transfer reaction, and weather the structural conformations adopted by the enzyme are due to its intrinsic property or initiated by the ligands, the role of substrate binding to the PGK domains remains essential step for catalysis (Zheng *et al*., 2012).

1.4.1.6 Hinge bending region

The switching of the PGK enzyme from the open to the closed structure requires conformational changes in the interdomain region (Adams and Pain, 1986). Blake *et al*, (1981) suggested that the two PGK domains are connected by three α-helices: 7, 14 and 15. The authors considered helices 7 and 14 as the hinges that undergo helix-helix interaction towards the closed conformation (Blake and Rice, 1981). The termini of helix 7 were identified later as C-hinge and N-hinge from T.brucei PGK crystal structure (Bernstein *et al*., 1997). Zheng *et al*, (2012) reported the presence of two flexible α-helices in the hinge region of BaPGK and CjBGK protein crystals which can regulate the distance between the two domains during catalysis (Zheng *et al*., 2012).

Another possible main hinge at β-stand L of the interdomain region of a pig muscle's PGK has been proposed and supported by simulation studies (Szilagyi *et al*., 2001; Szabo *et al*., 2008). The β-stand L hinge is located between N and C-domains and upon binding of the substrates, substantial conformational changes occurs to the hinge which resulted in further interaction of certain conserved residues towards other hinges, such as helix 7 facilitating the closure of the two domains (Varga *et al*., 2006).

1.4.1.7 The role of magnesium binding

The formation of a nucleotide-Mg complex is an essential step for the catalytic activity of PGK as the cation plays an important role in coordinating the phosphate groups of the nucleotide (Joao and Williams, 1993). Proton nuclear magnetic resonance (^{1}H NMR) measurements of yeast PGK indicated that the absence of Mg^{2+} causes the anionic oxygen

atoms of the diphosphate groups of ADP to interact electrostatically with the basic patch region of the N-domain whereas the addition of magnesium ions to ADP favours the binding of the nucleotide diphosphate to the hydrophobic site on the C-domain. It has been also suggested that the electrostatic binding of magnesium ion is shifted from βγ- to αβ-phosphate groups of ATP during the catalytic cycle of the PGK to promote the transfer of the terminal phosphate (Graham and Williams, 1991). Later studies indicated that the binding of magnesium ions to βγ- or αβγ-phosphates of ATP or GTP forms octahedral coordination sphere which is further completed by the binding of other oxygen anions from threonine, serine, aspartate or glutamate residues of the enzyme (Auerbach *et al*., 1997; Matte *et al*., 1998; Bugaev *et al*., 2016). A study conducted by Bernstein *et al*, (1979) suggested that the magnesium ions can align the β-phosphate group of the nucleotide with the phosphate group of the 3-phosphoglycerate providing the correct geometry to establish the phosphoryl transfer reaction (Bernstein *et al*., 1997).

1.5 Methods for nucleotide characterisation

X-ray crystallography and nuclear magnetic resonance (NMR) provide valuable experimental data useful in the characterisation of different natural and modified nucleotides and their interactions with metals and proteins (Neidle and Berman, 1983; Gacs-Baitz *et al*., 2004; Blackburn *et al*., 2006). Nucleotide-protein binding in aqueous phase has been investigated using solution NMR which mimics the physiological environment (Kay, 2005; Velyvis *et al*., 2007; Sugiki *et al*., 2017). Despite the wealth of experimental data obtained from X-ray crystallography and NMR, they have their own limitations. For example, nucleotide crystals do not necessarily reflect their functional conformations under physiological conditions. The irregular distribution of charge density of nucleic acids and the variation in their dynamic behaviour might affect their accurate structural determination by NMR methods (Ulyanov *et al*., 2006; Xia and Ren, 2013). Raman spectroscopy has been widely used for probing the chemical composition and the structure of various biomolecules, such as

nucleotides, nucleic acids and proteins (Barron *et al*., 2003). The technique can be also used to study the conformational changes associated with the binding of different ligands to enzymes (Kengne-Momo *et al*., 2012). Several studies illustrated the clinical applications of Raman spectroscopy in the *in vivo* detection of multiple pathological conditions affecting certain tissues and for the diagnosis of different tumors (Puppels, 2002; Wang *et al*., 2015; Gao *et al*., 2017).

The Raman technique is fast, non-invasive and highly sensitive for probing the structural changes of various compounds. The Raman spectra can be obtained from small volume of the sample and the method is suitable for studying molecules in aqueous environment as water provided weak Raman vibrations. Unlike X-ray crystallography and NMR, the Raman technique does not require further chemical modifications for the solvent or for the analyte and can be applied to study high molecular weight proteins (Fraser-Miller *et al*., 2016). Despite the advantages of the Raman spectroscopy, the method has some limitations, such as fluorescence which might arise from the analyte or from the impurities in the solution, and the destruction of some samples by the heat of the laser beam.

The absolute configuration of chiral biomolecules, such as DNA and amino acids and their dynamic features have been further investigated by applying a Raman-based technique known as Raman optical activity (ROA) (Blanch *et al*., 2002-2003). The ROA is a sensitive as well as non-invasive method which can provide detailed structural information on many molecules based on the small differences between right and left circulatory polarised light (Barron *et al*., 2003). The ROA was applied to probe the structural conformation of the sugar ring of different monosaccharides and the position of the surrounding hydroxyl groups in aqueous environment (Wen *et al*., 1993). The spectral markers that distinguish α-helix and β-sheets of human serum albumin and rabbit aldolase respectively were investigated using ROA spectroscopy (Barron *et al*., 2000). Therefore, combining Raman and ROA techniques can provide a great potential for investigating the structural characteristics of different molecules.

Despite the benefits of using the Raman and ROA as experimental tools for studying nucleotides, the application of computational methods, such as Density Functional Theory (DFT), can provide further insight about the assignment of particular vibrational modes. The DFT method is accurate, cost-effective and shown to be in agreement with the experimental measurements (Halls and Schlegel, 1999; Fairchild *et al*., 2009). Experimental Raman coupled with DFT calculations have been used by Paiva *et al*, (2017) to study D/L enantiomeric forms of valine and lysine amino acid crystals. The experimental results agreed with the theoretical simulations and showed detailed structural features and assignment of different vibrational modes of the racemic amino acids (Paiva *et al*., 2017). DFT was also used in combination with other spectroscopic techniques, such as infrared multiple photon dissociation spectroscopy (IRMPD) to investigate the molecular structure of the deprotonated form of adenosine 5'-diphosphate ([ADP–2H]-2) and adenosine 5'-triphosphate ([ATP–2H]-2) di-anions in gas phase (Schinle *et al*., 2013). The DFT simulation has been also applied with ^{1}H and ^{13}C NMR to provide further details about the structural features of cyclic uridine monophosphate in aqueous solution (Bango *et al*., 2008).

1.6 Raman and ROA spectroscopies: Overview, principles and instrumentation

1.6.1 Overview of the scattering phenomena

The interaction between photons of light with a target molecule can result in absorption or scattering of the incident photons. In some cases, the light does not react with the molecule and gets transmitted directly through it. Scattering occurs when a molecule absorbs a photon from the incident light. This photon transmits the molecule to a virtual state. The molecule then returns to its ground state and emits another photon with the same or different energy to the incident photon (Maher, 2010).

1.6.2 Principle of Raman spectroscopy

Raman scattering is considered as a vibrational spectroscopic technique that is used to detect the vibrational energy associated with the chemical bonds of the analyte (Smith and Dent, 2005). The technique relies on the inelastic scattering effect which results from the interaction between light of a given frequency and a molecule or a group of molecules. When a molecule is irradiated by a photon, the latter will change the polarisability of the electron cloud of the target molecule. As such, the distorted electrons will move to a higher energy (virtual state) at which, the molecule may have different electron geometry but its nuclei remain virtually unchanged. The new virtual state of the molecule is unstable and short lived and thus, the molecule will immediately return to its ground state and emits energy in the form of a second photon that might be scattered in any direction. The energy of the emitted photon depends on the energy of the incident light and the electronic properties of the molecule. Usually, the emitted photon will have the same amount of energy as contained in the incident photon; this is known as elastic or Rayleigh scattering. However, the second photon might be emitted with a different amount of energy producing a weak, approximately 10^{-5} of the incident radiation, such an emission is called the inelastic or Raman Scattering phenomenon (Ferraro *et al.*, 2003; Smith and Dent, 2005) (Figure 1.18).

The inelastic scattering photon can be emitted at different energy states: Stokes or anti-Stokes. The Stokes state is characterised by less energy compared to the incident photon and usually observed when the molecule is excited from its ground state. In contrast, the anti-Stokes photon has higher energy than the incident photon. This can occur because the molecule is already excited or in a high energy level (Figure 1.24). Observations from Raman spectroscopy indicate that Stokes scattering is more intense than the anti-Stokes (Hold *et al.*, 2005). This arises from the Boltzmann distribution of the vibrational states, which indicated that for typical conditions more molecules are found in ground state than in

excited states. Therefore, the Stokes lines are generally used in Raman measurements (Smith and Dent, 2005).

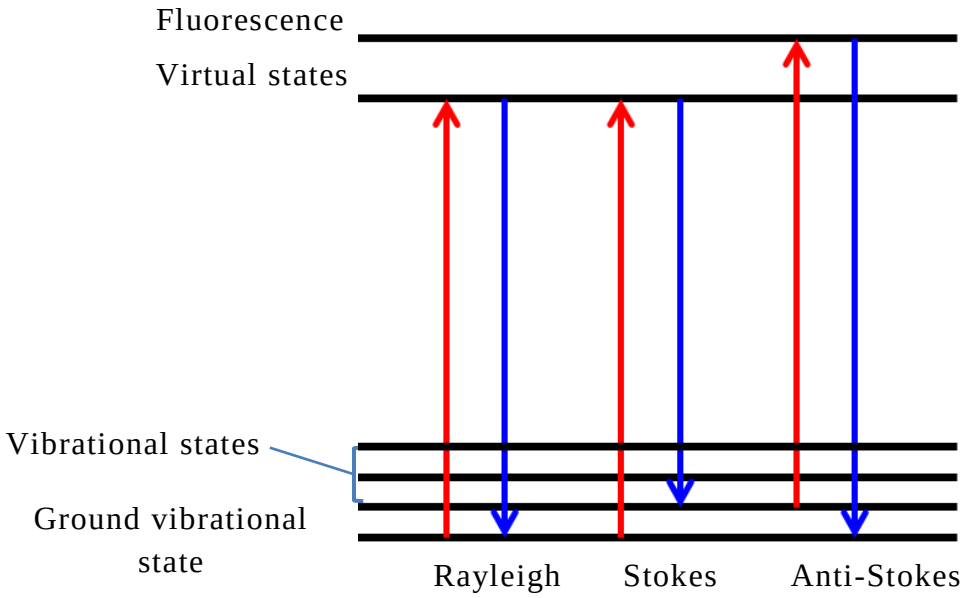

Figure 1.18. Energy level diagram describing the different states of Raman scattering. When the energy of the incident photon (red arrows) is similar to the energy of the scattered photon (blue arrows), this is called Rayleigh scattering. The energy of the scattered photons can be less than that of the incident photon, this is known as Stokes scattering. Sometimes, the molecule exists in excited state therefore; the energy of the scattered photon is higher than that of the incident photon, this is called anti-Stokes scattering. This illustration is adopted from (Smith and Dent, 2005).

The vibrations of a given molecule can be described by its normal modes as: (3N-5) for linear and (3N-6) for non-linear molecules, where N is the number of atoms in a single molecule. Water molecule, for example, has three normal modes while oxygen molecule (O_2) has only one normal mode of vibrations. , i.e., N = 3 for water, (3 x 3) - 6 = 3 modes. There are several types of molecular vibrations based on the bond type and the molecular structure. These vibrations can be categorised into: stretching vibrations and bending vibrations. The former is characterised by a change in the bond length and can be symmetric or asymmetric. The bending (or deformation) vibrations are characterised by a change in the angle of the bond and can be in-plane, (such as rocking and scissoring) or out-of-plane,

(such as wagging and twisting vibrations) (Smith and Dent, 2005) (Figure 1.19).

For polyatomic molecules, the vibrational modes become more complicated and might result in the formation of coupled or degenerate vibrations (Ferraro *et al*., 2003). For example, in some cases, certain atoms (groups) in a molecule might have similar vibrational frequency (energy). This causes some of their possible vibrations to be coupled (combined) and appeared as a single unique vibration, e.g., the acetone molecule, (CH_3–C=O–CH_3), contains two methyl groups that might have similar vibrational energy and thus, these groups are said to have: one asymmetric stretching vibration (Rather than two separate CH_3 asymmetric stretching vibrations) and one out-of-plane bending vibration (Rather than two separate CH_3 out-of-plane bending vibrations) (Popp and Reichenbacher, 2012).

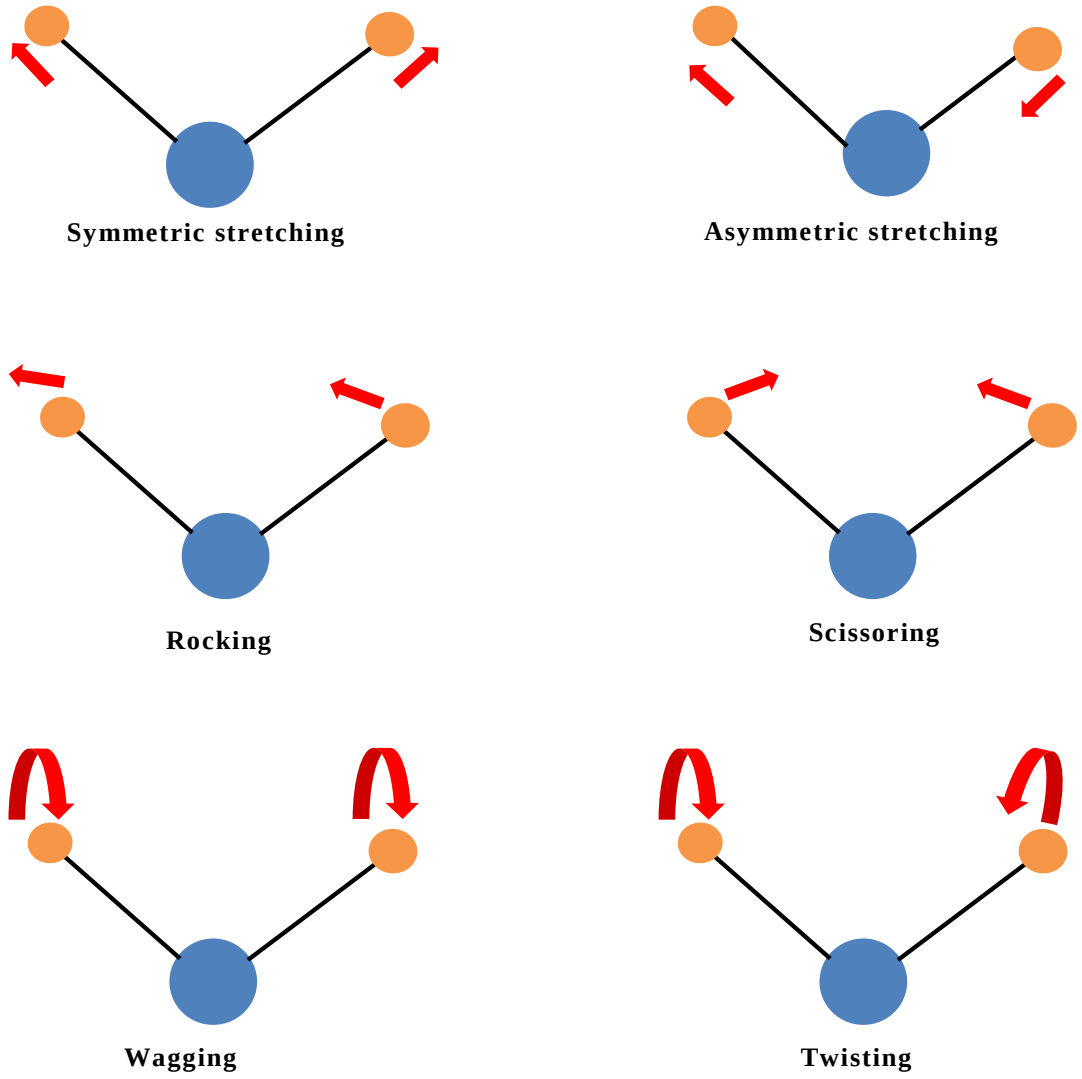

Figure 1.19. Spring and ball model illustrating different types of molecular vibrations. Stretching vibrations involve a change in the bond length and can be symmetric or asymmetric. Bending vibrations involves a change in the bond angles and can be in plane (rocking and scissoring) or out of plane (wagging and twisting). This illustration is adopted from (Ferraro *et al.*, 2003).

Raman and infra-red (IR) are considered as vibrational spectroscopic techniques as they both detect the change in the vibrational energy of the molecules (Smith and Dent, 2005). However, the mechanism of excitation is different. In the Raman method, as discussed earlier, the incident photon should change the polarizability of the molecule. However, in infrared spectroscopy the incident photon should change the dipole moment of the molecule. Therefore, some vibrational modes are Raman active but IR inactive and vice versa. Other vibrational modes can be active for both Raman and IR methods. For example, the symmetric starching of the CO_2 changes the polarisability of the molecule but does not change its dipole moment; as a result, it is Raman active and IR inactive. Another example is H_2O molecule which exists in three normal vibrational modes: symmetric, asymmetric and bending. All of these vibrational modes are Raman and IR active because they result in changes in the polarizability and the dipole moments of the molecule (Aroca, 2007).

1.6.3 Principle of Raman optical activity (ROA)

The phenomenon of Raman optical activity was first discovered by Atkins and Barron (Atkins and Barron, 1969). The authors demonstrated that the intensity of the Raman scattered light from a chiral molecule depends on the degree of circular polarization of the incident light and on the circular components of the scattered light. In 1971, Barron and Buckingham developed the ROA theory and introduced the dimensionless circular intensity difference (CID) which is described by equation (1):

$$\Delta = (IR - IL) / (IR + IL) \qquad (1)$$

Where Δ is (CID), IR and IL are the scattered intensities in right and left circulatory polarised light (Barron and Buckingham, 1971).

CID can be used as a more powerful experimental observable in measuring the difference in the intensities between the right and left polarised light with respect to the absolute Raman intensities obtained from different instruments.

In practice, ROA can be observed by applying one of two types of the incident beams: the incident circular polarisation (ICP-ROA) or the scattered circular polarisation (SCP-ROA). In (ICP-ROA), a circulatory polarised incident light (right and left) is applied then the difference in the light intensity is measured. Applying the SCP-ROA, which is used in this study, entails the use of the incident light with fixed polarisation following by detecting the intensities of the circulatory polarised light. The ICP-ROA or the SCP-ROA methods can be applied for collecting the backscattering ROA spectra. Both methods, nevertheless, can be used irrespective of the different design required for each method (Zhu *et al*., 2005).

1.6.4 Instrumentation

The Raman spectrometer is generally composed of four major parts: a laser source, optics, a monochromator, and a detector (Schrader, 2007). The availability of an intense and stable laser beam is important to irradiate the analyte at specific wavelength. Therefore, different laser sources are used in Raman spectrometers, e.g., Argon ion laser (488 and 514.5 nm), Helium–Neon diode laser (632.8 nm), Near Infrared (NIR) diode lasers (785 and 830 nm) and Neodymium–Yttrium Ortho-Vanadate (Nd:YVO4) diode laser (532 nm) (Bumbrah and Sharma, 2016). The Raman spectrometer comprises a group of optics, which are collection of lenses, used to direct the laser bream to the sample and collect the light scattered from it. Optimising the optics in the correct alignment increases the intensity of the Raman signal and enhances its quality especially for samples with low concentrations and samples examined in gaseous phase (Petrov *et al*., 2016). The monochromator is usually used with Rayleigh line filters, e.g., edge and notch filters to remove and separate the Rayleigh line from the Raman scattering radiation (Ferraro *et al*., 2003). Modern Raman spectrometers are equipped with highly sensitive charge-transfer device (CTD) detectors, in which the emitted photon from the sample strikes the silicon layer in the detector, and resulted in the generation of electric charges which are accumulated and measured. The amount of the generated charges is proportional to the number of photons

entered the detector (Sweedler, 1993). Common types of the CTD include charge-coupled device (CCD) and charge-injection device (CID) detectors (Skoog *et al.*, 2007).

For ROA measurements, the instrument is optimised in a backscattering geometry to enhance the detection of ROA signals (Blanch *et al.*, 2006). In ICP-ROA, the incident laser beam passes through an electro-optic modulator (EOM) to control the interchange of the left and the right circulatory polarised light states. The backscattering radiation emitted from the sample is then reflected off by 45°-mirror then passes through an edge filter to remove the Rayleigh line the transmitted to a group of optics which direct the beam to the CCD detector (Barron *et al.*, 2000) (Figure 1.20).

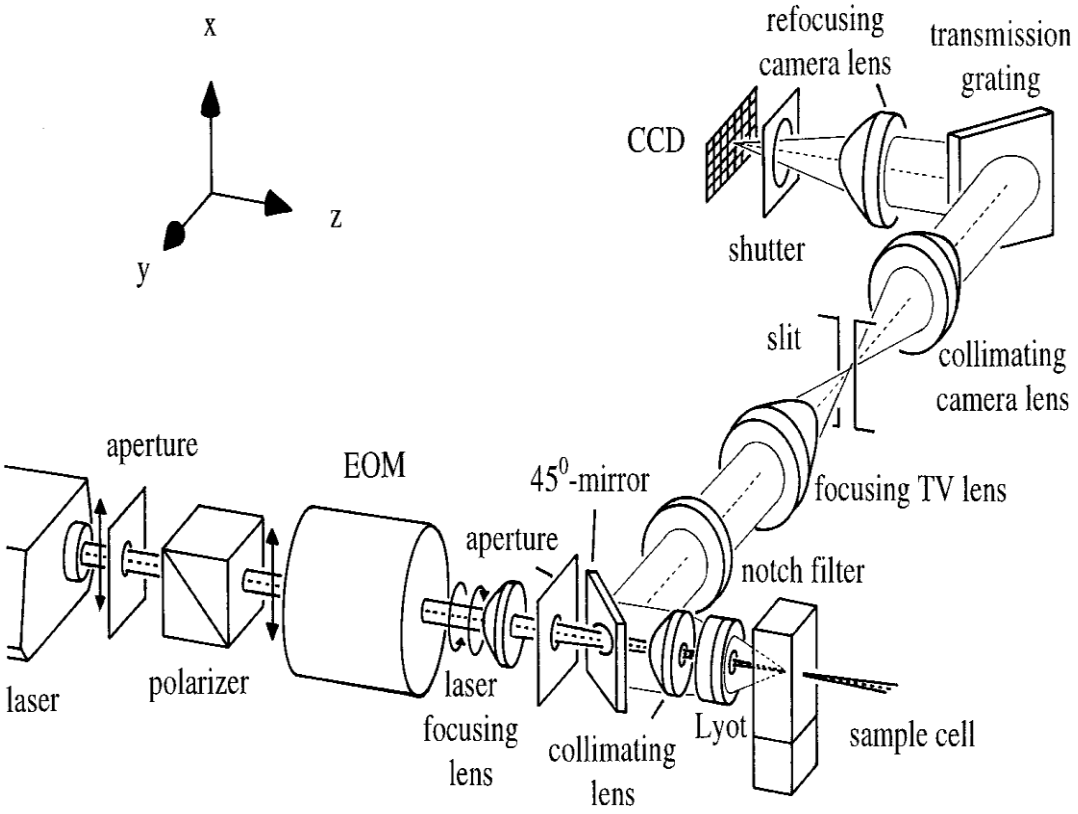

Figure 1.20. The ICP-ROA instrumentation. The instrument is optimised in backscattering geometry to improve ROA signals. The incident laser beam passes through a polariser to the electro-optic modulator (EOM) to control the interchange of the left and right circulatory polarised light states. The backscattered light from the sample reflected off by45°-mirror and passes to an edge filter to remove the Rayleigh radiation then directed by optics to the CCD detector. This illustration is adopted from (Blanch *et al.*, 2006).

1.7 The use of Raman and ROA spectroscopies for structural characterisation of nucleotides

Despite the discovery of the Raman phenomena in 1928 by the independent work of C. V. Raman and L. I. Mandelstam (Singh, 2002), the technique was considered as insensitive and time-consuming method. However, the development of fiber optics, multi-channel array detectors and enhanced data interpretation software enhances the sensitivity and improves the applicability of the Raman spectroscopy (Kim *et al*., 1993; Griffiths and de Haseth, 2007). The use of Raman methods for nucleotide characterisation began in 1967 when Lord and Thomas used Cary Model 81 Raman spectrometer to study the structure of different purine and pyrimidine nucleotides and their monophosphate derivatives in solid and liquid state at different pH environments (Lord and Thomas, 1967). Later on, Fanconi *et al*, (1969) demonstrated the Raman spectra of some monophosphate nucleotides, including 5'-AMP, 5'-GMP, 5'-CMP and 5'-UMP, and their polynucleotide counterparts (Fanconi *et al*., 1969). Rimai *et al*, (1969) explored the Raman spectra of 5'-AMP, 5'-ADP and 5'-ATP in liquid phase and investigated the spectral changes associated with the adenosine derivatives as a function of pH. Some of the phosphate related vibrations were assigned based on previous work on infrared spectra (Rimai *et al*., 1969). Medeiros and Thomas (1971) investigated the structure of inosine and inosine-5'-monophosphate in aqueous and deuterated solution (Medeiros and Thomas, 1971). The binding of different divalent cations such as, Ca^{2+}, Mg^{2+}, CO^{2+}, Cu^{2+}, and Hg^{2+} to ATP at different pH environments was examined by Lanir and Yu (1979). The work identified different metal-ATP binding sites based on the change in the protonation and deprotonation states of the nitrogenous base and the phosphate chain (Lanir and Yu, 1979). Carmona *et al*., (1988) applied the Raman spectroscopy to assess the interaction of copper ions with AMP and GMP nucleotides in solution. The study revealed the binding of the nucleotide phosphate groups with the copper ions (Carmona *et al*., 1988). As the Raman technique becomes more desirable in the investigating the structural changes of various molecules, Kopecky *et al*, (2002) compared

the ionisation states of the antiviral nucleotide analogue 9-[2-(Phosphonomethoxy) ethyl] adenine (PMEA) with their natural adenosines (5′-AMP, 3′-AMP, and 2′-AMP) at different pH values in order to observe the impact of protonation/deprotonation on the binding sites and the PK_a values of the antiviral drug (Kopecky *et al*., 2002). In 2012, Ostovarpour and Blanch, (2012) conducted the first study that combined Raman and ROA measurement for examining the structure of different adenosine derivatives and the influence of phosphorylation on their Raman and ROA profiles. The study identified certain Raman marker bands and reported the high sensitivity of ROA method for the structural changes associated with the adenosine derivatives (Ostovarpour and Blanch, 2012). The previously illustrated studied reflect the growing interest for using the Raman and ROA as a tools for structural analysis and clinical diagnosis. Despite the structural information gathered from Raman and ROA, the techniques are still in their early stages compared to x-ray and NMR methods. There is a need to establish a comprehensive experimental and computational Raman studies for various biomolecules and their interactions.

1.8 The use of Raman and ROA spectroscopies for structural characterisation of proteins

Early applications of Raman spectroscopy in determining protein structures were carried out in the late 1960s and aimed to examine the Raman profile of α-helical poly-L-alanine chain (Fanconi *et al*., 1969; Koenig and Sutton, 1969). Fanconi *et al*, (1969) identified the Raman vibrations for poly-L-alanine in fibres after irradiating the sample with laser beam for an hour to eliminate fluorescence. Moreover, Koenig and Sutton, (1969) presented the Raman spectrum of poly-L-alanine in aqueous solution and compared their results with infrared (IR) measurements reported in an earlier study by Miyazawa and Blout, (1961) (Miyazawa and Blout, 1961). Interestingly, Koenig and Sutton,(1969) determined six major amide regions in the Raman profile of the poly-L-alanine and analysed their related frequencies. A year later, Lord and Yu, (1970) conducted a Raman experiment on the lysozyme and identified its

constituent amino acids in solution, where the authors identified characteristic Raman bands at 1660 and 1150 cm^{-1} which corresponded to the Amide I and the Amide III regions respectively (Lord and Yu, 1970).

The use of Raman and Raman-based techniques, such UV resonance Raman spectroscopy (UVRR), for probing the structural properties of proteins has extended and involved a wide range of biologically important polypeptides, for example, haemoglobin (Bangcharoenpaurpong *et al.*, 1984), albumin (Dingari *et al.*, 2012), cytochrome c (Okada *et al.*, 2012) and globulin (Artemyev *et al.*, 2016)

Kinalwa *et al*, (2010) investigated the secondary structure of different proteins using Raman spectroscopy. In this study, the Amide I, II and III regions were considered as key markers for distinguishing α- helices, β-sheets and other forms of the protein secondary structure (Kinalwa *et al.*, 2010). Rygula *et al*, (2013) used different excitation wavelengths and reported the Raman spectra of 26 proteins (Rygula *et al.*, 2013).

The influence of post-translational modifications such as glycosylation and metal binding, of some polypeptides were analysed by Ashton *et al*, (2017) using a combination of Raman spectroscopy and chemometric methods. The study identified, the influence of glycosylation and iron binding on the structures of the apo- and holo- forms of the transferrin. The authors then applied a quantitative analytical approach to detect glycosylation in a mixture of glycosylated and non-glycosylated transferrin (Ashton *et al.*, 2017).

Surface enhance Raman scattering (SERS), a Raman based technique used to enhance the Raman signals by adsorbing the analyte to a synthesised nanoparticles, was used as a tool for the detection of tumor marker proteins, such as α-fetoprotein (AFP) and carcinoembryonic antigen (CEA) (Wang *et al.*, 2013; Song *et al.*, 2017).

ROA spectroscopy provides rich structural information for the secondary and tertiary structure of polypeptides. The technique is also applicable for identifying different conformations and probing the folding/non-folding

states of different proteins in aqueous solution (Matousek and Morris, 2010). Unlike conventional Raman spectroscopy, ROA spectra reflected signals originate mainly from the backbone of the polypeptide chain while the side chains provided less dominant vibrations (Barron *et al*., 2000). Therefore, the ROA method features higher sensitivity in identifying the small structural modifications and the dynamic properties of many proteins in aqueous environment. Blanch *et al*, (2000) applied ROA measurement for studying the structure of equine and hen lysozyme in addition to the calcium bound bovine α-lactoalbumin (Blanch *et al*., 2000).The secondary structure of different polypeptides and proteins including poly (L-lysine), human serum albumin, human immunoglobulin G, bovine ribonuclease A and bovine β-casein was investigated in aqueous phase by ROA spectroscopy (Zhu *et al*., 2006).The above mentioned studies showed the growing interest for applying Raman and ROA methods as powerful tools to investigating the structural features and the dynamics of certain proteins and their interactions.

It is worth noting that the most important Raman vibrations for polypeptides can be defined by: The backbone skeletal stretch region, Amide A and B regions and Amide I-VII. The former region is usually observed at ~870–1150 cm^{-1} and originates mainly from Cα–C, Cα–Cβ and C-N stretching vibrations (Blanch *et al*., 2000). Amide A and B regions are observed at 3500 and 3100 cm^{-1} respectively and arise specifically from NH group vibrations. Therefore, these regions not affected by the structural changes of the protein (Barth, 2007). Amide I to VII are mainly observed at: (I: 1600–1690 cm^{-1}, II: 1480–1580 cm^{-1}, III: 1230–1300 cm^{-1}, IV: 625–770 cm^{-1}, V: 640–800 cm^{-1}, VI: 540–600 cm^{-1}, and VII: 200 cm^{-1}) (Rygula *et al*., 2013). Unlike amide A and B, Amide I-III are sensitive to the alterations of the polypeptide secondary structures; therefore, they are widely used as diagnostic markers for protein structural analysis (Barth, 2007).

1.9 Research aim and objectives

It is well known that nucleotides participate in a wide variety of biochemical processes. Phosphorylation is one of the most common biological reactions. In many phosphorylation reactions, a phosphoryl group is transferred from a nucleotide to the target substrate. Often this occurs via the action of kinases, such as phosphoglycerate kinase (PGK), where ATP is used to deliver the phosphoryl group. During phosphorylation, magnesium ions bind to the nucleotide, which can cause significant conformational alterations in the nucleotide, in the enzyme (such as in PGK) or in the substrate. The structure of nucleotide-Mg complexes in solution and the mode of coordination of the metal ion by the phosphate oxygen atoms remain controversial.

The PGK enzyme requires the purine nucleotides, such as adenosines (ATP/ADP) as phosphate donors. Guanosine nucleotides (GTP/GDP), in addition, are also used by other enzymes, such as G-proteins for several phosphoryl transfer reactions. As this study focuses mainly on phosphorylation reactions, the light was shed on purine rather than pyrimidine nucleotides. Therefore, this project aims to:

- Apply Raman spectroscopy, coupled with using Density Functional Theory (DFT) models to assign the vibrational spectra, to characterise purine nucleosides (adenosines and guanosines) and their nucleotide derivatives.
- Investigate the influence of magnesium binding on the spectral profile of adenosine and guanosine mono-, di-and tri- phosphates in aqueous solution, including as a function of pH.
- Explore the Raman profile of the human phosphoglycerate kinase (hPGK) in its open conformation, when no ligands are bound, and in its fully closed conformation, when ADP, 3-phosphoglycerate and a metal fluoride mimic of the transferring phosphoryl group are all bound in a transition state analogue arrangement. The influence of conformational changes on the amide I and amide III regions of the enzyme spectrum were investigated using uniform isotopic substitution of nitrogen atoms with ^{15}N (^{15}N-hPGK).

1.10 References

Acharya, P., Cheruku, P., Chatterjee, S., Acharya, S. and Chattopadhyaya, J. (2004). 'Measurement of nucleobase pK_a values in model mononucleotides shows RNA-RNA duplexes to be more stable than DNA-DNA duplexes', *Journal of the American Chemical Society,* 126(9)**,**pp. 2862-2869.

Adams, B. and Pain, R. H. (1986). 'The effect of substrates on the inter-domain interactions of the hinge-bending enzyme 3-phosphoglycerate kinase', *FEBS Letters,* 196(2)**,**pp. 361-364.

Ahalawat, N. and Murarka, R. K. (2017). 'Molecular mechanism of nucleotide-dependent allosteric Regulation in AMP-Activated Protein Kinase', *The Journal of Physical Chemistry B,* 121(14)**,**pp. 2919-2930.

Alberts, B., Johnson, A., Lewis, J., Raff, M., Roberts, K. and Walter, P. (2008). *Molecular biology of the cell.* 5th edn. USA: Garland Science and Taylor and Francis Group.

Altona, C. and Sundaralingam, M. (1972). 'Conformational analysis of the sugar ring in nucleosides and nucleotides. New description using the concept of pseudorotation', *Journal of the American Chemical Society,* 94(23)**,**pp. 8205-8212.

Aroca, R. (2007). Theory of molecular vibrations. The origin of infrared and Raman spectra, in Ricardo,A.(ed.) *Surface-enhanced vibrational spectroscopy.* John Wiley and Sons, Ltd,pp.1-33.

Artemyev, D. N., Bratchenko, I. A., Khristoforova, Y. A., Lykina, A. A., Myakinin, O. O., Kuzmina, T. P., Davydkin, I. L. and Zakharov, V. P. (2016). 'Blood proteins analysis by Raman spectroscopy method'. *Proceedings of SPIE, Biophotonics: Photonic Solutions for Better Health Care V,* 9887,pp. 98871Y-1-98871Y-8.

Ashton, L., Brewster, V. L., Correa, E. and Goodacre, R. (2017). 'Detection of glycosylation and iron-binding protein modifications using Raman spectroscopy', *Analyst,* 142(5)**,**pp. 808-814.

Atkins, P. W. and Barron, L. D. (1969). 'Rayleigh scattering of polarized photons by molecules', *Molecular Physics,* 16(5)**,**pp. 453-466.

Auerbach, G., Huber, R., Grattinger, M., Zaiss, K., Schurig, H., Jaenicke, R. and Jacob, U. (1997). 'Closed structure of phosphoglycerate kinase from Thermotoga maritima reveals the catalytic mechanism and determinants of thermal stability', *Structure,* 5(11)**,**pp. 1475-1483.

Balog, E., Laberge, M. and Fidy, J. (2007). 'The influence of interdomain interactions on the intradomain motions in yeast phosphoglycerate kinase: A molecular dynamics study', *Biophysical Journal,* 92(5)**,**pp. 1709-1716.

Bangcharoenpaurpong, O., Schomacker, K. T. and Champion, P. M. (1984). 'Resonance Raman investigation of myoglobin and hemoglobin', *Journal of the American Chemical Society,* 106(19)**,**pp. 5688-5698.

Bango, A., Rastrelli, F. and Saielli, G. (2008). 'Predicting the NMR spectra of nucleotidesby DFT calculations: cyclic uridinemonophosphate', *Magnetic Resonance in Chemistry,* 46**,**pp. 518-524.

Barron, L. D., Blanch, E. W., McColl, I. H., Syme, C. D., Hecht, L. and Nielsen, K. (2003). 'Structure and Behaviour of Proteins, nucleic acids and viruses from vibrational Raman optical activity', *Spectroscopy,* 17(2-3),pp. 101-126.

Barron, L. D. and Buckingham, A. D. (1971). 'Rayleigh and Raman scattering from optically active molecules', *Molecular Physics*, 20(6)**,**pp. 1111-1119.

Barron, L. D., Hecht, L., Blanch, E. W. and Bell, A. F. (2000). 'Solution structure and dynamics of biomolecules from Raman optical activity', *Progress in Biophysics and Molecular Biology*, 73(1)**,**pp. 1-49.

Barth, A. (2007). 'Infrared spectroscopy of proteins', *Biochimica et Biophysica Acta (BBA) - Bioenergetics*, 1767(9)**,**pp. 1073-1101.

Bernstein, B. E., Michels, P. A. and Hol, W. G. (1997). 'Synergistic effects of substrate-induced conformational changes in phosphoglycerate kinase activation', *Nature*, 385(6613)**,**pp. 275-278.

Beste-Kerstin, Y. and Seifert, R. (2013). cCMP, cUMP, cTMP, cIMP and cXMP as possible second messengers: Development of a hypothesis based on studies with soluble guanylyl cyclase α1β1. *Biological Chemistry*.394(2),pp. 261-270.

Birnbaumer, L. and Zurita, A. R. (2010). 'On the roles of Mg in the activation of G proteins', *Journal of Receptors and Signal Transduction Research*, 30(6)**,**pp. 372-375.

Blackburn, G. M., Gait, M. J., Loakes, D. and Williams, D. M. (2006). *Nucleic acids in chemistry and biology*. 3rd edn. Cambridge: The Royal Sociaty of Chemistry.

Blake, C. (1997). 'Phosphotransfer hinges in PGK', *Nature*, 385**,**pp. 204-205.

Blake, C. C. F. and Evans, P. R. (1974). 'Structure of horse muscle phosphoglycerate kinase: Some results on the chain conformation, substrate binding and evolution of the molecule from a 3 Å Fourier map', *Journal of Molecular Biology*, 84(4)**,**pp. 585-601.

Blake, C.C.F.and Rice, D. W. (1981). 'Phosphoglycerate kinase', *Philosophical Transactions of the Royal Society of London B: Biological Sciences*, 293(1063)**,**pp. 93-104.

Blanch, E. W., Hecht, L. and Barron, L. D. (2003). 'Vibrational Raman optical activity of proteins, nucleic acids, and viruses', *Methods*, 29(2)**,**pp. 196-209.

Blanch, E. W., Hecht, L. and Barron, L. D. (2006). Raman optical activity, in Kenneth, B and Marianna,B.(eds.) *Chiral Analysis*. Texas: Elsevier Science,pp. 545-594.

Blanch, E. W., Hecht, L., Syme, C. D., Volpetti, V., Lomonossoff, G. P., Nielsen, K. and Barron, L. D. (2002). 'Molecular structures of viruses from Raman optical activity', *Journal of General Virology* , 83**,**pp. 2593-600.

Blanch, E. W., Morozova-Roche, L. A., Hecht, L., Noppe, W. and Barron, L. D. (2000). 'Raman optical activity characterization of native and molten globule states of equine lysozyme: Comparison with hen lysozyme and bovine α-lactalbumin', *Biopolymers*, 57(4)**,**pp. 235-248.

Brito-Arias, M. (2016). *Synthesis and Characterization of Glycosides*.2nd edn. *Springer International Publishing*[Online]. Available at: http://www.springer.com.

Bueno, J., Torres, M., Almendros, A., Carmona, R., Nunez, M. C., Rios, A. and Gil, A. (1994). 'Effect of dietary nucleotides on small intestinal repair after diarrhoea. Histological and ultrastructural changes', *Gut*, 35(7)**,**pp. 926-933.

Bugaev, A. L., Guda, A. A., Yefanov, O. M., Lorenz, U., Soldatov, A. V. and Vartanyants, I. A. (2016). 'X-ray absorption spectroscopy and coherent X-ray diffraction imaging for time-resolved investigation of the biological

complexes: Computer Modelling towards the XFEL experiment', *Journal of Physics: Conference Series,* 712(1)**,**pp. 1-4.

Bumbrah, G. S. and Sharma, R. M. (2016). 'Raman spectroscopy – Basic principle, instrumentation and selected applications for the characterization of drugs of abuse', *Egyptian Journal of Forensic Sciences,* 6(3)**,**pp. 209-215.

Carmona, P., Huong, P. V. and Gredilla, E. (1988). 'Raman spectra and binding of CuII to purine nucleotides', *Journal of Raman Spectroscopy,* 19(5)**,**pp.315-319.

Carver, J. D., Pimentel, B., Cox, W. I. and Barness, L. A. (1991). 'Dietary nucleotide effects upon immune function in infants', *Pediatrics,* 88(2)**,**pp. 359-363.

Carver, J. D. and Walker, A. W. (1995). 'The role of nucleotides in human nutrition', *The Journal of Nutritional Biochemistry,* 6(2)**,**pp. 58-72.

Chen, J., McAllister, M. A., Lee, J. K. and Houk, K. N. (1998). 'Short, strong hydrogen bonds in the gas phase and in solution: Theoretical exploration of pK_a matching and environmental effects on the strengths of hydrogen bonds and their potential roles in enzymatic catalysis', *The Journal of Organic Chemistry,* 63(14)**,**pp. 4611-4619.

Claire, S. (2001). *Nucleoside mimetics their chemistry and biological properties*. Amesterdam: Gordon and Breach Science Publishers.

Clay, M. C., Ganser, L. R., Merriman, D. K. and Al-Hashimi, H. M. (2017). 'Resolving sugar puckers in RNA excited states exposes slow modes of repuckering dynamics', *Nucleic Acids Research,* 45(14),pp. 1-11.

Cliff, M. J., Bowler, M. W., Varga, A., Marston, J. P., Szabo, J., Hounslow, A. M., Baxter, N. J., Blackburn, G. M., Vas, M. and Waltho, J. P. (2010). 'Transition State Analogue Structures of Human Phosphoglycerate Kinase Establish the Importance of Charge Balance in Catalysis', *Journal of the American Chemical Society,* 132(18)**,**pp. 6507-6516.

Corvetta, A., Della Bitta, R., Luchetti, M. M. and Pomponio, G. (1991). '5-Methylcytosine content of DNA in blood, synovial mononuclear cells and synovial tissue from patients affected by autoimmune rheumatic diseases', *Journal of Chromatography,* 566(2)**,**pp. 481-491.

Danshina, P. V., Geyer, C. B., Dai, Q., Goulding, E. H., Willis, W. D., Kitto, G. B., McCarrey, J. R., Eddy, E. M. and O'Brien, D. A. (2010). 'Phosphoglycerate Kinase 2 (PGK2) is essential for sperm function and male fertility in mice', *Biology of Reproduction,* 82(1)**,**pp. 136-145.

Davies, D. B. (1978). 'Conformations of nucleosides and nucleotides', *Progress in Nuclear Magnetic Resonance Spectroscopy,* 12(3)**,**pp. 135-225.

de Crecy-Lagard, V., Brochier-Armanet, C., Urbonavicius, J., Fernandez, B., Phillips, G., Lyons, B., Noma, A., Alvarez, S., Droogmans, L., Armengaud, J. and Grosjean, H. (2010). 'Biosynthesis of wyosine derivatives in tRNA: an ancient and highly diverse pathway in Archaea', *Molecular biology and evolution,* 27(9)**,**pp. 2062-2077.

Delbaere,L.T.J.,Sudom,A.M.,Prasad,L., Leduc, Y. and Goldie, H. (2004). 'Structure/function studies of phosphoryl transfer by phosphoenolpyruvate carboxykinase', *Biochimica et Biophysica Acta (BBA) - Proteins and Proteomics,* 1697(1)**,**pp. 271-278.

Dingari, N. C., Horowitz, G. L., Kang, J. W., Dasari, R. R. and Barman, I. (2012). 'Raman spectroscopy provides a powerful diagnostic tool for ccurate determination of albumin glycation', *PLoS One,* 7(2)**,**pp.1-11.

Eric, A.V. and Dennis, D. A. (2005). *Modern physical organic chemistry*.California: University Science Books.

Evich, M., Spring-Connell Alexander, M. and Germann Markus, W. (2017). Impact of modified ribose sugars on nucleic acid conformation and function. *Heterocyclic Communications*,23(3),pp.155-165.

Fairchild, S. Z., Bradshaw, C. F., Su, W. and Guharay, S. K. (2009). 'Predicting Raman spectra using density functional theory', *Applied Spectroscopy*, 63(7)**,**pp. 733-41.

Fanconi, B., Tomlinson, B., Nafie, L. A., Small, W. and Peticolas, W. L. (1969). 'Polarized laser Raman studies of biological polymers', *Journal of Chemical Physics*, 51(9)**,**pp. 3993-4005.

Farias, P. A. M. and Castro, A. A. (2014). 'Determination of xanthine in the presence of hypoxanthine by adsorptive stripping voltammetry at the mercury film electrode', *Analytical Chemistry Insights*, 9**,**pp. 49-55.

Ferraro, J. R., Nakamoto, K. and Brown, C. W. (2003). *Introductory Raman Spectroscopy*.2nd edn.San Diego: Academic Press.

Fraser-Miller, S. J., Saarinen, J. and Strachan, C. J. (2016). Vibrational spectroscopic imaging, In Mullertz, A., Perrie,Y., and Rades,T.(eds.) *Analytical Techniques in the Pharmaceutical Sciences.* New York: Springer New York,pp. 523-589.

Gabba, M., Poblete, S., Rosenkranz, T., Katranidis, A., Kempe, D., Zuchner, T., Winkler, Roland G., Gompper, G. and Fitter, J. (2014). 'Conformational state distributions and catalytically relevant dynamics of a hinge-bending enzyme studied by single-molecule FRET and a coarse-grained simulation', *Biophysical Journal*, 107(8)**,**pp. 1913-1923.

Gacs-Baitz,E., Kajtar-Peredy, M. and Sagi, G. (2004). 'NMR study of some diastereomeric nucleoside-3′-thiophosphate derivatives in solution', *Analytical and Bioanalytical Chemistry*, 379(1)**,**pp. 56-59.

Gao, P., Han, B., Du, Y., Zhao, G., Yu, Z., Xu, W., Zheng, C. and Fan, Z. (2017). 'The clinical application of Raman spectroscopy for breast cancer detection', *Journal of Spectroscopy*, 2017**,**pp. 1-10.

Gollnest, T., Dinis de Oliveira, T., Rath, A., Hauber, I., Schols, D., Balzarini, J. and Meier, C. (2016). 'Membrane-permeable triphosphate prodrugs of nucleoside analogues', *Angewandte Chemi International Edition in English*, 55(17)**,**pp. 5255-5258.

Graham, H. C. and Williams, R. J. P. (1991). 'The roles of ADP^{2-} and Mg^{2+} in control steps of phosphoglycerate kinase', *European Journal of Biochemistry*, 197(1)**,**pp. 81-91.

Griffiths, P. R. and de Haseth, J. A. (2007). *Frontmatter, in fourier transform infrared spectrometry.* 2nd edn. USA: John Wiley and Sons, Inc.

Halls, M. D. and Schlegel, H. B. (1999). 'Comparison study of the prediction of Raman intensities using electronic structure methods', *The journal of chemical physics*, 111(19)**,**pp. 8819-8824.

Hanrahan, J. R. and Hutchinson, D. W. (1992). 'The enzymatic synthesis of antiviral agents', *Journal of Biotechnology*, 23(2)**,**pp. 193-210.

Hengge, R., Gründling, A., Jenal, U., Ryan, R. and Yildiz, F. (2016). 'Bacterial signal transduction by cyclic di-GMP and other nucleotide second messengers', *Journal of Bacteriology*, 198(1)**,**pp. 15-26.

Hess, J. R. and Greenberg, N. A. (2012). 'The Role of nucleotides in the immune and gastrointestinal systems:Potential clinical applications', *Nutrition in Clinical Practice*, 27(2)**,**pp. 281-294.

Hold, K. E., Johnson, W. and HO, P. S. (2005). *Principles of physical biochemistry.* 2nd edn. USA: Prentice Hall.

Huang, I. Y., Fujii, H. and Yoshida, A. (1980). 'Structure and function of normal and variant human phosphoglycerate kinase', *Hemoglobin,* 4(5-6)**,**pp. 601-609.

Huse, M. and Kuriyan, J. (2002). 'The conformational plasticity of protein kinases', *Cell,* 109(3)**,**pp. 275-282.

Jeremy, B. M., John, T. L. and Lubert, S. (2015). *Biochemistry.*8th edn. New York: W. H. Freeman and Company

Jin, M. B., Yamaguchi, T., Shimahara, Y., Ichimiya, M., Kinoshita, K., Oka, T., Ozawa, K. and Yamaoka, Y. (1996). 'Significance of nucleosides and a nucleotide mixture infusion on hepatic energy metabolism of 70% hepatectomized rabbits in postoperative phase', *Journal of Parenteral and Enteral Nutrition,* 20(3)**,**pp. 211-214.

Joao, H. C. and Williams, R. J. P. (1993). 'The anatomy of a kinase and the control of phosphate transfer', *European Journal of Biochemistry,* 216(1)**,**pp. 1-18.

Jordheim, L. P., Durantel, D., Zoulim, F. and Dumontet, C. (2013). 'Advances in the development of nucleoside and nucleotide analogues for cancer and viral diseases', *Nature Reviews Drug Discovery,* 12(6)**,**pp. 447-464.

Kay, L. E. (2005). 'NMR studies of protein structure and dynamics', *Journal of Magnetic Resonance,* 173(2)**,**pp. 193-207.

Kengne-Momo, R. P., Daniel, P., Lagarde, F., Jeyachandran, Y. L., Pilard, J. F., Durand-Thouand, M. J. and Thouand, G. (2012). 'Protein interactions investigated by the Raman spectroscopy for biosensor applications', *International Journal of Spectroscopy,* 2012**,**pp. 1-7.

Kim, Jeong J., Lorenz, R., Arold, Stefan T., Reger, Albert S., Sankaran, B., Casteel, Darren E., Herberg, Friedrich W. and Kim, C. (2016). 'Crystal structure of PKG I:cGMP complex reveals a cGMP-mediated dimeric interface that facilitates cGMP-induced activation', *Structure,* 24(5)**,**pp. 710-720.

Kim, M., Owen, H. and Carey, P.R. (1993). 'High-performance Raman spectroscopic system based on a single spectrograph, CCD, notch filters, and a Kr^+ laser ranging from the near-IR to near-UV regions', *Applied Spectroscopy,* 47(11)**,**pp. 1780-1783.

Kinalwa, M. N., Blanch, E. W. and Doig, A. J. (2010). 'Accurate determination of protein secondary structure content from Raman and Raman optical activity spectra', *Analytical Chemistry,* 82(15)**,**pp. 6347-6349.

Koenig, J. L. and Sutton, P. L. (1969). 'Raman spectrum of the right-handed α-helix of poly-L-alanine', *Biopolymers,* 8(2)**,**pp. 167-171.

Kopecky, V., Jr., Mojzes, P., Burda, J. V. and Dostal, L. (2002). 'Raman spectroscopy study of acid-base and structural properties of 9-[2-(phosphonomethoxy)ethyl]adenine in aqueous solutions', *Biopolymers,* 67(4-5)**,**pp. 285-288.

Kroeze, W. K., Sheffler, D. J. and Roth, B. L. (2003). 'G-protein-coupled receptors at a glance', *Journal of Cell Science,* 116(24)**,**pp. 4867-4869.

Kumar, S., Ma, B., Tsai, C. J., Wolfson, H. and Nussinov, R. (1999). 'Folding funnels and conformational transitions via hinge-bending motions', *Cell Biochem Biophys,* 31(2)**,**pp. 141-164.

Kunfermann, A., Witschel, M., Illarionov, B., Martin, R., Rottmann, M., Hoffken, H. W., Seet, M., Eisenreich, W., Knolker, H. J., Fischer, M., Bacher, A., Groll, M. and Diederich, F. (2014). 'Pseudilins: halogenated, allosteric inhibitors of

the non-mevalonate pathway enzyme IspD', *Angewandte Chemi International Edition in English,*, 53(8)**,**pp. 2235-2239.

Lallemand, P., Chaloin, L., Roy, B., Barman, T., Bowler, M. W. and Lionne, C. (2011). 'Interaction of human 3-phosphoglycerate kinase with its two substrates: Is substrate antagonism a kinetic advantage?', *Journal of Molecular Biology,* 409(5)**,**pp. 742-757.

Lane, A. N. and Fan, T. W. M. (2015). 'Regulation of mammalian nucleotide metabolism and biosynthesis', *Nucleic Acids Research,* 43(4)**,**pp. 2466-2485.

Lanir, A. and Yu, N. T. (1979). 'Raman-spectroscopic study of the interaction of divalent metal-ions with adenine moiety of adenosine 5'-triphosphate', *Journal of Biological Chemistry,* 254(13)**,**pp. 5882-5887.

Lee, J. H., Im, Y. J., Bae, J., Kim, D., Kim, M.-K., Kang, G. B., Lee, D.S. and Eom, S. H. (2006). 'Crystal structure of Thermus caldophilus phosphoglycerate kinase in the open conformation', *Biochemical and Biophysical Research Communications,* 350(4)**,**pp. 1044-1049.

Li, D., Fedeles, B. I., Singh, V., Peng, C. S., Silvestre, K. J., Simi, A. K., Simpson, J. H., Tokmakoff, A. and Essigmann, J. M. (2014). 'Tautomerism provides a molecular explanation for the mutagenic properties of the anti-HIV nucleoside 5-aza-5,6-dihydro-2'-deoxycytidine', *Proceedings of the National Academy of Science of the U S A,* 111(32)**,**pp. E3252-E3259.

Lord, R. C. and Thomas, G. J. (1967). 'Raman spectral studies of nucleic acids and related molecules—I ribonucleic acid derivatives', *Spectrochimica Acta Part A: Molecular Spectroscopy,* 23(9)**,**pp. 2551-2591.

Lord, R. C. and Yu, N.t. (1970). 'Laser-excited Raman spectroscopy of biomolecules: I. Native lysozyme and its constituent amino acids', *Journal of Molecular Biology,* 50(2)**,**pp. 509-524.

Lunn, F. A., MacDonnell, J. E. and Bearne, S. L. (2008). 'Structural requirements for the activation of *Escherichia coli* CTP synthase by the allosteric effector GTP are stringent, but requirements for inhibition are lax', *Journal of Biological Chemistry,* 283(4)**,**pp. 2010-2020.

Maher, S. A. (2010). *Raman Spectroscopy, fullerenes and nanotechnology*.Cambridge: The Royal Society of Chemistry.

Mahmoudian, M., Rudd, B. A. M., Cox, B., Drake, C. S., Hall, R. M., Stead, P., Dawson, M. J., Chandler, M., Livermore, D. G., Turner, N. J. and Jenkins, G. (1998). 'A versatile procedure for the generation of nucleoside 5′-carboxylic acids using nucleoside oxidase', *Tetrahedron,* 54(28)**,**pp. 8171-8182.

Manning, G., Whyte, D. B., Martinez, R., Hunter, T. and Sudarsanam, S. (2002). 'The protein kinase complement of the human genome', *Science,* 298(5600)**,**pp. 1912-1934.

Matousek, P. and Morris, M. D. (2010). *Emerging Raman applications and techniques in biomedical and pharmaceutical fields*. USA: Springer Berlin Heidelberg.

Matte, A., Tari, L. W. and Delbaere, L. T. (1998). 'How do kinases transfer phosphoryl groups?', *Structure,* 6(4)**,**pp. 413-419.

Mauro, C. D., Pesapane, A., Formisano, L., Rosa, R., D'Amato, V., Ciciola, P., Servetto, A., Marciano, R., Orsini, R. C., Monteleone, F., Zambrano, N., Fontanini, G., Servadio, A., Pignataro, G., Grumetto, L., Lavecchia, A., Bruzzese, D., Iaccarino, A., Troncone, G., Veneziani, B. M., Montuori, N., Placido, S. D. and Bianco, R. (2017). 'Urokinase-type plasminogen activator

receptor (uPAR) expression enhances invasion and metastasis in RAS mutated tumors', *Scientific Reports,* 7(1)**,**pp. 1-12.

Medeiros, G. C. and Thomas, G. J. (1971). 'Raman studies of nucleic acids IV: Vibrational spectra and associative interactions of aqueous inosine derivatives', *Biochimica et Biophysica Acta (BBA) - Nucleic Acids and Protein Synthesis,* 247(3)**,**pp. 449-462.

Mihaylova, M. M. and Shaw, R. J. (2011). 'The AMP-activated protein kinase (AMPK) signaling pathway coordinates cell growth, autophagy, and metabolism', *Nature cell biology,* 13(9)**,**pp. 1016-1023.

Miyazawa, T. and Blout, E. R. (1961). 'The Infrared spectra of polypeptides in various conformations: Amide I and II bands', *Journal of the American Chemical Society,* 83(3)**,**pp. 712-719.

Moss, G. P., Smith, P. A. S. and Tavernier, D. (1995). 'Glossary of class names of organic compounds and reactivity intermediates based on structure (IUPAC Recommendations 1995) '. *Pure and Applied Chemistry*,67(8-9),pp.1307-1375.

Mullins, J. I., Heath, L., Hughes, J. P., Kicha, J., Styrchak, S., Wong, K. G., Rao, U., Hansen, A., Harris, K. S., Laurent, J.-P., Li, D., Simpson, J. H., Essigmann, J. M., Loeb, L. A. and Parkins, J. (2011). 'Mutation of HIV-1 genomes in a clinical population treated with the mutagenic nucleoside KP1461', *PLoS One,* 6(1)**,**pp. 1-10.

Murthy, V. L., Srinivasan, R., Draper, D. E. and Rose, G. D. (1999). 'A complete conformational map for RNA', *Journal of Molecular Biology,* 291(2)**,**pp. 313-327.

Navarro, J., Ruiz-Bravo, A., Jimenez-Valera, M. and Gil, A. (1996). 'Modulation of antibody-forming cell and mitogen-driven lymphoproliferative responses by dietary nucleotides in mice', *Immunology Letters,* 53(2-3)**,**pp. 141-145.

Neidle, S. (2002). *Nucleic acid structure and recognition*:Oxford:Oxford University Press.

Neidle, S. (2008). *Principles of nucleic acid structure.* New York: Academic Press.

Neidle, S. and Berman, H. M. (1983). 'X-ray crystallographic studies of nucleic acids and nucleic acid-drug complexes', *Progress in Biophysics and Molecular Biology,* 41**,**pp. 43-66.

Nelson, D. L., Nelson, D. L., Lehninger, A. L. and Cox, M. M. (2008). *Principles of biochemistry*. New York: W.H. Freeman.

Ogino, T., Iwama, M., Kinouchi, J., Shibagaki, Y., Tsukamoto, T. and Mizumoto, K. (1999). 'Involvement of a cellular glycolytic enzyme, phosphoglycerate kinase, in Sendai virus transcription', *Journal of Biological Chemistry,* 274(50)**,**pp. 35999-36008.

Okada, M., Smith, N. I., Palonpon, A. F., Endo, H., Kawata, S., Sodeoka, M. and Fujita, K. (2012). 'Label-free Raman observation of cytochrome c dynamics during apoptosis', *Proceedings of the National Academy of Sciences,* 109(1)**,**pp. 28-32.

Oldham, W. M. and Hamm, H. E. (2008). 'Heterotrimeric G protein activation by G-protein-coupled receptors', *Nature Reviews Molecular Cell Biology,* 9**,**pp. 60-71.

Ostovarpour, S. and Blanch, E. W. (2012). 'Phosphorylation detection and characterization in ribonucleotides using Raman and Raman optical activity (ROA) spectroscopies', *Applied Spectroscopy,* 66(3)**,**pp. 289-293.

Paduch, M., Jelen, F. and Otlewski, J. (2001). 'Structure of small G proteins and their regulators', *Acta Biochimica Polonica,* 48(4)**,**pp. 829-850.

Paiva, F. M., Batista, J. C., Rêgo, F. S. C., Lima, J. A., Freire, P. T. C., Melo, F. E. A., Mendes Filho, J., de Menezes, A. S. and Nogueira, C. E. S. (2017). 'Infrared and Raman spectroscopy and DFT calculations of DL amino acids: Valine and lysine hydrochloride', *Journal of Molecular Structure,* 1127**,**pp. 419-426.

Palmai, Z., Chaloin, L., Lionne, C., Fidy, J., Perahia, D. and Balog, E. (2009). 'Substrate binding modifies the hinge bending characteristics of human 3-phosphoglycerate kinase: a molecular dynamics study', *Proteins,* 77(2)**,**pp. 319-329.

Patel, R. N. (2007). *Biocatalysis in the pharmaceutical and biotechnology industries*. USA: Taylor and Francis Group, LLC.

Petrov, D. V., Matrosov, I. I. and Sedinkin, D. O. (2016). 'Collection optics for a Raman spectrometer based on the 90° geometry of scattered light collection', *Applied Optics,* 55(29)**,**pp. 8293-8295.

Pinkse, M. W. H., Rijkers, D. T. S., Dostmann, W. R. and Heck, A. J. R. (2009). 'Mode of action of cGMP-dependent protein kinase-specific inhibitors probed by photoaffinity cross-linking mass spectrometry', *Journal of Biological Chemistry,* 284(24)**,**pp. 16354-16368.

Plavec, J., Tong, W. and Chattopadhyaya, J. (1993). 'How do the gauche and anomeric effects drive the pseudorotational equilibrium of the pentofuranose moiety of nucleosides?', *Journal of the American Chemical Society,* 115(21)**,**pp. 9734-9746.

Popp, J. and Reichenbacher, M. (2012). *Challenges in molecular structure determination*. Germany: Springer Berlin Heidelberg.

Puppels, G. J. (2002). 'Preface to the special issue on medical applications of Raman spectroscopy', *Journal of Raman Spectroscopy,* 33(7)**,**pp. 496-497.

Purrello, R., Molina, M., Wang, Y., Smulevich, G., Fresco, J. R., Spiro, T. G. and Fossella, J. (1993). 'Keto-iminol tautomerism of protonated cytidine monophosphate characterized by ultraviolet resonance Raman spectroscopy: implications of C^+ iminol tautomer for base mispairing', *Journal of the American Chemical Society,* 115(2)**,**pp. 760-767.

Qin, L., Reger, A. S., Guo, E., Yang, M. P., Zwart, P., Casteel, D. E. and Kim, C. (2015). 'Structures of cGMP-dependent protein kinase (PKG) Iα Leucine zippers reveal an interchain disulfide bond important for dimer stability', *Biochemistry,* 54(29)**,**pp. 4419-4422.

Rich, A. (2003). 'The double helix: a tale of two puckers', *Nature Structural and Molecular Biology,* 10(4)**,**pp. 247-249.

Rimai, L., Cole, T., Parsons, J. L., Hickmott, J. T. and Carew, E. B. (1969). 'Studies of Raman spectra of water solutions of adenosine tri-, di-, and monophosphate and some related compounds', *Biophysical Journal,* 9(3)**,**pp. 320-329.

Robert, M. K., Daryl, G. K., Peter, M. A. and Victor, R. W. (2003). *Harper's illustrated biochemistry* (26th edn.). New York: Lange Medical Books/McGraw-Hill.

Roger, L. L. and Fiona, m. M. (2010). *Handbook of biochemistry and molecular biology* (4th edn.): CRC press Inc-M.U.A.

Rosemeyer, H., Toth, G., Golankiewicz, B., Kazimierczuk, Z., Bourgeois, W., Kretschmer, U., Muth, H. P. and Seela, F. (1990). 'Syn-anti conformational

analysis of regular and modified nucleosides by ^{1}D ^{1}H NOE difference spectroscopy: A simple graphical method based on conformationally rigid molecules', *The Journal of Organic Chemistry,* 55(22)**,**pp. 5784-5790.

Roy, B., Depaix, A., Perigaud, C. and Peyrottes, S. (2016). 'Recent trends in nucleotide synthesis', *Chemical Reviews,* 116(14)**,**pp. 7854-7897.

Rygula, A., Majzner, K., Marzec, K. M., Kaczor, A., Pilarczyk, M. and Baranska, M. (2013). 'Raman spectroscopy of proteins: a review', *Journal of Raman Spectroscopy,* 44(8)**,**pp. 1061-1076.

Saenger,W.(1984). *Principles of nucleic acid structure*. NewYork: Springer-Verlag.

Schinle, F., Crider, P. E., Vonderach, M., Weis, P., Hampe, O. and Kappes, M. M. (2013). 'Spectroscopic and theoretical investigations of adenosine 5[prime or minute]-diphosphate and adenosine 5[prime or minute]-triphosphate dianions in the gas phase', *Physical Chemistry Chemical Physics,* 15(18)**,**pp. 6640-6650.

Schrader, B. (2007). *Infrared and Raman spectroscopy.* Germany: Wiley-VCH Verlag GmbH

Scott, J. D. (1991). 'Cyclic nucleotide-dependent protein kinases', *Pharmacology and Theraputics,* 50(1)**,**pp. 123-145.

Seifert, R. (2014). 'Is cIMP a second messenger with functions opposite to those of cGMP?', *Naunyn-Schmiedeberg's Archives of Pharmacology,* 387(9)**,**pp. 897-899.

Seifert, R. (2015). 'cCMP and cUMP: Emerging second messengers', *Trends Biochemical Sciences,* 40(1)**,**pp. 8-15.

Shabarova, Z. and Bogdanov, A. (2007). *Advanced Organic Chemistry of Nucleic Acids.*Germany: VCH Verlagsgesellschaft mbH.

Shelton, J., Lu, X., Hollenbaugh, J. A., Cho, J. H., Amblard, F. and Schinazi, R. F. (2016). 'Metabolism, biochemical actions, and chemical synthesis of anticancer nucleosides, nucleotides, and base analogs', *Chemical Reviews,* 116(23)**,**pp. 14379-14455.

Shetty, S., Ganachari, M., Liu, M.C., Azghani, A., Muniyappa, H. and Idell, S. (2005). 'Regulation of urokinase receptor expression by phosphoglycerate kinase is independent of its catalytic activity', *American Journal of Physiology-Lung Cellular and Molecular Physiology,* 289(4)**,**pp. L591-L598.

Shiragami, H., Koguchi, Y., Tanaka, Y., Takamatsu, S., Uchida, Y., Ineyama, T. and Izawa, K. (1995). 'Synthesis of 9-(2-Hydroxyethoxymethyl)guanine (Acyclovir) from Guanosine', *Nucleosides and Nucleotides,* 14(3-5)**,**pp. 337-340.

Sigel, H. and Griesser, R. (2005). 'Nucleoside 5[prime or minute]-triphosphates: self-association, acid-base, and metal ion-binding properties in solution', *Chemical Society Reviews,* 34(10)**,**pp. 875-900.

Singh, R. (2002). 'C. V. Raman and the Discovery of the Raman Effect', *Physics in Perspective,* 4(4)**,**pp. 399-420.

Singh, V., Fedeles, B. I. and Essigmann, J. M. (2015). 'Role of tautomerism in RNA biochemistry', *RNA,* 21(1)**,**pp. 1-13.

Skoog, D., Holler, F. J. and Crouch, S. R. (2007). *Principles of instrumental analysis*. 6th edn. UK: Thomson Brooks/Cole.

Smith, E. and Dent, G. (2005). Modern Raman spectroscopy – A practical approach. Chichester: John Wiley and Sons, Ltd.

Sokoloski, J. E., Godfrey, S. A., Dombrowski, S. E. and Bevilacqua, P. C. (2011). 'Prevalence of syn nucleobases in the active sites of functional RNAs', *RNA*, 17(10)**,**pp. 1775-1787.

Song, G., Zhou, H., Gu, J., Liu, Q., Zhang, W., Su, H., Su, Y., Yao, Q. and Zhang, D. (2017). 'Tumor marker detection using surface enhanced Raman spectroscopy on 3D Au butterfly wings', *Journal of Materials Chemistry B*, 5(8)**,**pp. 1594-1600.

Sperlagh, B. and Vizi, E. S. (2011). 'The role of extracellular adenosine in chemical neurotransmission in the hippocampus and basal ganglia: Pharmacological and clinical aspects', *Current Topics in Medicinal Chemistry*, 11(8)**,**pp. 1034-1046.

Sprang, S. R. (2016). 'Invited review: Activation of G proteins by GTP and the mechanism of Gα-catalyzed GTP hydrolysis', *Biopolymers*, 105(8)**,**pp. 449-462.

Su, Z., Ning, B., Fang, H., Hong, H., Perkins, R., Tong, W. and Shi, L. (2011). 'Next-generation sequencing and its applications in molecular diagnostics', *Expert Review of Molecular Diagnostics*, 11(3)**,**pp. 333-343.

Sugiki, T., Kobayashi, N. and Fujiwara, T. (2017). 'Modern technologies of solution nuclear magnetic resonance spectroscopy for three-dimensional structure determination of proteins open avenues for life scientists', *Computational and Structural Biotechnology Journal*, 15**,**pp. 328-339.

Sweedler, J. V. (1993). 'Charge transfer device detectors and their applications to chemical analysis', *Critical Reviews in Analytical Chemistry*, 24(1)**,**pp. 59-98.

Szabo, J., Varga, A., Flachner, B., Konarev, P. V., Svergun, D. I., Zavodszky, P. and Vas, M. (2008). 'Communication between the Nucleotide site and the main molecular hinge of 3-phosphoglycerate kinase', *Biochemistry*, 47(26)**,**pp. 6735-6744.

Szilagyi, A. N., Ghosh, M., Garman, E. and Vas, M. (2001). 'A 1.8 Å resolution structure of pig muscle 3-phosphoglycerate kinase with bound MgADP and 3-phosphoglycerate in open conformation: New insight into the role of the nucleotide in domain closure, *Journal of Molecular Biology*, 306(3)**,**pp. 499-511.

Taylor, S. S., Kim, C., Cheng, C. Y., Brown, S. H. J., Wu, J. and Kannan, N. (2008). 'Signaling through cAMP and cAMP-dependent protein kinase: Diverse strategies for drug design', *Biochimica et biophysica acta*, 1784(1)**,**pp. 16-26.

Burtis, C., Ashwood, E. and Bruns, D. (2006). *Tietz textbook of clinical chemistry and molecular diagnostics*. 5th edn.USA: Saunders.

Traut, T. W. (1994). 'Physiological concentrations of purines and pyrimidines', *Molecular Cell Biochemistry*, 140(1)**,**pp. 1-22.

Tuteja, N. (2009). 'Signaling through G protein coupled receptors', *Plant Signaling and Behavior*, 4(10)**,**pp. 942-947.

Uauy, R., Stringel, G., Thomas, R. and Quan, R. (1990). 'Effect of dietary nucleosides on growth and maturation of the developing gut in the rat', *Journal of Pediatric Gastroenteroenterology and Nutrition*, 10(4)**,**pp. 497-503.

Ulyanov N.B., Du Z., James T.L. (2008) Refinement of nucleic acid structures with residual dipolar coupling restraints in cartesian coordinate space, in: Graham, A., W. (ed.) *Modern magnetic resonance*. Dordrecht: Springer,pp.665-670.

Vaidehi, N. and Goddard, W. A. (2000). 'Domain motions in phosphoglycerate kinase using hierarchical NEIMO molecular dynamics simulations', *The Journal of Physical Chemistry A,* 104(11)**,**pp. 2375-2383.

Varga, A., Flachner, B., Konarev, P., Graczer, E., Szabo, J., Svergun, D., Zavodszky, P. and Vas, M. (2006). 'Substrate-induced double sided H-bond network as a means of domain closure in 3-phosphoglycerate kinase', *FEBS Letters,* 580(11)**,**pp. 2698-2706.

Varga, A., Szabo, J., Flachner, B., Gugolya, Z., Vonderviszt, F., Zavodszky, P. and Vas, M. (2009). 'Thermodynamic analysis of substrate induced domain closure of 3-phosphoglycerate kinase', *FEBS Letters,* 583(22)**,**pp. 3660-3664.

Velikyan, I., Acharya, S., Trifonova, A., Foldesi, A. and Chattopadhyaya, J. (2001). 'The pK_a's of 2‘-hydroxyl group in nucleosides and nucleotides', *Journal of the American Chemical Society,* 123(12)**,**pp. 2893-2894.

Velyvis, A., Yang, Y. R., Schachman, H. K. and Kay, L. E. (2007). 'A solution NMR study showing that active site ligands and nucleotides directly perturb the allosteric equilibrium in aspartate transcarbamoylase', *Proceedings of the National Academy of Sciences,* 104(21)**,**pp. 8815-8820.

Ventura, C. and Maioli, M. (2001). 'Protein kinase C control of gene expression', *Critical Reviews in Eukaryotic Gene Exprssion,* 11(1-3)**,**pp. 243-267.

Vivet-Boudou, V., Isel, C., El Safadi, Y., Smyth, R. P., Laumond, G., Moog, C., Paillart, J.C. and Marquet, R. (2015). 'Evaluation of anti-HIV-1 mutagenic nucleoside analogues', *Journal of Biological Chemistry,* 290(1)**,**pp. 371-383.

Voet, D. and Voet, J. G. (2011). *Biochemistry* (4th edn.). USA: John Wiely and Sons Inc.

Walko, C. M. and Lindley, C. (2005). 'Capecitabine: A review', *Clinical Theraputics,* 27(1)**,**pp. 23-44.

Wang, A., Ruan, W., Song, W., Chen, L., Zhao, B., Jung, Y. M. and Wang, X. (2013). 'Detection of the potential tumor marker of AFP using surface-enhanced Raman scattering-based immunoassay', *Journal of Raman Spectroscopy,* 44(12)**,**pp. 1649-1653.

Wang, L. and Hosmane, R. S. (2001). 'A unique ring-expanded acyclic nucleoside analogue that inhibits both adenosine deaminase (ADA) and guanine deaminase (GDA; guanase): Synthesis and enzyme inhibition studies of 4,6-diamino-8H-1-hydroxyethoxymethyl-8-iminoimidazo[4,5-e][1,3]diazepine', *Bioorganic and Medicinal Chemistry Letters,* 11(22)**,**pp. 2893-2896.

Wang, W., Zhao, J., Short, M. and Zeng, H. (2015). 'Real-time *in vivo* cancer diagnosis using Raman spectroscopy', *Journal of Biophotonics,* 8(7)**,**pp. 527-545.

Wang, Z. and Cole, P. A. (2014). 'Catalytic mechanisms and regulation of protein kinases', *Methods in Enzymology,* 548**,**pp. 1-21.

Watson, H. C., Wendell, P. L. and Scopes, R. K. (1971). 'Crystallographic study of yeast phosphoglycerate kinase', *Journal of Molecular Biology,* 57(3)**,**pp. 623-625.

Wen, Z. Q., Barron, L. D. and Hecht, L. (1993). 'Vibrational Raman optical activity of monosaccharides', *Journal of the American Chemical Society,* 115(1)**,**pp. 285-292.

Wild, J. R., Loughrey-Chen, S. J. and Corder, T. S. (1989). 'In the presence of CTP, UTP becomes an allosteric inhibitor of aspartate transcarbamoylase', *Proceedings of the National Academy of Sciences of the U S A,* 86(1)**,**pp. 46-50.

Williams, A. A., Darwanto, A., Theruvathu, J. A., Burdzy, A., Neidigh, J. W. and Sowers, L. C. (2009). 'The impact of sugar pucker on base pair and mispair stability', *Biochemistry,* 48(50)**,**pp. 1-25.

Wishart, D. S., Feunang, Y. D., Guo, A. C., Lo, E. J., Marcu, A., Grant, J. R., Sajed, T., Johnson, D., Li, C., Sayeeda, Z., Assempour, N., Iynkkaran, I., Liu, Y., Maciejewski, A., Gale, N., Wilson, A., Chin, L., Cummings, R., Le, D., Pon, A., Knox, C. and Wilson, M. (2018). 'DrugBank 5.0: a major update to the DrugBank database for 2018', *Nucleic Acids Research,* 46(D1)**,**pp. D1074-D1082.

Xia, Z. and Ren, P. (2013). Prediction and coarse-grained modeling of RNA structures. In Rick, R. (ed.) *Biophysics of RNA folding.* New York: Springer.pp.53-68.

Xiao, Y. and Wang, Y. (2016). 'Global discovery of protein kinases and other nucleotide-binding proteins by mass spectrometry', *Mass Spectrometry Reviews,* 35(5)**,**pp. 601-619.

Zecchinon, L., Oriol, A., Netzel, U., Svennberg, J., Gerardin-Otthiers, N. and Feller, G. (2005). 'Stability domains, substrate-induced conformational changes, and hinge-bending motions in a psychrophilic phosphoglycerate kinase: A microcalorimetric study', *Journal of Biological Chemistry,* 280(50)**,**pp. 41307-41314.

Zerrad, L., Merli, A., Schroder, G. F., Varga, A., Graczer, E., Pernot, P., Round, A., Vas, M. and Bowler, M. W. (2011). 'A spring-loaded release mechanism regulates domain movement and catalysis in phosphoglycerate kinase', *Journal of Biological Chemistry,* 286(16)**,**pp. 14040-14048.

Zhao, H., French, J. B., Fang, Y. and Benkovic, S. J. (2013). 'The purinosome, a multi-protein complex involved in the de novo biosynthesis of purines in humans', *Chemical Communications,* 49(40)**,**pp. 4444-4452.

Zheng, H., Filippova, E. V., Tkaczuk, K. L., Dworzynski, P., Chruszcz, M., Porebski, P. J., Wawrzak, Z., Onopriyenko, O., Kudritska, M., Grimshaw, S., Savchenko, A., Anderson, W. F. and Minor, W. (2012). 'Crystal structures of putative phosphoglycerate kinases from B.anthracis and C.jejuni', *Journal of structural and functional genomics,* 13(1)**,**pp. 15-26.

Zhu, F., Isaacs, N. W., Hecht, L. and Barron, L. D. (2005). 'Raman optical activity: A tool for protein structure analysis', *Structure* 13(10)**,**pp. 1409-1419.

Zhu, F., Isaacs, N. W., Hecht, L., Tranter, G. E. and Barron, L. D. (2006). 'Raman optical activity of proteins, carbohydrates and glycoproteins', *Chirality,* 18(2)**,**pp. 103-115.

Chapter 2: Adenosines and their phosphorylated forms: Raman Spectroscopic Characterization and Density Functional Theory Analysis

Contributing authors and their roles:

Omer Azher is the main author who proposed the idea of supporting the Raman measurements with DFT calculations and generated the concept of the averaged atom displacement approach. Alex L. Wilson contributed to the DFT calculations. Shaun T. Mutter contributed to the preliminary DFT results. Paul L. A. Popelier, Ewan W. Blanch and Jonathan P. Waltho contributed to this work through supervision and guidance

2.1 Abstract

Phosphorylation is an important metabolic process in which a phosphoryl group is transferred from a substrate to nucleotide or between two nucleotides by the influence of kinases. The transfer of a (PO_3^-) group involves the binding of magnesium to the nucleotide. This binding results in significant conformational alterations in the nucleotides, enzymes or substrates. The structure of the adenosine nucleotide-Mg complex and the mode of coordination remain controversial. This study reports the use of Raman spectroscopy, peak deconvolution and Density Functional Theory (DFT) to characterise adenosine nucleotides and examine the influence of magnesium ions and pH on the spectral profile of adenosine mono-, di-and tri- phosphate in aqueous solution. These studies into the effects of Mg^{2+} and pH are supported by ^{31}P NMR measurements. Our results show that the Raman spectroscopy is sensitive to the degree of phosphorylation of different adenosine nucleotides and is able to identify the primary markers for adenosine and its phosphate containing derivatives. Combining Raman spectroscopy with a quantitative displacement approach from DFT provided a powerful diagnostic tool which determines a spectral fingerprint of each phosphorylated derivative of adenosine in aqueous environments. Raman and ^{31}PNMR measurements supported a model where the coordination of Mg^{2+} involves both α- and β-phosphate groups of 5'-ADP and β- and γ-phosphate groups of 5'-ATP in aqueous solution at pH 7.0. Results also indicated that the acidic pH has a remarkable impact on the magnesium bound phosphate groups in 5'-AMP, 5'-ADP and 5'-ATP. However, the alterations in the pH environment from pH 5-8 did not change the binding sites of magnesium ions and did not facilitate the binding of the divalent cation to other parts of the adenosine nucleotide molecule.

2.2 Introduction

The transfer of a phosphoryl (PO_3^-) group between a substrate and a nucleotide or between two nucleotides is essential to numerous cellular processes, such as energy management, gene expression, and the initiation of cell signalling cascades (Blackburn *et al.*, 2006; Ardito *et al.*, 2017). Phosphorylation of adenosine or guanosine diphosphates to form ATP or GTP is the most common reactions metabolically. The transmission of the phosphoryl group is usually accompanied by the binding of an essential magnesium ion (Mg^{2+}) to the nucleotide (Black *et al.*, 1994; Bazydlo *et al.*, 2014) and substantial conformational changes in the enzymes, substrates or nucleotides (Jai and Horowitz, 1999).The structure of nucleotide-Mg complexes in solution and the mode of coordination remain controversial (Szabo *et al.*, 2008; Hercend *et al.*, 2011), despite the widespread availability of experimental data provided by NMR spectroscopy and X-ray crystallography (Watson and Gamblin, 1985; Graham and Williams, 1991; Bango *et al.*, 2008). Though solution NMR methods can simulate the aqueous environment, there is an irregular distribution of proton density in the ribonucleotide molecule and limitations associated with describing conformational ensembles accurately (Gong *et al.*, 2009; Dingley and Pascal, 2011; Ostovarpour and Blanch, 2012). Moreover, crystals of ribonucleotides do not necessarily accurately reflect the conformations of the molecules under physiological conditions. For adenosines, most reports suggested the exclusive binding of the metal cation to the phosphate chain but, in some, the interaction of the magnesium ions with the nitrogenous base or the hydroxyl group(s) of the ribose sugar is proposed (Jiang and Mao, 2001). The studies are further complicated by the effects of variations in the experimental conditions, such as pH and concentrations, which may lead to some of the differences in the proposed models of adenosine nucleotide-Mg complexes.

Raman spectroscopy is a vibrational spectroscopic tool with which to examine the structural characteristics of proteins, viruses and nucleic acids (Black *et al.*, 1994). Compared with X-ray crystallography and NMR, the

application of Raman spectroscopy for studying nucleotides is still in its early stages. However, there is a growing body of evidence that supports the high sensitivity of Raman techniques to the structural composition and chemical constituent of different molecules. Raman spectroscopy is highly suitable for aqueous solutions since water provides only weak Raman vibrations (Smith and Dent, 2005). Density functional theory (DFT) calculations offer a complementary powerful computational approach for the prediction and assignment of vibrational bands in Raman spectra (Jimenez-Hoyos *et al*., 2008; Fairchild *et al*., 2009).The combination of Raman spectroscopy and DFT calculations, therefore, has the potential to lead to a detailed understanding of the ensemble of structures adopted by adenosine nucleotides and the ligation and conformational changes associated with the binding to magnesium. Such an analysis would form the basis from which the mechanism of action of many kinases could be examined in great detail, with an overall goal of understanding their catalytic activity under physiological and pathological conditions. In this paper we report the characterisation of the Raman spectra of common adenosine nucleotides and identify the frequencies of vibrational modes associated strongly with their phosphate groups using DFT methods. The results are compared with ^{1}H and ^{31}P NMR spectra of the same nucleotides under identical conditions. The influence of magnesium binding on the Raman spectra of adenosine mono-, di- and triphosphates is investigated, along with the impact of environmental pH. We find that in aqueous solution, both the α- and β-phosphate groups of 5'-ADP are coordinated by Mg^{2+} while in 5'-ATP coordination involves the β- and γ-phosphate groups at pH 7. Acidification does not alter the coordination of magnesium ions but does significantly affect the vibrational modes associated with the phosphate groups in 5'-AMP, 5'-ADP and 5'-ATP.

2.3 Material and methods

2.3.1 Chemicals

Samples of adenosine, 5'- adenosine monophosphate sodium salt, 5'- adenosine diphosphate sodium salt, 5'- adenosine triphosphate sodium salt hydrate, magnesium chloride and deuterium oxide (99.9 %) were purchased from Sigma-Aldrich Ltd and used without further purification.

2.3.2 Sample preparation

Adenosine samples were prepared with a concentration of 50 mM in 0.5 ml deionised water. Three replicates of each adenosine nucleotide were made. The pH of each solution was adjusted to 7.0 (± 0.1) using 1 M NaOH solution. Samples were centrifuged at 9500 g for 5 minutes to eliminate dust contamination. 100 µL of each nucleotide sample was transferred to a quartz microflourescence cell for spectral analysis. Raman measurements on the adenosine nucleotides were carried out without any further purification. For 5'-AMP-Mg, 5'- ADP-Mg and 5'-ATP-Mg complexes, each sample was prepared by mixing 0.5 ml of 100 mM adenosine nucleotide with 0.5 ml of 200 mM $MgCl_2$.

2.3.3 Variation of pH

Analyte complexes were prepared at pH 5.0, 6.0, 7.0 and 8.0. The pH measurements were examined using a Hanna pH 209-laboratory pH meter with accuracy of (± 0.05) pH and a resolution of 0.01 pH units. Each magnesium bound nucleotide was centrifuged and Raman spectra were measured on the ChiralRaman instrument.

2.3.4 NMR samples

A 100 mM solution of each nucleotide was prepared in 0.5 mL of 99.9 % deuterated water (D_2O) and then 0.5 mL of 200 mM $MgCl_2$ was added to each adenosine nucleotide sample then 0.7 mL of each analyte and 1 µL of 0.5 % (w/w) of tetramethylsilane was added to a 5 mm NMR tube.

2.3.5 Raman measurements

A ChiralRaman spectrometer (BioTools Inc., Jupiter FL, USA) operating in backscattering mode was used to measure all Raman spectra. The set-up of the instrument includes: Laser wavelength of 532 nm, spectral resolution of 7 cm^{-1}, power at the laser head of 1.20 W, length of illumination period was 1.029 seconds, total data acquisition times of 0.166 hrs. Data analysis was carried out using MATLAB R2013a, software that includes an inbuilt Raman toolbox.

2.3.6 Raman data analysis and peak deconvolution

The averaged Raman spectra were processed using Matlab software version R2013a. In this application, the Raman data for each adenosine nucleotide were summed and baselined. The resulting data were plotted using Origin 8.5 software. Peak deconvolution techniques were applied to enhance the resolution and to discriminate between the overlapping Raman peaks (Lorenz-Fonfria and Padros, 2005; Aragao and Messaddeq, 2008). The Origin 8.5.1 software was used for this purpose and the Gaussian function was chosen for deconvolution modelling. The second derivative was generated in each case to decrease the bandwidth and identify the position of the hidden peaks. The quality of the fitting was assessed by calculating the adjusted r square values. Peak deconvolution with the adjusted r square values near 1 (~ 0.95) indicated the goodness of the data (Miles, 2014). A more complete analysis of the deconvoluted peaks is provided in appendix 2. The results for the number of component peaks were verified using the DFT analysis of the same spectral region(s).

2.3.7 NMR measurements

^{1}H NMR measurements of the adenosine nucleotides at 300K were carried out using a Bruker Avance III 400 MHz spectrometer. To test for the saturation of binding of magnesium to the nucleotides, increasing concentrations of $MgCl_2$ were added up to 500 mM at pH 7.0 (Figures S2-8, S2-9). The nucleotide concentrations were 50 mM, dissolved in D_2O. ^{31}P NMR measurements were also carried out for each nucleotide-Mg complex

over the pH range 5.0 to 8.0, using ^{1}H decoupling. Data were processed using TopSpin 3.2 software. Spectra were referenced using internal tetramethylsilane. A complete illustration of the NMR spectra for adenosine nucleotides is provided in appendix 2

2.3.8 Density functional theory calculations

All calculations were carried out using the Gaussian09 package (Frisch, 2009). Structures for adenosine (A), 5'-adenosine monophosphate (5'-AMP), 5'- adenosine diphosphate (5'-ADP) and 5'-adenosine triphosphate (5'-ATP) were constructed by hand and a stochastic conformational search was carried out in MOE to find the lowest energy conformers (ULC, 2013). The lowest energy conformers were then optimised in Gaussian09 at B3LYP/6-311+G (d,p) (Lee *et al.*, 1988; Becke, 1993; Naaman and Vager, 2012). Vibrational frequencies and Raman intensities were also calculated at the same level of theory for geometry optimisation. The polarisable continuum model (PCM) was used to implicitly model the presence of solvent in each system (Miertus *et al.*, 1981). Raman intensities were scaled to 1.00 arb. units. according to the most intense Raman vibration, which was common to both adenosine and its nucleotide derivatives.

2.3.9 Analysis of vibrational modes

Visualisation of vibrational modes and the generation of Raman spectra were carried out using GaussView 5 (Lee *et al.*, 1988; Becke, 1993). DFT-derived vibrations for each adenosine derivative were analysed by measuring the displacement of individual atoms within each vibrational mode and classified according to which atoms were affected to the greatest extent (Figure S-1). Quantification of the relative displacement of each atom in every computed vibration for each Adenosine-based structure allows for the construction of a 'vibrational profile' for every computed vibration for each Adenosine-based structure. For example, ATP consists of five readily definable groups: purine ring, ribose ring, α-phosphate, β-phosphate and γ-phosphate. Summation of the relative atomic displacements in each group in a particular vibration allows the

quantification of the relative contributions to overall molecular displacement from each group. Hence, vibrations are described as, for example, comprising 84 % ribose ring and 16 % purine ring contributions. The assignment of DFT-derived Raman bands to the experimentally observed modes is proposed on the basis of both the relative frequency and intensity of vibrations computed using DFT. A more complete analysis of the proposed assignment of these bands is provided in appendix 1 (Table 1.1).

2.4 Results

2.4.1 Adenosine and its phosphates, without Mg^{2+}

Raman spectra of adenosine, and adenosine 5'-mono-, di- and tri-phosphates, in the absence of Mg^{2+}, were measured at pH 7.0 over the range 600-1800 cm^{-1} (Figure 2.1). The spectra are very similar to each other above 1205 cm^{-1} and below 760 cm^{-1}. The main differences between the experimental spectra of the various nucleotides are observed in Raman bands in the 760-1205 cm^{-1} region.

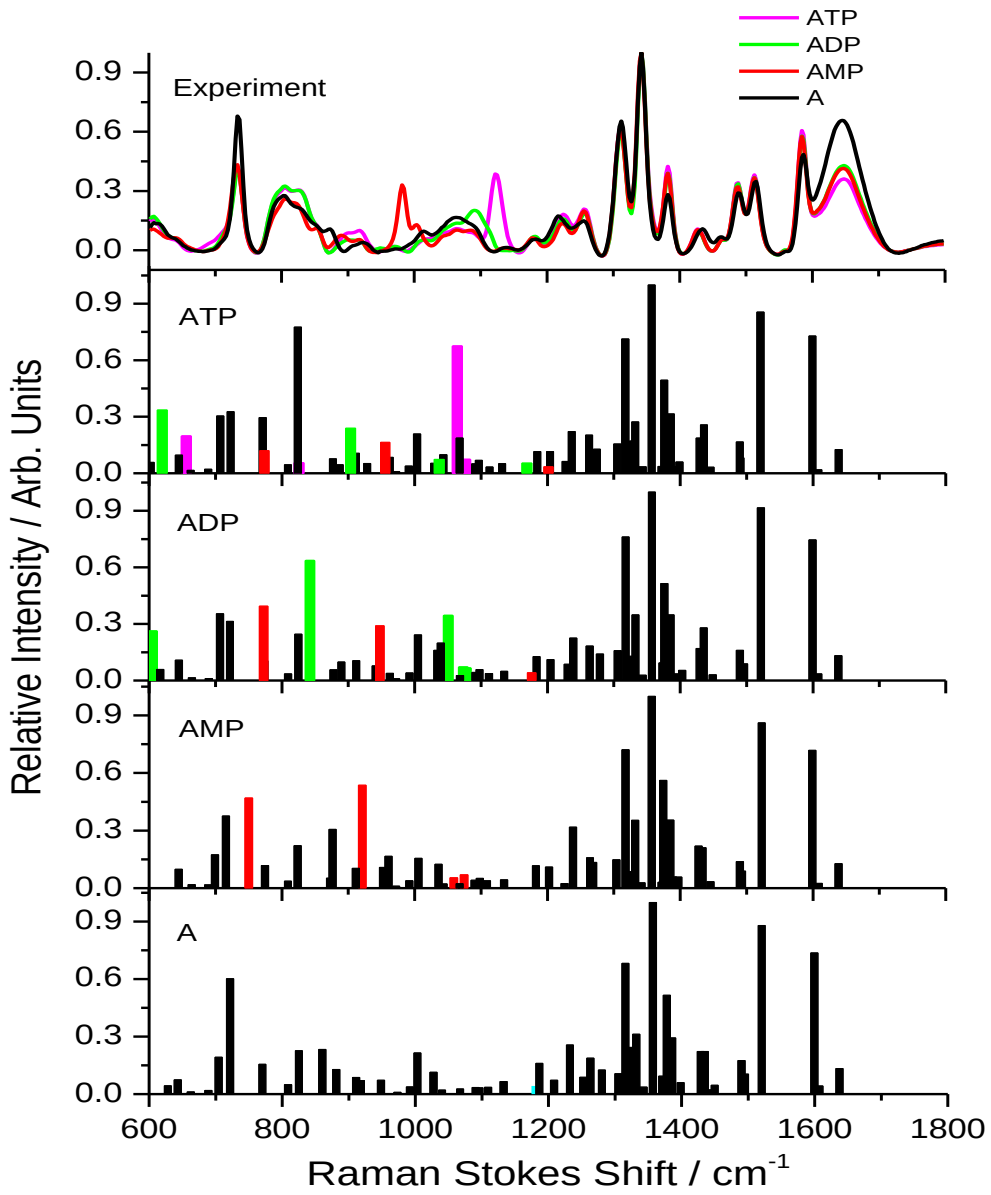

Figure 2.1. Experimental (top) and DFT calculated (bottom) Raman spectra for adenosine, 5'- adenosine monophosphate (AMP), 5'- adenosine diphosphate (ADP) and 5'- adenosine triphosphate (ATP) at pH 7.0. The experimental and DFT spectra showed similar intensities and frequencies above 1205 cm^{-1} and below 760 cm^{-1} regions. The main spectral differences are observed at 760-1205 cm^{-1} region.

600-760 and 1205-1800 cm^{-1}: For adenosine and all of the nucleotide derivatives studied here, there is a strong correlation between the experimental Raman spectra in the 1205-1800 cm^{-1} region, consistent with the component vibrational modes not involving the phosphate moieties. The region is dominated by major bands at 1584 cm^{-1}, a doublet at 1488 and 1512 cm^{-1}, and a triplet at 1312, 1342 and 1382 cm^{-1} (Figures 2.1, 2-2 –2-5). More surprisingly, there is also a strong correlation between the experimental Raman spectra in the 600-760 cm^{-1} region, where vibrations involving the phosphate moieties are more likely. However, the 600-760 cm^{-1} region is relatively devoid of intense bands; it dominated by a single band at 734 cm^{-1} (Figures 2.1, 2-2-2-5).

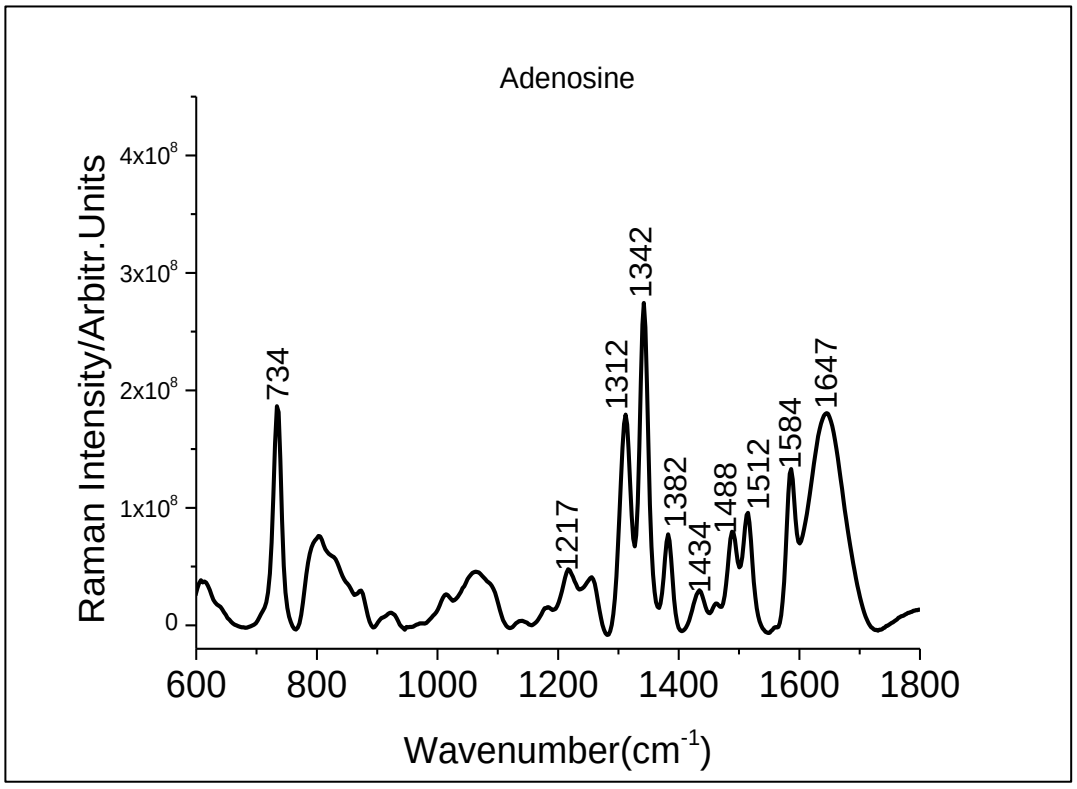

Figure 2-2. Raman spectrum for adenosine at pH 7.0.

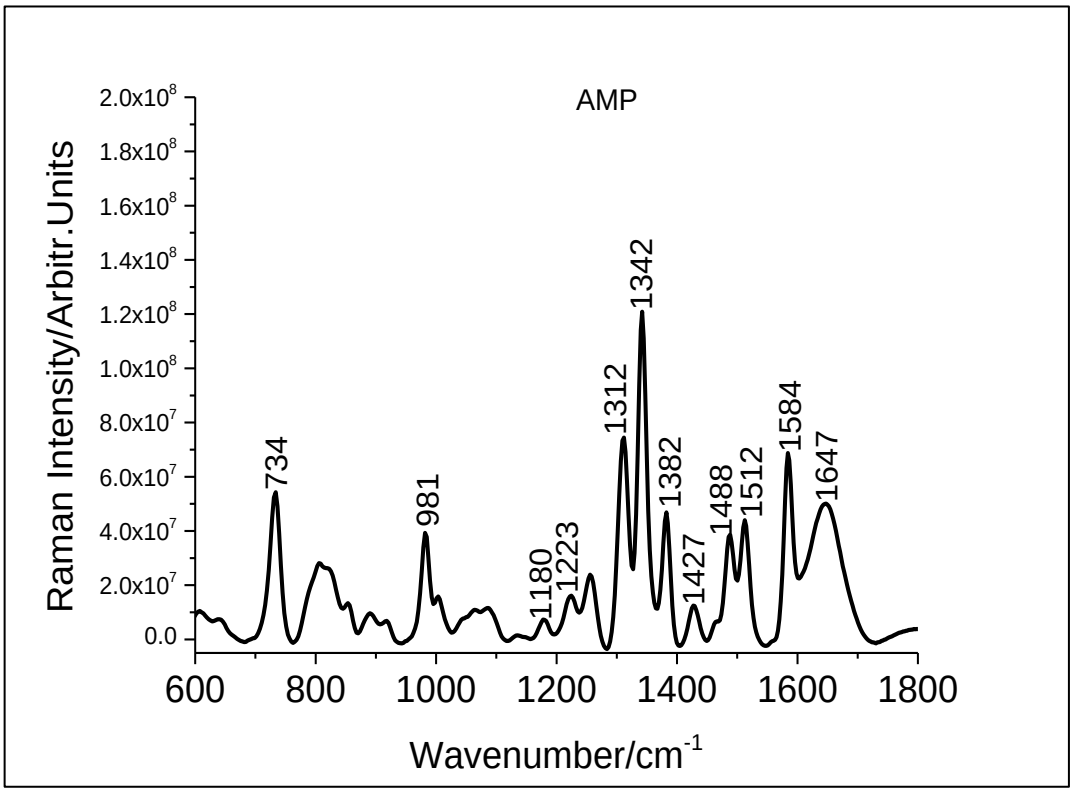

Figure 2-3. Raman spectrum for 5'- adenosine monophosphate (AMP) at pH 7.0.

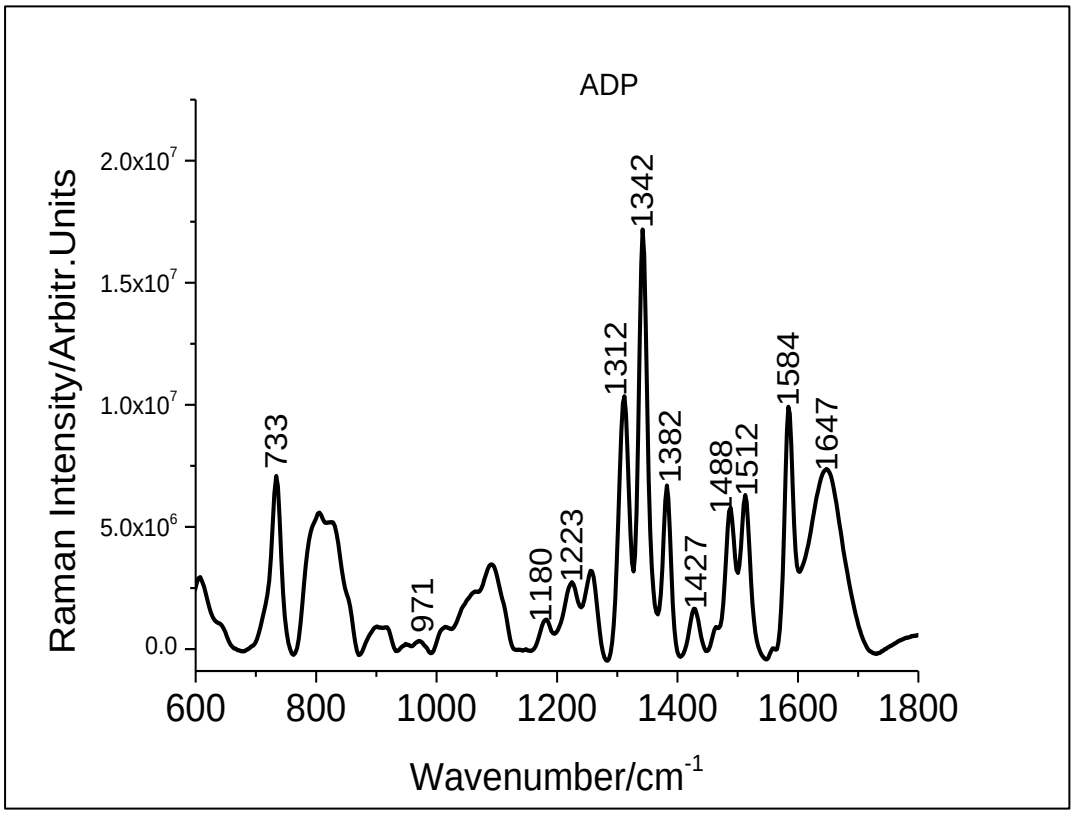

Figure 2-4. Raman spectrum for 5'- adenosine diphosphate (ADP) at pH 7.0.

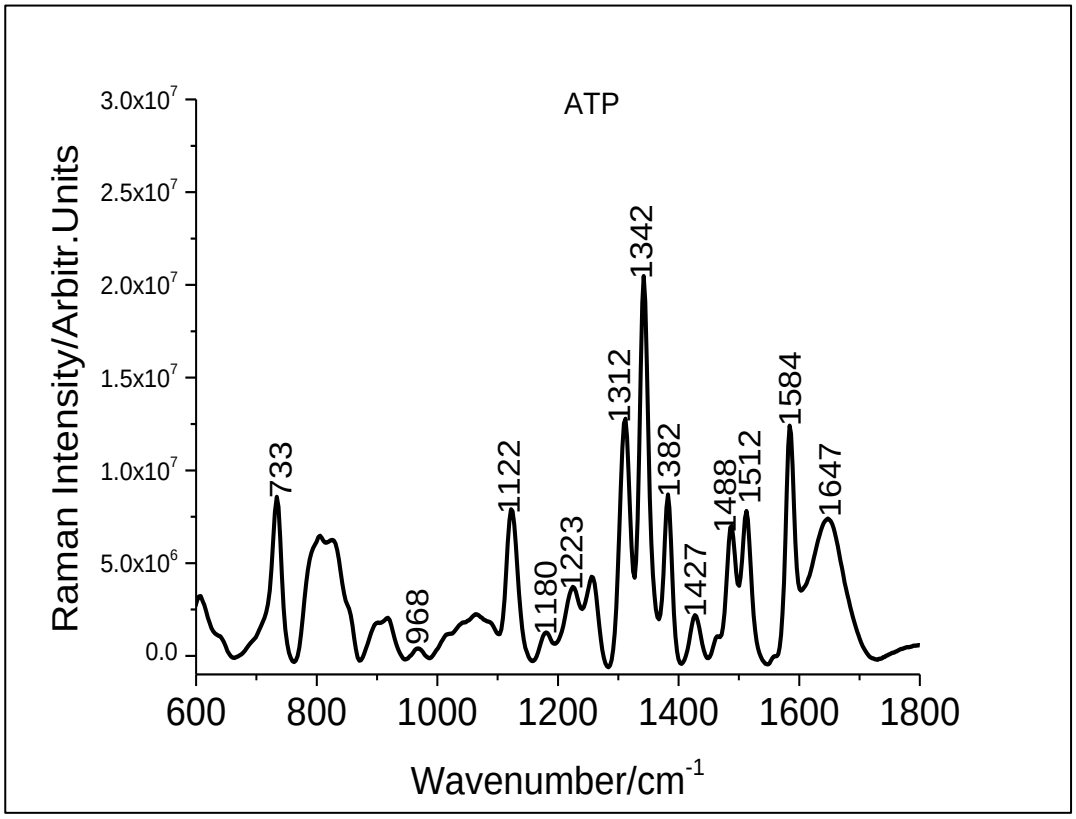

Figure 2-5. Raman spectrum for 5'- adenosine triphosphate (ATP) at pH 7.0.

760-1205 cm^{-1}: This region contains two broad peaks that are common to adenosine and all of the nucleotide derivatives, one in the range 760-870 cm^{-1} and one in the range 990-1205 cm^{-1} (Figure 2-6). Deconvolution of these peaks was performed in order to establish the features of the underlying components. For adenosine, deconvolution of the lower frequency (760-870 cm^{-1}) peak revealed three bands, at 785, 800, and 825 cm^{-1} (Figure 2-6), while deconvolution of the higher frequency (1020–1120 cm^{-1}) peak revealed five bands, at 1040, 1055, 1073, 1091, and 1100 cm^{-1} (Figure 2-6). For 5'-adenosine monophosphate (5'-AMP), in addition to the 760-870 cm^{-1} and 1020-1120 cm^{-1} peaks observed for adenosine, there is a distinct new peak at 981 cm^{-1} (Figure 2.1). The broad peaks at 760-870 cm^{-1} and 1020-1120 cm^{-1} show some differences in shape compared to the equivalent peaks for adenosine. Deconvolution reveals four bands (788, 803, 821, 853 cm^{-1}) for the lower frequency peak and four bands (1042, 1063, 1087 and 1099 cm^{-1}) for the higher frequency peak. The primary differences to the bands observed for adenosine are changes in relative intensities. This is particularly noticeable for the band at 853 cm^{-1}, for which there is only a hint in the Raman spectrum of adenosine. Also, in the higher frequency peak the band at 1087 cm^{-1} becomes dominant in 5'-AMP, and the band at 1063 cm^{-1} substitutes for the bands at 1055 and 1073 cm^{-1} in adenosine, the latter being the dominant band in the absence of phosphorylation.

For 5'-adenosine diphosphate (5'-ADP), the large peak at 981 cm^{-1} in 5'-AMP appears to have moved to higher frequency in the experimental spectrum, where it overlaps with the main 1020-1120 cm^{-1}peak (Figure 2.1). The broad peak at 1020-1120 cm^{-1} has a different shape and intensity compared to the equivalent peak for 5'-AMP. Deconvolution of the 1020-1120 cm^{-1} peak for 5'-ADP revealed six bands (1038, 1046, 1061, 1087, 1102, 1114 cm^{-1}), with the most intense peak at 1087 cm^{-1}, as observed for 5'-AMP. However, the 1087 cm^{-1} band dominates the intensity of this broad peak far more for 5'-ADP than for 5'-AMP.

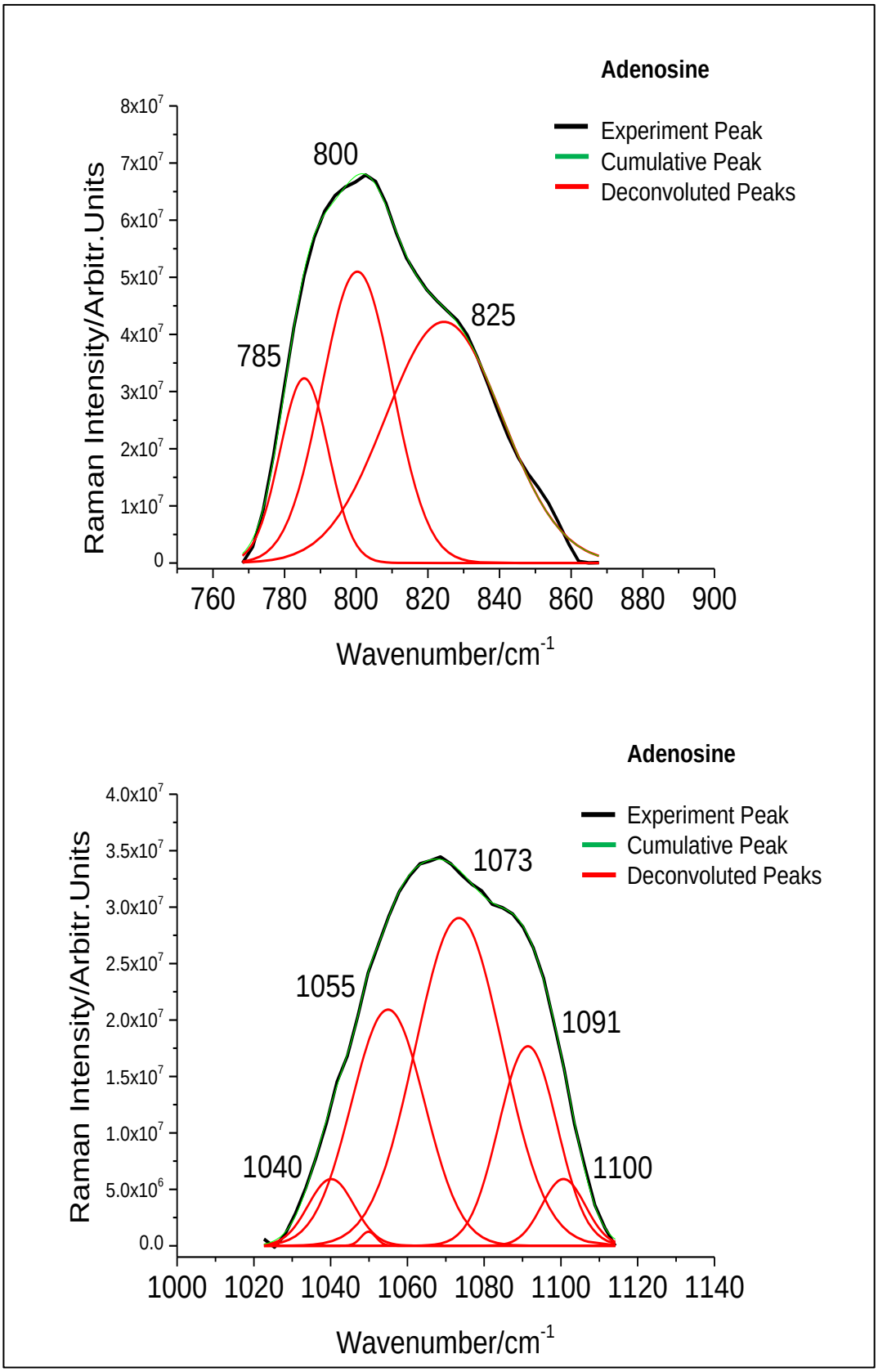

Figure 2-6. Peak deconvolution of the Raman spectrum for adenosine in the regions 760-870 cm^{-1} (top) and 1020-1120 cm^{-1} (bottom) at pH 7.0.

The other primary differences compared with the spectrum of 5'-AMP are the resolvable bands at both the low (1038 cm^{-1}) and high frequency (1114 cm^{-1}) ends of the broad peak, and the reduction in relative intensity of the 1061 cm^{-1} band. Deconvolution of the 760-870 cm^{-1} peak revealed four bands (784, 801, 829, 855 cm^{-1}) at similar frequencies to the equivalent bands observed for 5'-AMP, except for a +8 cm^{-1} shift for the 829 cm^{-1} band. There is also a significant reduction in intensity in the 801 cm^{-1} band.

For 5'-adenosine triphosphate (5'-ATP), an intense peak is observed at 1122 cm^{-1} (Figure 2.1,). Deconvolution of the 1020-1120 cm^{-1} region was insufficient to define all of the major component bands owing to the new, intense peak at 1122 cm^{-1} and so the deconvoluted region was extended to 990-1150 cm^{-1}. This deconvolution revealed four bands in addition to the 1122 cm^{-1} band (1013, 1037, 1067, 1091 cm^{-1}). The band at 1013 cm^{-1} for 5'-ATP did not appear in the spectrum of the other nucleotides. The 1067 cm^{-1} band is now dominant in intensity and the 1037 cm^{-1} band is much larger than the equivalent band in 5'-ADP. Deconvolution of the 760-870 cm^{-1} peak revealed four bands (784, 801, 829, 855 cm^{-1}), which are indistinguishable in frequency and intensity from the equivalent bands for 5'-ADP. This indicates that the addition of the γ-phosphate group has no detectable influence on these vibrations.

2.4.2 Adenosine phosphates, with Mg^{2+}

For 5'-adenosine monophosphate (Figures 2.7, 2-8), the major diagnostic band at 981 cm^{-1} is shifted by +3 cm^{-1} on saturation with Mg^{2+}. This relatively minor change in the Raman spectrum is reflected in the equivalent ^{31}P NMR spectra on Mg^{2+} saturation, where the chemical shift of the phosphate group moves downfield slightly (0.2 ppm) on addition of Mg^{2+}. Deconvolution of the broad Raman peak at 760-870 cm^{-1} also identified only a minor change in the frequencies of the component bands as a result of metal binding, while the 1020-1120 cm^{-1} peak did not reveal

any resolvable differences compared with unbound 5'-AMP (Figures S2-7, S2-13).

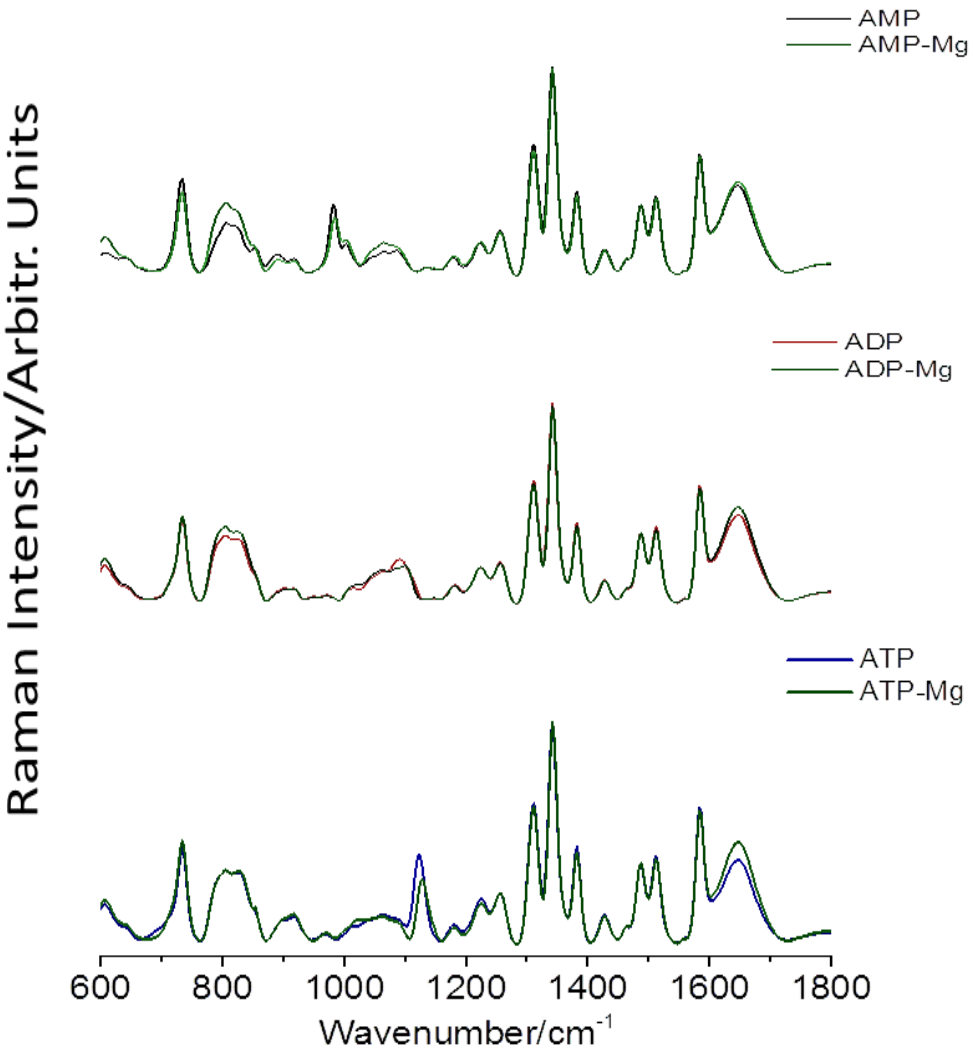

Figure 2.7. Experimental Raman spectra for 5'- adenosine monophosphate (AMP), 5'-adenosine monophosphate-magnesium complex (AMP-Mg), 5'- adenosine diphosphate (ADP),5'- adenosine diphosphate-magnesium complex (ADP-Mg), 5'-adenosine triphosphate and 5'-adenosine triphosphate-magnesium complex. The major spectral differences observed on saturation with Mg^{2+} are the +3 and +5 shifts of the bands at 981 and 1122 cm^{-1} for 5'-AMP and 5'-ATP respectively.

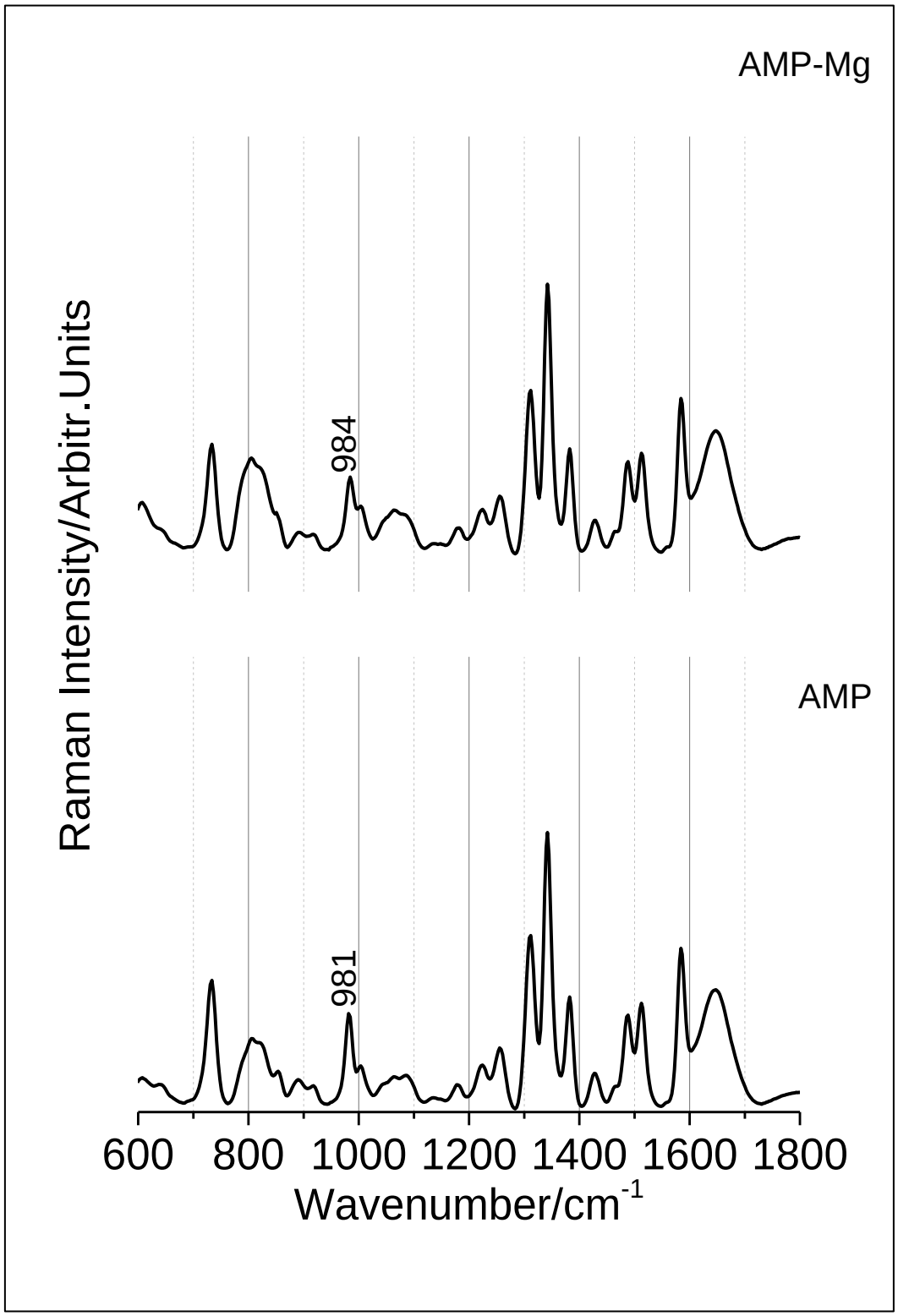

Figure 2-8. Experimental Raman spectra for 5'- adenosine monophosphate complex (AMP-Mg) and 5'- adenosine monophosphate (AMP) at pH 7.0.

For 5'-adenosine diphosphate (Figures 2.2, 2-9), Mg^{2+} binding has no resolvable effect on the broad peak at 760-870 cm^{-1}. On deconvolution of the 1020-1120 cm^{-1}, differences were detectable in the Raman bands following saturation with Mg^{2+}. The distribution of component bands moves the overall intensity to higher frequency, in line with the behaviour of the 981 cm^{-1} band of 5'-AMP, and the band at 1087 cm^{-1} no longer dominates. The peak of intensity of the experimental spectrum is now ca. 1100 cm^{-1}. It is difficult to ascribe changes to individual bands in the deconvolution spectrum, though the general trend of the component peaks is to higher frequency by approximately +3 cm^{-1}. In the equivalent ^{31}P NMR spectra, the changes in chemical shift are greater than that observed in 5'-AMP at pH 7.0, likely as a result of its increased pK_a compared with the mononucleotide, whereby the α- and β-phosphate resonances move downfield by 0.7 and 1.3 ppm, respectively, on binding of Mg^{2+}. These results support a model where the coordination of Mg^{2+} involves a substantial contribution from both the α- and β-phosphate groups of 5'-ADP, which would affect multiple bands in the broad peak at 1020-1120 cm^{-1}.

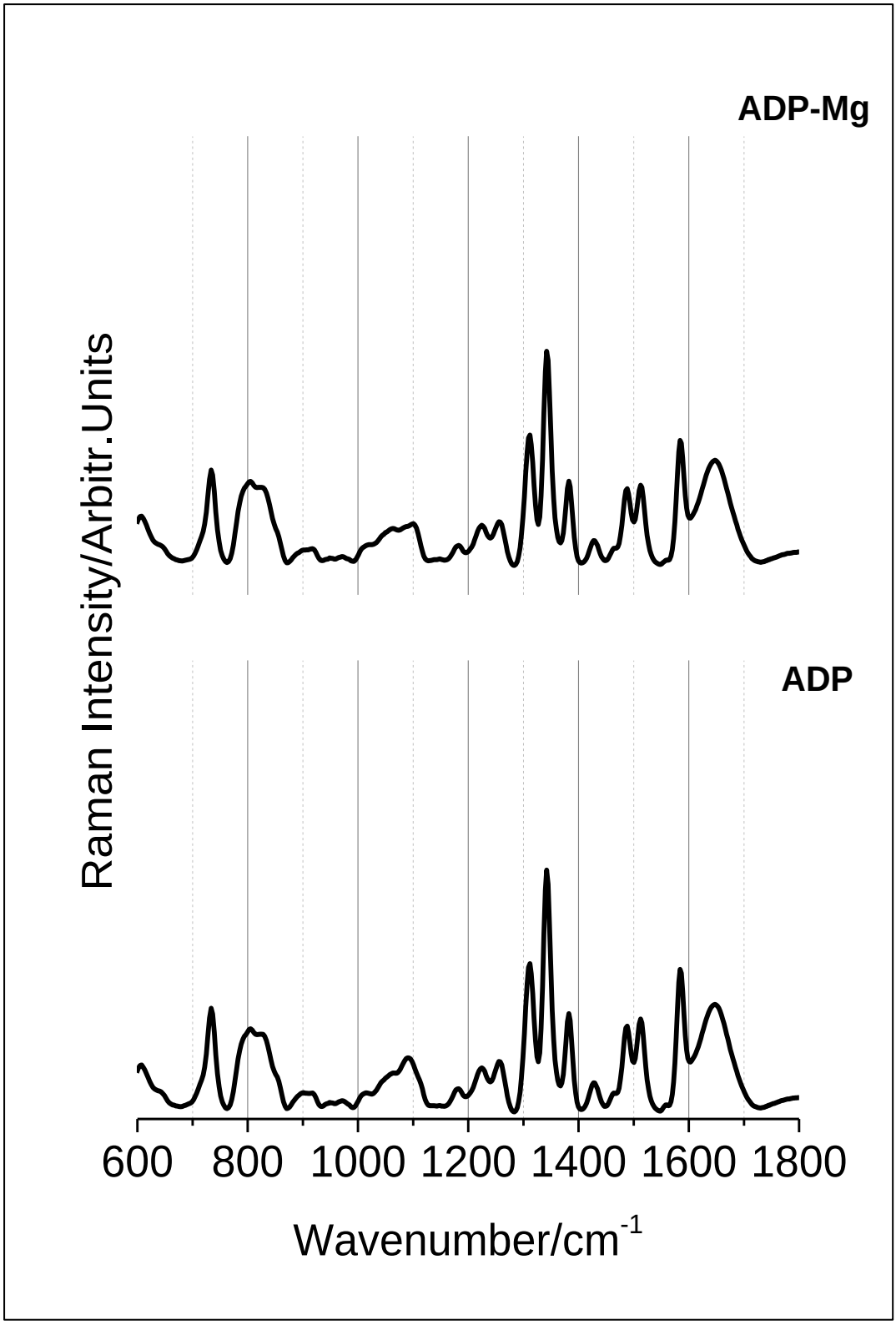

Figure 2-9. Raman spectra for 5'- adenosine diphosphate-magnesium complex (ADP-Mg) and 5'- adenosine diphosphate (ADP) at pH 7.0.

For 5'-adenosine triphosphate (Figures 2.2, 2-10), the major diagnostic band at 1122 cm^{-1} is shifted by +5 cm^{-1} on saturation with Mg^{2+}. As for 5'-ADP, deconvolution of the broad Raman peak at 760-870 cm^{-1} identified no changes in the frequencies or intensities of the bands on binding of Mg^{2+}. However, deconvolution of the 990-1150 cm^{-1} peak indicated a significant shift to higher frequency of component bands at 1013, 1037 and 1067 cm^{-1} by +10, +16 and +5 cm^{-1}, respectively, which is consistent with their assignment as having substantial contributions from the phosphate groups . In the equivalent ^{31}P NMR spectra, downfield chemical shift changes for the β- and γ-phosphate groups (by 2.5 and 1.3 ppm, respectively) are observed on binding of Mg^{2+}. The ^{31}P chemical shift of the α-phosphate shifts downfield by only 0.1 ppm, supporting a model where the coordination of Mg^{2+} is dominated by the β- and γ-phosphate groups.

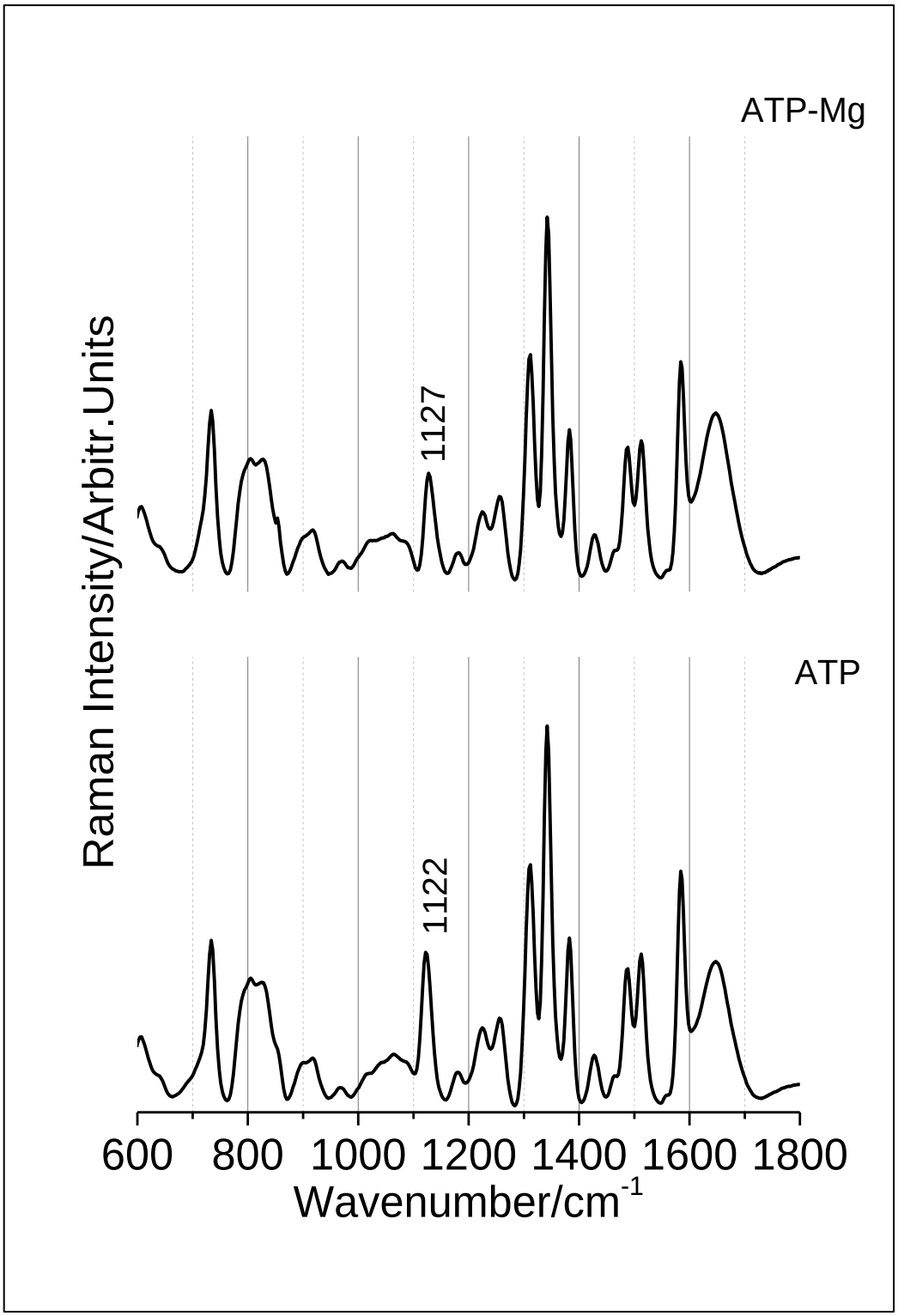

Figure 2-10. Experimental Raman spectra for 5'- adenosine triphosphate complex (ATP-Mg) and 5'- adenosine triphosphate (ATP) at pH 7.0.

2.4.3 The pH effects on adenosine phosphates-Mg^{2+} complexes

For 5'-adenosine monophosphate-Mg (Figures 2.3, 2-11), the Raman spectra were relatively unaffected between pH 7.0 and 8.0. However, by pH 5.0, the 981 cm^{-1} and 1020-1120 cm^{-1} peaks displayed a significant alteration. The 981 cm^{-1} peak is no longer visible to a significant extent, and there is no clear evidence that it has moved to a nearby frequency. Deconvolution of the 1020-1120 cm^{-1} peak revealed changes in intensity of the two major components. The component peak at ca. 1063 cm^{-1} falls in intensity as the pH falls, whereas the peak at ca. 1087 cm^{-1} increases substantially. In the ^{31}P NMR spectra over the same pH range, the chemical shift of the phosphate group moves upfield by 2.6 ppm at pH 5.0 (δ = 0.7 ppm) compared with at pH 7.0 (δ = 3.3 ppm), consistent with protonation of the Mg-bound phosphate group under the experimental conditions used. Deconvolution of the 760-870 cm^{-1} peak also revealed changes in intensity of components bands. Here, the band at ca. 800 cm^{-1} increases from pH 8.0 to 6.0 before falling again by pH 5.0, the latter effect of which may be related to the onset of protonation of the N1 atom in the purine ring (Corfu *et al.*, 1990).

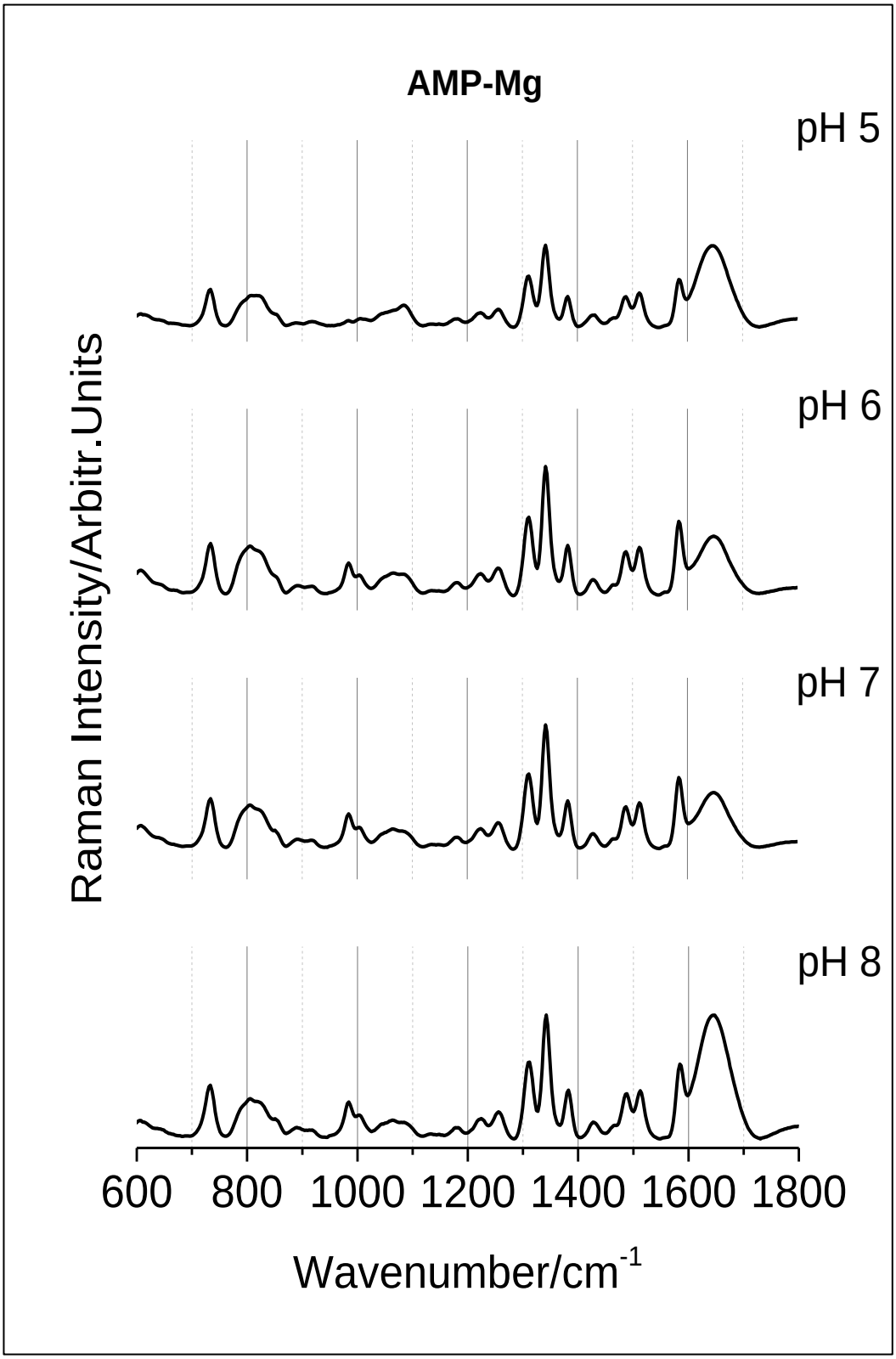

Figure 2-11. The Raman spectra for 5'- adenosine monophosphate-magnesium complex (AMP-Mg) at different pH environments.

For 5'-adenosine diphosphate-Mg (Figures 2.3, S2-23), like for 5'-AMP-Mg, the Raman spectra were relatively unaffected between pH 7.0 and 8.0. At pH 5.0, the broad peak at 1020-1150 cm^{-1} is affected dramatically; deconvolution revealed the peak becomes dominated by the component band at 1104 cm^{-1}, and a new band appears at 1132 cm^{-1} (Figure S2-24). In the ^{31}P NMR spectra over the same pH range, the chemical shifts of the α- and β-phosphates move upfield by 0.2 (-10.2 to -10.4 ppm) and 1.0 ppm (-6.1 to -7.1 ppm), respectively, (Figure S2-25), consistent with protonation reversing some of the chemical shift changes associated with Mg binding. Deconvolution of the 760-870 cm^{-1} peak revealed changes in intensity of components bands moderately similar to those observed in 5'-AMP-Mg (Figure S2-24). The band at ca. 800 cm^{-1} falls substantially in intensity between pH 6.0 and 5.0, though the increase in intensity between pH 8.0 and 6.0 observed for 5'-AMP-Mg is not visible for 5'-ADP-Mg, where the ca. 800 cm^{-1} is intense throughout this pH range.

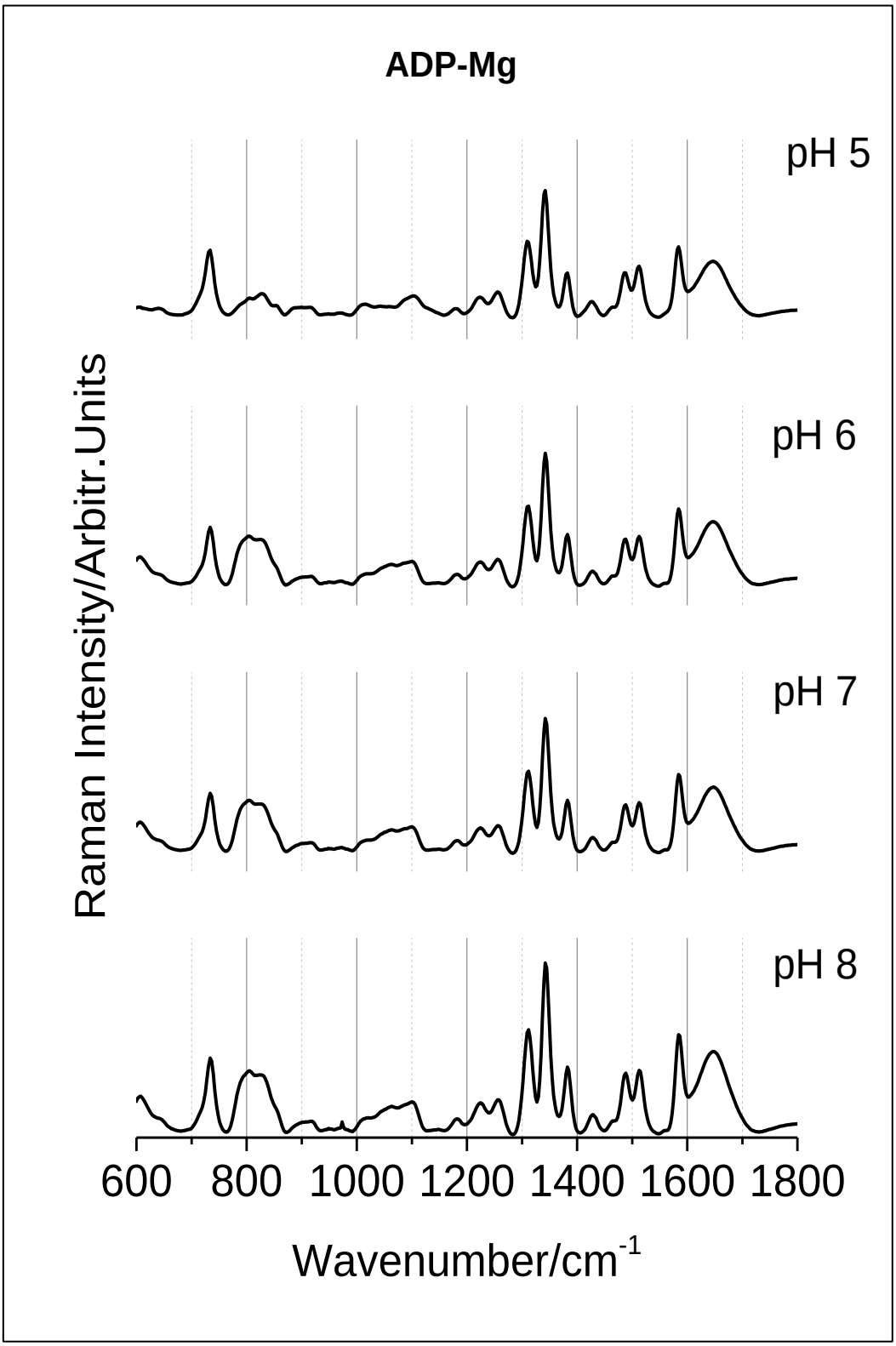

Figure 2-12. The Raman spectra for 5'- adenosine diphosphate-magnesium complex (ADP-Mg) at different pH environments.

For 5'-adenosine triphosphate-Mg (Figures 2.13, 2-14), like the other two nucleotides the Raman spectra were relatively unaffected between pH 7.0 and 8.0. At pH 5.0, the Raman peak at 1127 cm^{-1} is shifted +3 cm^{-1}. Deconvolution of the broad 990–1150 cm^{-1} peak was not successful but the primary observation is that a band at 1019 cm^{-1} becomes dominant in intensity at pH 5.0 compared with higher frequency bands. This behaviour contrasts with that of the 1020-1150 cm^{-1} peak for 5'-ADP-Mg, where the higher frequency components become dominant. In the ^{31}P NMR spectra over the same pH range, the chemical shifts of the β- and γ-phosphate groups move upfield by 0.8 and 1.0 ppm, respectively, over the same pH range (-19.3 to -20.1 ppm, and -5.9 to -6.9 ppm), consistent with protonation having a large effect on both of these phosphate groups. In contrast, the chemical shift of the α-phosphate group remains relatively unchanged (-10.9 to -11.1 ppm). Deconvolution of the 760-870 cm^{-1} peak revealed similar changes in intensity of components bands to those observed in 5'-ADP-Mg. The band at ca. 800 cm^{-1} falls substantially in intensity between pH 6.0 and 5.0.

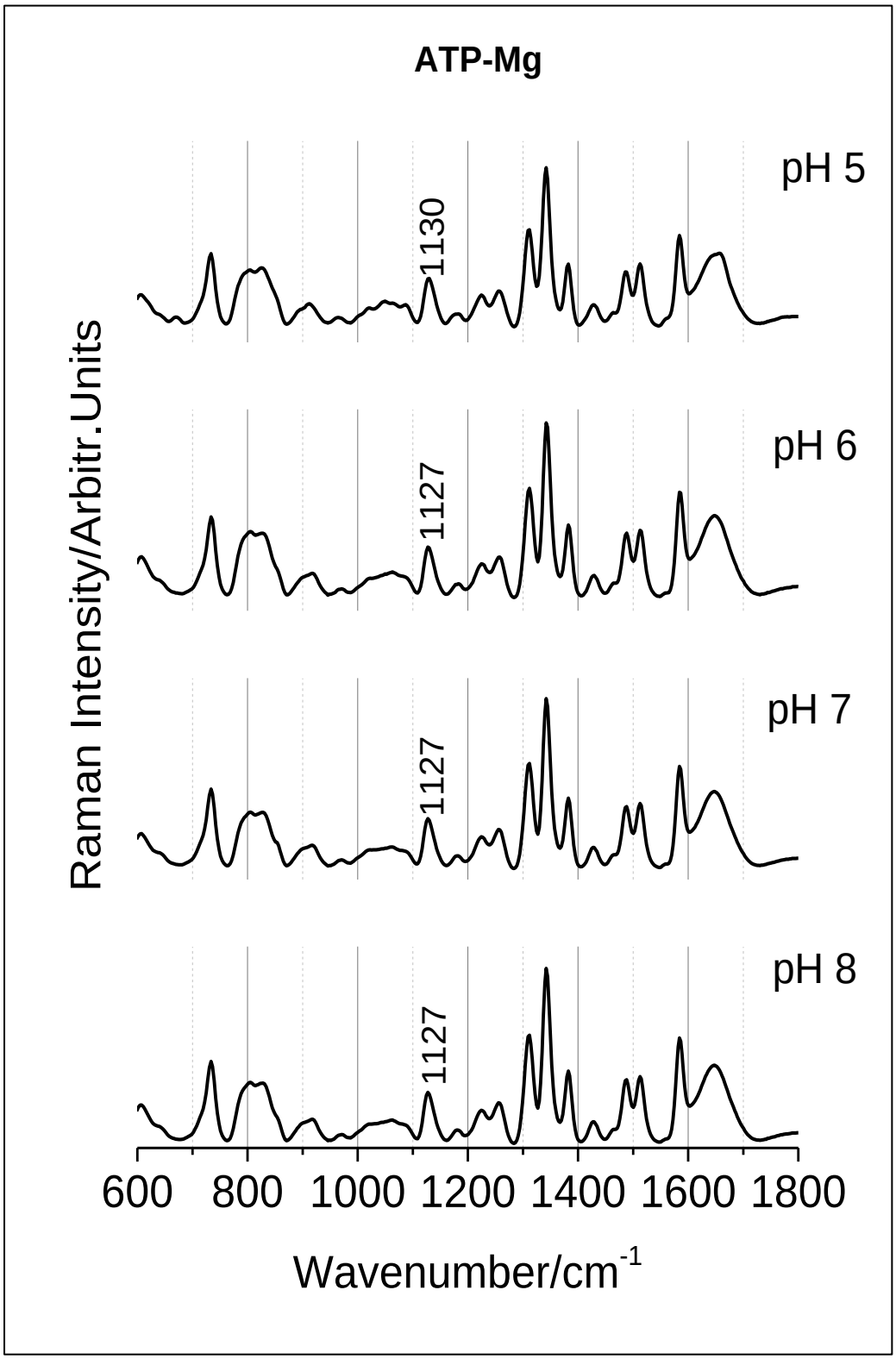

Figure 2-13.The Raman spectra for 5'- adenosine triphosphate-magnesium complex (ATP-Mg) at different pH environments.

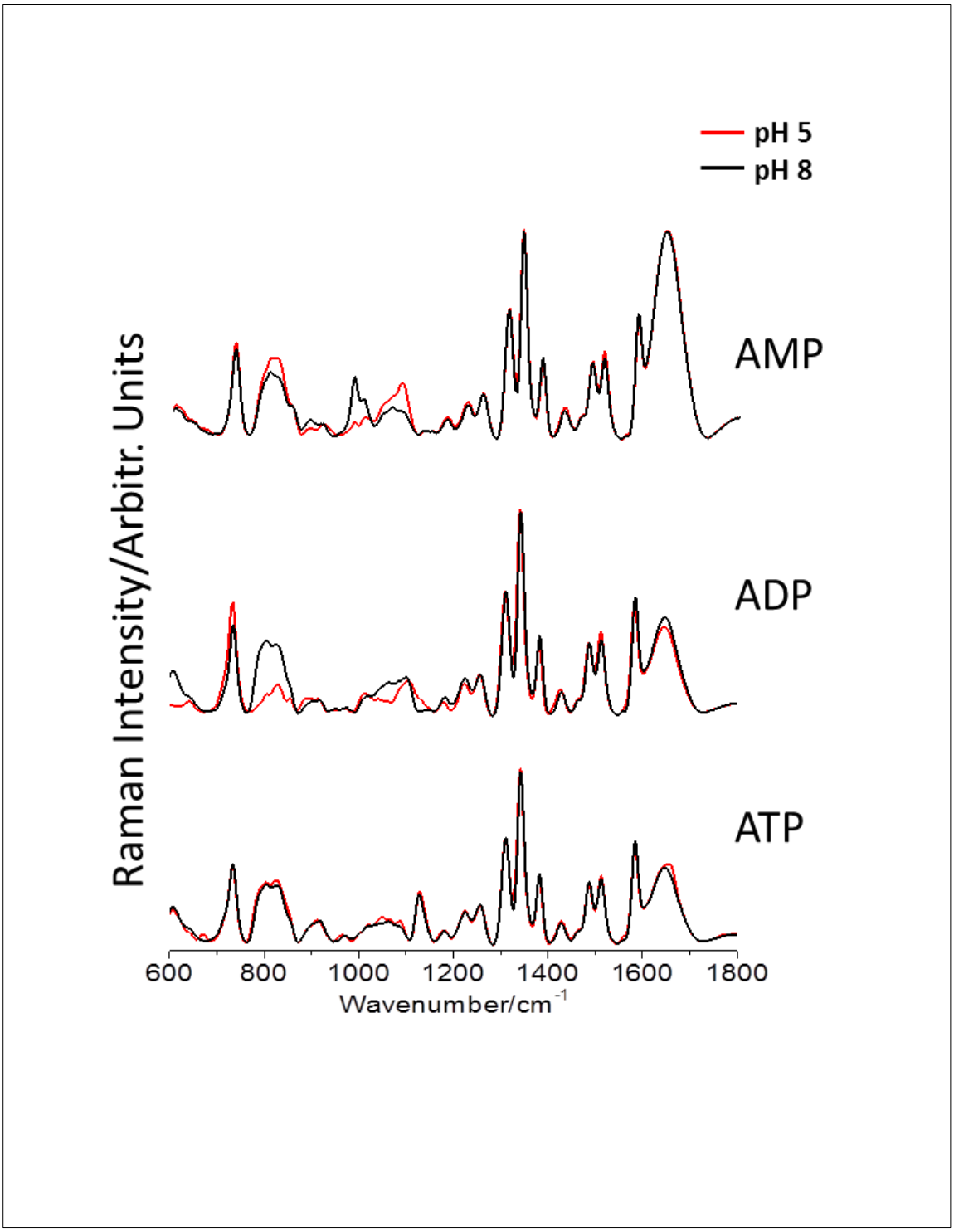

Figure 2.14 Experimental Raman spectra for 5'-adenosine monophosphate-magnesium complex (AMP-Mg), 5'- adenosine diphosphate-magnesium complex (ADP-Mg) and 5'-adenosine triphosphate-magnesium complex (ATP-Mg) at pH 5.0 and 8.0. Acidification decreases the intensity of the 5'-AMP band at 981 cm^{-1} and shifts the 5'-ATP band at 1127 cm^{-1} by +3 cm^{-1}.

2.4.4 Assignment of Raman bands using DFT models

In order to understand more thoroughly the differences in the experimental Raman spectra of adenosine, and adenosine 5'-mono-, di- and tri-phosphates, the Raman bands of the different species were calculated using a DFT approach. From this, some assignments of individual bands to specific vibrations are proposed.

Raman Vibrations above 1205 cm^{-1}: For adenosine and all of the nucleotide derivatives studied here, there is a strong correlation between the experimental and the DFT-derived Raman spectra in this region. According to the DFT calculations, the experimental 1584 cm^{-1} band corresponds to a vibration of significant relative Raman intensity (0.74 a.u., averaged across adenosine and the nucleotide derivatives - see methods section, (Figure 2.1) in which the purine ring atoms contribute to 95 % of atomic displacement. The 1488/1512 cm^{-1} doublet bands actually comprise 3 vibrational modes; a very intense (0.88 a.u.) purine-dominated (91 %) band, and two less intense (0.10 a.u., 0.18 a.u.) bands, ribose-dominated (99 %) and purine-dominated (94 %), respectively. The 1312/1342/1382 cm^{-1} triplet bands contain a very intense (1.00 a.u.) purine-dominated (87 %) band at 1342 cm^{-1}, whereas the bands at 1312 cm^{-1} and 1382 cm^{-1} are comprised of multiple less intense vibrational modes with more equal contributions (56 %: 44 % and 66 % :34 %) from the purine and ribose groups, respectively. As expected on the basis of the similarity in the experimental spectra in this region, the phosphate groups do not contribute to any vibrational modes in this region of the spectra. Therefore no significant frequency or intensity changes of any DFT bands in this region across adenosine and its derivatives are found.

Raman Vibrations below 760 cm^{-1}: The experimental Raman spectra for adenosine and all of the nucleotide derivatives are dominated in this region by a band at 734 cm^{-1} (Figure 2.1). According to DFT calculations, there are 3 vibrational modes that are potential contributors to this band, one of which is close in frequency (722 cm^{-1}) and two within 40 cm^{-1} (705 and 770 cm^{-1} for adenosine). For adenosine, the 722 cm^{-1} mode is dominant in

intensity (0.60 a.u., compared with 0.19 a.u. for the 705 cm^{-1} mode and 0.16 a.u. for the 770 cm^{-1} mode, and all three modes have near 50 % contributions from the purine and ribose groups. Unlike the region above 1205 cm^{-1}, vibrations in this region can include phosphate character, which may alter both the frequency and intensity of bands. For the adenosine derivatives, each of these modes gains a contribution from the phosphate group(s) in the nucleotides (up to a maximum of 14 %) but the frequencies are only moderately affected (a shift of up to 6 cm^{-1}). The intensities are more strongly affected, the 722 cm^{-1} mode falls from 0.60 a.u. in adenosine to 0.33 a.u. in 5'-ATP, whereas the 705 cm^{-1} and 770 cm^{-1} modes rise from 0.19 a.u. to 0.30 a.u. and from 0.16 a.u. to 0.30 a.u., respectively. Experimentally, an intensity drop in the 734 cm^{-1} band is observed from adenosine to its phosphate derivatives. This is not reflected in the sum of the behaviour of the 705 cm^{-1}, 722 cm^{-1} and 770 cm^{-1} modes in the DFT calculations, but is consistent with the behaviour of the 722 cm^{-1} mode in isolation.

Raman Vibrations in the region 760-1205 cm^{-1}: In the experimental spectra this region contains the major diagnostic peaks for the nucleotide derivatives, in addition to two broad peaks that they share in common with adenosine, one in the range 760-870 cm^{-1} and one in the range 990-1150 cm^{-1}.

In 5'-AMP, the major diagnostic band that appears at 981 cm^{-1} can be related to a new intense vibration in the DFT calculations (921 cm^{-1}, 0.54 a.u.), which has significant (74 %) phosphate contribution. This peak is reduced in intensity in 5'-ADP and 5'-ATP, which is consistent with its absence in the spectra of these derivatives. In 5'-ADP, the diagnostic band around 1087 cm^{-1} can be rationalized by the increase in intensity of DFT vibrations in this region, particularly a new relatively intense vibration (1051 cm^{-1}, 0.34 a.u.) with significant (41 % α-, 11 % β-) phosphate contribution. In terms of DFT, this vibration is not seen in adenosine and 5'-AMP, and is reduced in intensity in 5'-ATP, which is consistent with its absence in the other spectra. In 5'-ATP, the diagnostic peak appears at

1122 cm^{-1}, which can be rationalized by the appearance in the DFT calculations of a very intense peak (1064 cm^{-1}, 0.67 a.u.) with significant (29 % α-,24 % β-, 6 % γ-) phosphate character that is not observed in adenosine or its other derivatives.

In the 760-870 cm^{-1} range, there are multiple DFT-derived Raman modes in that approximate area that potentially contributes to the shape of the broad peak in this region. There are five modes that are common to all species (including the 770 cm^{-1} mode discussed above), though the 809 cm^{-1} mode is predicted to have low intensity throughout. The 825 cm^{-1} mode has substantial contributions from both purine and ribose groups in adenosine but has a 58 % contribution from the phosphate groups in 5'-ATP, where its intensity has increased from 0.23 a.u. to 0.78 a.u. In contrast, the 860 cm^{-1} mode decreases in intensity from 0.23 a.u. to 0.05 a.u. between adenosine and 5'-AMP, stays at approximately that level in the other nucleotides, moves to higher frequency by up to 18 cm^{-1} and picks up little contribution from the phosphate groups. The 881 cm^{-1} mode peaks in intensity in 5'-AMP (0.31 a.u) and is dominated by the atoms of the ribose ring. There are a further three modes, one present for 5'-AMP, 5'-ADP and 5'-ATP, one for 5'-ADP and 5'-ATP and one for 5'-ATP alone. The overall complexity makes it difficult to assign DFT modes to the experimental bands identified using deconvolution. However, there are similarities in behaviour. Experimentally, an increased intensity at approximately 825 cm^{-1} is observed for both 5'-ADP and 5'-ATP. This is also found in the DFT-derived spectra. In adenosine and 5'-AMP, there are no peaks in this region with a calculated relative intensity greater than 0.3. However in 5'-ADP and 5'-ATP, there are vibrations in this region with large relative intensities (0.64 in 5'-ADP, 0.78 in 5'-ATP) that contain significant contributions from phosphate groups (80 % and 58 % respectively).

In the 990-1150 cm^{-1} range, there are over 15 DFT-derived Raman bands that contribute to the shape of the broad peak in this region for adenosine, making any attempts at assignment to be very subjective.

2.5 Discussion

The Raman spectra recorded in this study identify primary marker bands for 5'-AMP, 5'-ADP and 5'-ATP at 981 cm^{-1}, 1087 cm^{-1} and 1122 cm^{-1}, respectively. By comparison with DFT-derived spectra of the same compounds, these bands appear be have substantial contributions from vibrations of the α-phosphate atoms for 5'-AMP, and 5'-ADP, and the α- or β-phosphate atoms for 5'-ATP. It is noticeable that the assigned modes are displaced from the experimental bands to lower frequency by 60, 36 and 58 cm^{-1}, respectively, for 5'-AMP, 5'-ADP and 5'-ATP. The source of this offset is unknown but may relate to the DFT calculations using in vacuo structures, while experimental measurements were in aqueous solution.

Secondary markers are observable, particularly in the variations in shape of the broad peaks in the 760-870 cm^{-1} and 1020-1120 cm^{-1} regions, but the contributing modes are difficult to assign owing to the number of contributory vibrations and any offsets between DFT-derived and experimental frequencies introduced when the vibrations involved phosphate group atoms. The Raman spectra above 1205 cm^{-1} are indistinguishable and according to DFT-derived spectra these vibrations do not involve phosphate group atoms.

The binding of Mg^{2+} to adenosine nucleotides has only a small effect on the primary diagnostic bands, ranging from +3 cm^{-1} for the 981 cm^{-1} band of 5'-AMP to +5 cm^{-1} for the 1122 cm^{-1} band of 5'-ATP. It is more difficult to ascribe the change in 5'-ADP owing to the overlap between the 1087 cm^{-1} band observed in the absence of Mg^{2+} overlapping with a broad peak in the 1020-1120 cm^{-1} region. It is intriguing that in both resolvable cases the change is consistently to higher frequency, despite the expected increase in mass afforded by coordination of the phosphate group atoms to a Mg^{2+} ion. A shift to higher frequency on metal binding has been proposed (Iyandurai.N *et al.*, 2009) to result from the transient interruption of the adjacent hydrogen bonds as a result of the binding of the metal to the oxygen atoms.

Protonation of the Mg-bound adenosine nucleotides has no dramatic effect on the Raman spectrum of adenosine or its nucleotide derivatives in the pH range 6.0 – 8.0. The ^{31}P NMR spectra are consistent with Mg binding selecting for the dianion state of AMP, the trianion state of ADP and the tetraanion anion state of ATP at neutral pH. Each nucleotide exhibits protonation with a pK_a value between 5.0 and 6.0, with the primary protonation event most strongly affecting the α-, β-, and γ-phosphate groups for 5'-AMP, 5'-ADP and 5'-ATP, respectively. The Raman spectra at pH 5.0 differ substantially from the spectra at neutral pH, but this effect cannot be confidently ascribed solely to the protonation of the phosphate moieties, since significant protonation of the N1 atom of the base is likely at this pH.

The experimental results presented here for adenosine and its nucleotide derivatives in the absence of Mg are in general agreement with previously reported Raman profiles (Rimai *et al.*, 1969; Carmona *et al.*, 1988; Ostovarpour and Blanch, 2012). The major diagnostic Raman band for 5'-ATP was reported previously (at 1123 cm^{-1}) (Takeuchi *et al.*, 1988), and it has been proposed that different vibrations for phosphate groups in adenosine nucleotides occur in the 850-1205 cm^{-1} region (Carmona *et al.*, 1988; Kopecky *et al.*, 2002). Also, the equivalent band to that reported here at 734 cm^{-1} was reported in an earlier study (Ostovarpour and Blanch, 2012), but occurred at 754 cm^{-1} for adenosine, 731 cm^{-1} for 5'AMP and 5'ADP, and 693 cm^{-1} for 5'-ATP. A likely source of the previously observed variation is the solution pH, which was 6.0 for 5'-AMP, 5.2 for 5'-ADP and 4.2 for 5'-ATP.

The Raman spectra of adenosine nucleotides in solution indicated greater spectral differences than similar molecules measured in solid state. A previous study (Gorelik *et al.*, 2008) reported the Raman spectrum of 5'-ADP in its crystalline form. There are significant spectral variations between the spectrum in crystallo and the results for 5'ADP in solution from this study, and a previous study in solution (albeit at low pH) (Ostovarpour and Blanch, 2012).

In conclusion, the results from this study have shown that Raman spectroscopy is sensitive to the degree of phosphorylation of different adenosine nucleotides. Raman spectroscopy was able to provide diagnostic spectral fingerprints for adenosine, 5'-AMP, 5'-ADP and 5'-ATP in aqueous solution. The representation of the fundamental Raman vibrations derived from DFT a model using an averaged atom displacement is a useful tool to provide a quantitative description of the contribution of the different moieties to the vibrational mode, and thus the experimental spectrum. By combining this approach with experimental spectra and peak deconvolution, secondary markers of the adenosine nucleotides are identified. This has allowed us to describe more fully the effects of the binding of magnesium ions, and the effects of pH variation on the spectra, thus paving the way for more detailed investigations of these nucleotides in the variety of environments in which they function in nature.

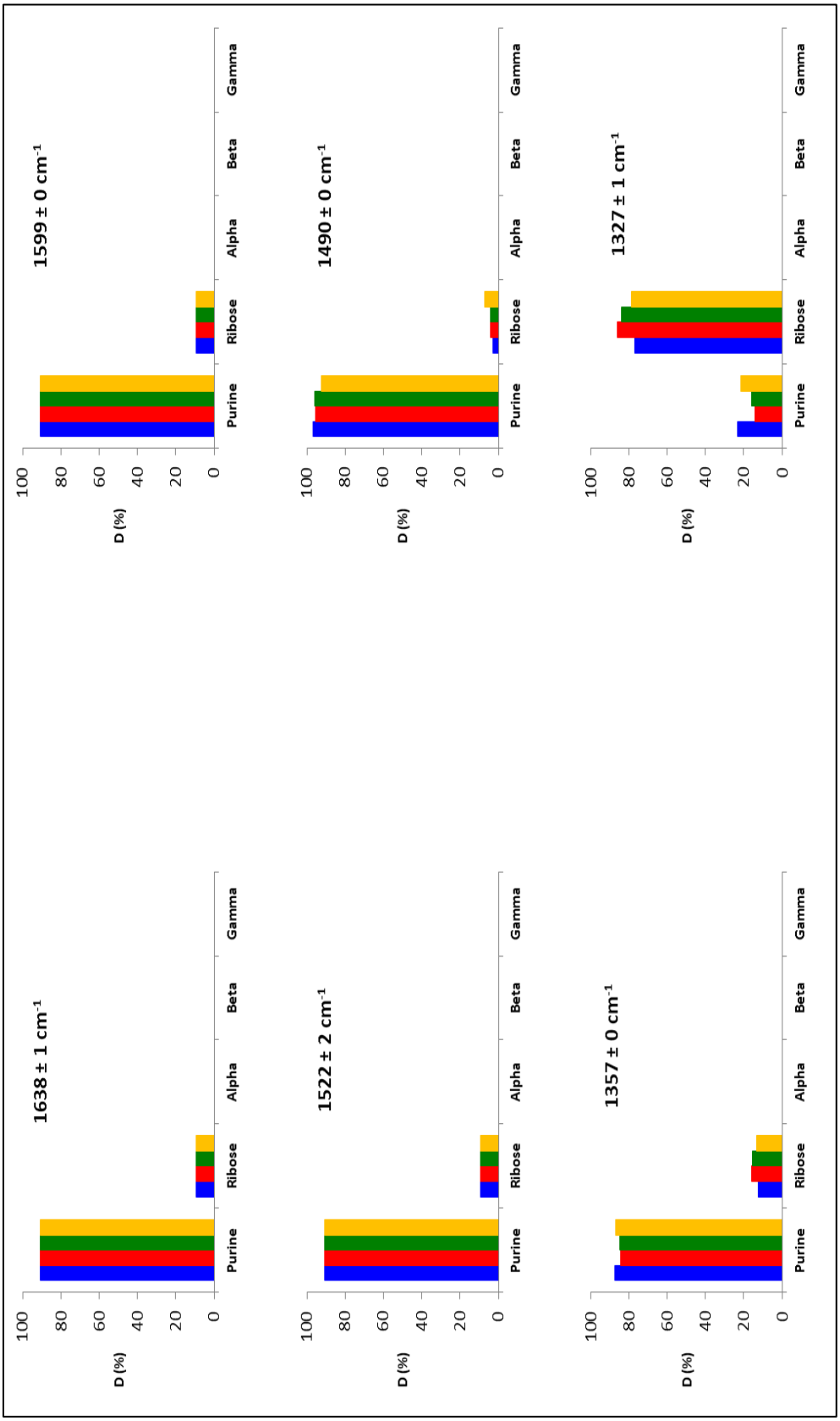

Figure 2.15. Averaged atom displacements (D) for adenosine (blue bands), 5'-adenosine monophosphate (AMP) (Red bands) 5'- adenosine diphosphate (ADP) (green bands) and 5'- adenosine triphosphate (ATP) (yellow bands).

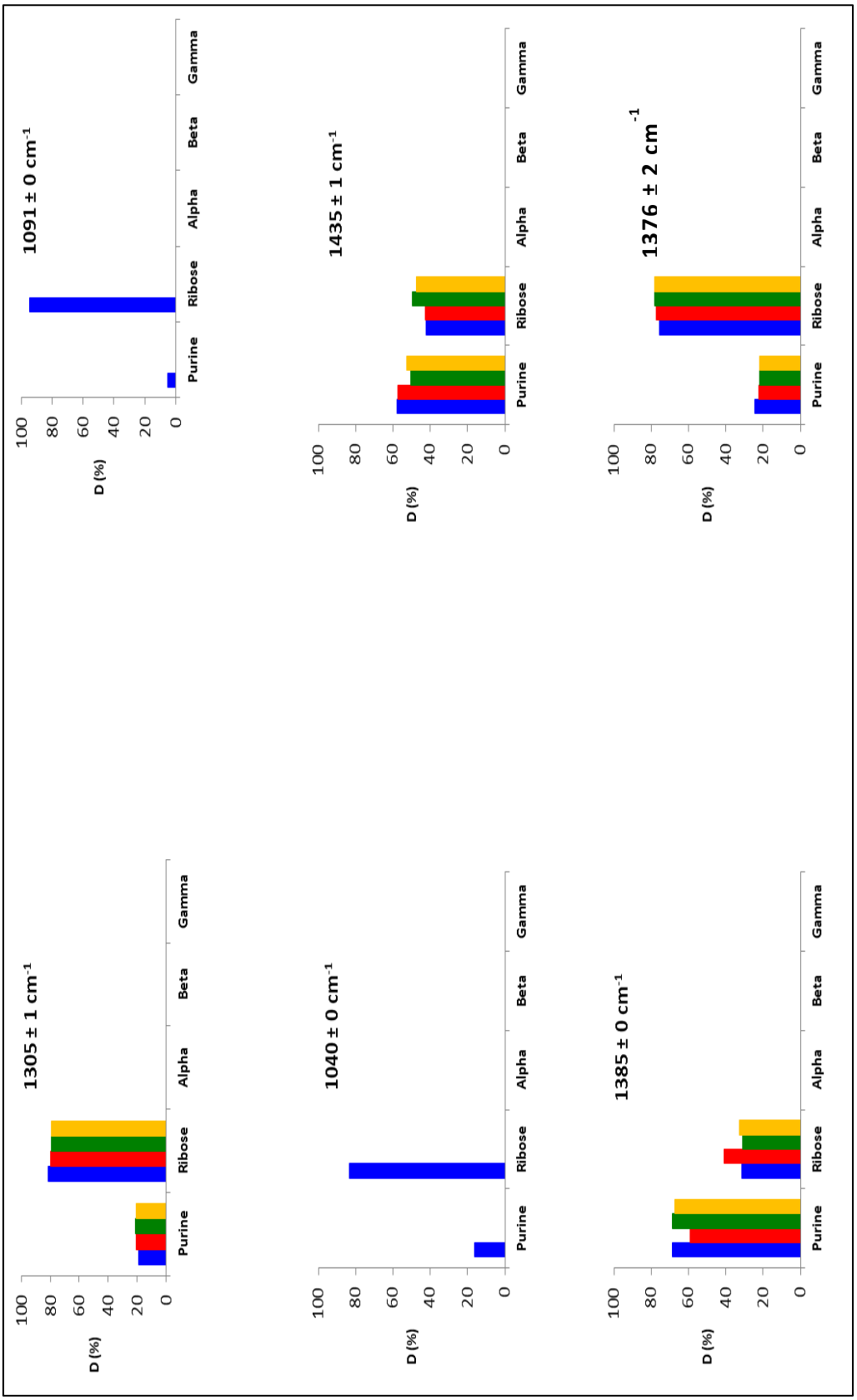

Figure 2.15. Continued.

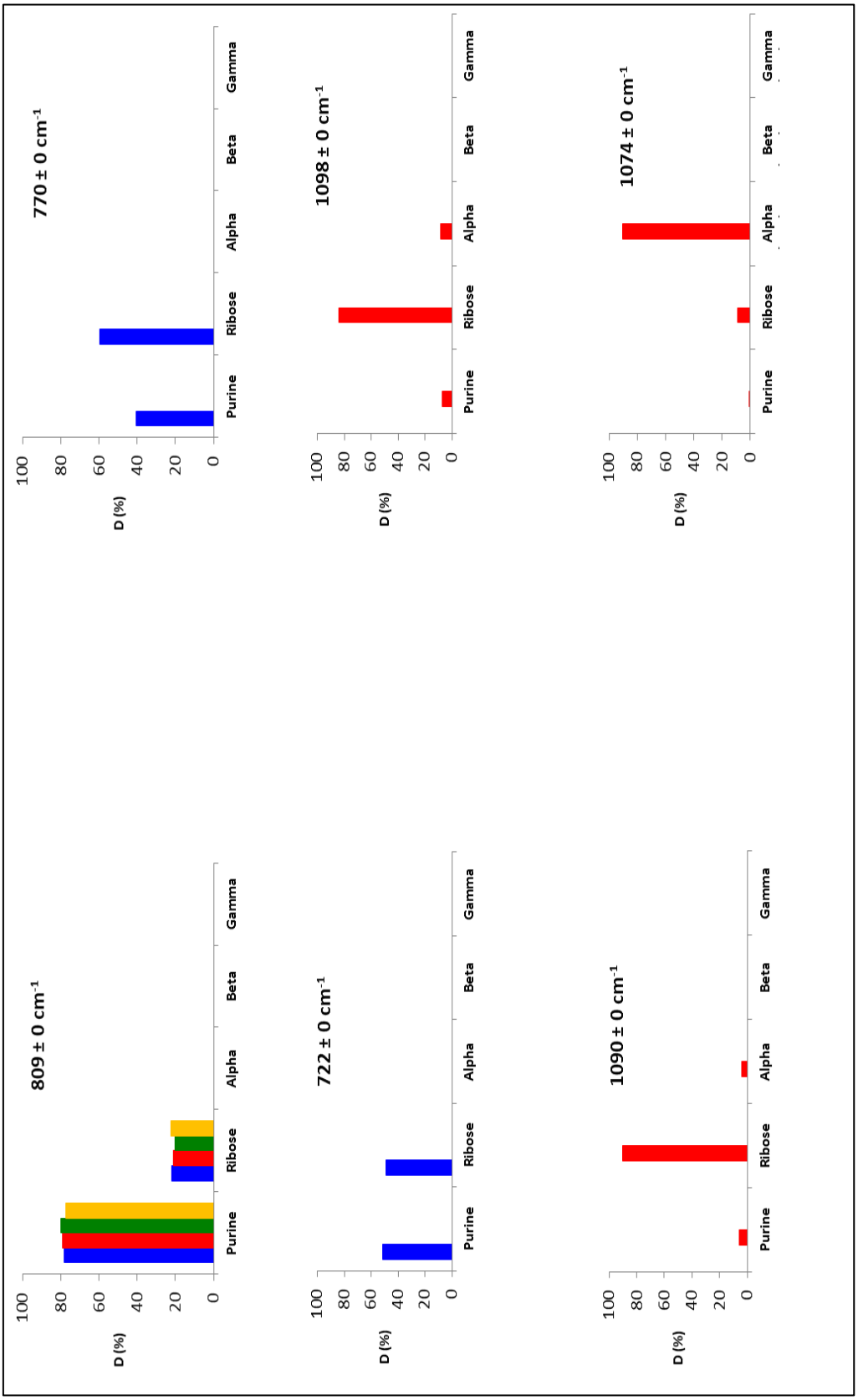

Figure 2.15. Continued.

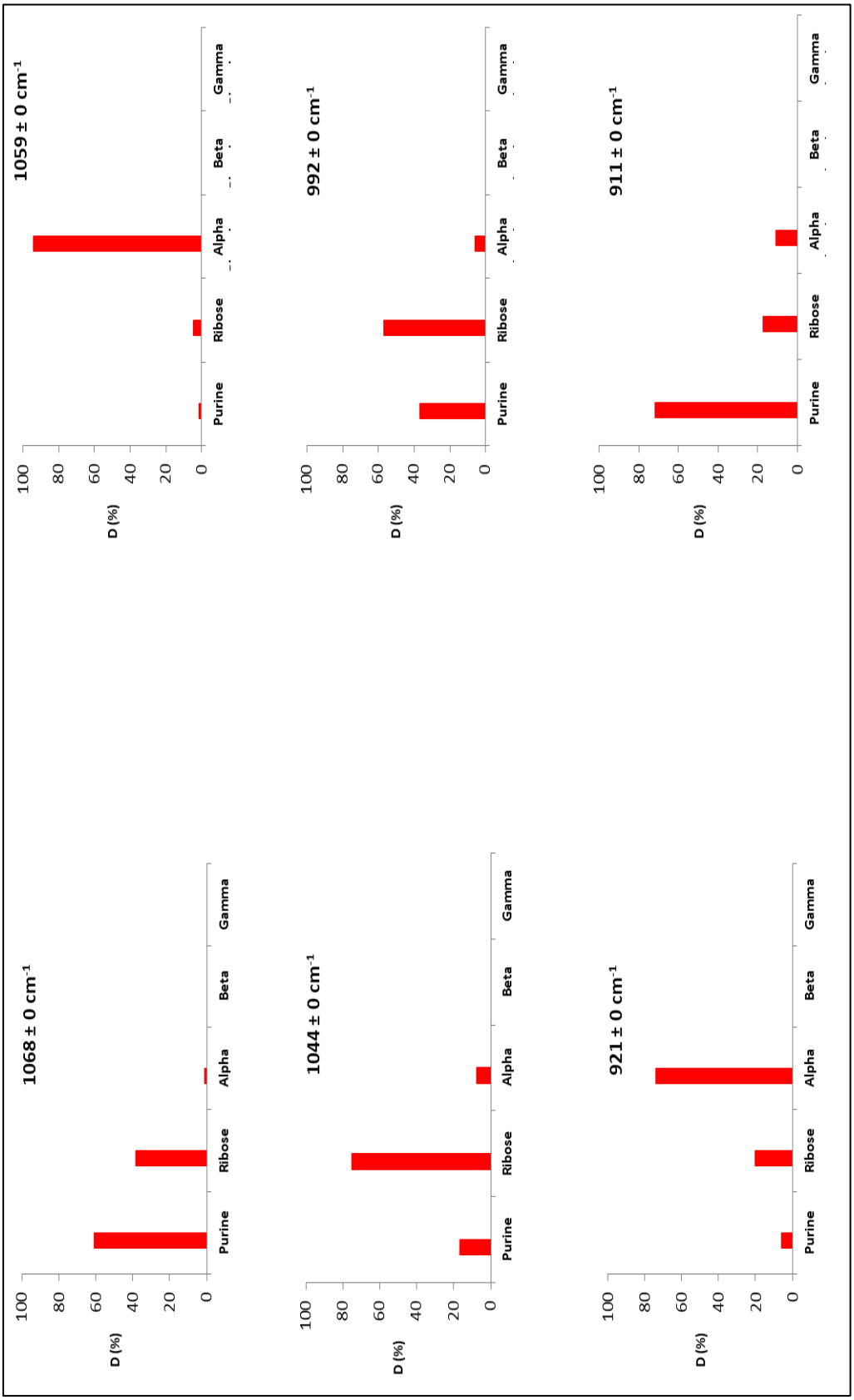

Figure 2.15. Continued.

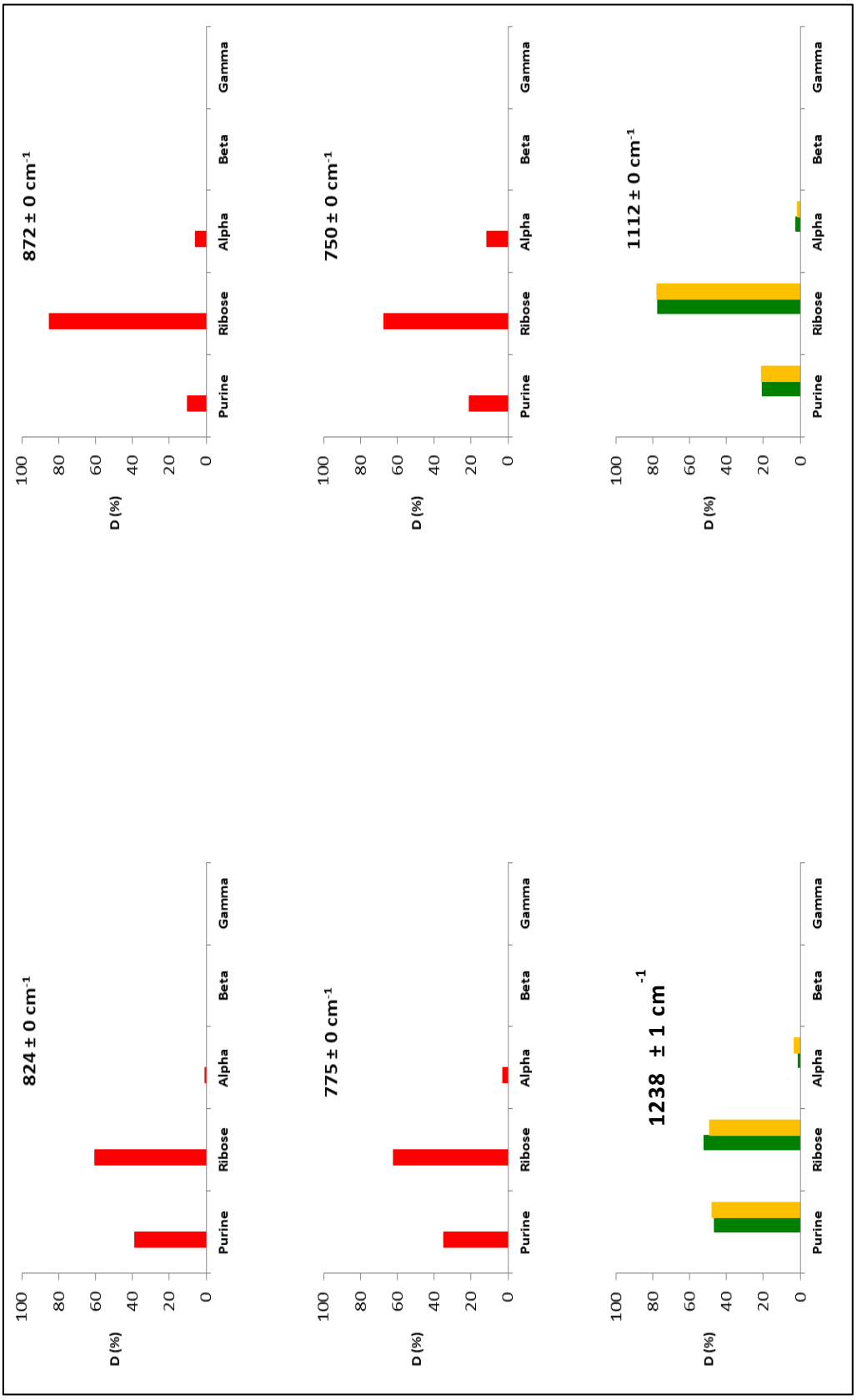

Figure 2.15. Continued.

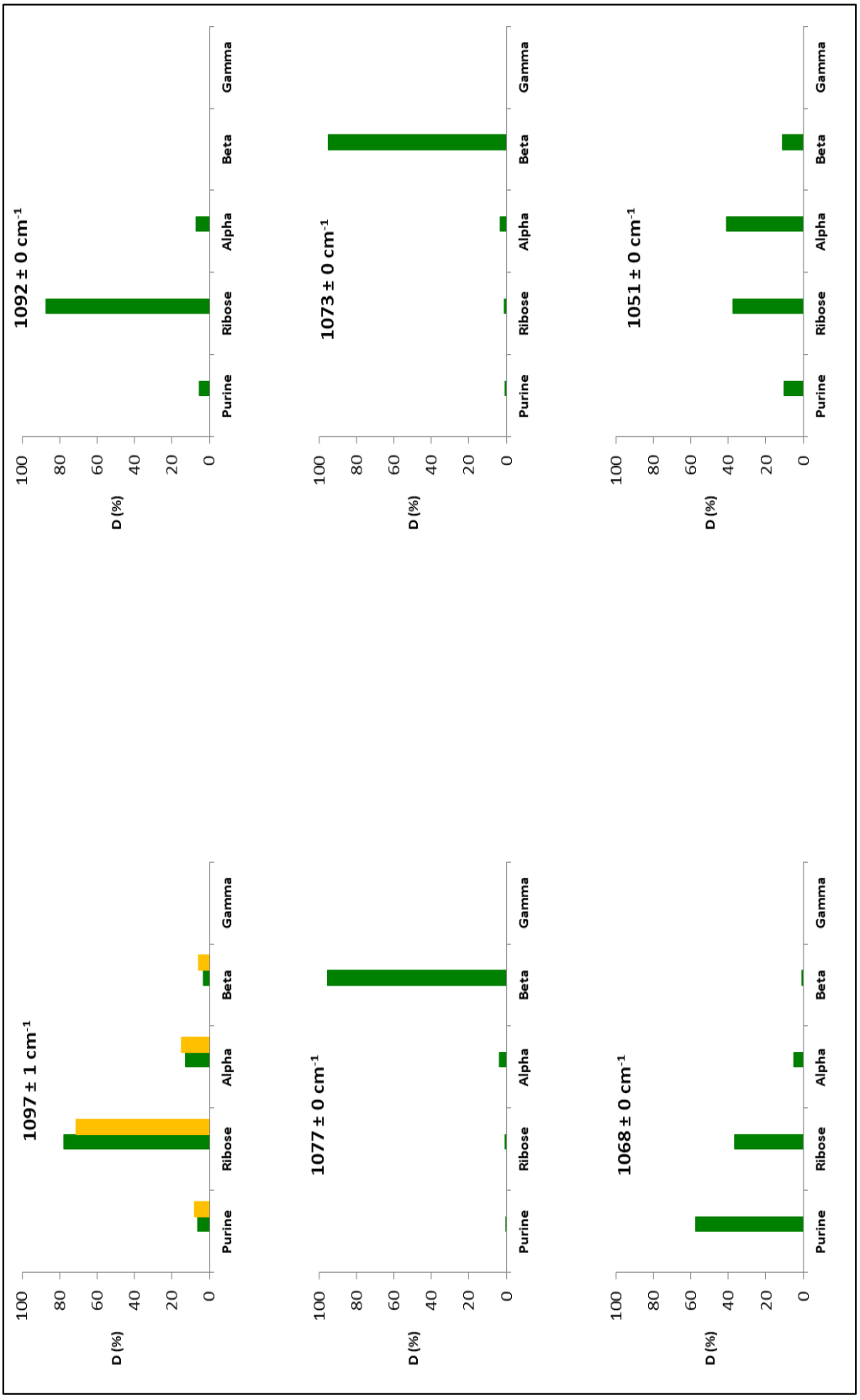

Figure 2.15. Continued.

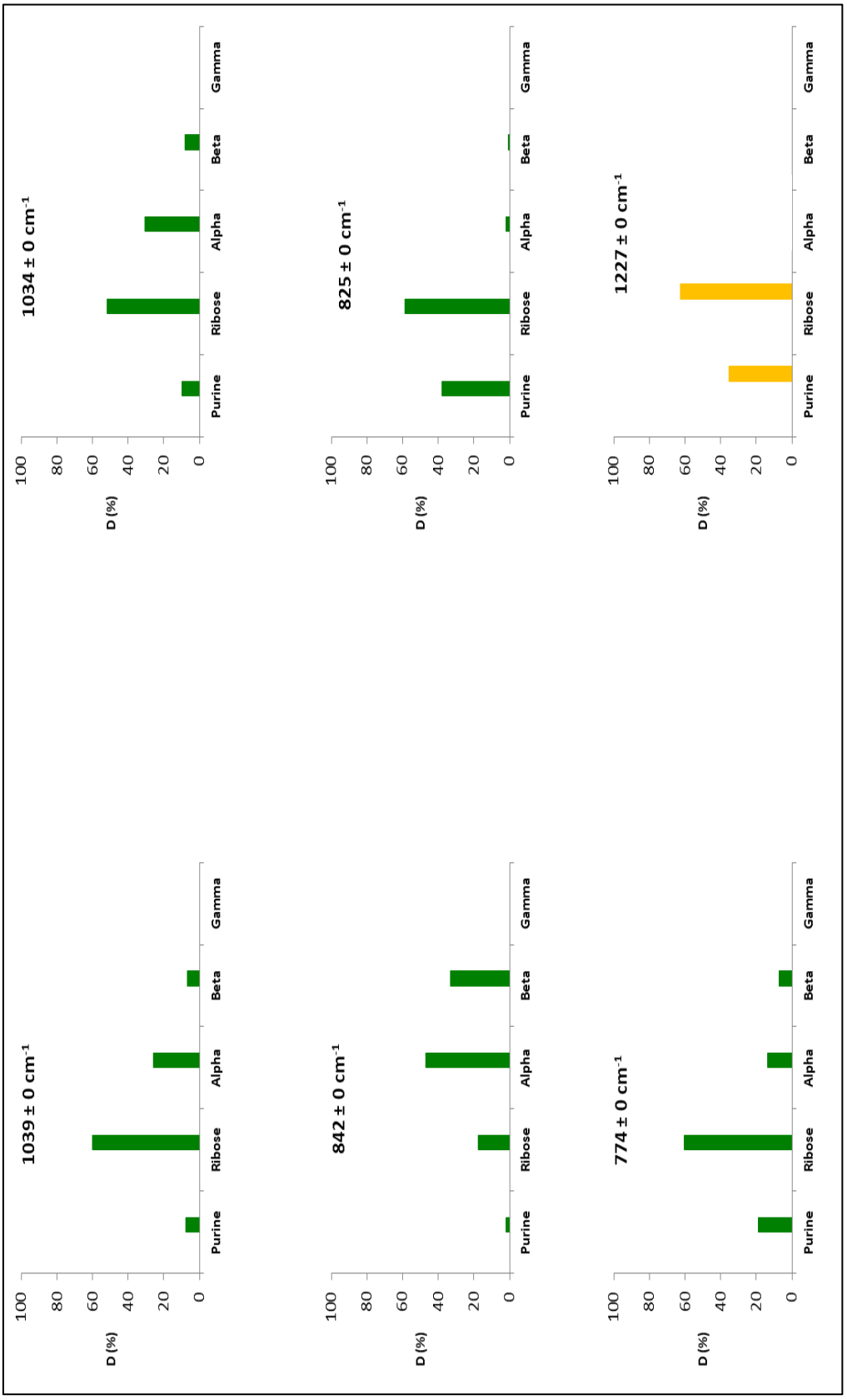

Figure 2.15. Continued.

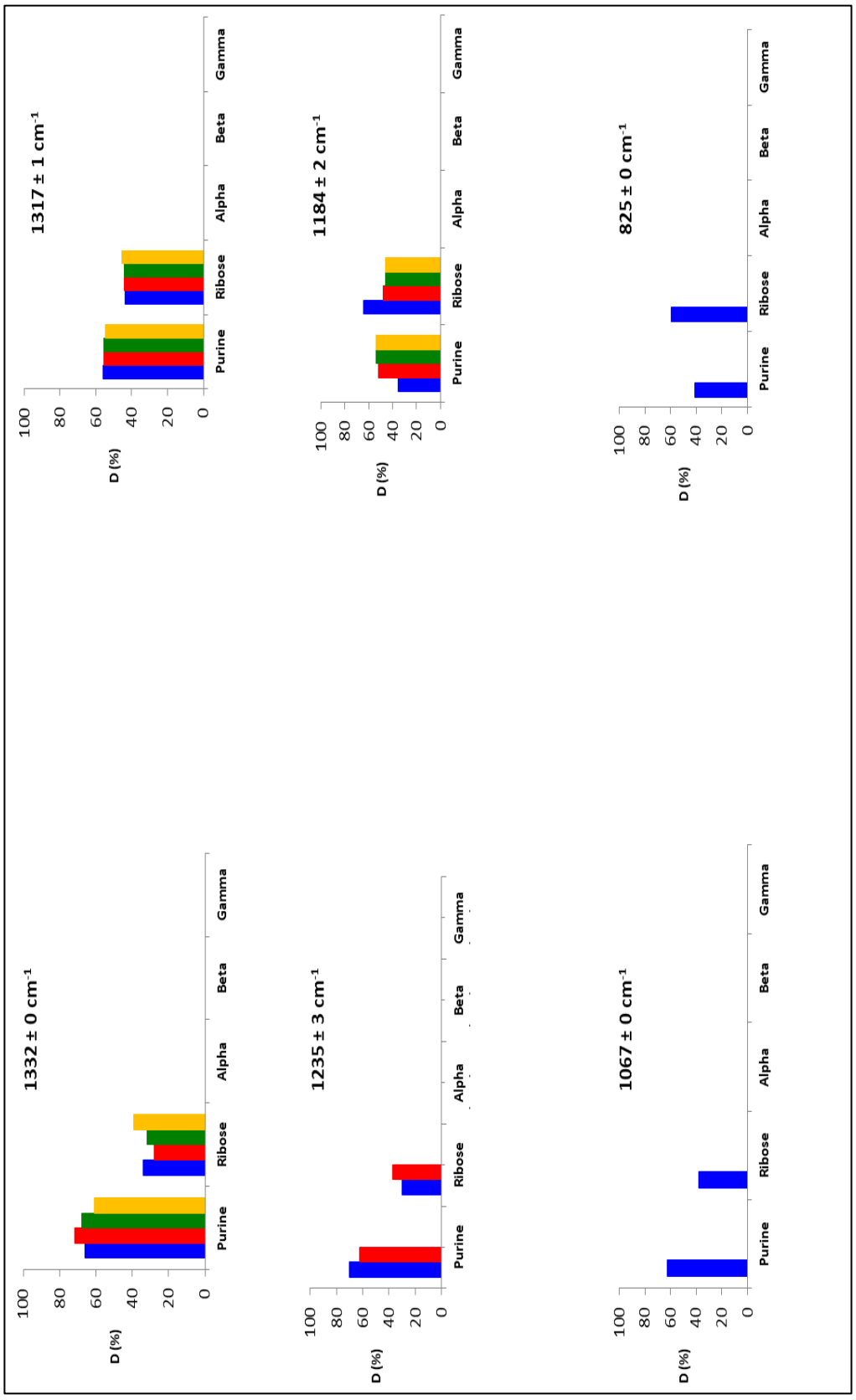

Figure 2.15. Continued.

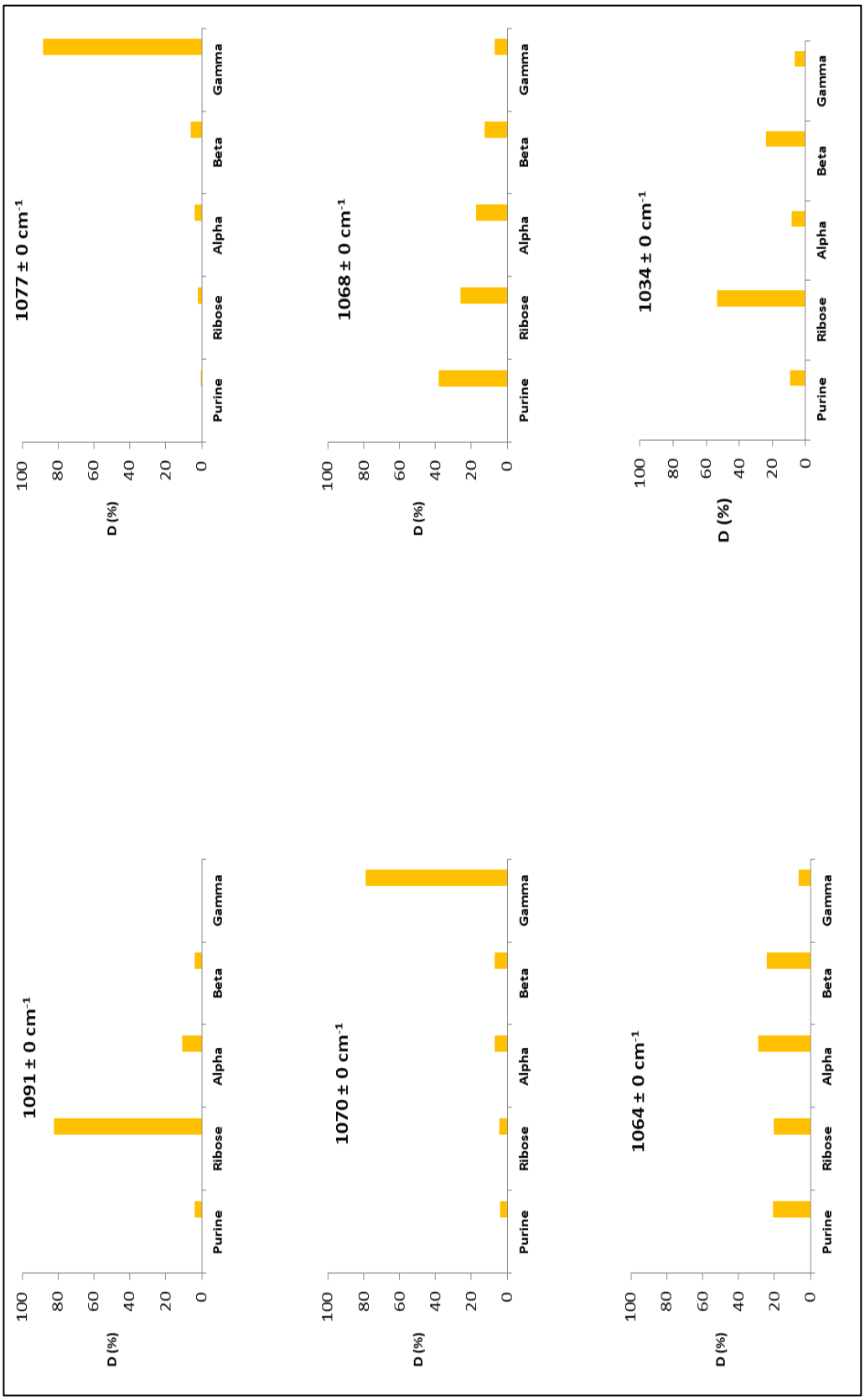

Figure 2.15. Continued.

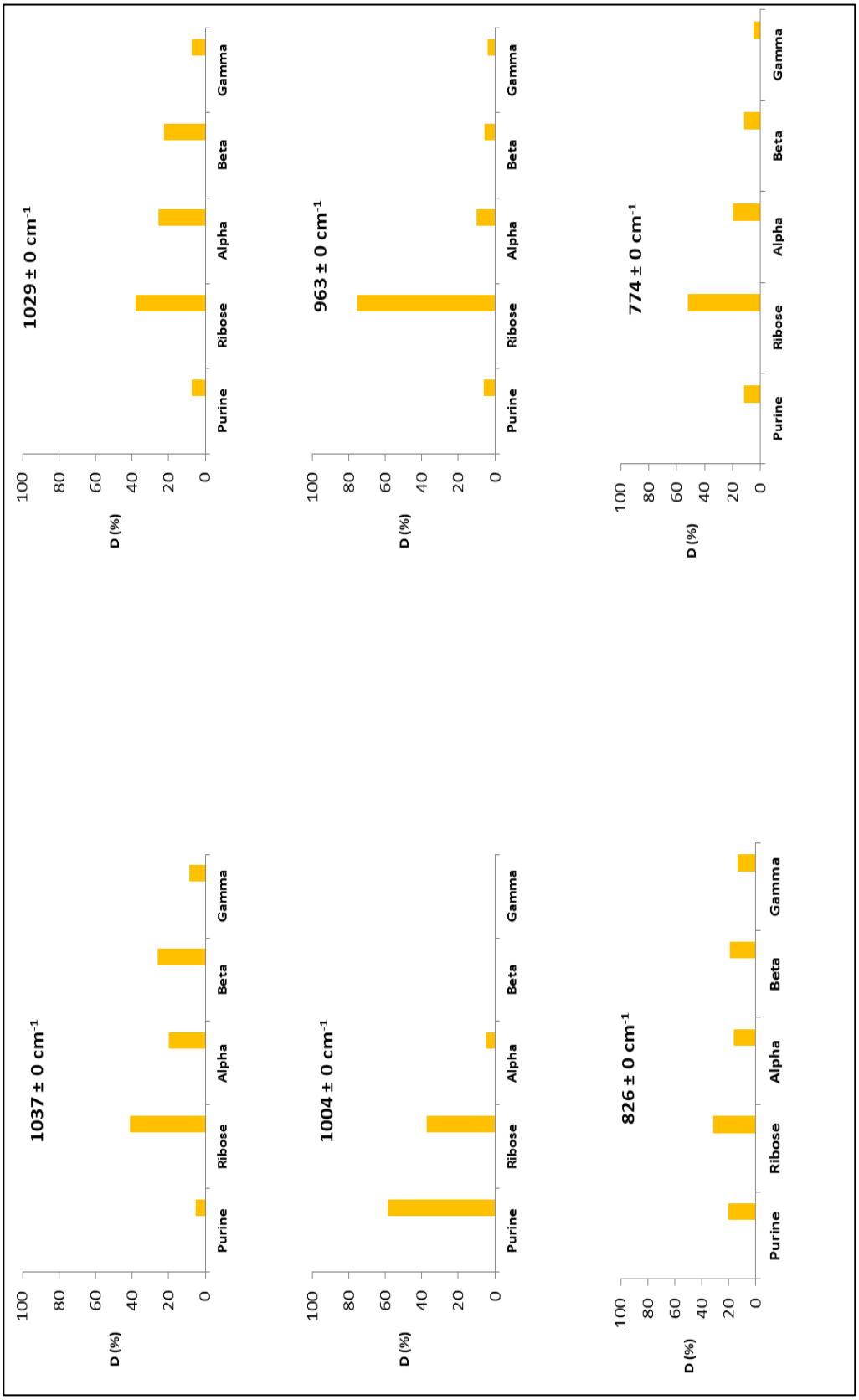

Figure 2.15. Continued.

2.6 References

Aragao, B. J. G. d. and Messaddeq, Y. (2008). 'Peak separation by derivative spectroscopy applied to ftir analysis of hydrolized silica', *Journal of the Brazilian Chemical Society,* 19,pp. 1582-1594.

Ardito, F., Giuliani, M., Perrone, D., Troiano, G. and Muzio, L. L. (2017). 'The crucial role of protein phosphorylation in cell signaling and its use as targeted therapy (Review)', *International Journal of Molecular Medicine,* 40(2),pp. 271-280.

Bango, A., Rastrelli, F. and Saielli, G. (2008). 'Predicting the NMR spectra of nucleotides by DFT calculations: cyclic uridinemonophosphate', *Magnetic Resonance in Chemistry,* 46,pp. 518-524.

Bazydlo, L. A. L., Needham, M. and Harris, N. S. (2014). 'Calcium, magnesium, and phosphate', *Laboratory Medicine,* 45(1),pp. e44-e50.

Becke, A. D. (1993). 'Density-functional thermochemistry. III. The role of exact exchange', *The journal of chemical physics,* 98,pp. 5648-5652.

Black, C. B., Huang, H. W. and Cowan, J. A. (1994). 'Biological coordination chemistry of magnesium, sodium, and potassium-ions - protein and nucleotide-binding sites ', *Coordination Chemistry Reviews,* 135,pp. 165-202.

Blackburn, M. G., Gait, M. J., Loakes, D. and Williams, D. M. (2006). *Nucleic acids in chemistry and biology* (3rd edn.). UK: The Royal Sociaty of Chemistry.

Carmona, P., Huong, P. V. and Gredilla, E. (1988). 'Raman spectra and binding of CuII to purine nucleotides', *Journal of Raman Spectroscopy,* 19(5),pp. 315-319.

Corfu, N. A., Tribolet, R. and Sigel, H. (1990). 'Comparison of the self-association properties of the 5′-triphosphates of inosine (ITP), guanosine (GTP), and adenosine (ATP)', *European Journal of Biochemistry,* 191(3),pp. 721-735.

Dingley, A. J. and Pascal, S. M. (2011). *Biomolecular NMR spectroscopy* (Vol. 3). Netherland: IOS Press.

Fairchild, S. Z., Bradshaw, C. F., Su, W. and Guharay, S. K. (2009). 'Predicting Raman spectra using density functional theory', *Applied Spectroscopy,* 63(7),pp. 733-41.

Frisch, M. J. T., G. W.; Schlegel, H. B.; Scuseria, G. E.; Robb, M. A.; Cheeseman, J. R.; Scalmani, G.; Barone, V.; Mennucci, B.; Petersson, G. A.; Nakatsuji, H.; Caricato, M.; Li, X.; Hratchian, H. P.; Izmaylov, A. F.; Bloino, J.; Zheng, G.; Sonnenberg, J. L.; Hada, M.; Ehara, M.; Toyota, K.; Fukuda, R.; Hasegawa, J.; Ishida, M.; Nakajima, T.; Honda, Y.; Kitao, O.; Nakai, H.; Vreven, T.; Montgomery, J. A., Jr.; Peralta, J. E.; Ogliaro, F.; Bearpark, M.; Heyd, J. J.; Brothers, E.; Kudin, K. N.; Staroverov, V. N.; Kobayashi, R.; Normand, J.; Raghavachari, K.; Rendell, A.; Burant, J. C.; Iyengar, S. S.; Tomasi, J.; Cossi, M.; Rega, N.; Millam, J. M.; Klene, M.; Knox, J. E.; Cross, J. B.; Bakken, V.; Adamo, C.; Jaramillo, J.; Gomperts, R.; Stratmann, R. E.; Yazyev, O.; Austin, A. J.; Cammi, R.; Pomelli, C.; Ochterski, J. W.; Martin, R. L.; Morokuma, K.; Zakrzewski, V. G.; Voth, G. A.; Salvador, P.; Dannenberg, J. J.; Dapprich, S.; Daniels, A. D.; Farkas, Ö.; Foresman, J. B.; Ortiz, J. V.; Cioslowski, J.; Fox, D. J. Gaussian, Inc., Wallingford CT. (2009). 'Gaussian 09, Revision'.

Gong, B., Chen, J. H., Yajima, R., Chen, Y., Chase, E., Chadalavada, D. M., Golden, B. L., Carey, P. R. and Bevilacqua, P. C. (2009). 'Raman crystallography of RNA', *Methods,* 49(2),pp. 101-11.

Gorelik, V. S., Kaminskii, A. A., Melnik, N. N., Sverbil, P. P., Voinov, Y. P., Zavaritskaya, T. N. and Zlobina, L. I. (2008). 'Spontaneous Raman scattering spectra of ADP and DADP crystals in different polarization schemes', *Journal of Russian Laser Research,* 29(4),pp. 357-363.

Graham, H. C. and Williams, R. J. P. (1991). 'The roles of ADP^{2-} and Mg^{2+} in control steps of phosphoglycerate kinase', *European Journal of Biochemistry,* 197(1),pp. 81-91.

Hercend, C., Bauvais, C., Bollot, G., Delacotte, N., Chappuis, P., Woimant, F., Launay, J.-M. and Manivet, P. (2011). 'Elucidation of the ATP7B N-domain Mg^{2+}-ATP coordination site and Its allosteric regulation', *PLoS One,* 6(10),pp. e26245.

Iyandurai.N, Senthil.K and Sarojini.R (2009). 'FT-Raman spectroscopy of heavy metal-nucleotide complexes', *Asian Jornal of Chemistry,* 21(6),pp. 4241-4245.

Jai, E. A. and Horowitz, P. M. (1999). 'Nucleotide and Mg^{2+} induced conformational changes in GroEL can be Detected by Sulfhydryl labeling', *Journal of Protein Chemistry,* 18(3),pp. 387-396.

Jiang, L. and Mao, X.-A. (2001). 'NMR evidence for Mg(II) binding to N1 of ATP', *Spectrochimica Acta Part A: Molecular and Biomolecular Spectroscopy,* 57(8),pp. 1711-1716.

Jimenez-Hoyos, C. A., Janesko, B. G. and Scuseria, G. E. (2008). 'Evaluation of range-separated hybrid density functionals for the prediction of vibrational frequencies, infrared intensities, and Raman activities', *Physical Chemistry Chemical Physics,* 10(44),pp. 6621-6629.

Kopecky, V., Jr., Mojzes, P., Burda, J. V. and Dostal, L. (2002). 'Raman spectroscopy study of acid-base and structural properties of 9-[2-(phosphonomethoxy)ethyl]adenine in aqueous solutions', *Biopolymers,* 67(4-5),pp. 285-288.

Lee, C., Yang, W. and Parr, R. G. (1988). 'Development of the Colle-Salvetti correlation-energy formula into a functional of the electron density', *Physical Review. B, Condensed Matter and Materials Physics,* 37(2),pp. 785-789.

Lorenz-Fonfria, V. A. and Padros, E. (2005). 'Maximum entropy deconvolution of infrared spectra: use of a novel entropy expression without sign restriction', *Applied Spectroscopy,* 59(4),pp. 474-86.

Miertus, S., Scrocco, E. and Tomasi, J. (1981). 'Electrostatic interaction of a solute with a continuum. A direct utilizaion of AB initio molecular potentials for the prevision of solvent effects', *Chemical Physics,* 55(1),pp. 117-129.

Miles, J. (2014). R squared, adjusted R squared. *Wiley StatsRef: Statistics Reference Online.* John Wiley and Sons, Ltd.

Naaman, R. and Vager, Z. (2012). *The structure of small molecules and ions*. New York: Springer Science and Business Media.

Ostovarpour, S. and Blanch, E. W. (2012). 'Phosphorylation detection and characterization in ribonucleotides using Raman and Raman optical activity (ROA) spectroscopies', *Applied Spectroscopy,* 66(3),pp. 289-293.

Rimai, L., Cole, T., Parsons, J. L., Hickmott, J. T. and Carew, E. B. (1969). 'Studies of Raman spectra of water solutions of adenosine tri-, di-, and monophosphate and some related compounds', *Biophysical Journal,* 9(3),pp. 320-329.

Smith, E. and Dent, G. (2005). Introduction, basic theory and principles, in Ewen, S. and Geoffrey,D.(eds.) *Modern Raman spectroscopy – A practical approach.* Chichester: John Wiley and Sons, Ltd,pp.1-20

Szabo, J., Varga, A., Flachner, B., Konarev, P. V., Svergun, D. I., Zavodszky, P. and Vas, M. (2008). 'Communication between the nucleotide site and the main molecular hinge of 3-Phosphoglycerate Kinase', *Biochemistry,* 47(26),pp. 6735-6744.

Takeuchi, H., Murata, H. and Harada, I. (1988). 'Interaction of adenosine 5'-triphosphate with Mg^{2+}: vibrational study of coordination sites by use of 18O-labeled triphosphates', *Journal of the American Chemical Society,* 110(2),pp. 392-397.

ULC, C. C. G. (2013). *Molecular operating environment (MOE)* [Online]. Canada. Available: http://www.chemcomp.com/index.htm [Accessed 08 2017].

Watson, H. C. and Gamblin, S. J. (1985). 'The magnesium protein interaction in nucleotide complexes of phos-phoglycerate kinase', *Journal of Biosciences,* 8(1),pp. 499-506.

Chapter 3: Spectroscopic Characterisation of Guanosine Nucleotides and their Interaction with Magnesium Using Raman, Raman Optical Activity and Density Functional Theory Analysis

Contributing authors and their roles:

Omer Azher is the main author who proposed the idea of supporting the Raman measurements with DFT calculations and generated the concept of the averaged atom displacement approach. Alex L. Wilson contributed to the DFT calculations. Shaun T. Mutter contributed to preliminary DFT data. Paul L. A. Popelier, Ewan W. Blanch and Jonathan P. Waltho contributed to this work through supervision and guidance

3.1 Abstract

Phosphorylation is a metabolic process by which a phosphate group is transferred enzymatically from a donor to an acceptor. Often the phosphate donor is ATP or GTP, the latter often undergoing enzyme-catalysed hydrolysis to GDP where the acceptor is water. The transfer of phosphate between guanosine nucleotides relies on the binding of magnesium ions to form nucleotide-Mg^{2+} complex. This binding can exert substantial conformational changes in the nucleotides, enzymes or substrates. In the absence of enzymes, the role of magnesium ions in coordinating guanosine nucleotides remains elusive. This study applies Raman spectroscopy, peak deconvolution, Density Functional Theory (DFT) and Raman Optical Activity to characterise guanosine nucleotides and compare their diagnostic Raman bands with those observed for adenosines mono-, di-, and triphosphates. The study also investigates the impact of magnesium ion binding and different pH values on the spectral profile of guanine mono-, di-and tri- phosphate in aqueous solution. The effects of Mg^{2+} and pH are further supported by ^{31}P NMR measurements, which are used to determine the protonation state of the phosphate groups. The results provide a sensitive and diagnostic approach to identify the primary and secondary marker bands of different forms of guanosine nucleotides and these bands are described using DFT-derived assignment and an averaged atom displacement.approach. Mg^{2+} binding to guanosine nucleotides was consistent with a model where it coordinates both α- and β- phosphate groups of 5'-GDP and β- and γ-phosphate groups of 5'-GTP in aqueous solution at pH 7.0. Acidification exerted a substantial impact on the Raman spectra of phosphorylated forms of guanosine. However, the magnesium binding sites remain unchanged at pH 5-8.

3.2 Introduction

Guanosine nucleotides are essential molecules for different cellular activities. In addition to their role as one of the basic units of DNA and RNA molecules, they are also involved in signal transduction, energy transfer, coenzyme synthesis and allosteric regulation (Brosh *et al.*, 1992; Nelson *et al.*, 2008). The activity of the nucleotide mono-, di- and tri phosphates during phosphorylation reaction depends largely on the binding of metal ions, most importantly magnesium (Anastassopoulou and Theophanides, 1995). The binding of the metal cation to the nucleotide helps to stabilise the molecule via neutralising its negatively charged phosphate groups (Anastassopoulou and Theophanides, 2002). This can result in substantial conformational changes of the nucleotide, the enzyme or the substrate (Rudack *et al.*, 2012). The role of Mg ions in coordinating the nucleotide and the modes of interaction are controversial (de la Fuente *et al.*, 2004). Therefore, studying the dynamic behaviour of the nucleotide-Mg complex and the mode of interaction in aqueous solution at physiological pH is important for further understanding of the role of these metal ions and their influence on the structure of guanosine nucleotides, which in turn affect the catalytic activity of various kinase enzymes.

The use of X-ray crystallography and NMR spectroscopy as powerful tools for studying the properties of nucleotides and nucleic acids has provided rich information about the structure and properties of these molecules (Watson and Gamblin, 1985; Dingley and Pascal, 2011). However, these techniques are associated with some experimental limitations when examining the nucleotides in aqueous environments.

Solution NMR methods, for instance, experience an irregular distribution of the proton density in the ribonucleotide molecule (Ulyanov *et al.*, 2006). Other challenges of solution NMR include the preparation of the target analyte in deuterated solvents and the large volume of sample required for the measurements (Gong *et al.*, 2009; Ostovarpour and Blanch, 2012). Raman spectroscopy is a powerful tool for studying the structural conformations of different biological molecules, such as proteins,

enzymes, nucleotides and nucleic acids (Black *et al.*, 1994; Ostovarpour and Blanch, 2012). The technique is characterized by its high sensitivity to minor structural changes in addition to its suitability to be used for aqueous samples since water molecules generate weak Raman signals (Smith and Dent, 2005). The measurements of the Raman technique can be also made using low volumes of sample (~100 microliter) without the need for further chemical modification of the target analyte.

Raman Optical Activity (ROA) is a Raman-based vibrational spectroscopic technique that relies on detecting the minor Raman scattering differences from chiral molecules (Nafie, 2011). ROA is considered to be a more sensitive technique than the corresponding Raman for studying the structural differences of various biological molecules, such as nucleic acids and proteins, carbohydrates and viruses. The technique was previously used to probe a variety of conformational changes of nucleic acids, such as the orientation of the ribose ring and the nitrogenous base around the glycosidic bond (Blanch *et al.*, 2003).

Density functional theory (DFT) is a computational modelling technique which can be applied for the prediction and assignment of the Raman vibrational bands of different molecules (Balbuena and Seminario, 1995; Hanlon *et al.*, 2000; Koch and Holthausen, 2001). Combining Raman measurements and DFT calculations can enhance our understanding of the dynamic structure of guanosine mono-, di-, and tri- phosphates and the conformational changes associated with the binding of magnesium. The use of ROA along with the Raman spectroscopy can offer further details about the structural differences between guanosine nucleotides in aqueous solution. The application of Raman, ROA and DFT analysis can expand our knowledge about mechanism of action of many nucleotide binding proteins and their structural variations in different conditions.

The aim of this study is to use Raman, ROA and NMR to characterize the structure of the guanosine mono, di- and triphosphate molecules in aqueous solution and investigate the impact of the binding of the magnesium ions and pH on their Raman profiles.

3.3 Material and methods

3.3.1 Chemicals

Samples of guanosine, 5'- guanosine monophosphate sodium salt hydrate (5'-GMP), 5'- guanosine diphosphate sodium salt (5'-GDP), 5'- guanosine triphosphate sodium salt hydrate (5'-GTP), magnesium chloride and deuterium oxide (99.9 %) were purchased from Sigma-Aldrich Ltd.

3.3.2 Sample preparation

Samples of guanosine, 5'-GMP, 5'-GDP and 5'-GTP were prepared with a concentration of 50 mM in 0.5 ml deionised water. Metal guanosine nucleotide complexes were prepared by adding 0.5 ml of 100 mM guanosine nucleotide and 0.5 ml of 200 mM $MgCl_2$. For each guanosine nucleotide, three biological replicates and four technical replicates were made for the Raman measurements and three replicates were made for the ROA analysis. Samples are prepared at pH 7.0 (±0.1) using 1M NaOH (w/v) and 2.3 % (v/v) HCl solutions and centrifuged at 9500 g for 5 minutes to exclude contaminants. 100 µL of each nucleotide sample was transferred to a quartz microflourescence cell for Raman analysis.

3.3.3 Variation of pH

Magnesium bound guanosine nucleotides were prepared at pH 5.0, 6.0, 7.0 and 8.0. The pH measurements were adjusted using a Hanna pH 209-laboratory pH meter with accuracy of (±0.05) pH and a resolution of 0.01 pH units.

3.3.4 NMR samples

Each guanosine nucleotide was prepared with a concentration of 50 mM in 0.5 ml of 99.9 % deuterated water (D_2O). Guanosine-Mg samples were prepared adding 0.5 ml of 100 mM guanosine nucleotide and 0.5 ml of 200 mM $MgCl_2$. Samples were transferred to a 5 mm NMR tube and 1µL of 0.5 % (w/w) of tetramethylsilane was added to each sample.

3.3.5 Raman measurements

The Raman and ROA measurements were applied using a ChiralRaman spectrometer (BioTools Inc., Jupiter FL, USA). The set-up of the instrument includes: Laser wavelength of 532 nm, spectral resolution of 7 cm^{-1}, power at the laser head of 1.20 W, length of illumination period was 1.029 seconds, total data acquisition times of 0.166 hrs. Data analysis was carried out using MATLAB R2013a software that includes an inbuilt Raman toolbox. Data were analysed using MATLAB R2013a software that includes an inbuilt Raman and ROA toolbox.

3.3.6 Raman data analysis and peak deconvolution

Matlab software version R2013a was used to process the averaged Raman spectra. In this software, the Raman data for each Guanosine nucleotide were summed and baselined then plotted using Origin 8.5 software. A peak deconvolution technique was performed to identify the overlapped peaks in the broaden areas of the Raman spectra (Hobro *et al.*, 2007; Szabo, 2008). Origin 8.5.1 software was also used for deconvolution and the Gaussian function was selected for deconvolution modelling. The second derivative was obtained in in each case to decrease the bandwidth and enhance the resolution of the overlapped peaks. The quality of the fitting was assessed by calculating adjusted r square values. Peak deconvolution with adjusted r square values near 1 (~ 0.95) indicated the goodness of the data (Miles, 2014). A more complete analysis of the deconvoluted peaks is provided in appendix 3. The results for the number of component peaks were verified using the DFT analysis of the same spectral region(s).

3.3.7 NMR measurements

^{1}H NMR measurements of the guanosine nucleotides at 300K were carried out using a Bruker Avance III 400 MHz spectrometer. To test for the saturation of binding of magnesium to the nucleotides, increasing concentrations of $MgCl_2$ were added up to 500 mM at pH 7.0. The guanosine, mono-, di-, and triphosphate concentrations were 50 mM, dissolved in D_2O. ^{31}P NMR measurements were also carried out for each

nucleotide and nucleotide-Mg complex over the pH range 5.0 to 8.0, using ^{1}H decoupling. Data were processed using TopSpin 3.2 software. Spectra were referenced using internal tetramethylsilane. A complete illustration of the NMR spectra for guanosine nucleotides is provided in appendix 3.

3.3.8 Density functional theory calculations

Gaussian09 package was applied for DFT calculations (Frisch, 2009). Molecular structures of guanosine, 5'-GMP, 5'-GDP and 5'-GTP were constructed manually and a stochastic conformational search was carried out in MOE to identify the lowest energy structural orientations. The lowest energy conformers were optimised in Gaussian09 at B3LYP/6-311+G (d,p)(Becke, 1993; Naaman and Vager, 2012). The calculations of the Raman frequencies and intensities were achieved at the same level of theory for geometry optimisation. The polarisable continuum model (PCM) was used to implicitly simulate the presence of solvent in the systems. Visualisation of vibrational modes and generation of Raman spectra was carried out using GaussView 5(Lee *et al.*, 1988; Becke, 1993; Luque *et al.*, 2001).

3.3.9 Analysis of vibrational modes

Visualisation of vibrational modes and the generation of Raman spectra were carried out using GaussView 5(Lee *et al.*, 1988; Becke, 1993; Luque *et al.*, 2001). DFT-derived vibrations for each guanosine derivative were analysed by measuring the displacement of the individual atoms within each vibrational mode and classified according to which atoms were affected to the greatest extent (Figure S3-1). Quantification of the relative displacement of each atom in every computed vibration for each 5'-GMP, 5'-GDP and 5'GTP allows for the construction of a 'vibrational profile' for every computed vibration for each guanosine-based structure. For example, GTP consists of five readily definable groups: purine ring, ribose ring, α-phosphate, β-phosphate and γ-phosphate. Summation of the relative atomic displacements in each group in a particular vibration allows the quantification of the relative contributions to overall molecular displacement from each group.

Hence, vibrations are described as, for example, comprising 84 % ribose ring and 16 % purine ring contributions. The assignment of DFT-derived Raman bands to the experimentally observed modes is proposed on the basis of both the relative frequency and intensity of vibrations computed using DFT. A more complete analysis of the proposed assignment of these bands is provided in appendix 1 (Table 1.2).

3.4 Results

The Raman spectra for guanosine, 5'-guanosine monophosphate (5'-GMP), 5'-guanosine diphosphate (5'-GDP) and 5'-guanosine triphosphate (5'-GTP) showed general spectral similarities above 1150 cm^{-1} and below 760 cm^{-1} (Figures 3.1, 3.2). However, The Raman spectrum for guanosine revealed multiple variations in the frequency of their Raman bands compared to its phosphate derivatives. These variations are inconsistent with the DFT calculations nor with the Raman spectra for adenosine and its phosphate derivatives, which showed comparable Raman spectra above 1150 cm^{-1} and below 760 cm^{-1} (Figure 2.1). The reason behind these spectral differences between guanosine and its phosphate derivatives is unknown but it could be related to the self-aggregation of the guanosine molecules at the time of the Raman measurements. Unlike 5'-ADP and 5'-ATP, the results of the saturation curves of 5'-GDP and 5'-GTP reflected a very complicated series of binding equilibria with magnesium ions.

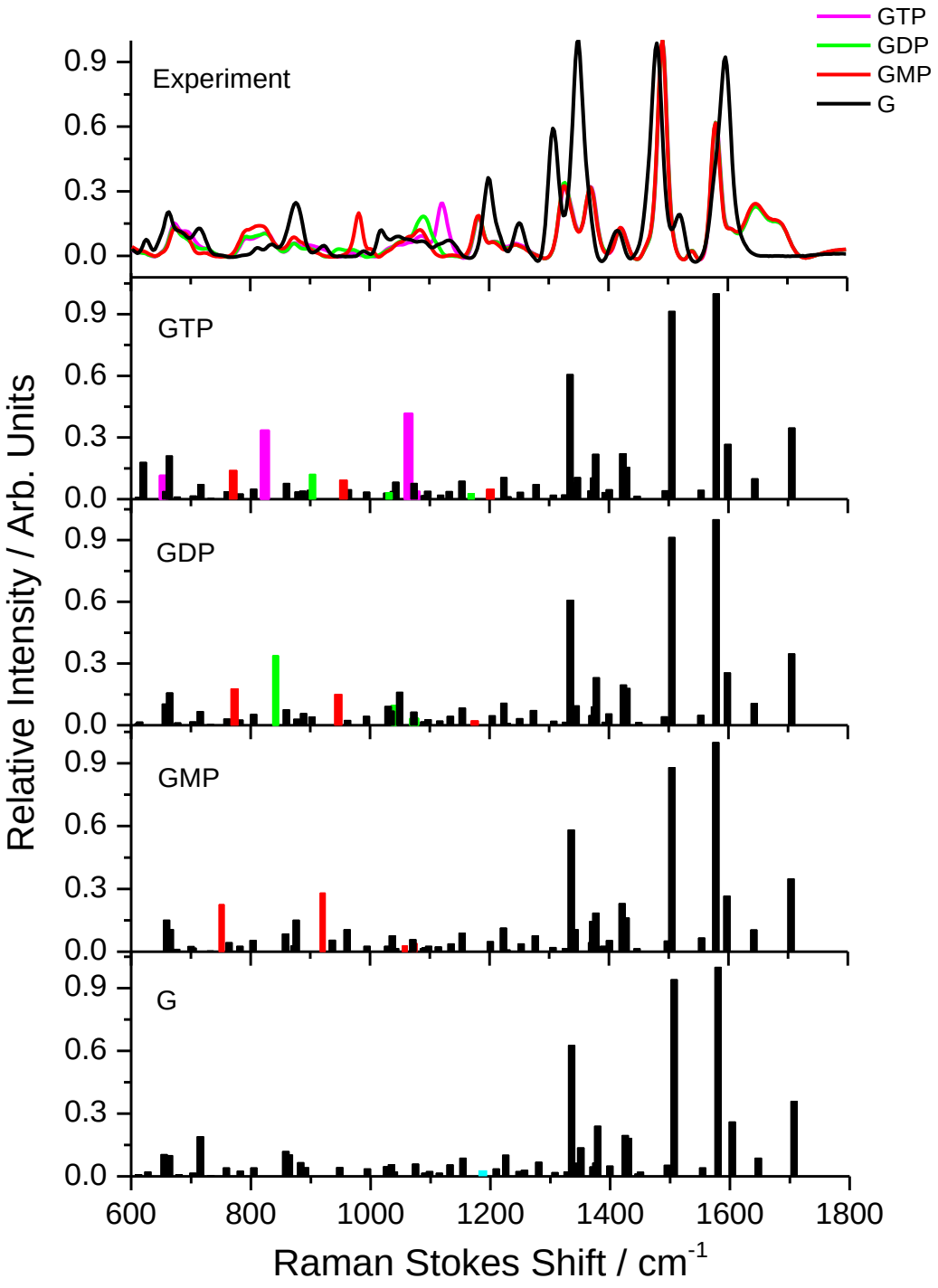

Figure 3-1. Experimental (top) and DFT calculated (bottom) Raman spectra for guanosine (G), 5'- guanosine monophosphate (GMP), 5'- guanosine diphosphate (GDP) and 5'- guanosine triphosphate (GTP) at pH 7.0. The experimental Raman spectrum for guanosine differs from its phosphate derivatives. This is inconsistent with the DFT calculation. The reason behind this is unknown but it could be due to self-aggregation of guanosine molecules in aqueous solution.

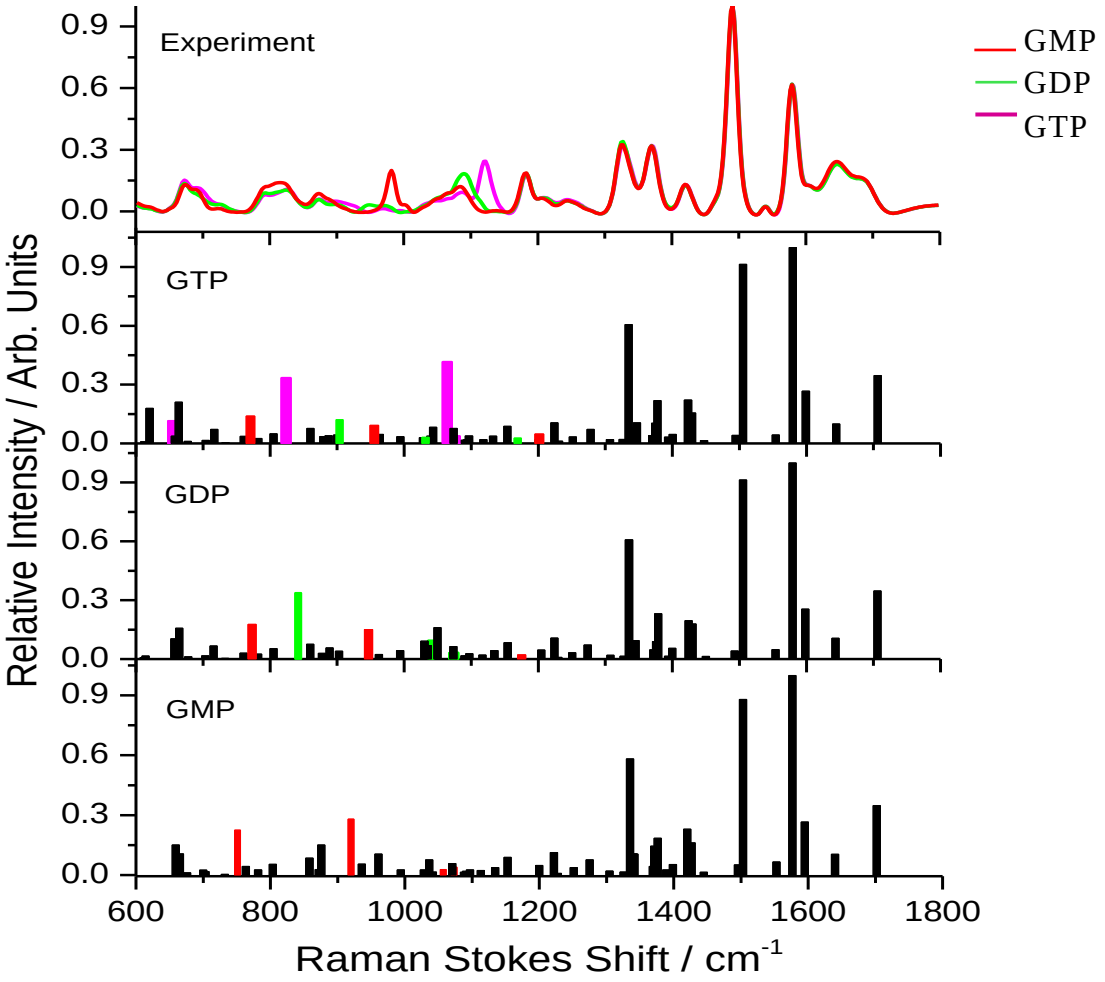

Figure 3.2 Experimental (top) and DFT calculated (bottom) Raman spectra for 5'-guanosine monophosphate (GMP), 5'- guanosine diphosphate (GDP) and 5'-guanosine triphosphate (GTP) at pH 7.0. The experimental and DFT spectra showed similar intensities and frequencies above 1150 cm^{-1} and below 760 cm^{-1} regions. The main spectral differences are observed at 760-1150 cm^{-1} region.

3.4.1 Raman spectra for guanosines vs adenosines

The chemical structure of the nitrogenous base of guanosine differs from that of the adenosine by the presence of (C=O) and (NH) groups. The amino group (NH_2) of the guanosine's base is attached to C2' compared to C6' of its adenosine analogue (Figures 3.3, 3.4). The Raman profile for 5'-GMP, 5'-GDP and 5'-GTP recorded over the range of 600-1800 cm^{-1} showed some spectral variations as well as similarities between guanosine mono-, di- and tri-phosphates and their adenosine analogues (Figure 3.5). For example, the strong Raman band detected at 1490 cm^{-1} for 5'-GMP, 5'-GDP and 5'-GTP is absent in 5'-AMP, 5'-ADP and 5'-ATP. The doublet identified in the guanosine nucleotides at 1370 and 1327 cm^{-1} is replaced by a triplet in adenosine molecules at 1312, 1342 and 1382 cm^{-1}. The sharp Raman band at 734 cm^{-1} for adenosine nucleotides is shifted in all phosphate containing guanosines to 672 cm^{-1} (Figures 3-5).

The region at 760-1200 cm^{-1} is characterised by general similarities in the Raman features for adenosine and guanosine nucleotides (Figure 3.4). Deconvolution of the overlapped regions at, 760-870 and 1020-1120 cm^{-1}, for guanosine derivatives showed some similarities as well as variations compared to the same regions for adenosine nucleotides. The deconvoluted regions and the spectral variations between guanosine and adenosine molecules are illustrated in appendix 2.

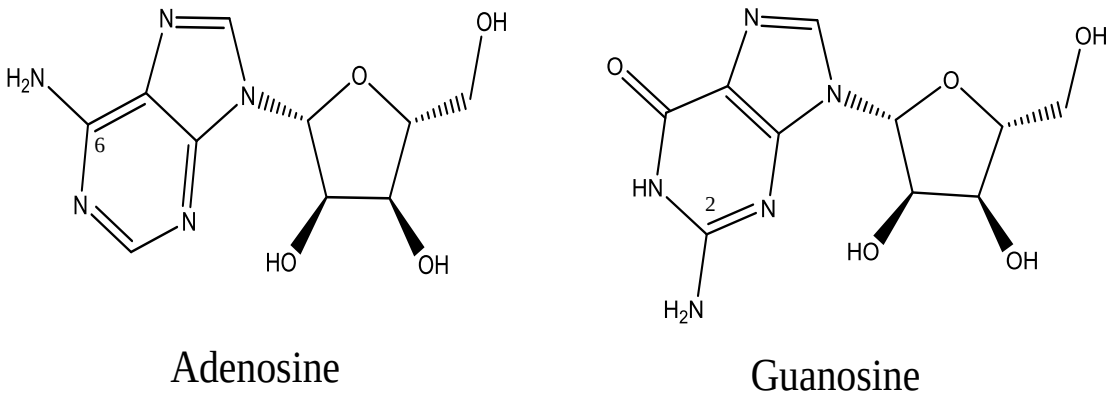

Figure 3.3 The structural differences of the nitrogenous bases of the purine nucleosides adenosine and guanosine

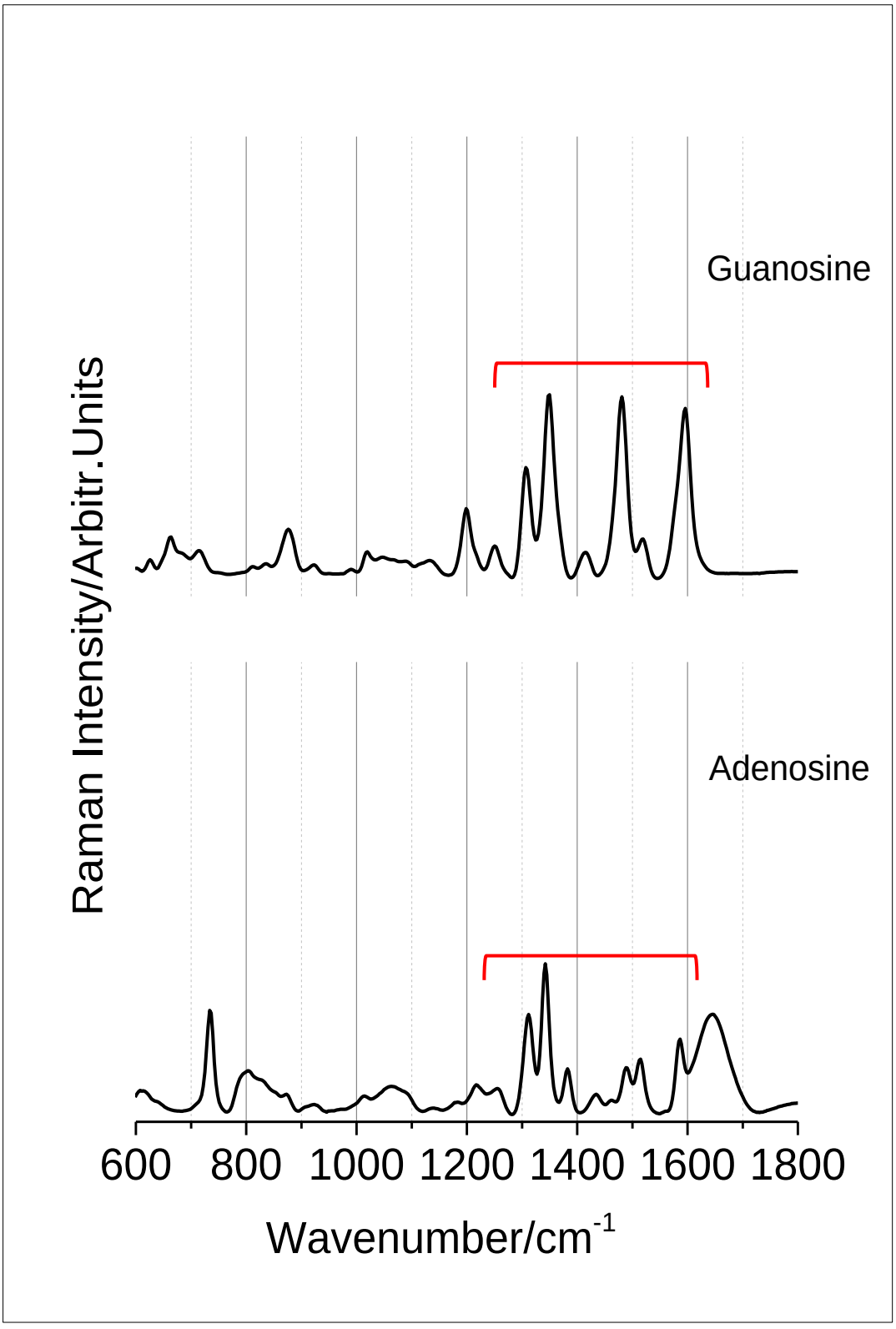

Figure 3.4. The Raman spectra for guanosine adenosine at pH 7.0.

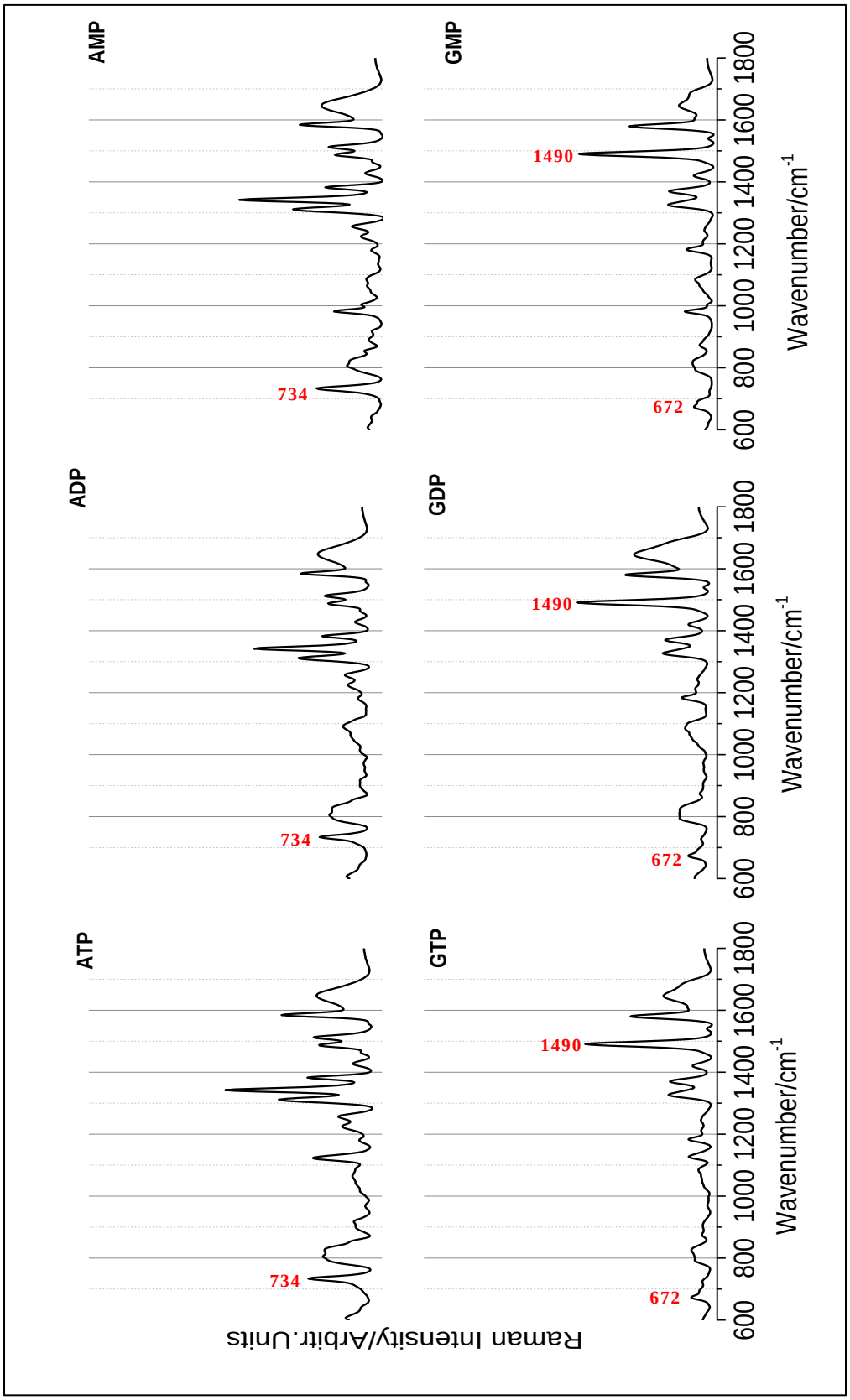

Figure 3.5. The Raman spectra for 5'- adenosine monophosphate (5'-AMP), 5'- adenosine diphosphate (5'-ADP) 5'- adenosine triphosphate (5'-ATP), 5'- guanosine monophosphate (5'-GMP), 5'- guanosine diphosphate (5'-GDP) and 5'- guanosine triphosphate (5'-GTP).

3.4.2 Guanosine mono-, di- and tri-phosphates, without Mg^{2+}

The Raman spectra for guanosine 5'-mono-, di- and tri- phosphates, in the absence of magnesium, were recorded over the range from 600-1800 cm^{-1} at pH 7.0 (Figure 3.2). The Raman spectra of all guanosine nucleotides are comparable above 1150 cm^{-1} and below 760 cm^{-1}. The major spectral alterations between the guanosine phosphate molecules are mainly appeared in the region at 760-1150 cm^{-1} (Figures 3.6-3.8).

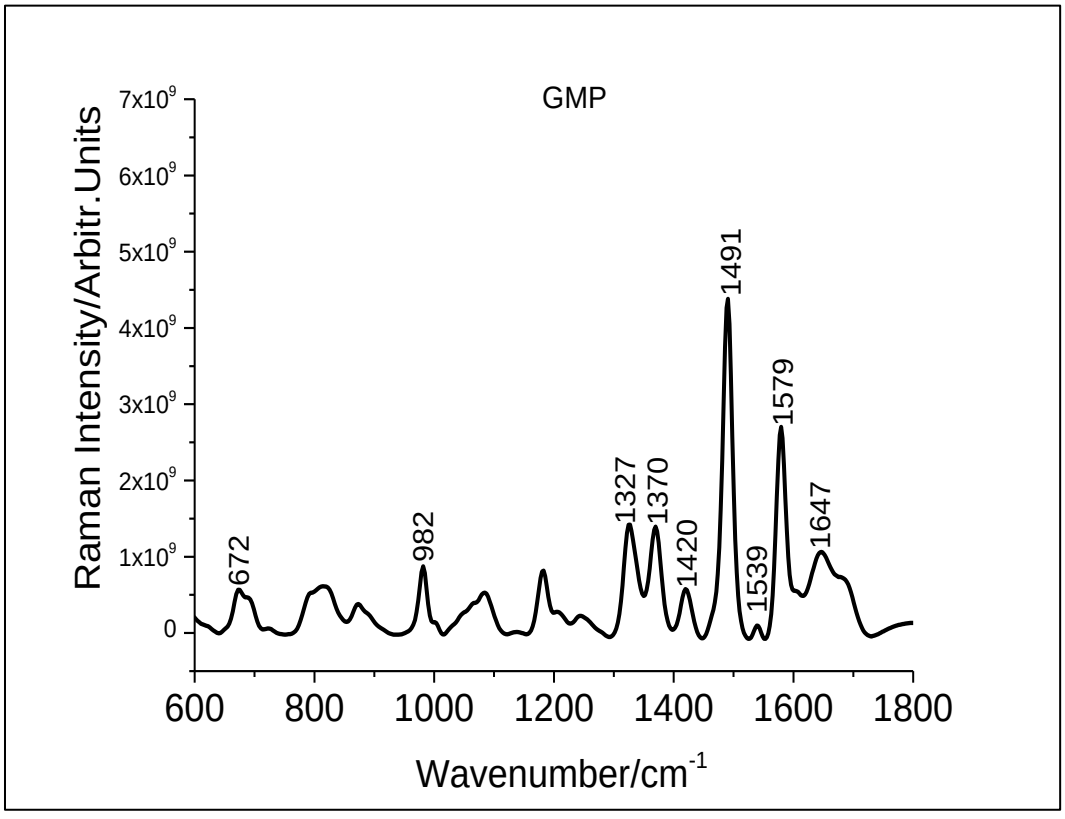

Figure 3.6. Raman spectrum for 5'-guanosine monophosphate (GMP) at pH 7.0.

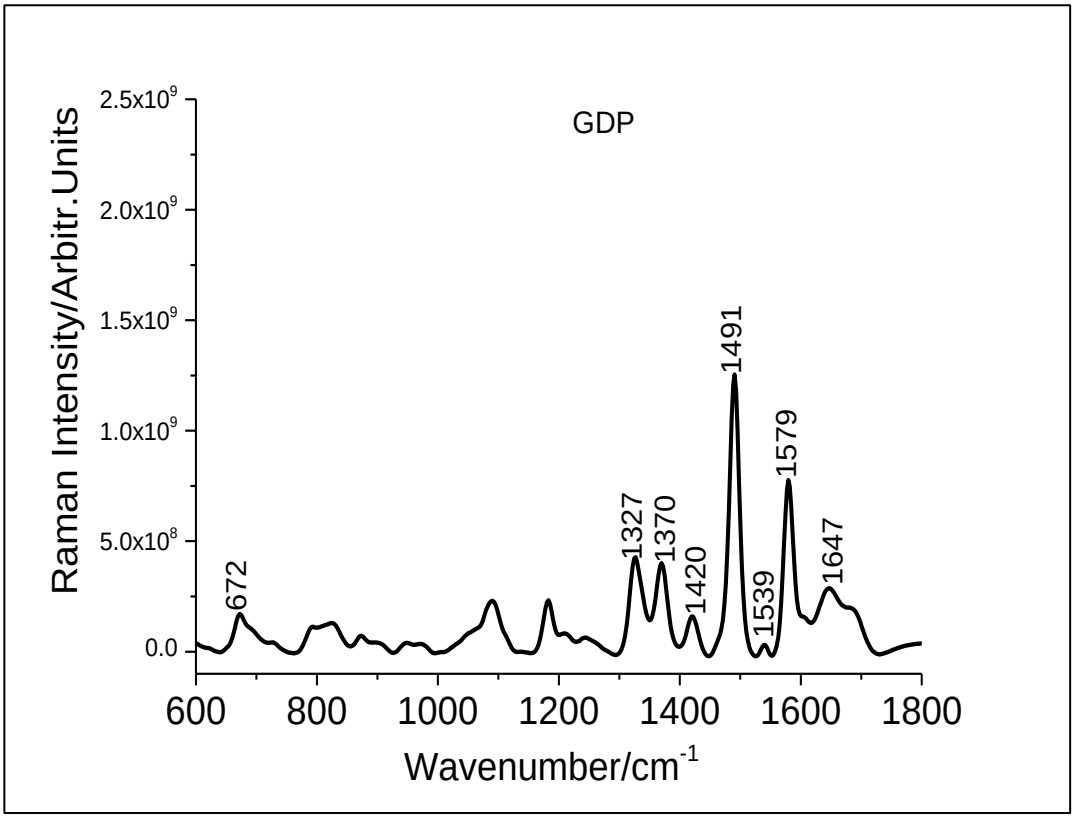

Figure 3.7. Raman spectrum for 5'-guanosine diphosphate (GDP) at pH 7.0.

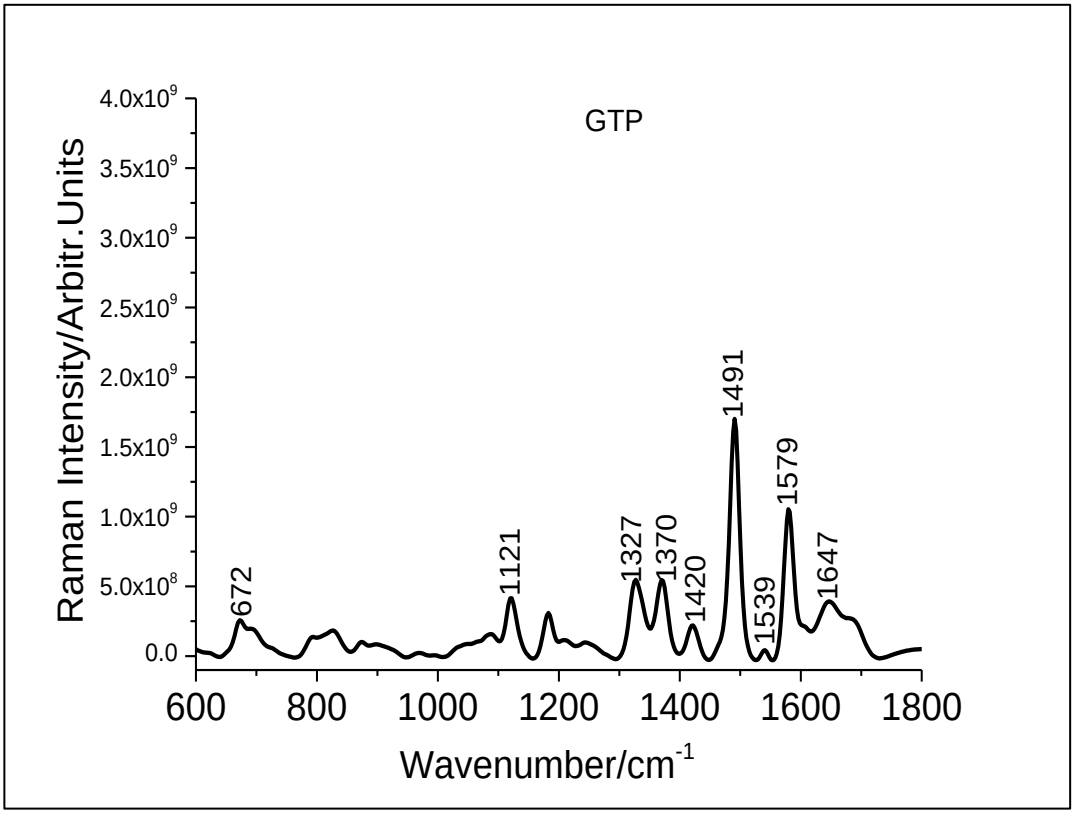

Figure 3.8. Raman spectrum for 5'-guanosine triphosphate (GTP) at pH 7.0.

600-760 and 1150-1800 cm^{-1}: The 1150-1800 cm^{-1} region showed similar Raman features for all the guanosine mono-, di, and triphosphates. These spectral similarities are supported by the DFT calculations which also reflected consistent bands with similar frequencies and intensities (Figure 3.2). The high intensity Raman bands observed at 1579 cm^{-1}, 1491 cm^{-1} and the doublet at 1370 and 1327 cm^{-1} are the characteristic features of this region. The region at 600-760 cm^{-1} is dominated by a Rama band at 672 cm^{-1} for all the guanosine derivatives.

760-1150 cm^{-1}: This region of the Raman profile is dominated by two broad and asymmetric peaks, one at 760 - 870 cm^{-1} and the other one at 990 - 1160 cm^{-1}. These broad peaks were deconvoluted to identify the overlapped bands for comparison with the DFT analysis (Griffiths and de Haseth, 2007; Aragao and Messaddeq, 2008).

For 5'-GMP, a distinct Raman band is detected at 982 cm^{-1}(Figure 3-6), which is absent in 5'-GDP and 5'-GTP. Deconvolution of the 1020-1120 cm^{-1} identified three bands at 1053, 1064 and 1085 cm^{-1} , with the band at 1085 cm^{-1} having the highest intensity of the three. The deconvoluted region at 760-870 cm^{-1} resolved to three overlapped bands, at 790, 809 and 825 cm^{-1}.

For 5'-GDP, the peak at 982 cm^{-1} in 5'-GMP disappears and a new peak appears at higher frequency, where it overlaps with the broad 1020-1120 cm^{-1} peak. Deconvolution of the 1020-1120 cm^{-1} peak for 5'-GDP revealed three bands at 1058, 1091 and 1114 cm^{-1}, with the most intense peak at 1091 cm^{-1}. Deconvolution of the 760-870 cm^{-1} peak reflected the presence of three overlapped bands at 798, 810 and 830 cm^{-1}. The noticeable differences between 5'-GMP and 5'-GDP are the general shift in the resolved bands to higher frequency in 5'-GDP and the presence of a small band at 1114 cm^{-1} which is not present for 5'GMP.

For 5'-GTP, there is a distinctive new Raman band at 1121 cm^{-1} (Figure 3-8). Deconvolution of the 1020-1120 cm^{-1} peak was insufficient to include all of the fundamental bands and so the deconvoluted region was extended

to 990-1160 cm^{-1}. This deconvolution revealed three bands in addition to the band at 1121 cm^{-1}, at 1039, 1070 and 1090 cm^{-1}. The bands at 1039 and 1070 cm^{-1} did not appear in the Raman spectra of 5'-GMP or 5'-GDP. The band at 1090 cm^{-1} is dominant in intensity, similarly to the 5'GDP band at 1091 cm^{-1}. Deconvolution of the 760-870 cm^{-1} peak reflected three bands, all of which are similar to the ones observed for 5'-GDP, at 789, 810 and 830 cm^{-1}. This indicates that the addition of the γ-phosphate group has no discernible effect on the frequencies of these vibrations.

3.4.3 Guanosine mono-, di- and tri-phosphates, with Mg^{2+}

In vivo, guanosine nucleotides present in aqueous environment are normally associated with different metals, such as magnesium ions. Therefore, this study investigated the impact of magnesium ions on the Raman spectra of 5'-GMP, 5'-GDP and 5'-GTP.

For 5'-GMP (Figure 3.9), the Raman spectra of the unbound and magnesium-bound forms showed no observable spectral differences in the frequencies of the Raman bands. However, the intensity of the diagnostic band for 5'GMP, at 982 cm^{-1} was reduced by ~ 8.0 % for 5'-GMP-Mg (Figure 3-10). The deconvoluted regions at 760-870 cm^{-1} reflected minor spectral changes in the bands at 825 cm^{-1} which shifted to lower frequency (821 cm^{-1}) in the 5'-GMP-Mg complex , while the 1020-1120 cm^{-1} peak did not reveal any resolvable differences compared with unbound 5'-GMP. Equivalent ^{31}P NMR spectra showed that the chemical shift of the phosphate group for 5'-GMP moves only slightly downfield (0.1 ppm) on addition of Mg^{2+}, indicating little sensitivity of this group to magnesium binding.

For 5'-GDP (Figure 3.2), similarly to 5'-GMP, the binding of the magnesium has no resolvable effect on the overall spectral profile of 5'-GDP. However, the shape and the component bands of the broaden peak of the 5'-GDP-Mg complex at 1020-1120 cm^{-1} differ from that of the unbound 5'-GDP. The maximum intensity is now *ca.* 1083 cm^{-1} which has decreased in intensity by ~14 % compared to the dominant band at 1091 cm^{-1} for 5'-

GDP (Figure 3-10). It is difficult to ascribe changes to individual bands in the deconvoluted spectrum, though the general trend of the component peaks is to lower frequency by approximately -9 cm^{-1}. The ^{31}P NMR measurements of 5'-GDP showed more chemical shift changes in the phosphate resonance, upon magnesium saturation, compared with the 5'-GMP. In 5'-GDP-Mg complex, the α- phosphate peak moved downfield by 0.6 ppm and that of the β-phosphate shifted down field by 1.0 ppm. These results support a model where the coordination of Mg^{2+} involves a substantial contribution from both the α- and β-phosphate groups of 5'-GDP.

For 5'-GTP (Figure 3.9), a significant change is observed for the diagnostic band at 1121 cm^{-1}, which is shifted to higher frequency by +6 cm^{-1} on saturation with magnesium (Figure 3-11). The intensity of this band also decreased by ~31 % upon magnesium binding (Figure 3.10), whereas the deconvoluted peaks at 760-870 cm^{-1} for 5'-GTP overlay closely on binding to Mg^{2+}. In contrast, deconvolution of the 990-1160 cm^{-1} peak for the 5'-GTP-Mg complex indicated the presence of a new band at 1140 cm^{-1} and a shift in the frequency of the 5'-GTP component bands at 1039, 1070 and 1090 cm^{-1} by +9, +9 and -3 cm^{-1}, respectively, which is consistent with their assignment as having substantial contributions from the phosphate groups. In the equivalent ^{31}P NMR spectra, a downfield chemical shift was detected for the β- and γ-phosphate groups (by 2.3 and 1.0 ppm, respectively) for the 5'-GTP-Mg complex. However, the α-phosphate peak did not change chemical shift, supporting a model where the coordination of Mg^{2+} is dominated by the β- and γ-phosphate groups.

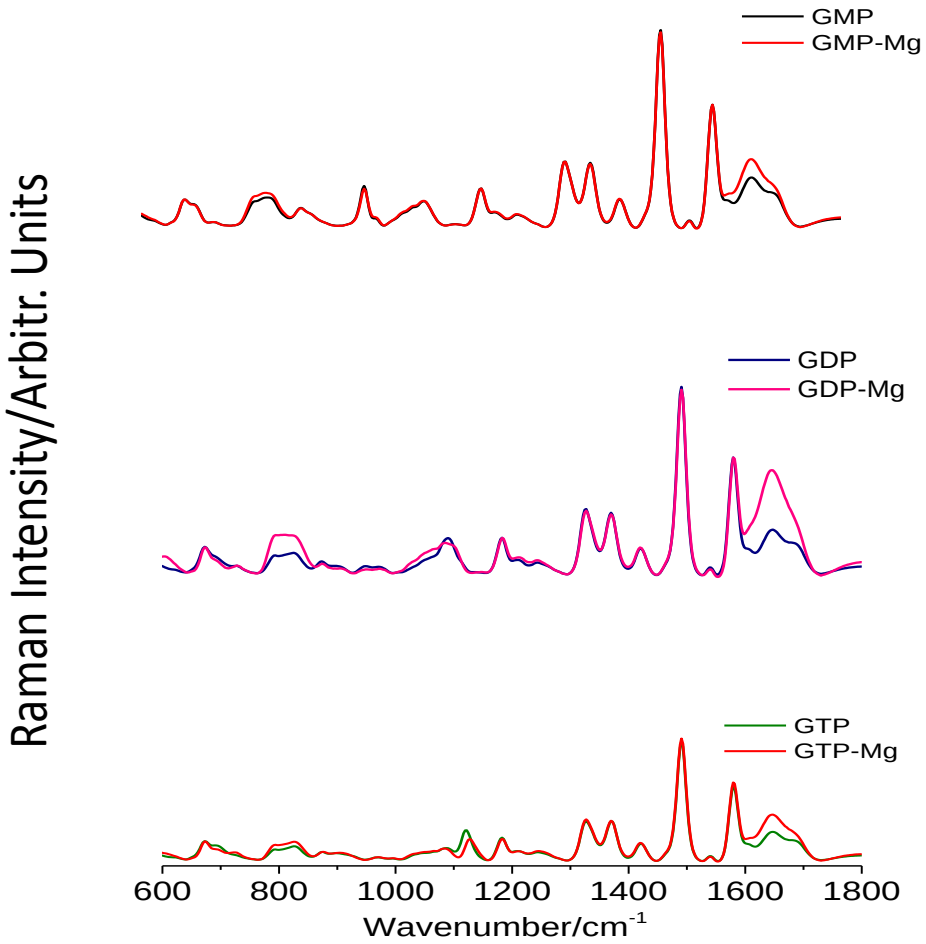

Figure 3.9. Experimental Raman spectra for 5'- guanosine monophosphate (GMP), 5'-guaosine monophosphate-magnesium complex (GMP-Mg), 5'- adenosine diphosphate (GDP), 5'- guanosine diphosphate-magnesium complex (GDP-Mg), 5'-guanosine triphosphate and 5'-guanosine triphosphate-magnesium complex. The major spectral differences observed on saturation with Mg^{2+} are the +5 shifts of the band at 1122 cm^{-1} for 5'-GTP.

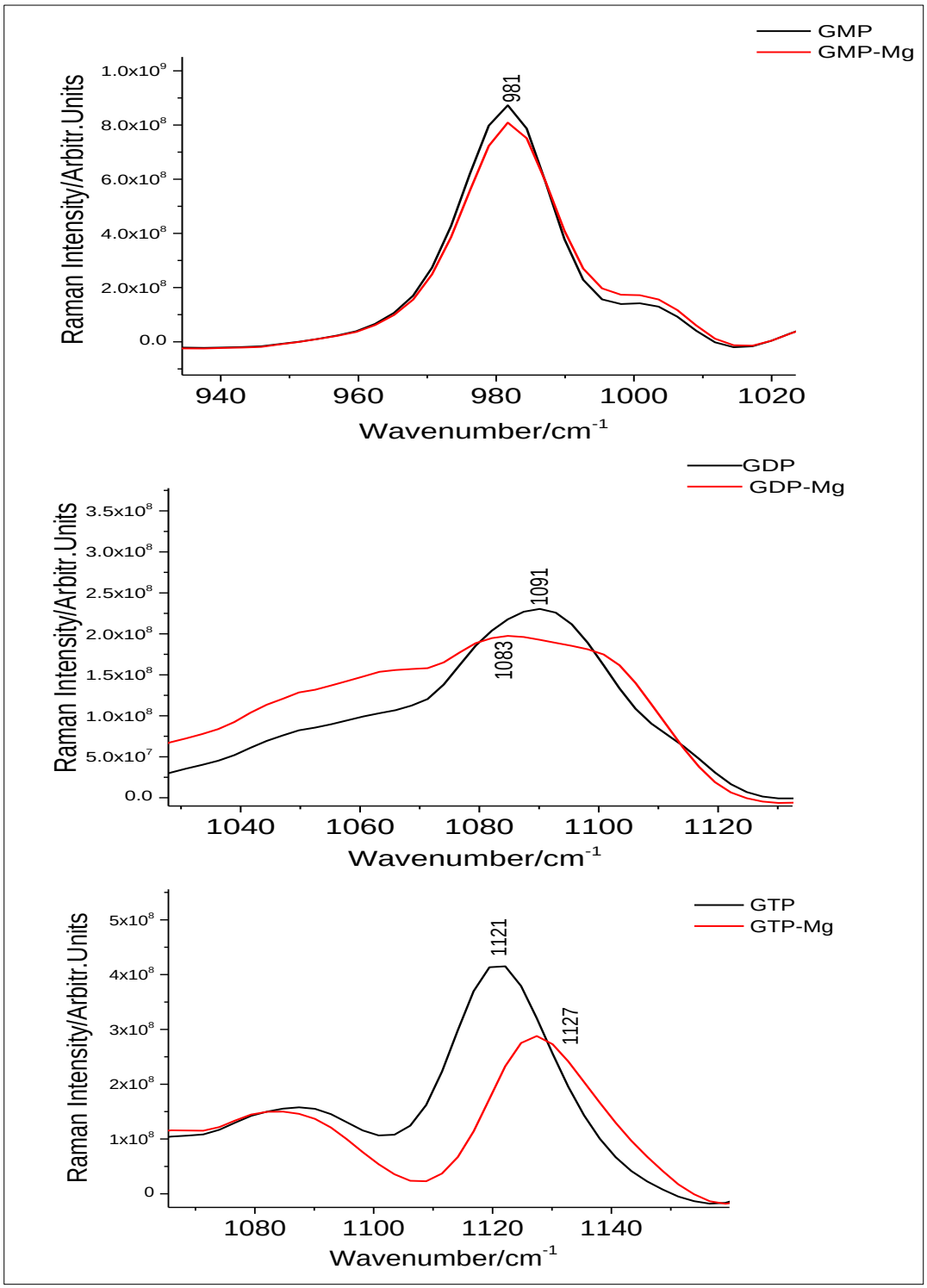

Figure 3.10. The difference in the experimental Raman intensities of the bound and free guanosine mono-, di- and triphosphate molecules. The intensity of the band at 981 cm^{-1} for 5'- guanosine monophosphate complex (5'-GMP-Mg) is reduced by~ 8 % , the intensity of the band at 1091 cm^{-1} for 5'-guanosine diphosphate complex (5'-GDP-Mg) decreased by ~14 % and the intensity of the band at 1127 cm^{-1} for 5'- guanosine triphosphate complex (5'-GTP-Mg) is reduced by 31 % at pH 7.0.

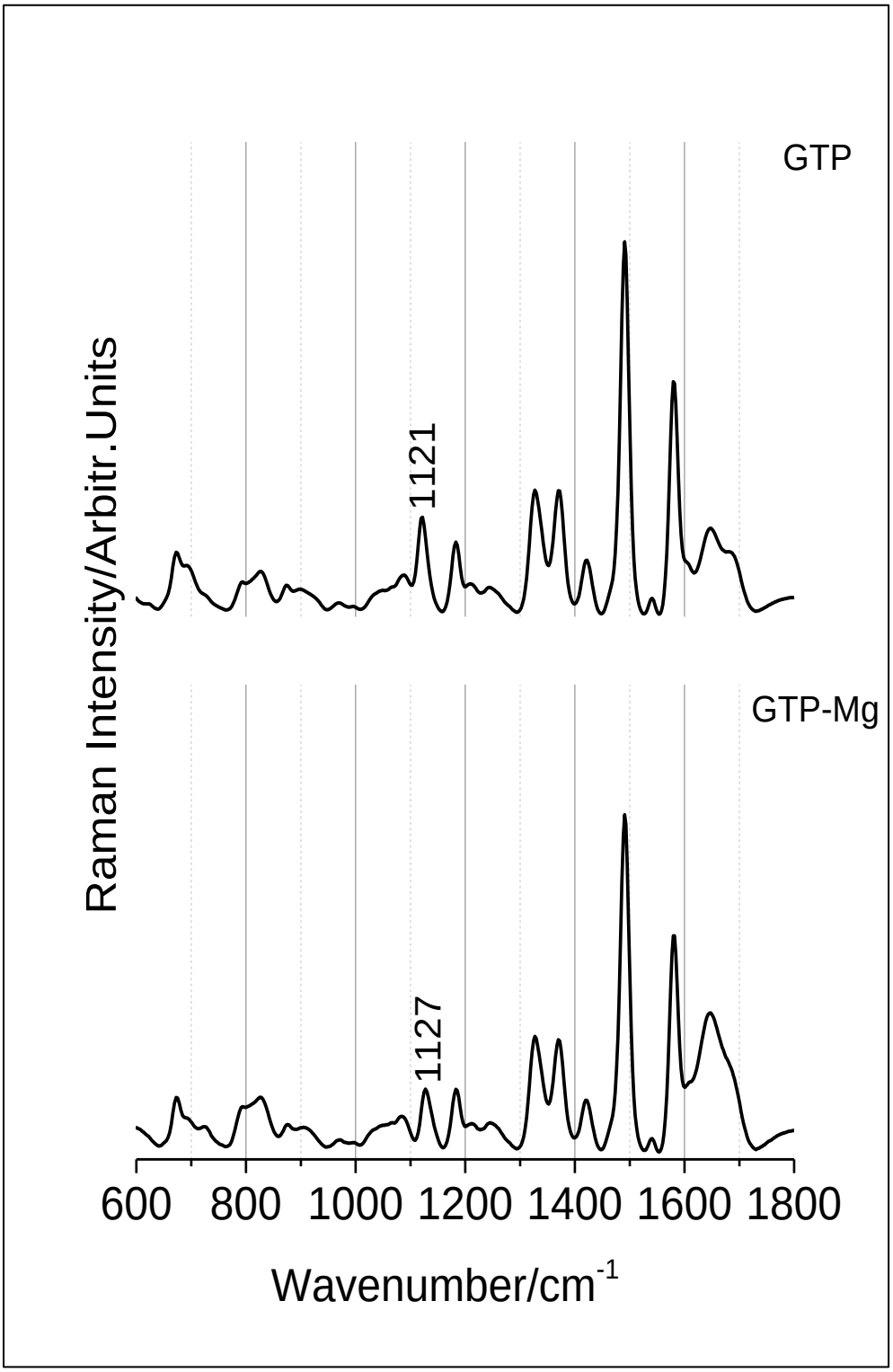

Figure 3.11. Experimental Raman spectra for 5'- guanosine triphosphate (GTP) and 5'- guanosine triphosphate complex (GTP-Mg) at pH 7.0.

3.4.4 The pH effects on guanosine phosphates-Mg^{2+} complexes

The influence of environmental pH on the Raman profiles of 5'-GMP-Mg, 5'-GDP-Mg, and 5'-GTP-Mg complexes was examined at pH 5.0, 6.0, 7.0 and 8.0 to determine whether this approach offered a signature of the protonation state of the phosphate groups.

For 5'-GMP -Mg (Figure 3.12, 3-13), the Raman profiles were unaltered between pH 7.0 and 8.0. However, at pH 5.0, the diagnostic band at 982 cm^{-1} showed a remarkable decrease in its intensity such that it is no longer visible in the Raman profile, and there is no evidence supporting its shift to a nearby frequency (Figure 3-13). Deconvolution of the peak at 1020-1120 cm^{-1} for 5-GMP-Mg reflected alterations in the intensities and frequencies of some of the component bands. For example, the dominant band at 1085 cm^{-1} falls in intensity at pH 5.0, whereas the band at 1064 cm^{-1} at pH 7.0 increases substantially and moved to lower frequency (1060 cm^{-1}). Deconvolution of the peak at 760-870 cm^{-1} reflected an overall shift to a lower frequency and a decrease in the intensity of all the component bands at pH 5.0. The protonation of the magnesium bound phosphate group was also investigated between pH 5.0 and 8.0 using ^{31}P NMR. The results reflected a substantial upfield chemical shift change of 1.8 ppm at pH 5.0 (δ = 1.4 ppm) compared with that at pH 7.0 and 8.0 (δ = 3.2 and 3.3 ppm respectively). This indicates that there is protonation of the magnesium-associated phosphate group over this pH range.

For 5'-GDP-Mg (Figures 3.12, 3-14), the Raman profiles were unaffected between pH 7.0 and 8.0. At pH 5.0, deconvolution of the peaks at 1020-1120 cm^{-1} and 760-870 cm^{-1} identified a decrease in the intensity of the dominant bands at 806 and 1082 cm^{-1} at low pH. However, the equivalent results obtained from ^{31}P NMR measurements indicated only a slight upfield shift of the α-and β-phosphate resonances by 0.3 (δ-10.1 to -10.4 ppm) and 1.3 ppm (δ-6.2 to -7.5 ppm), respectively, over the pH range 8.0 to 5.0. This is consistent with little change in the protonation state of either phosphate group in the presence of magnesium, which makes it

difficult to equate any changes in Raman spectra over this pH range with changes in protonation.

For 5'-GTP-Mg (Figures 3.12, 3-15), the Raman profiles were again unaltered between pH 7.0 and 8.0. At pH 5.0, the diagnostic band at 1127 cm^{-1} (at pH 7.0) shifted to higher frequency by +3 cm^{-1}. Similarly, deconvolution of the 990-1160 cm^{-1} region also indicated a shift in the component bands at 1079 and 1087 cm^{-1}. Deconvolution of the 760-870 cm^{-1} peak identified a small shift of the band at 807 cm^{-1} to higher frequency. In the equivalent ^{31}P NMR spectra, a upfield chemical shift changes for α-, β- and γ-phosphate groups (by 0.4, 0.4 and 0.8 ppm, respectively) are observed at pH 5.0. , which again indicate that there is no substantial protonation of the phosphate groups over this pH range.

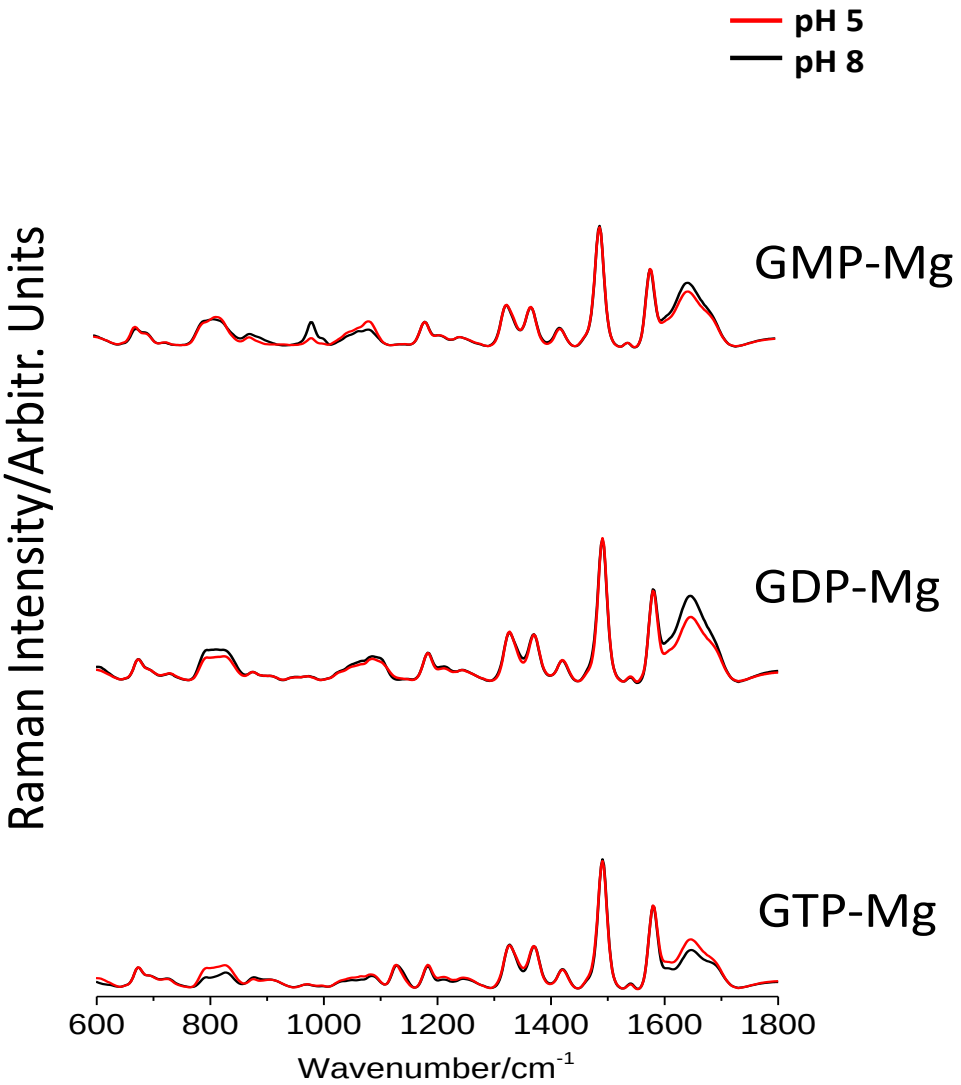

Figure 3.12. Experimental Raman spectra for 5'- guanosine monophosphate-magnesium complex (GMP-Mg), 5'-guanosine diphosphate-magnesium complex (GDP-Mg) and 5'-guanosine triphosphate-magnesium complex (GTP-Mg) at pH 5.0 and 7.0. Acidification decreases the intensity of the 5'-GMP band at 982 cm^{-1} and shifts the 5'-GTP band at 1127 cm^{-1} by +3 cm^{-1}.

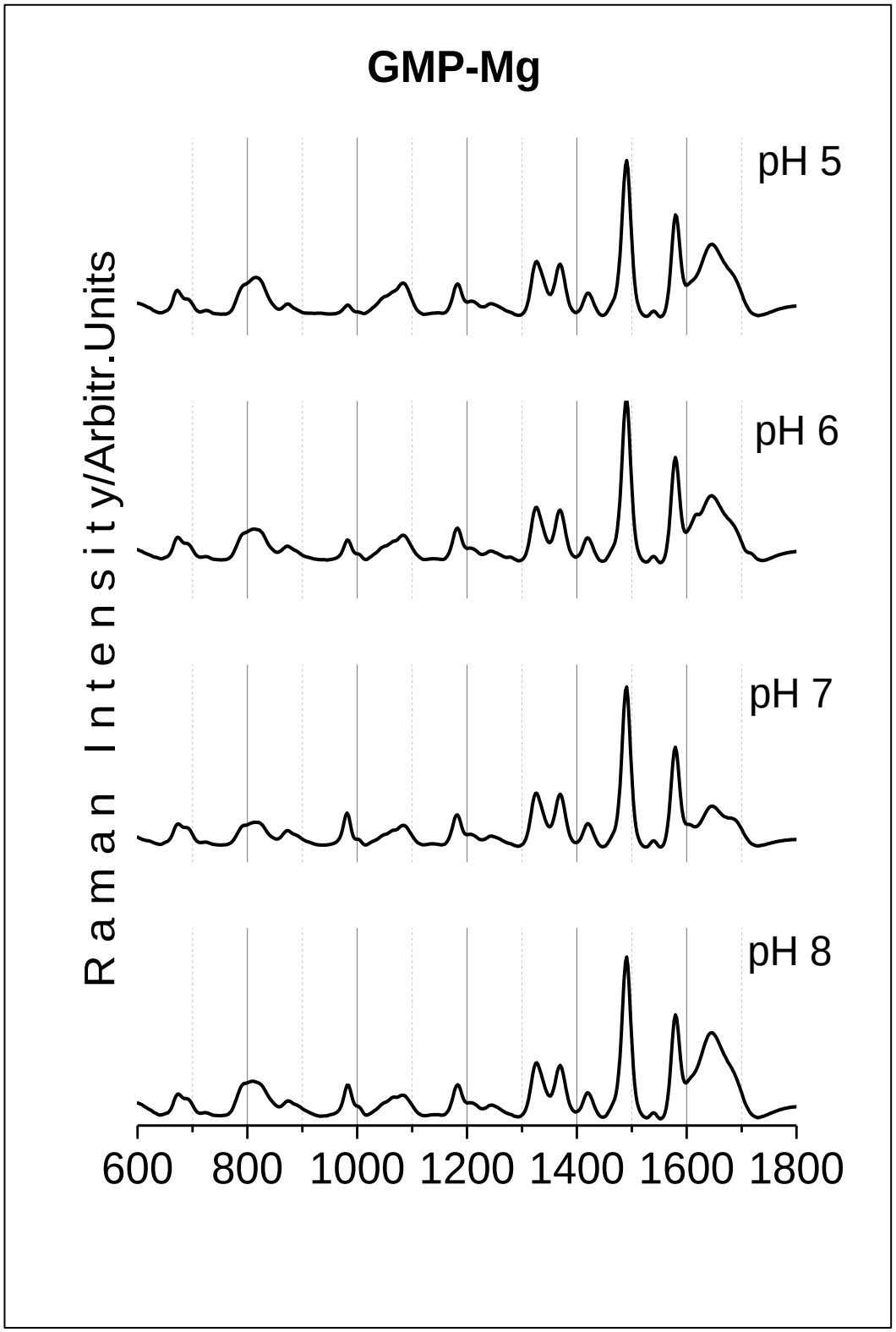

Figure 3.13. The Raman spectra for 5'- guanosine monophosphate-magnesium complex (GMP-Mg) at different pH environments.

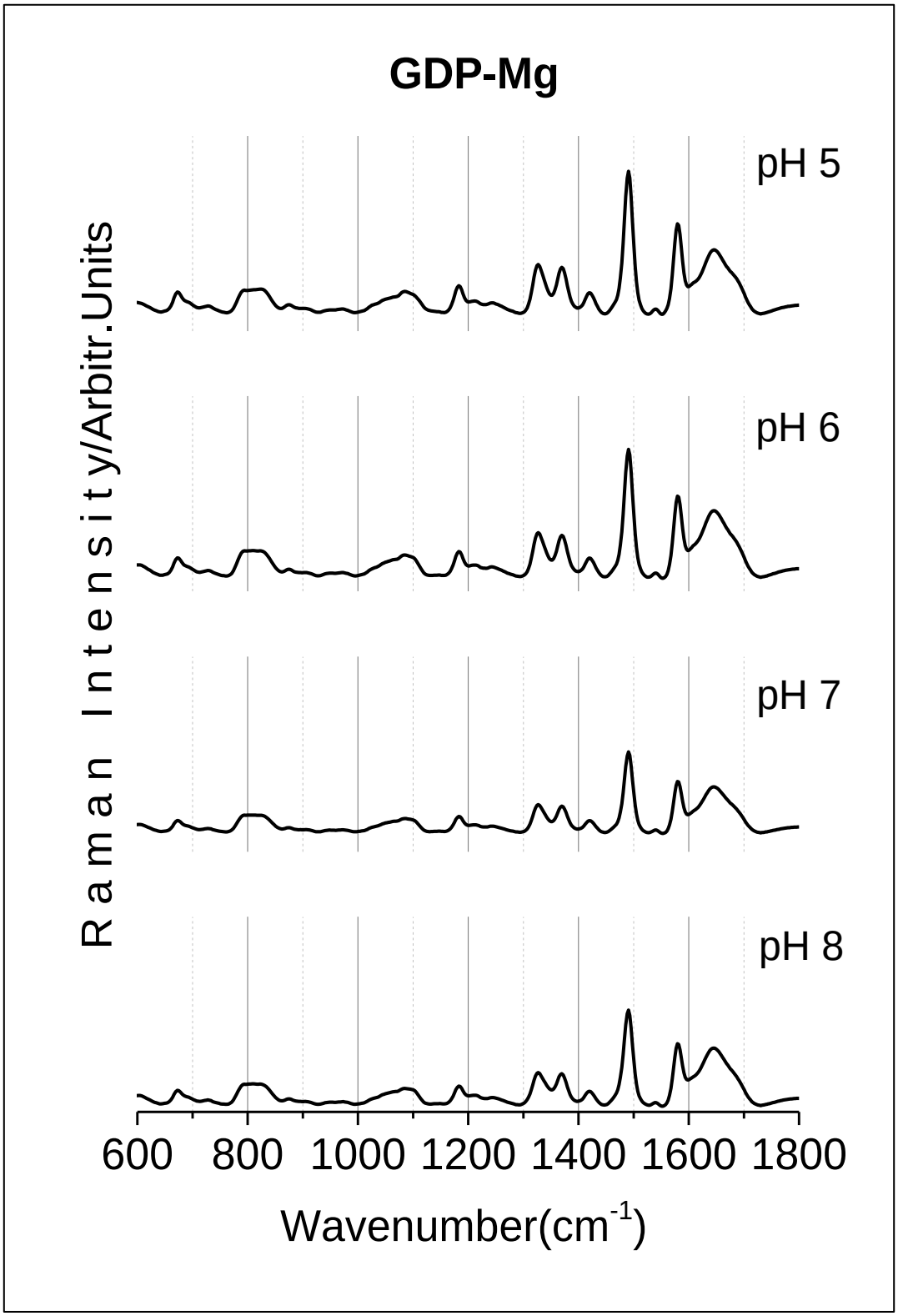

Figure 3.14. The Raman spectra for 5'- guanosine diphosphate-magnesium complex (GDP-Mg) at different pH environments.

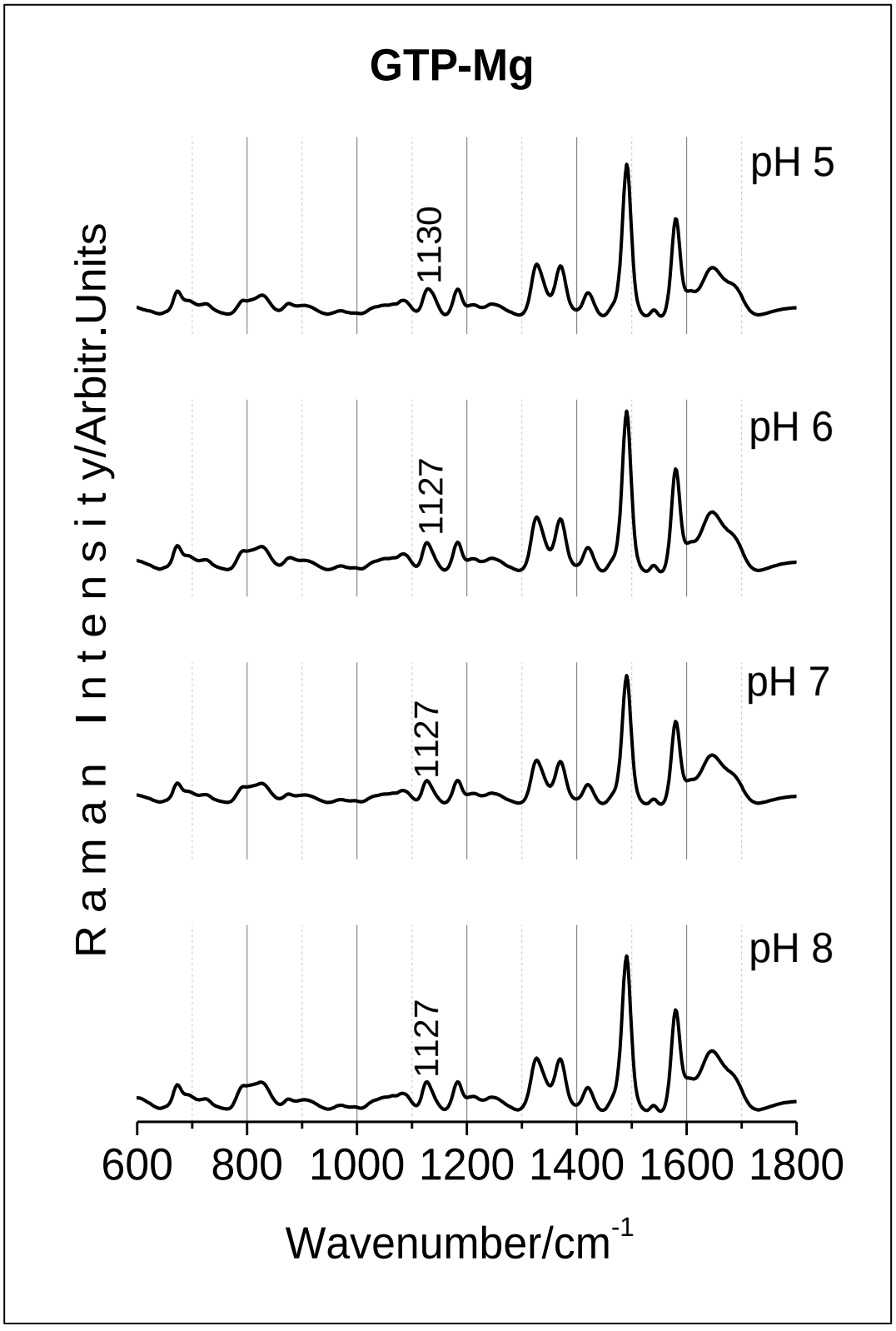

Figure 3.15. The Raman spectra for 5'- guanosine triphosphate-magnesium complex (GTP-Mg**)** at different pH environments.

3.4.5 *ROA spectra for Guanosine mono-, di- and triphosphates, without* Mg^{2+}

The ROA is sensitive to minor structural changes associated with chiral molecules. Therefore, the technique was applied to investigate the spectral differences between 5'-GMP, 5'-GDP and 5'-GTP. The ROA spectrum for each was recorded over the range of 600-1800 cm^{-1} at pH 7.0 (Figure 3.16). The resulting profiles identify multiple ROA bands across the spectra. The ROA region at 800-1250 cm^{-1} is characterised by several positive ROA bands, which can potentially be used as marker bands to distinguish between different guanosine nucleotides. The ROA band at 893 cm^{-1} for 5'-GMP is shifted to higher frequency by + 6 wavenumbers in 5'-GDP and 5'-GTP, while the band at 1135 cm^{-1} for 5'-GMP remains at the same frequency in 5'-GDP but shifts to higher frequency by + 8 wavenumbers in 5'-GTP. Interestingly, the region of the ROA spectra at 1250-1800 cm^{-1} also changes in a diagnostic way that distinguishes 5'-GTP from 5'-GMP and 5'-GDP, despite none of these vibrations having a direct contribution from atoms of the phosphate groups (see below). The positive ROA bands at 1493 and 1580 cm^{-1} for 5-GMP and 5'-GDP, moved to 1498 and 1584 cm^{-1}, respectively, for 5'-GTP.

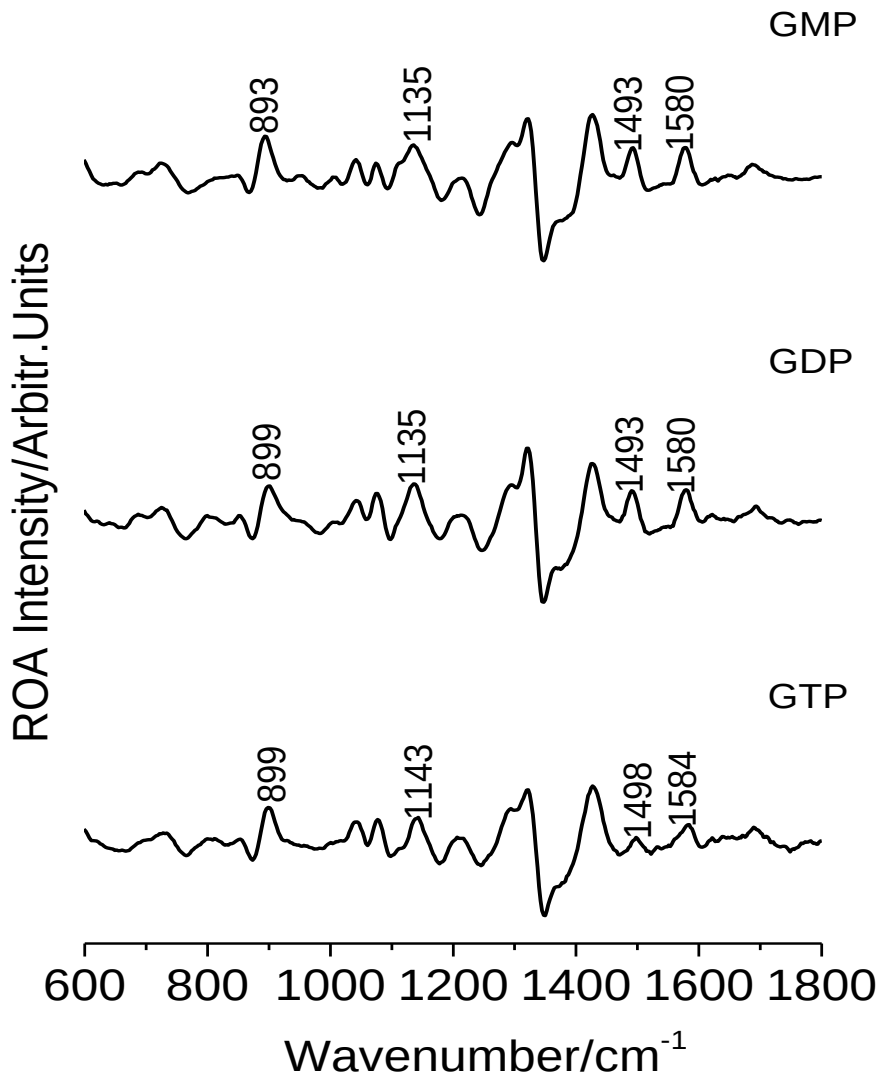

Figure 3.16. The ROA spectra for 5'- guanosine monophosphate (5'-GMP), 5'-guanosine diphosphate (5'-GDP) and 5'- guanosine triphosphate (5'-GTP) at pH 7.0. The spectra identified multiple positive ROA marker bands that can discriminate between each guanosine nucleotide.

3.4.6 Assignment of Raman bands using DFT models

For a more detailed understanding of the differences in the experimental Raman and ROA spectra of guanosine 5'-mono-, di- and tri- phosphates, the Raman bands of the different species were calculated using a DFT approach. From this, some assignments of individual bands to specific vibrations can be proposed (Figure 3.18).

Raman vibrations above 1150 cm^{-1}: In this region, the results of the experimental Raman measurements and the DFT-derived vibrational modes are significantly correlated for all of the nucleotide derivatives. The intense experimental Raman band at 1579 cm^{-1} can be assigned to a DFT mode at 1579 cm^{-1} (± 1), which is calculated to have substantial relative Raman intensity (1.0 a.u., averaged across guanosine and its phosphate derivatives - see methods section, figure 3.2). In this vibrational mode the purine ring atoms contribute to 90 % of atomic displacement. The small experimental band at 1539 cm^{-1} is assigned to a DFT mode with low predicted Raman intensity (0.05 a.u.) at 1554 cm^{-1} (± 1), where the atomic displacement is again dominated by purine atoms (94 %). The intense experimental band at 1491 cm^{-1} can be assigned to an intense DFT mode at 1505 cm^{-1} (0.9 a.u., 93 % purine vibration). The small experimental band at 1420 cm^{-1} can be assigned to two DFT modes; 1423 cm^{-1} (± 1) (0.22 a.u., 43 % purine vibration) and 1430 cm^{-1} (± 1) (0.16 a.u., 45 % purine vibration). The 1370 cm^{-1} band of the (1370/1327 cm^{-1}) doublet can be assigned to an intense DFT mode at 1378 cm^{-1} (± 1) (0.21 a.u.), with some contribution from weaker DFT modes at 1372 cm^{-1} (± 1) (0.04 a.u.) and 1374 cm^{-1} (± 2) (0.11 a.u.).All of these vibrational modes are dominated by ribose vibrations (71 %). The 1327 cm^{-1} band of the (1370/1327 cm^{-1}) doublet can be assigned to an intense DFT mode at 1335 cm^{-1} (± 2) (0.7 a.u.), with additional contribution from a weaker DFT mode at 1327 cm^{-1} (± 1) (0.02 a.u.). Both vibrational modes are dominated by ribose atom vibrations (67 %).As expected on the basis of the similarity in the experimental spectra in this region, the phosphate groups do not contribute directly to any vibrational modes in this region of the spectra. Therefore no

large frequency or intensity changes of any DFT modes in this region are found between guanosine and its nucleotide derivatives.

Raman vibrations below 760 cm^{-1}: The experimental Raman spectra for guanosine and its nucleotide derivatives are dominated in this region by bands in the 670-690 cm^{-1} region. According to DFT calculations, there are 3 vibrational modes that are likely contributors to these bands, one of which is close in frequency (677 ± 1 cm^{-1}, 0.01 a.u.) and two within 20 cm^{-1} (665 ± 1, 0.11 a.u. and 657 ± 2 cm^{-1}, 0.15 a.u.). All three modes have near 60 % contributions from the purine and 16 % from the ribose group. Unlike the region above 1150 cm^{-1}, vibrational modes in this region can include direct phosphate group atom contributions, which may alter both the frequency and intensity of bands. For the guanosine derivatives, each of these modes gains a contribution from the phosphate group(s) in the nucleotides (up to a maximum of 71 % in 5'-GTP) but the frequencies and intensities are only moderately affected (a shift of up to 4 cm^{-1} in the frequency and 0.1 a.u. in the intensity). The minor change in the intensity of the DFT modes is in agreement with the experimental spectra, which reflected no significant alterations in the intensity of the 670-690 cm^{-1} region bands in the guanosine nucleotides

Raman Vibrations in the region 760-1150 cm^{-1} region: In the experimental spectra, this region contains the major diagnostic peaks for the nucleotide derivatives, in addition to two broad peaks, one in the range 760-870 cm^{-1} and one in the range 990-1160 cm^{-1}.

For 5'-GMP, the diagnostic band at 982 cm^{-1} correlates to a DFT mode at 921 cm^{-1} (0.28 a.u.), which has a 76 % contribution of the phosphate group atoms (Figure 3.17). The calculated intensity of this mode is reduced for 5'-GDP and 5'-GTP, which is consistent with its absence in the experimental Raman spectra of these derivatives.

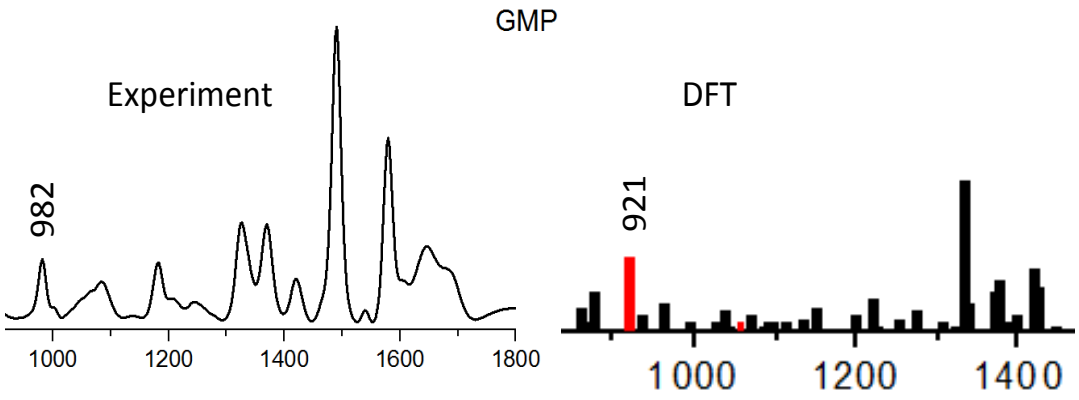

Figure 3.17. Comparison of the GMP experimental Raman band at 982 cm^{-1} with a similar DFT band at 921 cm^{-1}.

The deconvoluted 760-870 cm^{-1} region is associated with multiple DFT modes that can potentially contribute to the shape of the broad peak. For 5'-GMP, the 752 cm^{-1} (0.23 a.u.) mode is moved to 773 cm^{-1} (0.18 a.u.) and 771 cm^{-1} (0.14 a.u.) for 5'-GDP and 5'-GTP, respectively. These three DFT modes have substantial contribution of ribose atoms (58 %) and, to a lesser extent phosphate group atoms (12 % for 5'-GMP, 31 % for 5'-GDP and 41 % for 5'-GTP). The 842 cm^{-1} (0.34 a.u.) and 824 cm^{-1} (0.33 a.u.) DFT modes for 5'-GDP and 5'-GTP respectively, are characterised by a low contribution of the purine (3 % for 5'GDP and 2 % for 5'-GTP) and ribose (18 % for 5'GDP and 5'-GTP) atoms but a higher contribution of the phosphate group atoms (46 % α- and 33 % β- for 5'GDP and 26 % α-, 32 % β- and 22 % γ- for 5'-GTP).

Deconvolution of the 990-1150 cm^{-1} region revealed more than 12 DFT modes that potentially contribute to the shape of the broad peak in this region, making any attempts at assignment to be very subjective. While potential assignments of the diagnostic band for 5'-GDP at 1091 cm^{-1} can be proposed, the potential DFT modes are predicted to have low intensity, e.g. the DFT mode at 1076 cm^{-1} (0.03 a.u.), which has significant contributions from both the α- (4 %) and β- (94 %) phosphate groups). For 5'-GTP, the diagnostic peak at 1121 cm^{-1} can be assigned to a DFT mode

at 1064 cm^{-1} (0.42 a.u.), which is unique to 5'-GTP and has significant contributions from phosphate groups atoms (37 % α-, 30 % β-, 8 % γ-).

3.5 Discussion:

This study provides an analysis of the Raman and Raman Optical Activity spectra for guanosine and its nucleotides 5'-GMP, 5'-GDP and 5'-GTP. Assignments of the vibrational modes that give rise to the experimental spectra are proposed where possible on the basis of DFT calculations of the individual species. The primary guanosine marker bands are identified at 1490, 1370 and 1327 cm^{-1}, which are attributed to vibrational modes involving atoms from both the purine and the ribose rings, in line with previous proposals using different computational method (Rodriguez-Casado *et al.,* 1998). There was no evidence for a contribution of the phosphate group(s) atoms in any of these marker bands in the spectra of the nucleotides. The study also identified primary diagnostic bands for 5'-GMP (982 cm^{-1}), 5'-GDP (1091 cm^{-1}) and 5'-GTP (1121 cm^{-1}). The corresponding DFT-derived vibrational modes appear to have substantial contributions from the α-phosphate group for 5'-GMP (76 %), the β-phosphate group for 5'-GDP (94 %) (though this is a more tentative assignment owing to its low predicted intensity) and the α-, β and γ-phosphate groups for 5'-GTP (37 %, 30 % and 8 %, respectively). The assignment is supported by a focus on predicted vibrational modes that occur only when the relevant phosphate groups are present, and it is noticeable that the assigned diagnostic modes are displaced from the experimental bands to lower frequency by 61, 15 and 57 cm^{-1}, respectively, for 5'-GMP, 5'-GDP and 5'-GTP. The source of this offset is not established here but a likely contributory factor is the environmental differences between the DFT calculations (using *in vacuo* structures), and the experimental measurements in aqueous solution.

Secondary marker bands for the different species are present in the 670-870 and 1020-1120 cm^{-1} regions but their analysis depends on using a deconvolution approach to resolve component bands in heavily overlapped peaks. This leads to some uncertainties in the assignment of component bands owing to the number of potential contributing vibrations and any offsets between DFT-derived and experimental frequencies introduced when the vibrations involve phosphate group atoms.

The binding of Mg^{2+} to the guanosine nucleotides had relatively little effect on the Raman spectra. A minor shift to a higher frequency (1127 cm^{-1}) was observed for the diagnostic band of 5'-GTP at 1121 cm^{-1}, but not clearly for the other nucleotides. Such behaviour for metal bound nucleotide complexes has been proposed to arise from the transient interruption of hydrogen bonding as a result of the binding of the metal to the oxygen atoms (Iyandurai.N *et al.*, 2009). A more general observation is that the binding of magnesium ions to the guanosine nucleotides led a change in the Raman intensity in the phosphate containing bands in the normalised Raman spectra. For 5'-GMP-Mg, the decrease of the diagnostic band is small (981 cm^{-1}, ~ 8 %) but the decrease becomes more marked for the diagnostic bands of 5'-GDP-Mg (1083 cm^{-1}, ~ 16 %) and of 5'-GTP (1127 cm^{-1}, ~ 35 %). Such a decrease in the intensity of the Raman bands has previously been rationalised on the basis of an increase in the size of the molecule (Chio *et al.*, 2003; Smith and Dent, 2005), but the pattern between the nucleotides observed here does not fit the proportional increase in size afforded by a single magnesium ion.

The changes observed in the Raman spectra of the magnesium bound guanosine nucleotides as a function of environmental pH over the range 5.0 to 8.0 were much more variable. The spectra were unaltered for each between pH 7.0 and 8.0, with the changes confined to the low end of the pH range studied. The ^{31}P NMR spectra report on extensive protonation of 5'-GMP-Mg by pH 5.0 ($\Delta\delta$ = 1.8 ppm), with less change for 5'-GDP-Mg ($\Delta\delta$ = 0.3 and 1.3 ppm) and for 5'-GTP-Mg ($\Delta\delta$ = 0.8, 0.4 and 0.4 ppm).The corresponding changes in the Raman spectra ranged from a dramatic loss in intensity for the diagnostic band of 5'-GMP-Mg, through a modest loss in intensity for the some bands of 5'-GDP-Mg, to a +3 cm^{-1} shift for the diagnostic band of 5'-GTP. The lack of clear correlations between the behaviour of the different nucleotides reflects their disparate susceptibilities to protonation over this pH range, coupled with the potential to have significant protonation of the N1 atom of the base as a contributory factor at pH 5.0.

ROA spectra for guanosine and its nucleotide derivatives have not been reported previously. The ROA spectra over the range 600-1800 cm^{-1} reveal primary marker bands for the nucleotides. In the region where phosphate group atoms can contribute directly to the vibrational modes, the band at 893, cm^{-1} is diagnostic for 5'-GMP; it

occurs at 893 cm^{-1} for 5'-GDP and 5'-GTP. In contrast, the band at 1143 cm^{-1} is diagnostic for 5'-GTP; it occurs at 1135 cm^{-1} for 5'-GMP and 5'-GDP. More surprising is the influence of the length of the phosphate chain on vibrational modes where its atoms do not contribute directly. The bands at 1498 cm^{-1} and at 1584 cm^{-1} are diagnostic for 5'-GTP; they occur at 1493 cm^{-1} and 1580 cm^{-1} for 5'-GMP and 5'-GDP. Overall there is a general shift to higher frequency as a function of phosphorylation, and the effects are more widespread for 5'-GTP than for 5'-GDP. The source of this frequency shift is not established here but is consistent with the general shift to higher frequency of the diagnostic Raman bands of the three nucleotides, albeit significantly lower in magnitude. A plausible contributing factor is an influence of the phosphate groups on the conformational properties of the purine and ribose moieties, but this is not apparent in the respective crystal structures to a significant extent. Intriguingly, the primary diagnostic bands in the Raman spectra are not those highlighted by the ROA measurements.

In conclusion, Raman spectroscopy is a sensitive tool that can be used to discriminate guanosines from their adenosine analogues. The technique is sensitive to the phosphorylation state and able to distinguish between different guanosine nucleotides, their binding to magnesium ions and the environmental pH. ROA spectroscopy provides a complementary diagnostic of the phosphorylation state, with well defined bands reflecting different vibrational modes to those that dominate the Raman spectra. The description of the underlying DFT-derived vibrational modes using an averaged atom displacement method has provided a quantitative description of the contribution of the different moieties to the each mode. By combining this approach with experimental spectra and peak deconvolution, primary and secondary markers of the guanosine nucleotides can be characterised. This paves the way for more detailed investigations of these nucleotides in the variety of environments in which they function in nature.

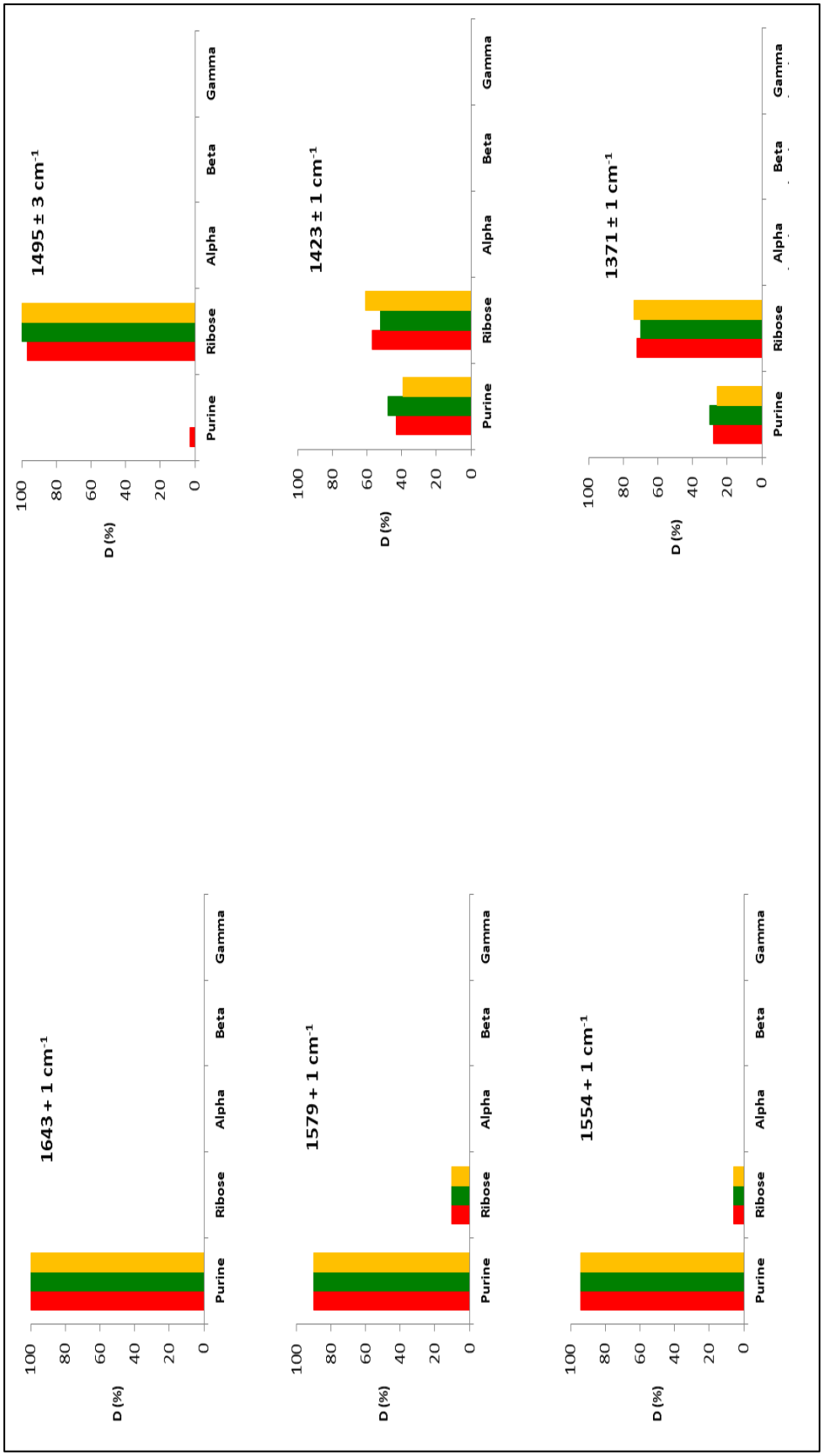

Figure 3.18. Averaged atom displacements (D) for 5'- guanosine monophosphate (GMP) (red bands), 5'- guanosine diphosphate (GDP) (green bands) and 5'- guanosine triphosphate (GTP) (yellow bands).

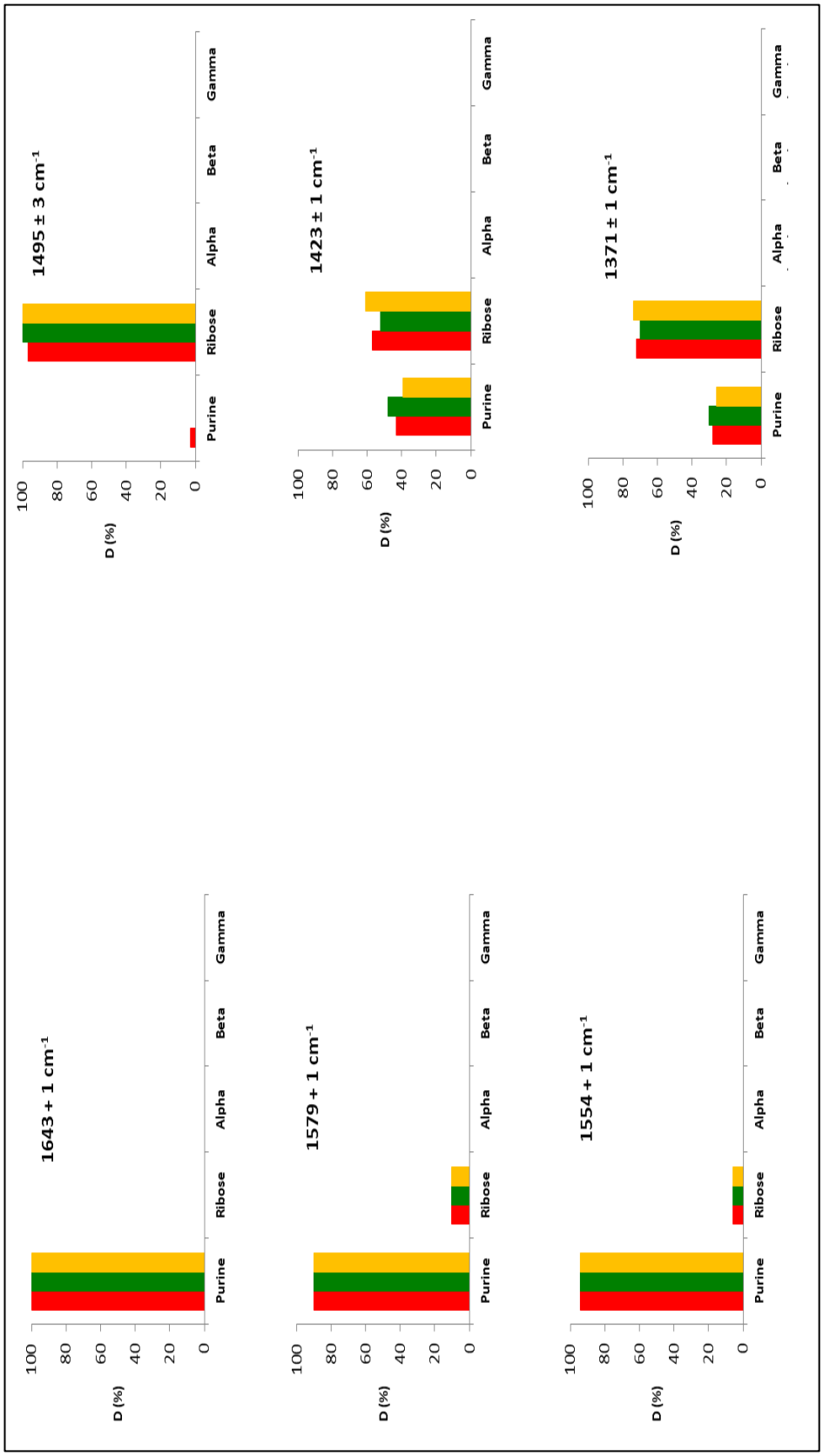

Figure 3.18. Averaged atom displacements (D) for 5'- guanosine monophosphate (GMP) (red bands), 5'- guanosine diphosphate (GDP) (green bands) and 5'- guanosine triphosphate (GTP) (yellow bands).

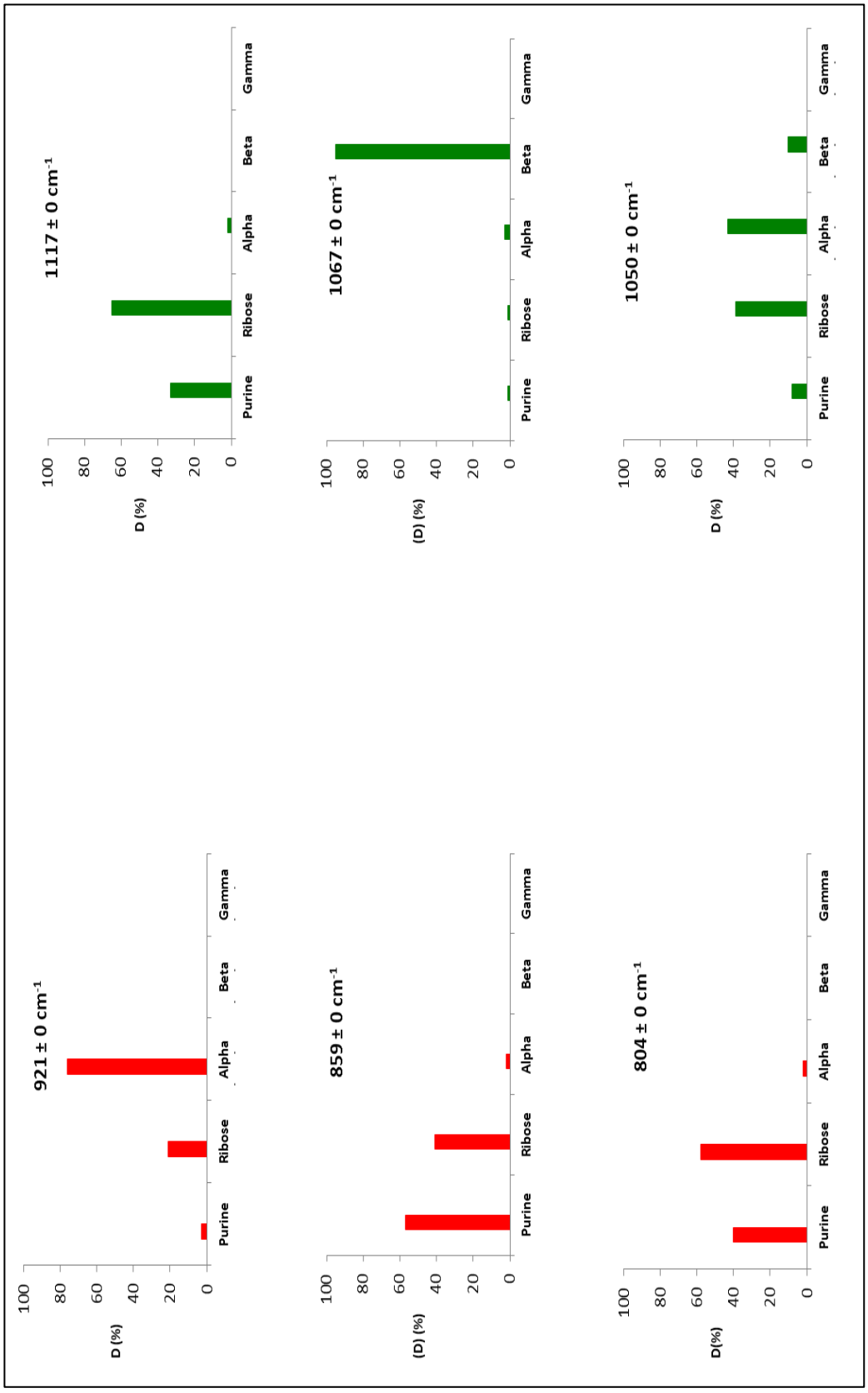

Figure 3.18. Continued.

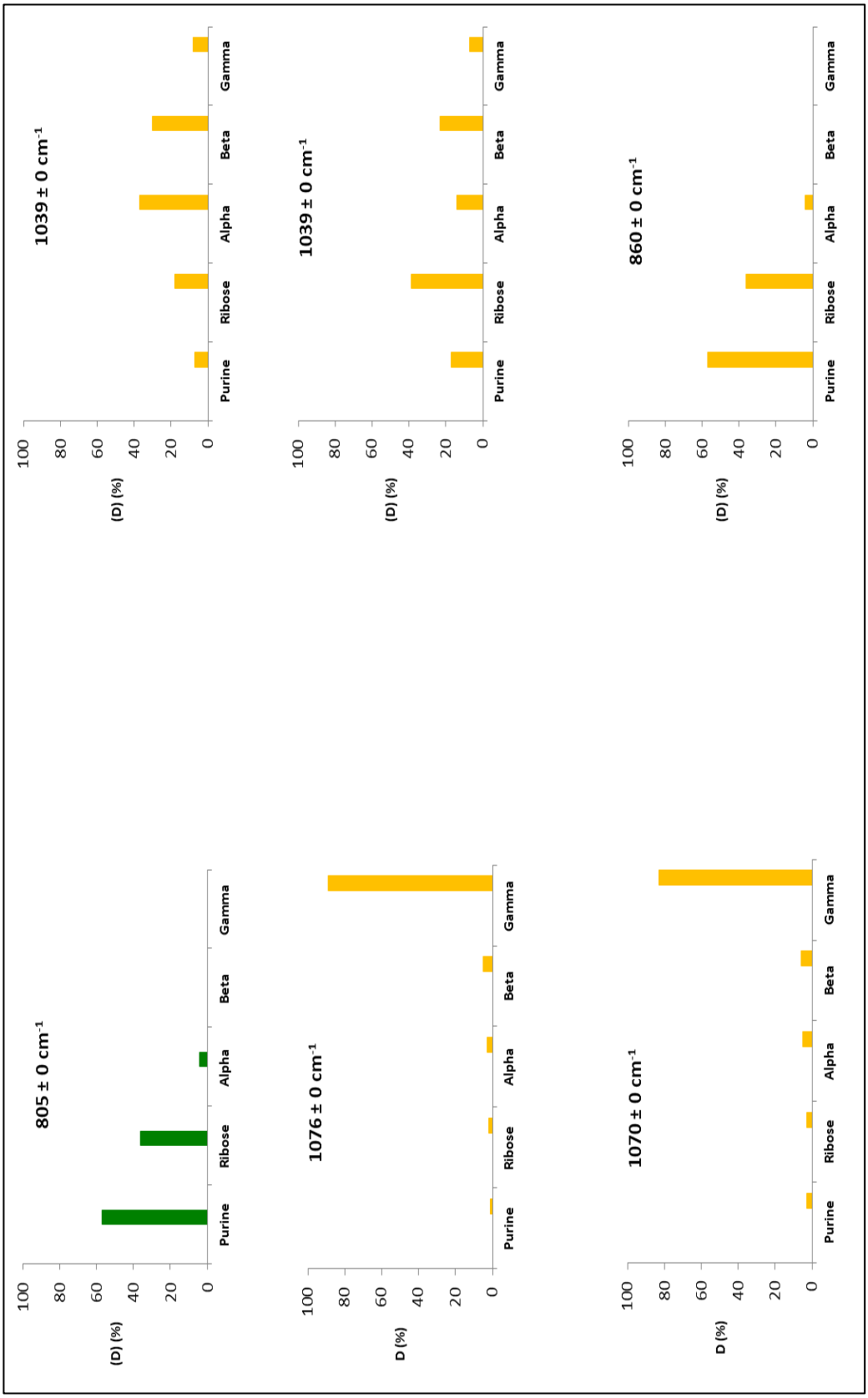

Figure 3.18. Continued.

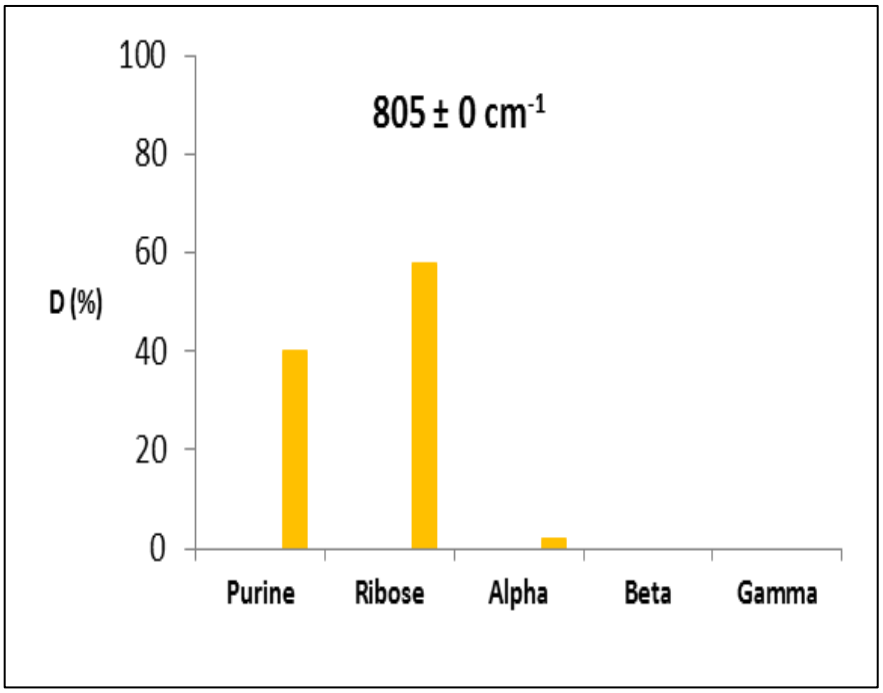

Figure 3.18. Continued.

3.6 References

Anastassopoulou, J. and Theophanides, T. (1995). The role of metal ions in biological systems and medicine, In Dimitris P,K.(ed.) *Bioinorganic chemistry: An inorganic perspective of life.* Dordrecht: Springer Netherlands,pp.209-2018.

Anastassopoulou, J. and Theophanides, T. (2002). 'Magnesium–DNA interactions and the possible relation of magnesium to carcinogenesis. Irradiation and free radicals', *Critical Reviews in Oncology/Hematology,*42(1)**,**pp.79-91.

Aragao, B.J.G.de. and Messaddeq,Y. (2008). 'Peak separation by derivative spectroscopy applied to ftir analysis of hydrolized silica', *Journal of the Brazilian Chemical Society,* 19**,**pp.1582-1594.

Balbuena, P. B. and Seminario, J. M. (1996). DFT study of nickel: Towards the MD simulation of the nickel-water interface, in Jorge, S. (ed.) *Recent developments and applications of modern density functional theory*.New Orland:Elsevier.pp.649-677.

Becke, A. D. (1993). 'Density-functional thermochemistry. III. The role of exact exchange', *The journal of chemical physics,* 98**,**pp.5648-5652.

Black, C. B., Huang, H. W. and Cowan, J. A. (1994). 'Biological coordination chemistry of magnesium, sodium, and potassium-ions - protein and nucleotide-binding sites ', *Coordination Chemistry Reviews,* 135**,**pp. 165-202.

Blanch, E. W., Hecht, L. and Barron, L. D. (2003). 'Vibrational Raman optical activity of proteins, nucleic acids, and viruses', *Methods,* 29(2)**,**pp.196-209.

Brosh, S., Sperling, O., Dantziger, E. and Sidi, Y. (1992). 'Metabolism of guanine and guanine nucleotides in primary rat neuronal cultures', *Journal of Neurochemistry,* 58(4)**,**pp.1485-1490.

Chio, C. H., Sharma, S. K., Lucey, P. G. and Muenow, D. W. (2003). 'Effects of particle size and laser-induced heating on the Raman spectra of alpha quartz grains', *Applied Spectroscopy,* 57(7)**,**pp.774-783.

de la Fuente, M., Hernanz, A. and Navarro, R. (2004). 'IR and Raman study on the interactions of the 5′-GMP and 5′-CMP phosphate groups with Mg(II), Ca(II), Sr(II), Ba(II), Cr(III), Co(II), Cu(II), Zn(II), Cd(II), Al(III) and Ga(III)', *JBIC Journal of Biological Inorganic Chemistry,* 9(8)**,**pp.973-986.

Dingley, A. J. and Pascal, S. M. (2011). *Biomolecular NMR spectroscopy*. Netherland: IOS Press.

Frisch, M. J. T., G. W.; Schlegel, H. B.; Scuseria, G. E.; Robb, M. A.; Cheeseman, J. R.; Scalmani, G.; Barone, V.; Mennucci, B.; Petersson, G. A.; Nakatsuji, H.; Caricato, M.; Li, X.; Hratchian, H. P.; Izmaylov, A. F.; Bloino, J.; Zheng, G.; Sonnenberg, J. L.; Hada, M.; Ehara, M.; Toyota, K.; Fukuda, R.; Hasegawa, J.;Ishida, M.; Nakajima, T.; Honda, Y.; Kitao, O.; Nakai, H.; Vreven, T.; Montgomery, J. A., Jr.; Peralta, J. E.; Ogliaro, F.; Bearpark, M.; Heyd, J. J.; Brothers, E.; Kudin, K. N.; Staroverov, V. N.; Kobayashi, R.; Normand, J.; Raghavachari, K.; Rendell, A.; Burant, J. C.; Iyengar, S. S.; Tomasi, J.; Cossi, M.; Rega, N.; Millam, J. M.; Klene, M.; Knox, J. E.; Cross, J. B.; Bakken, V.; Adamo, C.; Jaramillo, J.; Gomperts, R.; Stratmann, R. E.; Yazyev, O.; Austin, A. J.; Cammi, R.; Pomelli, C.;

Ochterski, J. W.; Martin, R. L.; Morokuma, K.; Zakrzewski, V. G.; Voth, G. A.; Salvador, P.; Dannenberg, J. J.; Dapprich, S.; Daniels, A. D.; Farkas, Ö.; Foresman, J. B.; Ortiz, J. V.; Cioslowski, J.; Fox, D. J. Gaussian, Inc., Wallingford CT. (2009). 'Gaussian 09, Revision'.

Gong, B., Chen, J. H., Yajima, R., Chen, Y., Chase, E., Chadalavada, D. M., Golden, B. L., Carey, P. R. and Bevilacqua, P. C. (2009). 'Raman crystallography of RNA', *Methods,* 49(2)**,**pp.101-111.

Griffiths, P. R. and de Haseth, J. A. (2007). *Fourier transform infrared spectrometry* (2nd edn.). USA: John Wiley and Sons, Inc.

Hanlon, E. B., Manoharan, R., Koo, T. W., Shafer, K. E., Motz, J. T., Fitzmaurice, M., Kramer, J. R., Itzkan, I., Dasari, R. R. and Feld, M. S. (2000). 'Prospects for *in vivo* Raman spectroscopy', *Physics in Medicine and Biology,* 45(2)**,**pp.R1-R59.

Hobro, A. J., Rouhi, M., Blanch, E. W. and Conn, G. L. (2007). 'Raman and Raman optical activity (ROA) analysis of RNA structural motifs in domain I of the EMCV IRES', *Nucleic Acids Research,*35(4)**,**pp.1169-1177.

Iyandurai.N, Senthil.K and Sarojini.R (2009). 'FT-Raman spectroscopy of heavy metal-nucleotide complexes', *Asian Jornal of Chemistry,* 21(6)**,**pp. 4241-4245.

Koch, W. and Holthausen, C. (2001). *A chemist's guide to density functional theory* (2nd edn.):Weinheim: John Wiley and Sons, Inc.

Lee, C., Yang, W. and Parr, R. G. (1988). 'Development of the Colle-Salvetti correlation-energy formula into a functional of the electron density', *Physical Review B. Condensed Matterand Materials Physics,* 37(2)**,**pp.785-789.

Luque, F. J., Lopez, J. M. and Orozco, M. (2001). Perspective on "Electrostatic interactions of a solute with a continuum. A direct utilization of ab initio molecular potentials for the prevision of solvent effects", in Christopher,C. and D. G., T. (eds.) *Theoretical chemistry accounts: New century issue.* Berlin: Springer Berlin Heidelberg,pp.343-345.

Miles, J. (2014).'R squared, adjusted R squared'. *Wiley StatsRef: Statistics Reference Online.* John Wiley and Sons, Ltd.

Naaman, R. and Vager, Z. (2012). *The structure of small molecules and ions*.Chicago: Springer Science and Business Media.

Nafie, L. A. (2011). *Vibrational Optical Activity.* New York: John Wiley and Sons, Ltd.

Nelson, D. L., Nelson, D. L., Lehninger, A. L. and Cox, M. M. (2008). *Principles of Biochemistry*.4th edn. New York: W.H. Freeman.

Ostovarpour, S. and Blanch, E. W. (2012). 'Phosphorylation detection and characterization in ribonucleotides using Raman and Raman optical activity (ROA) spectroscopies', *Appl Spectrosc,* 66(3)**,**pp. 289-93.

Rodriguez-Casado, A., Carmona, P. and Molina, M. (1998). 'Enzymatic synthesis of 18O(6)-guanosine and spectroscopic characterization of Hoogsteen and reverse Hoogsteen hydrogen-bonded guanosine Structures', *The Journal of Physical Chemistry B,* 102(27)**,**pp.5387-5393.

Rudack, T., Xia, F., Schlitter, J., Kotting, C. and Gerwert, K. (2012). 'The role of magnesium for geometry and charge in GTP hydrolysis, revealed by quantum mechanics/molecular mechanics simulations', *Biophysical Journal,* 103(2)**,**pp.293-302.

Smith, E. and Dent, G. (2005). Introduction, basic theory and principles, in Ewen,S. and Geoffrey, D.(eds) *Modern Raman spectroscopy –A Practical approach.*Chichester: John Wiley and Sons, Ltd.pp.1-20.

Smith, E. and Dent, G. (2005). The Raman experiment – Raman instrumentation, sample presentation, data handling and practical aspects of interpretation, in Ewen, S. and Geoffrey,D.(eds) *Modern Raman Spectroscopy – A Practical Approach.* John Wiley and Sons, Ltd, pp.23-70.

Szabo, Z. (2008). 'Multinuclear NMR studies of the interaction of metal ions with adenine-nucleotides', *Coordination Chemistry Reviews,* 252(21–22)**,**pp. 2362-2380.

Ulyanov, N. B., Du, Z. and James, T. L. (2006). Refinement of nucleic acid structures with residual dipolar coupling restraints in cartesian coordinate space. In Graham A, W.(ed.) *Modern magnetic resonance.* Dordrecht: Springer Netherlands.pp.665-670.

Watson, H. C. and Gamblin, S. J. (1985). 'The magnesium protein interaction in nucleotide complexes of phos-phoglycerate kinase', *Journal of Biosciences,* 8(1)**,**pp.499-506.

Chapter 4: Spectroscopic Characterisation of the Phosphoglycerate Kinase Transition State Using Raman Spectroscopy

Contributing authors and their roles:

Omer Azher is the main author. Zhalgas Serimbetov provided the phosphoglycerate kinase enzyme, Ewan W. Blanch and Jonathan P. Waltho contributed to this work through supervision and guidance

4.1 Abstract

Human phosphoglycerate kinase (hPGK) is a 415-residue glycolytic enzyme that catalyses the reversible transfer of a phosphoryl (PO_3^-) group from 1, 3-bisphosphoglycerate (1,3 BPG) to adenosine diphosphate (ADP) forming adenosine triphosphate (ATP) and 3-phosphoglycerate (3PG). During catalysis, the enzyme adopts a hinge bending motion forming a closed hPGK conformation, which is mimicked using a hPGK-ADP-AlF_4-3PG transition state analogue complex. Despite the wealth of structural data obtained from X-ray crystallography and NMR, the detailed mechanisms and the chemical interactions involved during the hinge bending motion of the hPGK remain ambiguous. This study uses the Raman spectroscopy to characterize the spectral profile of hPGK in aqueous solution and study the structural changes associated the enzyme during its catalytic cycle. The impact of isotopic substitution on Amide I and Amide III bands and the contribution of the ADP nucleotide were also explored. The results revealed the Raman profiles for apo-hPGK, hPGK-ADP, hPGK-3PG and hPGK-TSA complexes in aqueous environment at neutral pH. The marker bands from Amide I and III regions and the spectral changes associated with these bands for the different states of the enzyme are identified. The results also indicated that the spectral changes associated with binding of ADP or 3-PG corresponded mainly to some of the α-helices of the hPGK backbone. In the closed conformation of hPGK, both β-sheets and α-helices are involved, supporting the role of different hydrogen bonding in stabilizing the enzyme in different stages of its catalytic cycle. The results also suggested that Raman vibrations identified at 1030-1070 cm^{-1} in the hPGK-ADP complex could arise from ADP vibrations.

4.2 Introduction

Human phosphoglycerate kinase (hPGK) is a 45 kD monomeric protein composed of 415- residues. The enzyme plays a vital role in the glycolytic pathway as it reversibly transfers a phosphoryl (PO_3^{2-}) group from 1, 3-bisphosphoglycerate (1,3 BPG) to adenosine diphosphate (ADP) forming adenosine triphosphate (ATP) and 3-phosphoglycerate (3-PG) (Voet and Voet, 2011). Structurally, PGK comprises two similar size subunits (N- and C-domains) folded into α-helices and β-sheets and separated by a flexible hinge (Yon *et al.*, 1990). For hPGK, the N-domain is composed of 27 % α-helix and 11 % β-sheet conformations, while, the C-domain is composed of 42 % α-helix and 14 % β-sheet (Damaschun *et al.*, 1999). The hinge region of PGK also consists of a combination of α-helices and β- sheets in addition to other random coil-like structures (Watson *et al.*, 1982). The binding sites for 1, 3-BPG and ADP are located in the N- and the C-domains respectively (Hosszu *et al.*, 1997). X-ray studies have identified two structural conformations for PGK crystals (open and closed). The open conformation of the protein occurs in the absence of the bound substrates and is defined by separated N- and C-subunits.

During the catalytic cycle of the enzyme, the two domains move in a hinge bending motion towards each other bringing the substrates together and forming the closed PGK conformer (Szabo *et al.*, 2008). The movement of the two domains during catalysis is essential for the function and activity of the protein. Despite the wealth of experimental and computational information already established, the detailed molecular mechanisms and the diverse chemical interactions underlying the hinge bending motion remains elusive (Dhar *et al.*, 2010). X-ray crystallography and nuclear magnetic resonance (NMR) are considered as the fundamental techniques that provided valuable data about the structural modifications associated with PGK during its enzymatic activity. Nevertheless, X-ray crystallography and NMR have their own disadvantages. The former method is restricted in the information about the dynamic behavior of the molecules while NMR is limited to smaller to medium sized molecular weight proteins (Krishnan and Rupp, 2001).

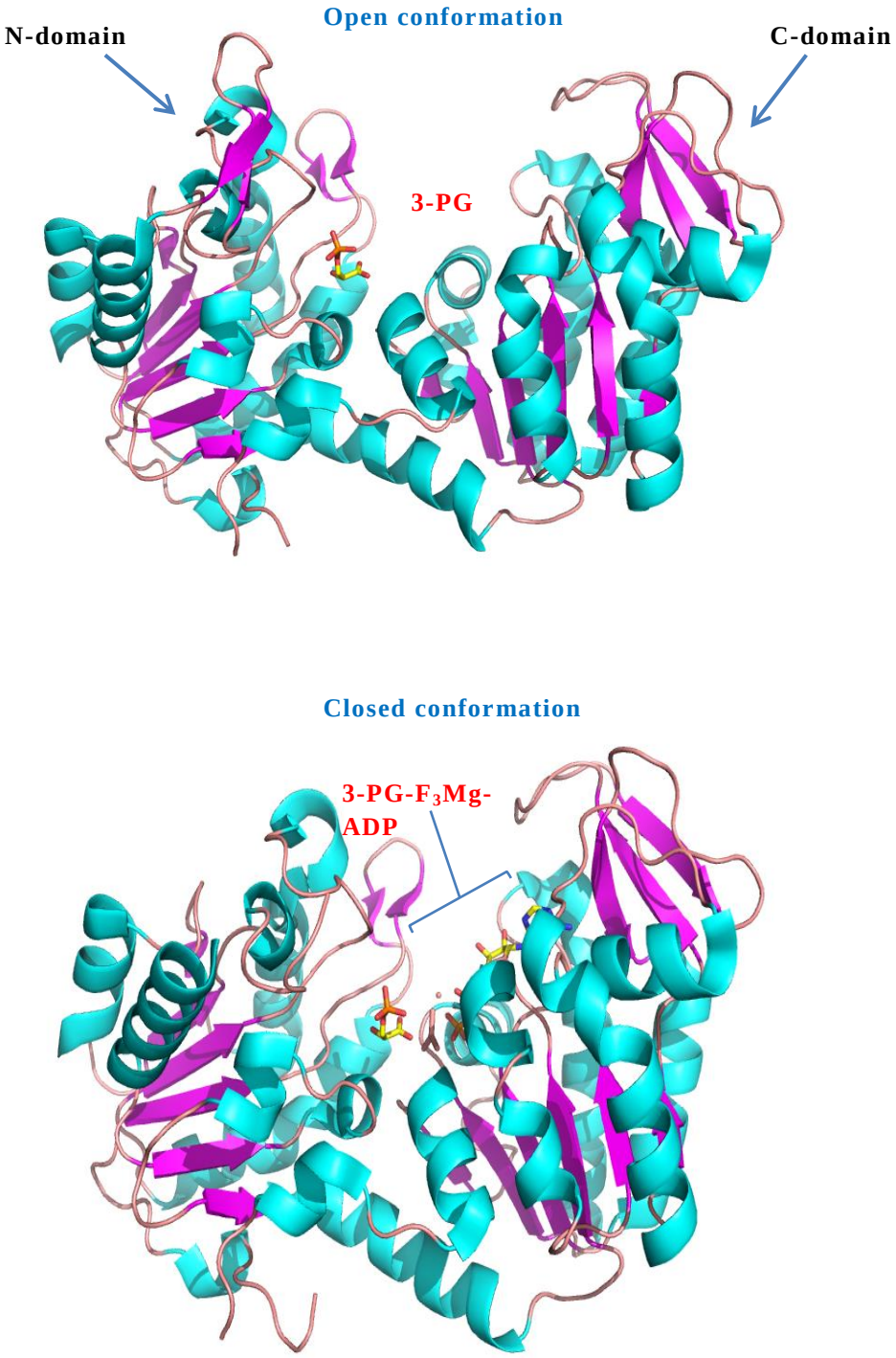

Figure 4.1. The structure of the open (top) and closed (bottom) conformation of human PGK.

Raman spectroscopy is a state of art vibrational spectroscopic technique that could overcome some of these limitations. It has been used successfully for studying and identifying the chemical constituents and the structural characteristics of proteins, viruses and nucleic acids in solid and aqueous environments (Black *et al.*, 1993). Samples for Raman analysis do not require chemical labeling and can be used for proteins of all sizes (Smith and Dent, 2005). Raman spectroscopy can also be applied to study the secondary structure of proteins and detect the structural changes accompanying different phases of the catalytic cycles of enzymes (Pappas *et al.*, 2000 ; Kinalwa *et al.*, 2010). Alterations in the protein secondary structures can be analyzed using certain vibrational frequencies that appear in characteristic regions of Raman spectra, most importantly those involving CONH groups, which are referred to as Amide A, B and I to VII modes (Kong and Yu, 2007). The Amide I and III regions are considered to contain the bands that are most sensitive to changes in the secondary structure of the protein backbone (Yang *et al.*, 2015; Cai and Singh, 2004). The Amide I region is located between 1600-1680 cm^{-1} and results from the stretching vibrations of the carbonyl group C=O. The Amide III region is located between 1230-1300 cm^{-1} and corresponds to a mix of C-C and C-N stretching with C-H deformation and N-H bending vibrations (Schulz and Baranska, 2007).

Studying the conformational changes of the enzymes leading to the formation of the transition state (TS) is fundamentally important in the development of a detailed understanding of the chemical interactions involved during the catalytic cycle of the enzyme. The lifetime for the enzymatic TS lasts for a few femtoseconds, therefore, direct monitoring of the TS remains a challenging task (Zewail, 2000; Schramm, 2015)'. The use of transition state analogues (TSAs) is considered as a valuable alternative approach for exploring the dynamic behavior of the target protein during catalysis (Schramm, 2007). Aluminium and magnesium fluoride derivatives have been used as TSAs for studying the catalytic activity of PGK as they are able to neutralise the charges in the active site of the protein and mimic the geometry of its TS (Cliff *et al.*, 2010; Bowler, 2013). This study aims to:

a) Characterize the Raman profile of hPGK and study the spectral changes associated with the Amide I and III regions of the enzyme during its catalytic cycle.

b) Identify bands in the Amide I and III region specifically associated with amide groups through the introduction of isotopic labels. .

c) Study the contribution of the nucleotide ADP and the coordination of α- and β-phosphate groups during catalysis.

4.3 Material and methods

4.3.1 Chemicals

Samples of 3-phosphoglycerate (3-PG), 5'- adenosine diphosphate sodium salt (5'-ADP), magnesium chloride ($MgCl_2$) and aluminium chloride ($AlCl_3$) were purchased from Sigma-Aldrich Ltd and used without further purification.

4.3.2 Sample preparation

Each sample of 3-PG, ADP, $MgCl_2$ and was prepared with a concentration of 2.8 mM in 50 mM Tris buffer. The pH of each solution was adjusted to 7.0 (±0.1) using 1 M NaOH solution. Samples were centrifuged at 9500 g for 5 minutes to eliminate dust contamination. $AlCl_3$ was prepared in a similar concentration and used as a transition state analogue to maintain the closed conformation of the enzyme (Zerrad *et al.*, 2011).

4.3.3 Human phosphoglycerate kinase (hPGK) enzyme

Expression and purification of the enzyme have been described earlier (Flachner *et al.*, 2005). The protein sample [20 mg/ml in 50 mM Tris buffer] was stored at -80 °C. Samples of hPGK-3-PG and hPGK-ADP were prepared with a concentration of 0.4 mM of the protein and 0.4mM of the substrate at pH 7.2. The protein complex was prepared at a concentration of 0.4 mM of hPGK and 0.4 mM of 3-PG, ADP, $MgCl_2$ and $AlCl_3$ at pH 7.2. For spectral analysis, each sample of apo-hPGK, hPGK-ADP, hPGK-3-PG and hPGK TSA complexes were replicated three times and 100 µL of each replicate was transferred to a quartz microfluorescence cells. The expression and purification of ^{15}N-labeled-hPGK have been described in a earlier study (Reed *et al.*, 2003).

4.4.4 Raman measurements

A ChiralRaman spectrometer (BioTools Inc., Jupiter FL, USA) operating in backscattering mode was used to measure all Raman spectra. The set-up of the instrument includes: Laser wavelength of 532 nm, spectral resolution of 7 cm^{-1}, power at the laser head of 1.20 W, length of illumination period was 1.029 seconds, total data acquisition times of 0.166 hrs. Data analysis was carried out using MATLAB R2013a software that includes an inbuilt Raman toolbox.

4.4.5 Raman data analysis and peak deconvolution

The Raman spectra were processed using Matlab version R2013a. In this software, the accumulated Raman data for each protein sample were summed and baselined. Spectral subtraction was performed for each replicate to eliminate the bands from buffer (Severcan and Parvez, 2012). The data were then plotted using Origin 8.5 software. Curve fitting was applied for the broaden bands of hPGK to improve the resolution and identify the overlapping Raman peaks (Lorenz-Fonfria and Padros, 2005; Aragao and Messaddeq, 2008). Origin 8.5.1 software was used for this purpose and the Gaussian function was chosen for deconvolution modelling. The second derivative was applied in each case to reduce the bandwidth and identify the frequency of each underlying bands. The quality of the fitting was assessed by calculating adjusted r square values. Peak deconvolution with adjusted r^2 values near 1 (~ 0.95) indicated the goodness of the data (Miles, 2014).

4.4 Results

The Raman spectra for apo-hPGK, hPGK-ADP, hPGK-3-PG and hPGK TSA complexes were recorded. To our knowledge, this is the first study to report the Raman spectra for hPGK and which probe the spectral changes associated with the enzyme during catalysis. The Raman profile for 0.4 mM apo-hPGK in Tris buffer is shown for the region at 950-1800 cm^{-1} (Figure 4.2). The general features of the spectrum are in agreement with spectra from earlier studies performed on different proteins (Figure 4.3), for example α-synuclein (Maiti *et al.*, 2004; Esmonde-White *et al.*, 2009). The main bands in the Amide I and III regions for apo-hPGK are located at 1668 and 1242 cm^{-1}, respectively (Figure 4.2). The results show broadened

bandwidth and asymmetry for the Amide I and III band profiles, which indicates the presence of overlapping Raman bands (Figure 4.4) (Maiti *et al.*, 2004).

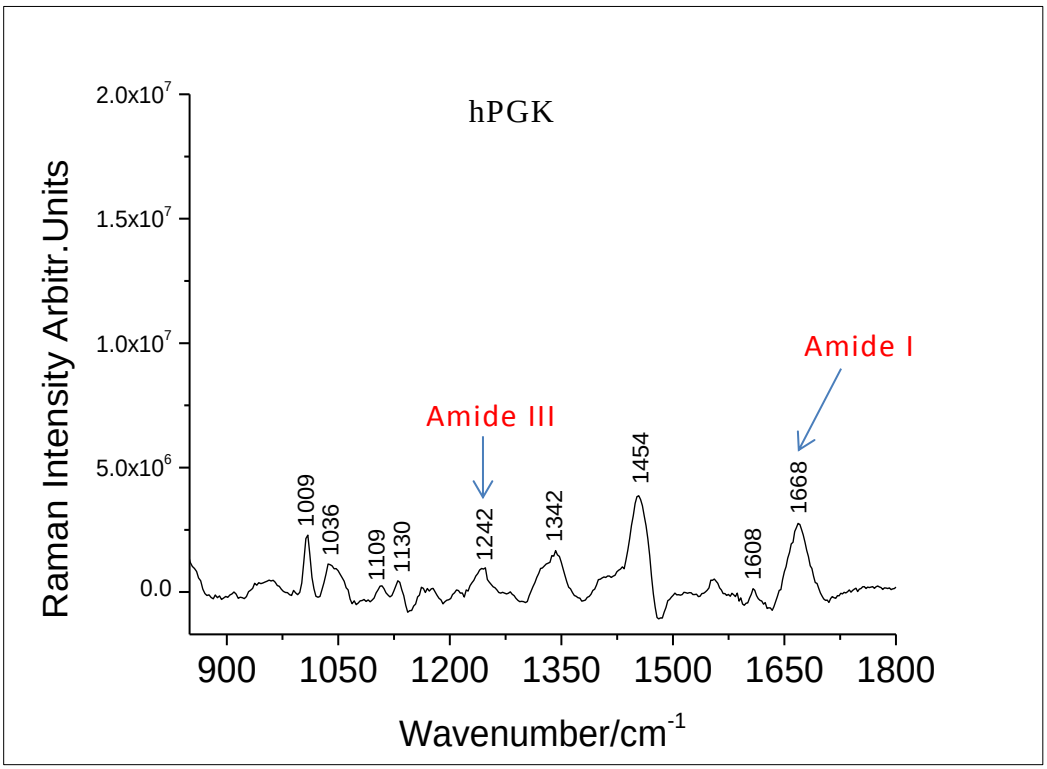

Figure 4.2. The Raman spectrum of 0.4mM hPGK at pH 7.2.

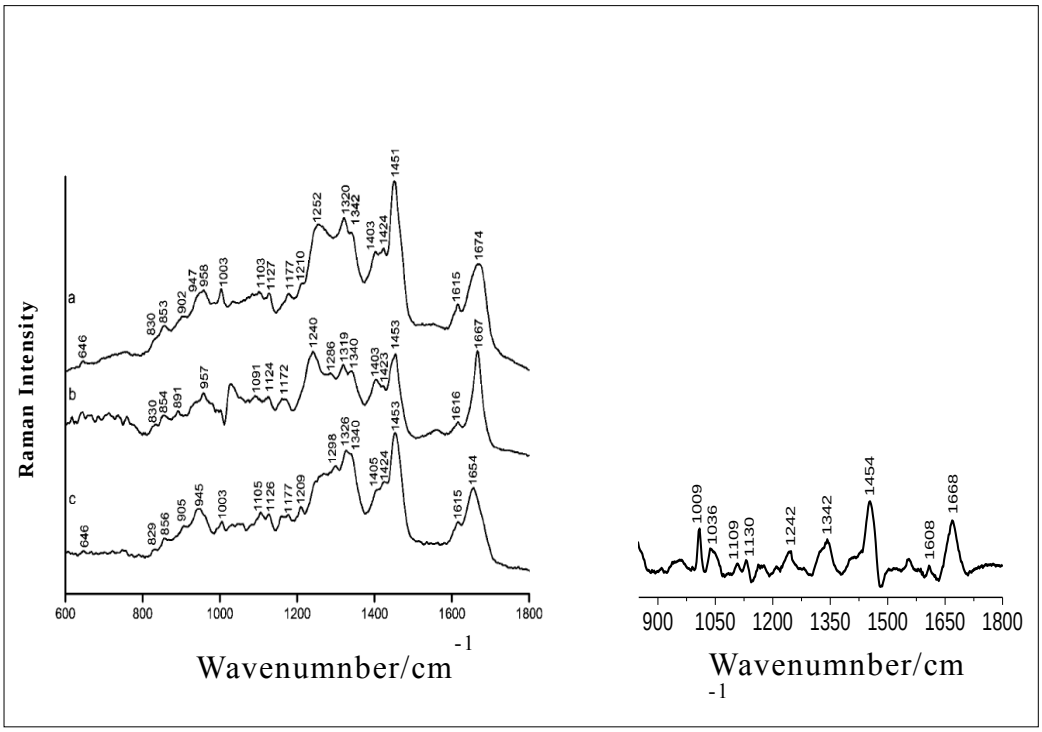

Figure 4.3. General similarities between the Raman spectra of α-synuclein (left) from earlier study and hPGK (right) in the present study.

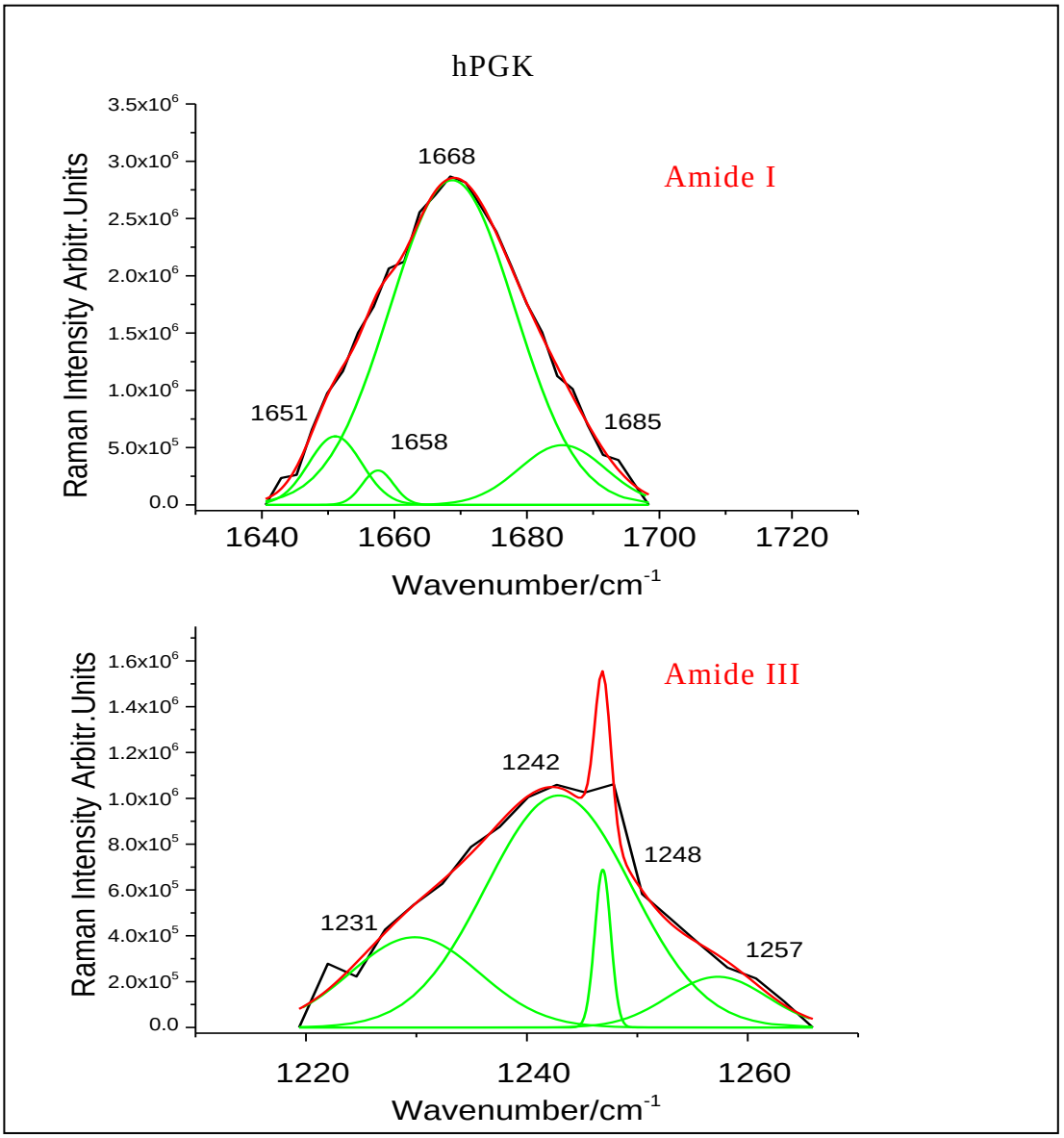

Figure 4.4. Peak deconvolution of the Amide I (above) and III regions (below) of hPGK. The black line represents the experimental band, red line represents the cumulative modelled band profile and green lines represent the deconvoluted band components.

In order to confirm that the assigned bands in the Amide I and III regions were from vibrational modes that included Amide group atoms, the Raman spectrum of apo-hPGK uniformly labelled with ^{15}N (^{15}N-hPGK) were also recorded over the range 900-1800 cm^{-1}. The spectra for ^{15}N-hPGK identified a general shift to lower frequency of the Amide I (by 5 cm^{-1}) and Amide III (by 2 cm^{-1}) bands. The Raman band at 1009 cm^{-1} also shifted to lower frequency (by 3 cm^{-1}) in ^{15}N-hPGK (Figure 4-5). A comparable change in the Raman frequency of aspartic acid and its isotopic analogues has been reported (Navarrete *et al.*, 1994).

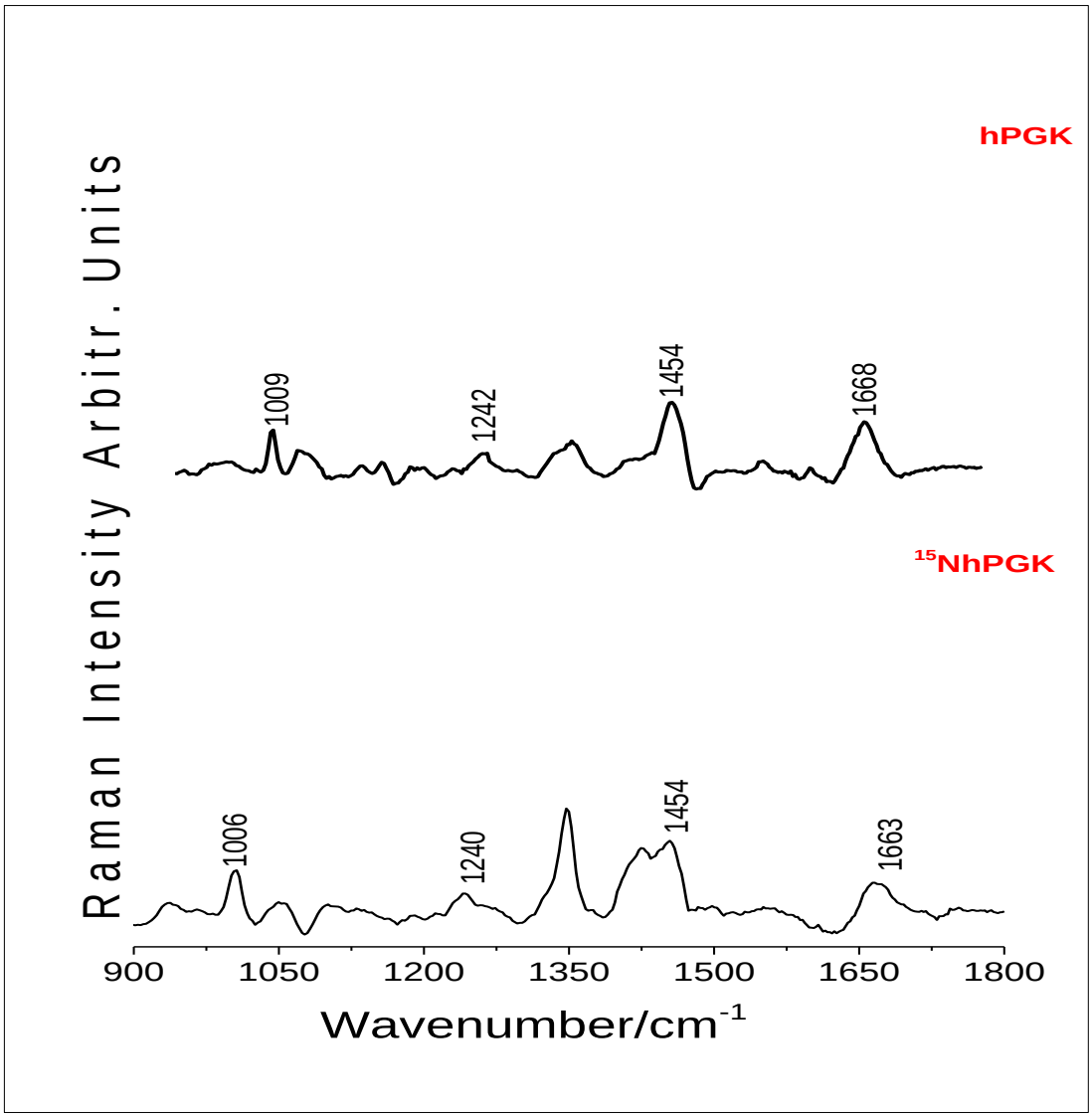

Figure 4.5. The Raman spectra of hPGK(top) and its isotope analogue ^{15}NhPGK (bottom). The Amide I and III bands at 1668 and 12480 cm^{-1} respectively are shifted to lower wavenumber in the ^{15}NhPGK molecule.

The Raman profiles for the enzyme bound substrate and TSA complexes are compared in Figure 4.6. This revealed general spectral similarities between apo-hPGK and its bound complexes. However, alterations are observed in the frequency and the shape of the bands in the Amide I and III regions. For the hPGK-ADP complex, the fitted bands in the Amide I region indicated a 3 cm^{-1} shift to higher frequency compared with apo-hPGK (1651 to 1654 cm^{-1}) for the band that is assigned to the α-helical structure. However, the band that is dominant in intensity at 1668 cm^{-1} (assigned to the β-sheet structure), revealed a similar frequency to that in apo-hPGK. For the hPGK-3-PG complex, the β-sheet band at 1668 cm^{-1} again remained unchanged while the α-helix band move to higher frequency by 3 cm^{-1} (1651 to 1657 cm^{-1}) compared with apo-hPGK (Figure 4.7).

The hPGK-TSA complex, on the other hand, there is a distinct change in the Amide I region, where both the α-helix (1651 to 1656 cm^{-1}) and the β-sheet (1668 to 1665 cm^{-1}) bands alter their frequency and intensity compared to apo-hPGK. The intensity of the β-sheet band, in particular, was decreased dramatically (Figure 4-7).

The Raman profiles also showed some distinctive spectral characteristics for apo-hPGK, hPGK-ADP, hPGK-3-PG and hPGK-TSA complexes in the amide III region (Figure 4-8). The Raman band assigned to the β-sheet vibration 1242 cm^{-1} does not change in frequency but there is a marked change in its relative intensity to other bands in the Amide III region. In the hPGK-3PG and hPGK-ADP complexes, the band in the 1257-1259 cm^{-1} range increases significantly compared with apo-hPGK. In the hPGK-TSA complex the equivalent band (at 1258 cm^{-1}) increases further in relative intensity such that it is almost equal in magnitude with the 1242 cm^{-1} band. The assignment of this band is not well established in the literature.

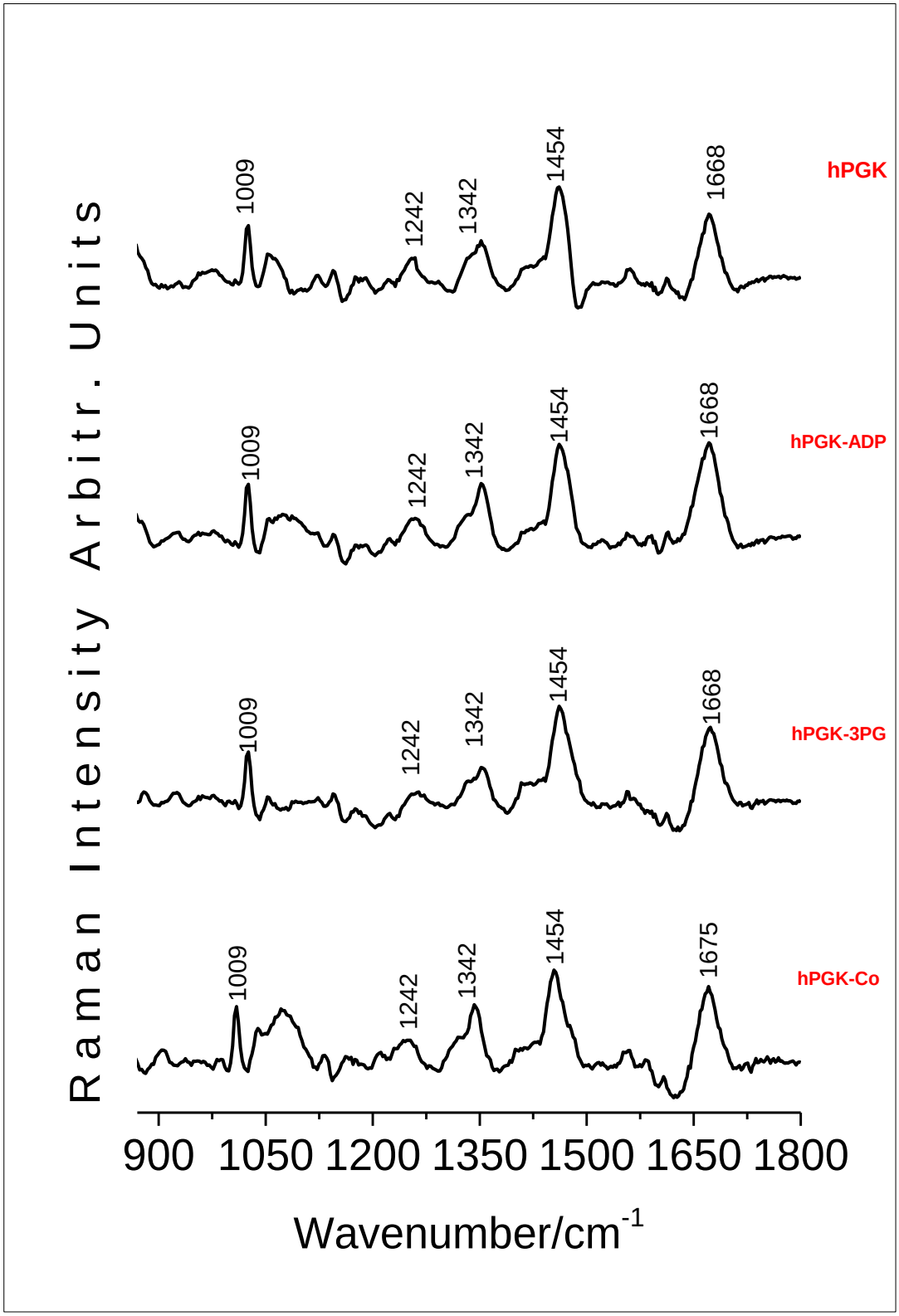

Figure 4.6. Raman spectra for 0.4 mM hPGK, hPGK-ADP, hPGK-3-PG and hPGK complex at pH 7.2.

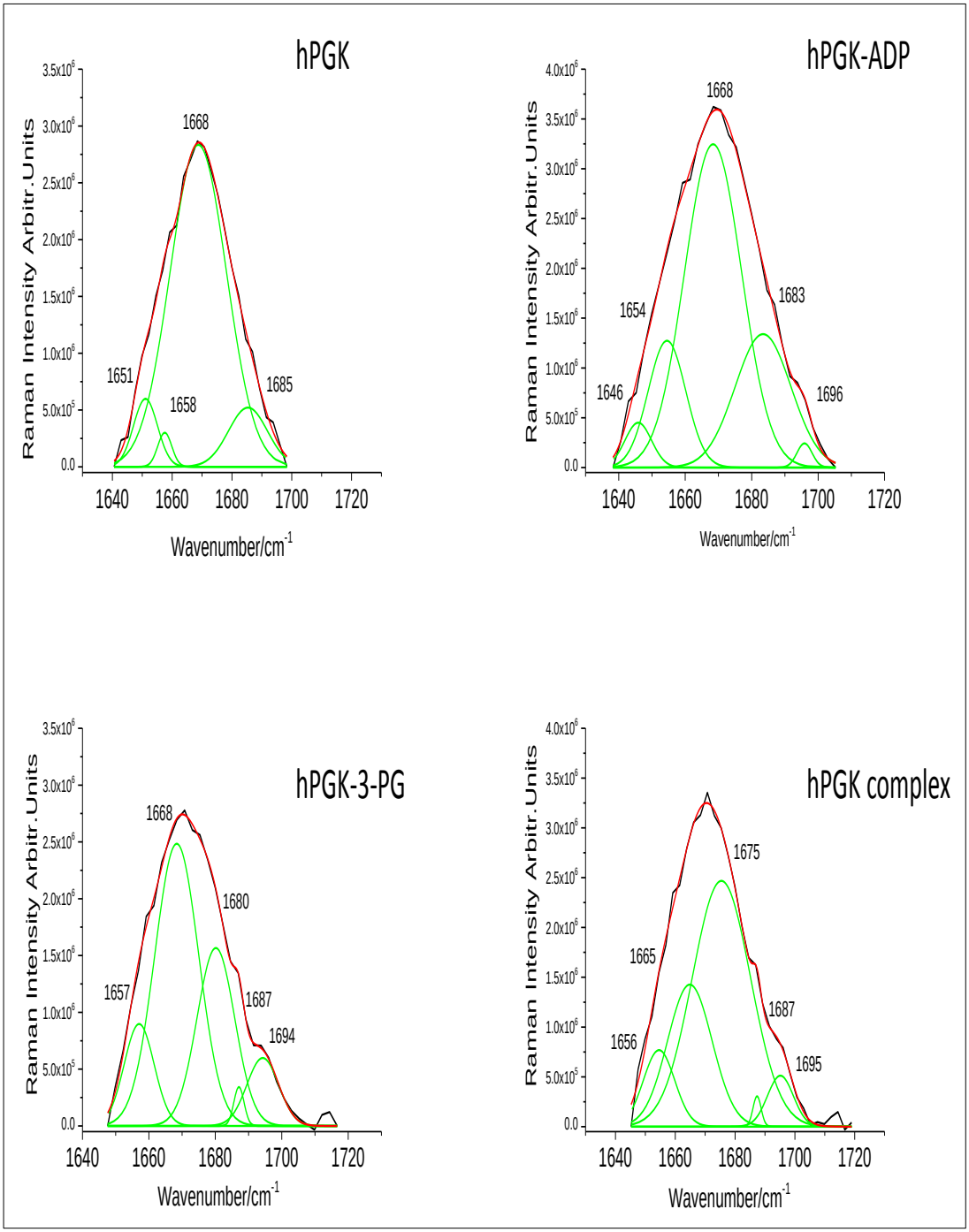

Figure 4-7. Peak deconvolution of the Amide I region of PGK, PGK-ADP, PGK-3-PG and PGK complex. The black line represents the experimental band, red line represents the cumulative modelled band profile and green lines represent the deconvoluted band components.

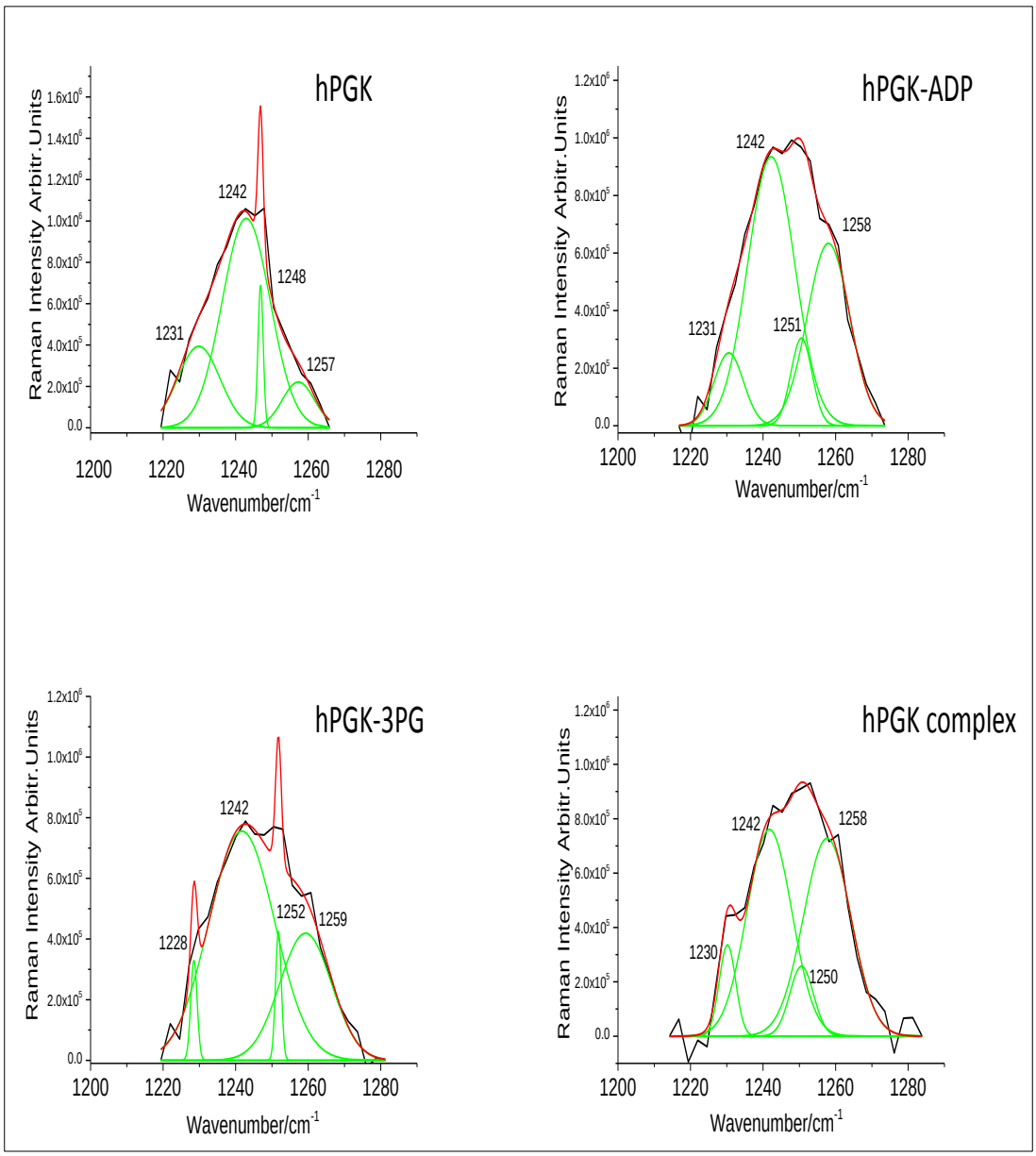

Figure 4.8. Peak deconvolution of the amide III region of PGK, PGK-ADP, PGK-3-PG and PGK complex. The black line represents the experimental band, red line represents the cumulative modelled band profile and green lines represent the deconvoluted band components.

The asymmetric broad Raman peak in the region 1030-1070 cm^{-1} revealed spectral changes, particularly between the hPGK-ADP and the hPGK-TSA complexes (Figure 4.9). Deconvolution of the peak in this region revealed the presence of seven bands in both the TSA complex and the nucleotide bound enzyme. Based on our DFT calculations conducted previously on 5'-ADP molecule, the Raman band at 1037 cm^{-1} for hPGK-ADP is potentially correlated to two DFT modes (1034 cm^{-1}, 0.16 a.u., and 1039 cm^{-1}, 0.02 a.u.) of the nucleotide. The 1047 cm^{-1} band for the PGK-ADP complex is also potentially correlated to a DFT-derived mode (1051 cm^{-1}, 0.34 a.u.). Finally, the high intensity band for the PGK-ADP complex observed at 1077 cm^{-1} potentially corresponds to the two DFT-derived nucleotide modes (1073 cm^{-1}, 0.07 a.u. and 1078 cm^{-1}, 0.07 a.u.). All of these vibrational modes have a 39 to 99 % contribution of the α- and β-phosphate groups.

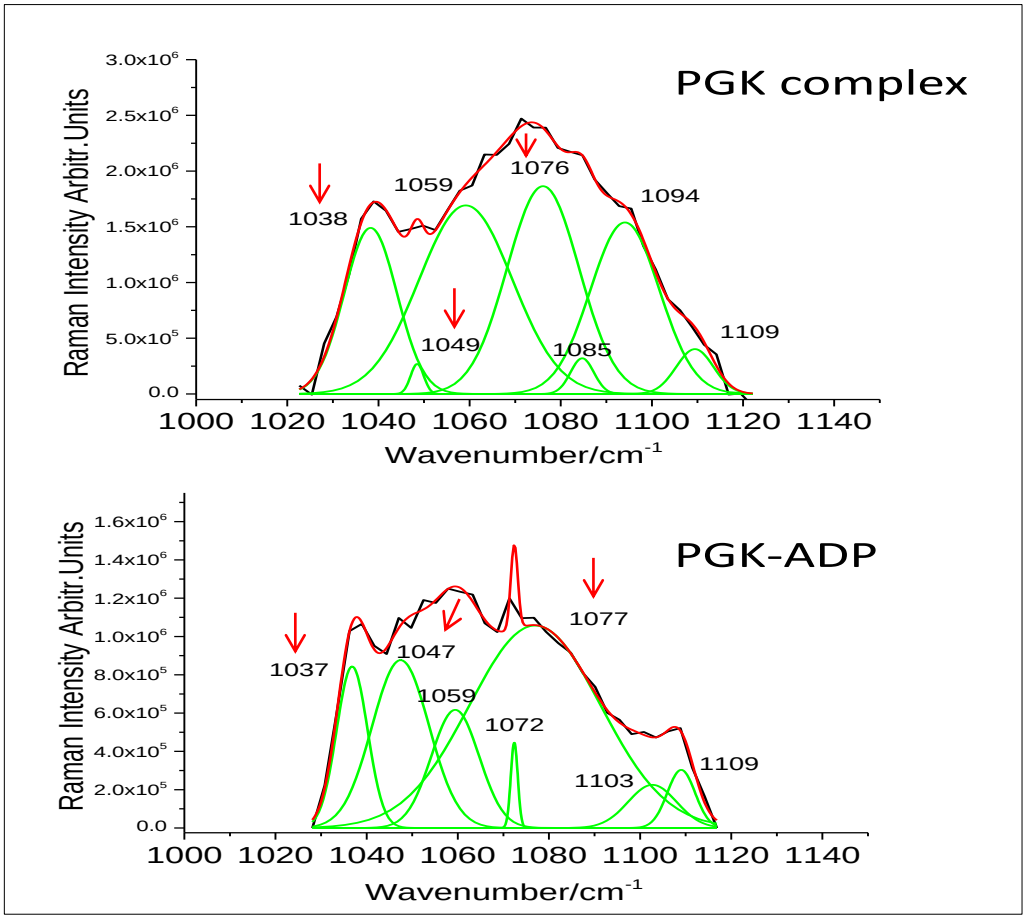

Figure 4.9. Peak deconvolution of the region at 1030-1070 cm^{-1} for hPGK complex (above) and hPGK-ADP (below). Black line represents the experimental band, red line represents the cumulative band and green lines represent the deconvoluted bands. The red arrows indicate the ADP Raman bands based on out DFT calculations.

4.5 Discussion

The Raman profiles in this study define the spectral characteristics for apo-hPGK, and the hPGK-ADP, hPGK-3PG and hPGK-TSA complexes. The work therefore explores the spectral alterations in the Amide I and III regions of the enzyme during its catalytic cycle. Isotopic substitution with ^{15}N confirmed that the primary bands analysed in the Amide I and III regions directly involved the backbone amide groups. The general features of the Raman spectrum of hPGK are the presence of intense Raman signals in the regions previously assigned to Amide I vibrations (at 1668 cm^{-1}), C-H deformation (at 1454 cm^{-1}) and phenylalanine vibrations (at 1009 cm^{-1}). Comparing the Raman profiles for hPGK with other proteins reviewed in an earlier study (Rygula *et al.*, 2013), it can be concluded that all of the intense bands can be used as spectral markers that distinguish hPGK from other proteins. For example, Dingari *et al*. (2012) recorded the Raman spectrum for albumin and revealed the presence of three high intensity Raman bands that are similar to the ones observed for hPGK, but with clear differences in frequencies (Dingari *et al*., 2012).

The Amide I and III bands, at 1668 and 1248 cm^{-1} respectively, reflect the large contribution of β–sheet secondary structure to the overall architecture of hPGK. The Raman vibrations of these bands correspond mainly to C=O stretching (Amide I) and C-H, N-H deformation (Amide III) (Merlino *et al.*, 2008). Alterations in the vibrational frequencies in these regions reveal chemical or structural modifications of the protein molecule. The Raman spectrum of ^{15}N-labelled apo-hPGK, demonstrated the impact of isotope substitution on Amide I and Amide III regions of the hPGK enzyme as these regions shifted by -5 and -2 cm^{-1} respectively compared to the unlabelled enzyme.

The Raman profiles for apo-hPGK, and the hPGK-ADP, hPGK-3PG and hPGK-TSA complexes revealed distinct spectral features. The deconvoluted Amide I region of the hPGK is dominated by bands at 1668 cm^{-1}, assigned to the β-sheets, in apo-hPGK and the two substrate complexes. The binding of ADP or 3-PG has no measureable effect on the frequency of this band, but a significant effect on its relative intensity, especially in the case of 3-PG binding The primary effect of substrate binding is to shift the band at 1651 cm^{-1}, assigned to the α-helices, to higher frequency (+ 3 cm^{-1} for ADP and + 6 cm^{-1} for 3-PG) and to increase the relative intensity of these bands.

These observations suggest that the binding of ADP or 3-PG can impart structural modifications to hPGK even when the enzyme remains in an open conformation. There is no crystal structure of apo-hPGK but small-angle X-ray scattering models of its structure indicate that it has a more open conformation than the ADP or 3-PG bound forms (Zerrad *et al*., 2011). This is consistent with changes in the hinge region, which is dominated by α-helices, between apo-hPGK and the substrate complexes. These changes in Raman spectra are also in agreement with molecular dynamic studies, which revealed that the binding of the nucleotide and bisphosphoglycerate can alter the PGK structure by decreasing the flexibility of the C-domain and increasing the fluctuations of the N-domain respectively (Palmai *et al.*, 2009).

A more substantial effect on the Amide I region is observed on formation of the TSA complex. The β-sheet band at 1668 cm^{-1} for apo-hPGK, hPGK-ADP and hPGK-3PG complexes moved to 1665 cm^{-1} in the hPGK-TSA complex with a notable reduction in intensity. The Amide I region became dominated in intensity by a band, also in the β-sheet region, at 1675 cm^{-1}. The α-helix band at 1651 cm^{-1} in apo-hPGK moved to 1656 cm^{-1} in the TSA complex, which is similar to the behavior observed for substrate binding. The marked alterations in the vibrational energy of the β-sheet bands between the open and closed conformation of the enzyme supports an important role of the β-sheet structures in the hinge bending motion of the enzyme that leads to closure, since the β-sheet, especially β-strand L, plays an important role in the function of main hinge region in PGK (Hayward, 1999; Szilagyi *et al.*, 2001). A further role of the α-helical conformation was proposed by Auerbach *et al,* (1997) who shed light on the contribution of the α-helix structure in enhancing the thermostability and facilitate the transfer of $(\gamma - PO_3^{2-})$ groups for Trypanosoma PGK (Auerbach *et al.*, 1997). This is consistent with the Raman shift (by 5 cm^{-1}) observed in the hPGK-TSA complex as this change can be due to the involvement of α-helical rearrangements during the closure of the two domains of the enzyme complex. However, the observed change in Raman spectra is similar without full closure of the enzyme. The closed conformation of PGK involves the formation of hydrogen bonding between the Amide groups of various amino acids to stabilise the structure and neutralise the negative charges on the γ-phosphate group, thus, decreasing its free energy (Auerbach *et al.*, 1997; Bernstein and Hol, 1998; Pelton

and McLean, 2000). The results of the deconvoluted bands in Amide I regions for the hPGK-TSA complex showed noticeable decreases in the intensity of the β-sheet vibrations compared to the unbound form of the protein. As the reduction in the intensity of the Raman bands can be used as an indicator of the formation of hydrogen bonding (Triggs and Valentini, 1992), we can conclude that the decrease in the intensity of the β-sheet bands in the Amide I regions of the hPGK complex indicated the involvement of these regions in H-bonding during the formation of the transition state conformation of the enzyme.

Although the assignment of Raman bands in the Amide III region is less robust than in the Amide I region, the changes observed in the two regions between apo-hPGK, the two substrate complexes and the hPGK-TSA complex mirror each other to some extent. The similarity is most apparent in that the dominant band (1242 cm^{-1} in Amide III and 1668 cm^{-1} in Amide I) reduce in intensity relative to a higher frequency band (1257-1259 cm^{-1} in Amide III and 1675-1685 cm^{-1} in Amide I), meaning that the overall change in shape remains similar. It is noteworthy though that there is not a one-to-one correspondence in the changes, and further interpretation of the underlying causes will require future efforts to assign the bands with more confidence.

Finally, the hPGK-ADP and hPGK-TSA complexes showed noticeable similarities in the 1030-1070 cm^{-1} region of the Raman spectrum, which distinguish them from apo-hPGK and the hPGK-3PG complex. The changes in the spectral profiles of the deconvoluted region at 1000-1140 cm^{-1} for hPGK-ADP and hPGK-TSA complex reflect nucleotide binding, and could be due to the hydrogen bonding network established as the C-domain of hPGK is occupied. The hydrogen bonding in this region helps to stabilise the oxygen anions in the phosphoryl groups and to coordinate them in a way that allows the terminal phosphate to be transferred to 3-phosphoglycerate, and *vice versa* (Szilagyi *et al.*, 2001). The interpretation of the of the deconvoluted Raman bands of the protein bound ADP based on the experimental measurements and DFT calculations can provide a comprehensive description of the dynamic behaviour of the nucleotide upon binding to the protein. This will also enable further investigations of the involvement of different chemical moieties of the nucleotide, such as phosphate group(s), during the activity of different proteins. Despite that, interpreting the spectral changes of the bound nucleotide using this

approach (Raman measurement and DFT) can have some limitations. For instance, the detection of the Raman bands of the bound nucleotide is difficult due to the small size of the nucleotide compared to the bound protein. The Raman bands of the buffer might interfere with the nucleotide bands; therefore, careful subtraction of the buffer is necessary to eliminate this interference. The Raman peak at which the Raman vibrations of the ADP are expected is broadened. Therefore deconvolution is required to detect the overlapped bands. The deconvoluted bands could have different frequencies than the real bands that arise from the actual vibration of the molecule Therefore, the frequencies and intensities of the deconvoluted bands should be comparable to their DFT counterparts to ensure the accuracy of the results.

In conclusion, this study reports the Raman profile for hPGK and identified three intense bands at at 1668, 1454 and 1009 cm^{-1} along with their assignments. Our experimental results showed that the binding of each of the substrates resulted in spectral changes in the Raman bands assigned for the α-helical structure from the Amide I regions. These changes are ascribed to modifications in the backbone of PGK, in agreement with previous molecular dynamics calculations. The Raman spectrum for the closed conformation of hPGK was recorded using aluminum fluoride to establish a transition state analogue with ADP and 3-PG. The changes in the Raman spectra of the hPGK-TSA complex for the bands assigned for α- helical and the β-sheet vibrations revealed the important role of both the α- helical and the β-sheet secondary structures hydrogen bonding in establishing the transition state of the enzyme. The results also supported the role of the hydrogen bonds in stabilizing the structure of the closed PGK complex. The Raman vibrations of the nucleotide are also identified in the region of 1030-1070 cm^{-1} and the coordination of α and β phosphate groups was indicated by the alterations in the vibrational energy associated with them on formation of the hPGK transition state.

4.6 References

Aragao, B. J. G. d. and Messaddeq, Y. (2008). 'Peak separation by derivative spectroscopy applied to ftir analysis of hydrolized silica', *Journal of the Brazilian Chemical Society,* 19**,**pp.1582-1594.

Auerbach, G., Huber, R., Grattinger, M., Zaiss, K., Schurig, H., Jaenicke, R. and Jacob, U. (1997). 'Closed structure of phosphoglycerate kinase from Thermotoga maritima reveals the catalytic mechanism and determinants of thermal stability', *Structure,* 5(11)**,**pp.1475-1483.

Bernstein, B. E. and Hol, W. G. J. (1998). 'Crystal structures of substrates and products bound to the phosphoglycerate kinase active site reveal the catalytic mechanism', *Biochemistry,* 37(13)**,**pp.4429-4436.

Black, C. B., Huang, H. w. and Cowan, J. A. (1993). 'Biological coordination chemistry of magnesium, sodium and potassium ions. Protein and nucleotide binding sites ', *Coordination Chemistry Reviews,* 135/136**,**pp.165-202.

Bowler, M. W. (2013). 'Conformational dynamics in phosphoglycerate kinase, an open and shut case?', *FEBS Letters,* 587(13)**,**pp.1878-1883.

Cai, S. and Singh, B. R. (2004). 'A distinct utility of the amide III infrared band for secondary structure estimation of aqueous protein solutions using partial least squares methods', *Biochemistry,* 43(9)**,**pp. 2541-2549.

Cliff, M. J., Bowler, M. W., Varga, A., Marston, J. P., Szabo, J., Hounslow, A. M., Baxter, N. J., Blackburn, G. M., Vas, M. and Waltho, J. P. (2010). 'Transition state analogue structures of human phosphoglycerate kinase establish the importance of charge balance in catalysis', *Journal of the American Chemical Society,* 132(18)**,**pp. 6507-6516.

Damaschun, G., Damaschun, H., Gast, K. and Zirwer, D. (1999). 'Proteins can adopt totally different folded conformations', *Journal of Molecular Biology,* 291(3)**,**pp.715-725.

Dhar, A., Samiotakis, A., Ebbinghaus, S., Nienhaus, L., Homouz, D., Gruebele, M. and Cheung, M. S. (2010). 'Structure, function, and folding of phosphoglycerate kinase are strongly perturbed by macromolecular crowding', *Proceedings of the National Academy of Sciences,* 107(41)**,**pp. 17586-17591.

Dingari, N. C., Horowitz, G. L., Kang, J. W., Dasari, R. R. and Barman, I. (2012). 'Raman spectroscopy provides a powerful diagnostic tool for accurate determination of albumin glycation', *PLoS One,* 7(2)**,**pp.1-11.

Esmonde-White, K. A., Mandair, G. S., Raaii, F., Jacobson, J. A., Miller, B. S., Urquhart, A. G., Roessler, B. J. and Morris, M. D. (2009). 'Raman spectroscopy of synovial fluid as a tool for diagnosing osteoarthritis', *Journal of Biomedical Optics,* 14(3)**,**pp.1-17.

Flachner, B., Varga, A., Szabo, J., Barna, L., Hajdu, I., Gyimesi, G., Zavodszky, P. and Vas, M. (2005). 'Substrate-assisted movement of the catalytic Lys 215 during domain closure: site-directed mutagenesis studies of human 3-phosphoglycerate kinase', *Biochemistry,* 44(51)**,**pp.16853-16865.

Hayward, S. (1999). 'Structural principles governing domain motions in proteins', *Proteins: Structure, Function, and Bioinformatics,*36(4)**,**pp.425-435.

Hosszu, L. L., Craven, C. J., Spencer, J., Parker, M. J., Clarke, A. R., Kelly, M. and Waltho, J. P. (1997). 'Is the structure of the N-domain of phosphoglycerate

kinase affected by isolation from the intact molecule?', *Biochemistry,* 36(2)**,**pp.333-340.

Kinalwa, M. N., Blanch, E. W. and Doig, A. J. (2010). 'Accurate determination of protein secondary structure content from Raman and Raman optical activity spectra', *Analytical Chemistry*,82(15),pp.6347-6349.

Kong, J. and Yu, S. (2007). 'Fourier transform infrared spectroscopic analysis of protein secondary structures', *Acta Biochimica Biophysica Sinica,* 39(8)**,**pp.549-59.

Krishnan, V. V. and Rupp, B. (2001). 'Macromolecular structure determination: Comparison of X-ray crystallography and NMR spectroscopy', *eLS.* John Wiley and Sons, Ltd.

Lorenz-Fonfria, V. A. and Padros, E. (2005). 'Maximum entropy deconvolution of infrared spectra: Use of a novel entropy expression without sign restriction', *Applied Spectroscopy,* 59(4)**,**pp.474-86.

Maiti, N. C., Apetri, M. M., Zagorski, M. G., Carey, P. R. and Anderson, V. E. (2004). 'Raman spectroscopic characterization of secondary structure in natively unfolded Pproteins: α-Synuclein', *Journal of the American Chemical Society,* 126(8)**,**pp. 2399-2408.

Merlino, A., Sica, F., Mazzarella, L., Zagari, A. and Vergara, A. (2008). 'Correlation between Raman and X-ray crystallography data of (Pro-Pro-Gly)10', *Biophys Chem,* 137(1)**,**pp. 24-7.

Miles, J. (2014). R squared, adjusted R squared. *Wiley StatsRef: Statistics Reference Online,* John Wiley and Sons, Ltd.

Miura, T. and Thomas, G. J., Jr. (1995). 'Raman spectroscopy of proteins and their assemblies', in Biswas, B.B. and Roy, S. (eds) *Subcellular biochemistry.*Boston:Springer, 24**,**pp.55-99.

Navarrete, J. T. L., Hernandez, V. and Ramirez, F. J. (1994). 'Ir and Raman spectra of L-aspartic acid and isotopic derivatives', *Biopolymers,* 34(8)**,**pp.1065-1077.

Ngarize, S., Herman, H., Adams, A. and Howell, N. (2004). 'Comparison of changes in the secondary structure of unheated, heated, and high-pressure-treated β-lactoglobulin and ovalbumin proteins using fourier transform Raman spectroscopy and self-deconvolution', *Journal of Agricultural and Food Chemistry,* 52(21)**,**pp.6470-6477.

Palmai, Z., Chaloin, L., Lionne, C., Fidy, J., Perahia, D. and Balog, E. (2009). 'Substrate binding modifies the hinge bending characteristics of human 3-phosphoglycerate kinase: A molecular dynamics study', *Proteins,* 77(2)**,**pp. 319-29.

Pappas, D., Smith, B. W. and Winefordner, J. D. (2000). 'Raman spectroscopy in bioanalysis', *Talanta,* 51(1)**,**pp.131-144.

Pelton, J. T. and McLean, L. R. (2000). 'Spectroscopic methods for analysis of protein secondary structure', *Analytical Biochemistry,* 277(2)**,**pp.167-176.

Reed, M. A. C., Hounslow, A. M., Sze, K. H., Barsukov, I. G., Hosszu, L. L. P., Clarke, A. R., Craven, C. J. and Waltho, J. P. (2003). 'Effects of domain dissection on the folding and stability of the 43 kDa protein PGK probed by NMR', *Journal of Molecular Biology,* 330(5)**,**pp.1189-1201.

Rygula, A., Majzner, K., Marzec, K. M., Kaczor, A., Pilarczyk, M. and Baranska, M. (2013). 'Raman spectroscopy of proteins: a review', *Journal of Raman Spectroscopy,* 44(8)**,**pp.1061-1076.

Schramm, V. L. (2007). 'Enzymatic transition state theory and transition state analogue Design', *Journal of Biological Chemistry,* 282(39)**,**pp. 28297-28300.

Schramm, V. L. (2015). 'Transition states and transition state analogue interactions with enzymes', *Accounts of Chemical Research,* 48(4)**,**pp. 1032-1039.

Schulz, H. and Baranska, M. (2007). 'Identification and quantification of valuable plant substances by IR and Raman spectroscopy', *Vibrational Spectroscopy,* 43(1)**,**pp.13-25.

Severcan, F. and Parvez, I. H. (2012). *Vibrational spectroscopy in diagnosis and screening*. Netherlands: IOS press.

Smith, E. and Dent, G. (2005). Introduction, Basic Theory and Principles, in Ewen,S. and Geofferey, D.(eds) *Modern Raman Spectroscopy – A Practical Approach.* John Wiley and Sons, Ltd,pp.1-20.

Szabo, J., Varga, A., Flachner, B., Konarev, P. V., Svergun, D. I., Zavodszky, P. and Vas, M. (2008). 'Communication between the nucleotide site and the main molecular hinge of 3-Phosphoglycerate kinase', *Biochemistry,* 47(26)**,**pp. 6735-6744.

Szilagyi, A. N., Ghosh, M., Garman, E. and Vas, M. (2001). 'A 1.8 Å resolution structure of pig muscle 3-phosphoglycerate kinase with bound MgADP and 3-phosphoglycerate in open conformation: New insight into the role of the nucleotide in domain closure', *Journal of Molecular Biology,* 306(3)**,**pp.499-511.

Triggs, N. E. and Valentini, J. J. (1992). 'An investigation of hydrogen bonding in amides using Raman spectroscopy', *The Journal of Physical Chemistry,* 96(17)**,**pp.6922-6931.

Voet, D. and Voet, J. G. (2011). *Biochemistry* (4th edn.). USA: John Wiely and Sons Inc.

Watson, H. C., Walker, N. P., Shaw, P. J., Bryant, T. N., Wendell, P. L., Fothergill, L. A., Perkins, R. E., Conroy, S. C., Dobson, M. J. and Tuite, M. F. (1982). 'Sequence and structure of yeast phosphoglycerate kinase', *The EMBO Journal,* 1(12)**,**pp.1635-1640.

Yang, H., Yang, S., Kong, J., Dong, A. and Yu, S. (2015). 'Obtaining information about protein secondary structures in aqueous solution using Fourier transform IR spectroscopy', *Nature Protocols,* 10(3)**,**pp. 382-396.

Yon, J. M., Desmadril, M., Betton, J. M., Minard, P., Ballery, N., Missiakas, D., S, G.-M., Perahia, D. and Mouawad, L. (1990). 'Flexibility and folding of phosphoglycerate kinase', *Biochimie,* 72(6)**,**pp.417-429.

Zerrad, L., Merli, A., Schroder, G. F., Varga, A., Graczer, E., Pernot, P., Round, A., Vas, M. and Bowler, M. W. (2011). 'A spring-loaded release mechanism regulates domain movement and catalysis in phosphoglycerate kinase', *Journal of Biological Chemistry,* 286(16)**,**pp.14040-14048.

Zewail, A. H. (2000). 'Femtochemistry: Atomic-scale dynamics of the chemical bond', *The Journal of Physical Chemistry A,* 104(24)**,**pp. 5660-5694.

Chapter 5: Conclusion and future works

Purine nucleotides (Adenosines and guanosines) and their phosphate derivatives are involved in different metabolic and cellular processes. Phosphorylation is one the important cellular reactions which involves the transfer of a phosphoryl group from the nucleotide to the target substrate via the influence of certain enzymes, such as phosphoglycerate kinase (PGK). During phosphorylation, a nucleotide molecule is used as a source of the phosphoryl group and the magnesium ions bind to the nucleotide and cause substantial conformational changes in the nucleotide, in the enzyme (PGK) or in the substrate. The structure of nucleotide-Mg complexes in solution and the mode of Mg^{2+}coordination remain controversial. Therefore, this project applies a combined Raman spectroscopy and Density Functional Theory (DFT) approach to characterise and assign the fundamental bands in the Raman profiles of the purine nucleotides and their phosphate derivatives in aqueous solution at physiological pH. The study investigates the influence of magnesium binding on the spectral profile of adenosine and guanosine mono-, di-and tri- phosphates in aqueous solution, as a function of pH. These studies into the effects of Mg^{2+} and pH are supported by ^{31}P NMR measurements. The study further applies Raman spectroscopy to explore the spectral profile of the human phosphoglycerate kinase (hPGK) in its open conformation, when no ligands are bound, and in its fully closed conformation, when ADP, 3-phosphoglycerate and a metal fluoride mimic of the transferring phosphoryl group are all bound in a transition state analogue arrangement. The influence of conformational changes on the Amide I and III regions of the enzyme spectrum were investigated using uniform isotopic substitution of nitrogen atoms with ^{15}N (^{15}N-hPGK).

In this study , the Raman spectra of purine nucleotides and their phosphate derivatives were recorded and the results have shown that the use of Raman spectroscopy coupled with averaged atom displacement method (obtained from DFT calculations) provide a powerful tool for characterising and assigning the Raman spectra of purine nucleotides. This tool is useful to provide a quantitative contribution of each atom in the

nucleotide molecule. The results of this study identified the primary and secondary markers for purine nucleotides and their phosphorylated forms. In the absence of the enzyme, the Raman and ^{31}PNMR measurements supported a model where the coordination of Mg^{2+} involves both α- and β-phosphate groups of the diphosphate purine nucleotides, (5'-ADP and 5'-GDP), and β- and γ-phosphate groups of the triphosphate purine nucleotides (5'-ATP and 5'-GTP) in aqueous solution at pH 7.0. Results also indicated that the acidification has a remarkable impact on the magnesium bound phosphate groups in adenosine and guanosine nucleotides. However, the alterations in the pH environment from pH 5-8 did not change the binding sites of the magnesium ions and did not facilitate the binding of the divalent cation to other parts of the purine nucleotide molecule.

The Raman spectra of PGK enzyme in its open and closed conformation were recorded over the range of 900-1800 cm^{-1} at physiological pH in Tris buffer. The Amide I and III regions were identified and the spectral changes of these regions in different forms of the PGK enzyme were detected and used to analyse the changes in the PGK secondary structure in the open and closed confirmation. The results supported the role of the α-helix, β-sheet and hydrogen bonds in switching the PGK enzyme from the open (inactive) to the closed (active) conformation. The study proposed some of the ADP Raman bands for the |PGK-ADP-magnesium complex in the 1030-1070 cm^{-1} region, and assigned these bands to include a considerable contribution of the α- and β- phosphate groups.

The Raman spectroscopy, peak deconvolution and averaged atom displacement approach from DFT used in this study provided a powerful diagnostic tool to probe the structural changes associated with many nucleotides and proteins. Therefore, the method can be further applied to investigate the primary and secondary marker bands for other nucleotides such as, cytidines, inosines, cAMP, etc. The combined Raman and DFT method can pave the way for further pharmaceutical studies to explore the structure and dynamic behaviour of different nucleoside and nucleotide

analogues and their interaction with other molecules in aqueous environments.

The dynamic structure of different proteins and the impact of the binding of certain nucleotide on changing the conformation of different enzymes during multiple biological processes, such as the binding of ATP to AMP-activated protein kinase and the binding of GTP to cytidine 5-triphosphate synthase, remain ambiguous. Therefore, applying Raman spectroscopy for studying these interactions can provide promising results and increase our knowledge of the dynamic behaviour of different biologically important molecules.

Appendix 1

Table 1.1. Averaged atom displacements for adenosine (A), 5'-adenosine monophosphate (5'-AMP), 5'-adenosine diphosphate (5'-ADP) and 5'-adenosine triphosphate (5'-ATP). ῡ= wavenumber (cm-1), RRI = relative Raman intensity (a.u.), P = purine ring atomic displacement (%), R = ribose ring atomic displacement (%), α = alpha phosphate atomic displacement (%), β = beta phosphate atomic displacement (%), γ = gamma phosphate atomic displacement (%) and D = total atomic displacement (Å).

A					AMP						ADP							ATP							
$\bar{\nu}$	RRI	P	R	D	$\bar{\nu}$	RRI	P	R	α	D	$\bar{\nu}$	RRI	P	R	α	β	D	$\bar{\nu}$	RRI	P	R	α	β	γ	D
628	0.04	29	71	4.63							617	0.06	12	33	32	23	5.12	602	0.06	15	30	15	25	15	5.51
											605	0.26	8	23	51	18	4.82	620	0.34	5	19	32	31	13	5.16
643	0.07	54	46	5.20	645	0.10	58	38	4	5.05	645	0.11	58	37	5	0	5.09	645	0.10	55	35	5	4	1	5.12
																		656	0.20	8	15	38	32	7	5.11
663	0.01	84	16	3.52	664	0.02	88	10	2	3.33	665	0.01	88	11	1	0	3.34	663	0.02	70	10	10	8	2	3.58
689	0.02	79	21	3.86	689	0.02	64	30	6	4.24	690	0.01	77	19	4	0	3.66	689	0.02	74	18	4	4	0	3.75
705	0.19	42	58	5.09	699	0.17	30	60	10	5.02	707	0.35	38	50	8	4	5.23	707	0.30	37	50	9	4	0	5.27
722	0.60	51	49	5.09	716	0.38	59	36	5	4.89	722	0.31	42	44	9	5	5.27	723	0.33	43	43	9	5	0	5.26
770	0.16	41	59	4.63	775	0.12	35	62	3	4.54	774	0.10	19	61	14	6	4.67	771	0.30	27	50	13	8	2	5.04
					750	0.47	21	67	12	4.41	772	0.39	26	53	13	8	4.94	774	0.12	12	52	19	12	5	4.70
809	0.05	78	22	4.05	809	0.04	79	21	0	3.91	809	0.04	80	20	0	0	3.89	809	0.05	77	23	0	0	0	4.03
825	0.23	41	59	4.51	824	0.22	39	60	1	4.40	825	0.25	38	59	2	1	4.42	824	0.78	14	28	19	23	16	5.27
																		826	0.05	20	31	16	19	14	5.16
860	0.23	9	91	3.70	872	0.05	10	84	6	3.84	878	0.06	12	82	6	0	3.77	877	0.08	12	77	3	4	4	3.84
881	0.13	16	84	3.57	876	0.31	11	80	9	3.91	890	0.10	9	69	14	8	4.11	887	0.05	7	53	11	12	17	4.39
											842	0.64	3	17	47	33	3.84	903	0.24	6	20	28	19	27	4.73
911	0.09	79	21	3.96	911	0.10	72	17	11	4.06	912	0.11	76	22	2	0	4.09	911	0.11	67	20	6	3	4	4.26
918	0.07	91	9	1.60	952	0.11	72	20	8	1.80	941	0.08	78	15	0	7	1.62	929	0.05	92	8	0	0	0	1.50
948	0.07	10	90	3.75	961	0.17	14	70	16	3.94	963	0.04	8	72	11	9	3.95	963	0.08	6	75	10	6	3	3.90
					921	0.54	6	20	74	3.80	948	0.29	4	10	31	55	3.84	956	0.16	0	7	13	35	45	3.69

Appendix 1

973	0.01	99	1	1.38	972	0.01	98	2	0	1.47	972	0.01	98	2	0	0	1.44	972	0.01	98	2	0	0	0	1.40
992	0.04	47	53	4.41	992	0.04	37	57	6	4.39	992	0.04	40	53	4	3	4.48	991	0.04	40	54	4	2	0	4.44
1003	0.21	59	41	3.74	1006	0.16	61	36	3	3.64	1005	0.24	58	37	5	0	3.70	1004	0.21	58	37	5	0	0	3.64
1027	0.11	14	86	4.02	1036	0.12	12	82	6	3.92	1034	0.16	10	52	31	7	4.37	1029	0.05	7	38	25	22	8	4.73
											1051	0.34	10	38	41	11	4.47	1037	0.07	5	41	20	26	8	4.57
1040	0.02	16	84	4.03	1044	0.02	17	75	8	4.05	1039	0.20	8	60	26	6	4.02	1043	0.10	9	53	8	24	6	4.35
																		1064	0.67	21	20	29	24	6	5.05
1067	0.03	62	38	4.16	1068	0.02	61	38	1	4.12	1068	0.03	58	37	4	1	4.21	1068	0.19	38	26	17	12	7	4.73
																		1070	0.06	4	4	7	6	79	2.91
																		1077	0.07	0	2	4	6	88	2.19
1091	0.03	5	95	3.79	1090	0.04	6	90	4	3.76	1092	0.04	6	87	7	0	3.81	1091	0.05	4	82	11	3	0	3.85
1096	0.03	7	93	3.97	1098	0.05	8	84	8	4.00	1098	0.06	6	78	13	3	4.04	1097	0.07	8	71	15	6	0	4.16
1109	0.04	22	78	4.40	1109	0.04	21	76	3	4.52	1112	0.04	21	77	2	0	4.38	1113	0.03	20	78	2	0	0	4.41
1133	0.07	11	89	3.78	1135	0.04	10	84	6	3.58	1135	0.05	9	84	7	0	3.55	1132	0.05	8	84	8	0	0	3.54
											1073	0.07	1	1	3	95	2.07	1169	0.05	0	0	3	94	3	1.86
											1078	0.07	0	1	3	96	1.99								
1182	0.04	28	72	3.74																					
1186	0.16	36	64	3.89	1183	0.12	52	48	0	4.23	1184	0.13	54	46	0	0	4.26	1185	0.12	54	46	0	0	0	4.19
					1059	0.05	2	4	94	2.22															
					1074	0.07	1	9	90	2.69	1176	0.04	2	9	87	2	2.58	1202	0.03	4	24	70	2	0	3.52
1208	0.07	12	88	3.14	1202	0.11	13	87	0	3.06	1205	0.11	13	87	0	0	2.98	1204	0.12	21	79	0	0	0	3.10
1232	0.26	70	30	3.47	1226	0.02	21	79	0	3.22	1231	0.09	40	60	0	0	3.52	1227	0.06	35	65	0	0	0	3.50
1252	0.09	20	80	3.26	1239	0.32	63	37	0	3.85	1239	0.23	47	53	0	0	3.89	1237	0.22	51	49	0	0	0	3.93
1263	0.19	68	32	3.99	1264	0.16	71	29	0	3.85	1264	0.18	74	26	0	0	3.78	1263	0.20	74	26	0	0	0	3.80
1280	0.13	2	98	2.65	1269	0.13	10	90	0	2.64	1279	0.14	2	98	0	0	2.49	1274	0.13	7	93	0	0	0	2.56
1305	0.11	19	81	3.43	1304	0.15	20	80	0	3.37	1306	0.16	21	79	0	0	3.37	1305	0.16	21	79	0	0	0	3.38
1316	0.68	56	44	3.56	1318	0.72	56	44	0	3.67	1318	0.76	56	44	0	0	3.65	1317	0.71	55	45	0	0	0	3.62
1326	0.24	23	77	3.19	1326	0.09	14	86	0	2.91	1327	0.13	16	84	0	0	2.97	1329	0.17	22	78	0	0	0	3.13
1332	0.31	66	34	4.17	1332	0.35	72	28	0	3.88	1333	0.35	68	32	0	0	4.03	1332	0.27	61	39	0	0	0	4.22
1343	0.04	10	90	2.89	1342	0.03	11	89	0	2.79	1343	0.03	11	89	0	0	2.80	1343	0.03	11	89	0	0	0	2.77

Appendix 1

1357	1.00	87	13	3.43	1357	1.00	84	16	0	3.50	1357	1.00	85	15	0	0	3.49	1357	1.00	87	13	0	0	0	3.46
1371	0.09	17	83	3.31	1372	0.03	14	86	0	3.21	1373	0.09	18	82	0	0	3.30	1372	0.04	15	85	0	0	0	3.25
1378	0.52	25	75	3.41	1374	0.56	22	78	0	3.25	1376	0.51	22	78	0	0	3.30	1376	0.49	22	78	0	0	0	3.25
1386	0.29	69	31	3.26	1385	0.36	59	41	0	3.61	1386	0.35	69	31	0	0	3.22	1386	0.32	67	33	0	0	0	3.26
1399	0.06	14	86	3.29	1389	0.06	21	79	0	3.41	1395	0.04	11	89	0	0	3.38	1395	0.04	13	87	0	0	0	3.40
1429	0.22	40	60	3.27	1397	0.06	11	89	0	3.23	1403	0.05	11	89	0	0	2.88	1399	0.06	12	88	0	0	0	3.08
1435	0.22	58	42	3.58	1428	0.22	40	60	0	3.26	1429	0.17	48	52	0	0	3.56	1429	0.19	43	57	0	0	0	3.38
1446	0.02	2	98	3.10	1434	0.21	57	43	0	3.44	1435	0.28	50	50	0	0	3.22	1436	0.26	53	47	0	0	0	3.40
1450	0.05	4	96	3.01	1446	0.03	5	95	0	2.75	1449	0.03	4	96	0	0	2.68	1446	0.03	6	94	0	0	0	2.75
1490	0.18	97	3	2.66	1490	0.14	96	4	0	2.66	1490	0.16	96	4	0	0	2.68	1490	0.17	93	7	0	0	0	2.81
1495	0.10	1	99	1.60	1493	0.09	1	99	0	1.60	1496	0.09	0	100	0	0	1.56	1491	0.08	5	95	0	0	0	1.62
1520	0.88	91	9	3.07	1523	0.86	91	9	0	2.96	1521	0.92	91	9	0	0	2.99	1521	0.86	91	9	0	0	0	3.01
1599	0.74	95	5	3.32	1599	0.72	95	5	0	3.44	1599	0.75	95	5	0	0	3.38	1599	0.73	95	5	0	0	0	3.44
1607	0.04	98	2	2.54	1609	0.02	98	2	0	2.57	1608	0.04	98	2	0	0	2.56	1608	0.02	98	2	0	0	0	2.55
1637	0.13	99	1	2.45	1639	0.13	99	1	0	2.40	1638	0.13	98	2	0	0	2.45	1639	0.13	98	2	0	0	0	2.41

Table 1.2. Averaged atom displacements for 5'-guanosine monophosphate (5'-GMP), 5'-guanosine diphosphate (5'-GDP) and 5'-gauanosine triphosphate (5'-GTP). ῡ= wavenumber (cm-1), RRI = relative Raman intensity (a.u.), P = purine ring atomic displacement (%), R = ribose ring atomic displacement (%), α = alpha phosphate atomic displacement (%), β = beta phosphate atomic displacement (%), γ = gamma phosphate atomic displacement (%) and D = total atomic displacement (Å).

GMP						GDP							GTP						
$\bar{\nu}$	RRI	P	R	α	D	$\bar{\nu}$	RRI	P	R	α	β	D	$\bar{\nu}$	RRI	P	R	α	β	γ	D
						612	0.01	81	8	9	2	1.98	612	0.01	97	3	0	0	0	1.77
						614	0.02	12	35	31	22	4.90	620	0.18	3	18	32	33	14	5.00
659	0.15	58	37	5	4.83	657	0.10	65	29	6	0	4.35	655	0.11	14	15	35	29	7	5.22
													658	0.04	49	19	14	14	4	4.55
665	0.11	69	30	1	4.43	665	0.16	62	34	4	0	4.61	664	0.21	55	34	7	4	0	4.93
676	0.01	84	16	0	3.83	678	0.01	85	15	0	0	3.77	677	0.01	84	15	1	0	0	3.79
704	0.02	59	35	6	4.81	703	0.02	86	13	1	0	3.72	704	0.02	85	14	1	0	0	3.75
700	0.03	35	55	10	5.19	716	0.07	26	57	12	5	5.13	717	0.07	25	56	12	7	0	5.16
733	0	96	4	0	2.98	733	0.00	96	4	0	0	2.95	734	0.00	97	3	0	0	0	2.91
764	0.04	35	64	1	4.48	760	0.03	35	65	0	0	4.49	761	0.04	34	64	2	0	0	4.50
752	0.23	20	68	12	4.45	773	0.18	11	58	19	12	4.51	771	0.14	9	50	22	14	5	4.56
782	0.03	79	21	0	3.58	782	0.03	81	19	0	0	3.53	783	0.03	50	50	0	0	0	3.57
													805	0.05	42	48	10	0	0	4.60
804	0.05	40	58	2	4.65	805	0.05	40	58	2	0	4.59	824	0.33	2	18	26	32	22	4.44
859	0.09	57	41	2	4.59															
						842	0.34	3	18	46	33	3.99	904	0.12	5	20	28	20	27	1.56
873	0.03	12	82	6	3.91	860	0.08	57	36	4	3	4.54	860	0.08	59	35	2	1	3	4.46
876	0.15	9	82	9	3.86	878	0.03	12	83	5	0	3.78	880	0.04	11	78	3	4	4	3.84

Appendix 1

921	0.28	3	21	76	3.55	947	0.15	1	11	32	56	3.70	955	0.09	0	5	13	36	46	3.51
937	0.06	82	9	9	1.45	903	0.04	87	13	0	0	1.47	900	0.04	69	8	7	8	8	4.50
962	0.11	6	76	18	3.84	962	0.02	5	74	12	9	3.86	964	0.05	4	76	11	6	3	3.86
995	0.03	21	71	8	4.05	994	0.04	21	69	7	3	4.43	994	0.03	21	71	7	1	0	4.05
1029	0.03	54	43	3	4.40	1030	0.09	43	37	15	5	4.76	1028	0.03	24	32	21	18	5	5.36
1037	0.08	32	64	4	4.43	1040	0.09	24	62	11	3	4.43	1032	0.03	35	23	18	18	6	4.75
						1035	0.07	25	38	29	8	5.27	1039	0.04	17	39	14	23	7	4.87
1043	0.02	16	76	8	4.12	1050	0.16	8	39	43	10	4.39	1043	0.08	17	54	5	18	6	4.45
													1064	0.42	7	18	37	30	8	4.56
1072	0.06	63	33	4	4.11	1074	0.06	63	32	4	1	4.10	1074	0.08	56	28	8	5	3	4.26
													1070	0.04	3	3	5	6	83	2.65
													1076	0.04	1	2	3	5	89	2.18
1089	0.01	40	56	4	4.40	1090	0.02	29	65	6	0	4.43	1091	0.02	48	45	5	2	0	4.21
1092	0.02	48	51	1	4.09	1094	0.01	53	42	5	0	4.06	1094	0.02	39	51	8	2	0	4.34
1198	0.03	10	82	8	4.12	1097	0.03	22	69	9	0	4.36	1097	0.04	16	66	13	5	0	4.41
1114	0.02	34	63	3	4.52	1117	0.02	33	65	2	0	4.48	1118	0.02	30	68	2	0	0	4.48
						1134	0.04	13	80	7	0	3.65	1133	0.04	12	81	7	0	0	3.63
						1154	0.08	81	19	0	0	3.97								
1136	0.04	12	82	6	3.61	1171	0.03	2	1	2	95	2.17	1154	0.09	82	18	0	0	0	3.90
1154	0.09	81	19	0	4.00	1076	0.03	1	1	4	94	1.96	1169	0.03	0	0	3	94	3	1.87
1058	0.03	0	5	95	2.14	1175	0.02	0	10	89	1	2.51	1201	0.02	6	48	45	1	0	3.49

Appendix 1

1075	0.04	6	9	85	3.10	1204	0.05	20	80	0	0	2.95	1202	0.05	8	63	29	0	0	3.15
1202	0.05	11	89	0	2.96	1224	0.11	62	38	0	0	3.52	1224	0.11	65	35	0	0	0	3.42
1223	0.11	57	43	0	3.67	1230	0.01	16	84	0	0	2.92	1231	0.01	16	80	4	0	0	3.05
1229	0.01	15	85	0	2.91	1250	0.03	49	51	0	0	3.22	1252	0.03	45	52	3	0	0	3.32
1253	0.04	53	47	0	3.17	1374	0.07	1	97	2	0	2.44	1278	0.07	2	95	3	0	0	2.47
1277	0.08	1	99	0	2.40	1308	0.02	6	94	0	0	3.06	1307	0.02	7	93	0	0	0	3.04
1306	0.02	6	94	0	3.03	1327	0.01	10	90	0	0	3.82	1326	0.02	12	88	0	0	0	2.90
1327	0.02	9	91	0	2.86	1335	0.61	56	44	0	0	3.55	1335	0.61	55	45	0	0	0	3.58
1337	0.85	55	45	0	3.48	1343	0.09	19	81	0	0	3.00	1343	0.08	15	85	0	0	0	2.89
1343	0.11	21	79	0	3.03	1345	0.09	92	8	0	0	2.33	1347	0.11	95	5	0	0	0	2.28
1342	0.11	81	19	0	2.64	1372	0.05	30	70	0	0	3.79	1370	0.04	26	74	0	0	0	3.68
1371	0.04	28	72	0	3.73	1376	0.09	20	80	0	0	2.99	1374	0.10	20	80	0	0	0	2.97
1373	0.15	12	88	0	2.75	1379	0.23	38	62	0	0	4.07	1378	0.22	42	58	0	0	0	4.18
1378	0.18	44	56	0	4.19	1394	0.02	7	93	0	0	3.21	1394	0.03	12	88	0	0	0	3.39
1391	0.03	11	89	0	3.36	1400	0.06	10	88	2	0	3.14	1401	0.05	10	87	4	0	0	2.80
1401	0.05	12	86	2	3.04	1424	0.20	48	52	0	0	3.88	1423	0.22	39	61	0	0	0	3.57
1422	0.23	43	57	0	3.70	1430	0.18	41	59	0	0	3.14	1429	0.16	49	51	0	0	0	3.39
1429	0.16	45	55	0	3.31	1450	0.01	3	97	0	0	2.66	1447	0.01	3	97	0	0	0	3.69
1447	0.01	3	97	0	2.70	1493	0.04	0	100	0	0	1.56	1495	0.04	0	100	0	0	0	1.59
1498	0.05	3	97	0	1.63	1505	0.91	93	7	0	0	3.33	1505	0.91	93	7	0	0	0	3.31
1505	0.88	92	8	0	3.36	1554	0.05	94	6	0	0	3.42	1554	0.04	94	6	0	0	0	3.44
1555	0.07	94	6	0	3.32	1579	1.00	90	10	0	0	3.39	1580	1.00	90	10	0	0	0	3.37
1579	1.00	90	10	0	3.43	1598	0.25	99	1	0	0	2.45	1599	0.27	99	1	0	0	0	2.45
1597	0.27	99	1	0	2.49	1643	0.11	100	0	0	0	1.98	1644	0.10	100	0	0	0	0	2.00

1643	0.10	100	0	0	2.00	1706	0.35	97	3	0	0	2.86	1706	0.35	97	3	0	0	0	2.88
1705	0.35	98	2	0	2.87															

Appendix 2

AMP, ADP and ATP saturation curves:

The dissociation constants (Kd) for adenosine mono-, di- and tri-phosphates were determined by monitoring changes in ^{1}H NMR chemical shifts for 50 mM nucleotide at pH 7.0 on increasing the $MgCl_2$ concentrations. The results for 5'-AMP reflected a very complicated series of binding equilibria. However, for 5'-ADP and 5'-ATP simple hyperbolic saturation curves were observed, reflecting nucleotide-Mg saturation at the concentrations used in this study.

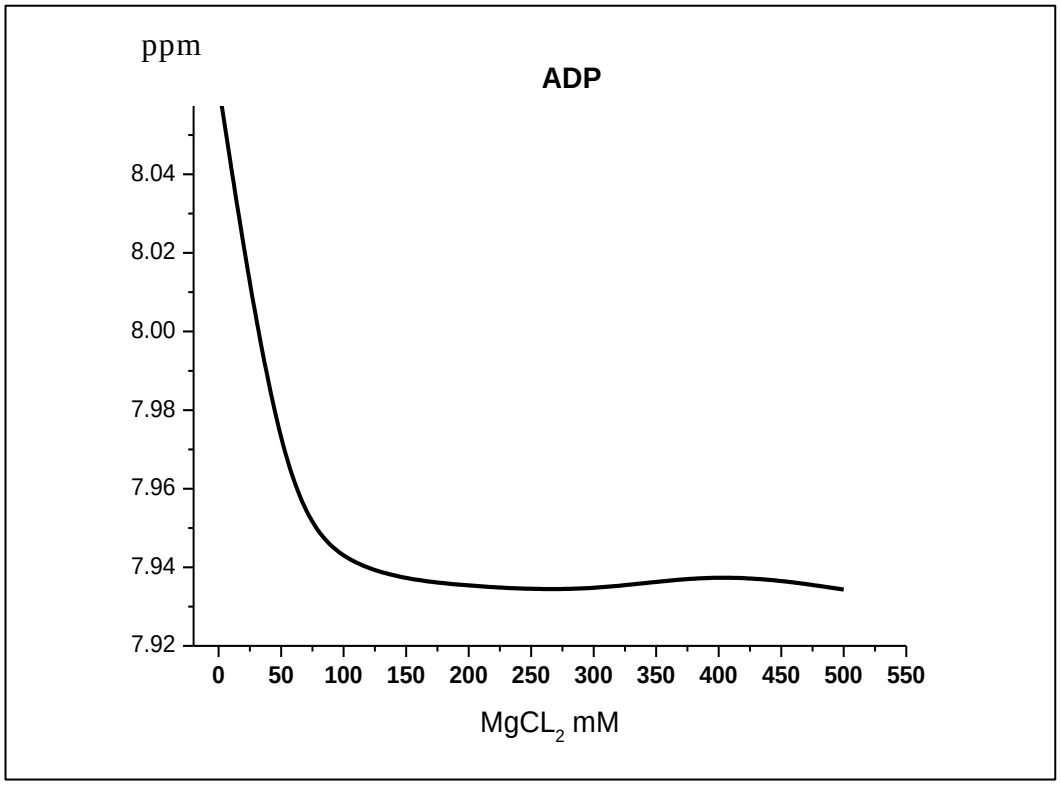

Figure 2-1. Saturation curve for 5'- adenosine diphosphate (ADP) at pH 7.0 (50 mM 5'-ADP + variable concentrations of ($Mg\ Cl_2$) at pH 7.0.

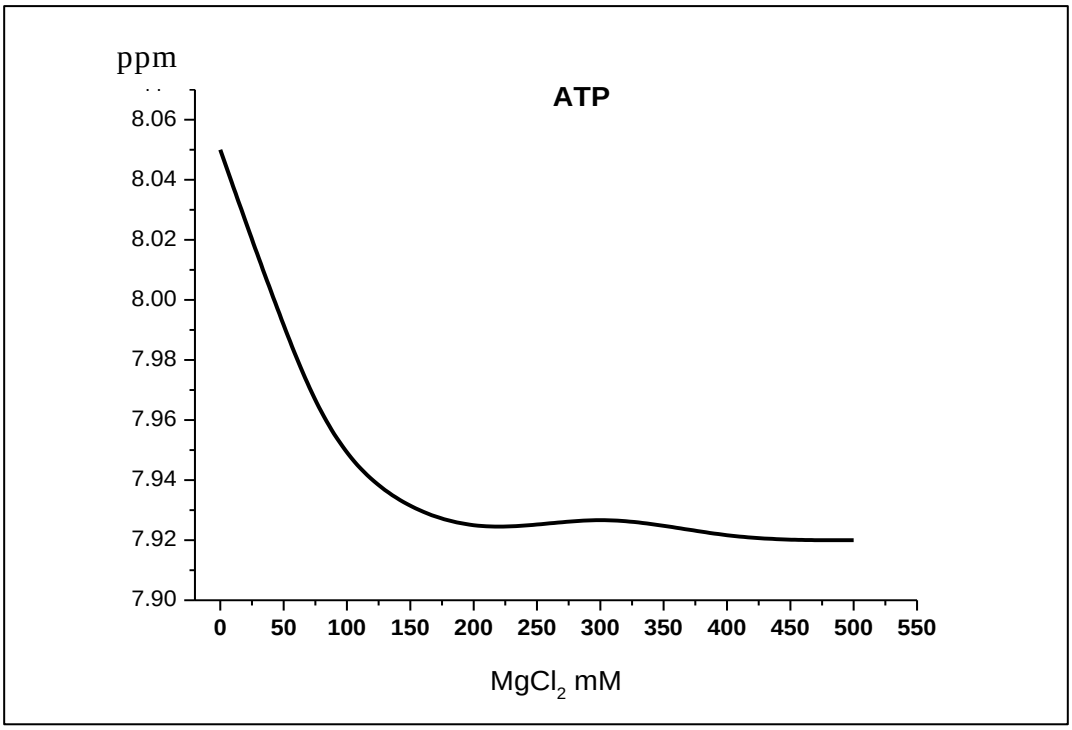

Figure 2-2. Saturation curve for 5'- adenosine triphosphate (ATP) at pH 7.0 (50 mM 5'-ATP + variable concentrations of ($Mgcl_2$) at pH 7.0.

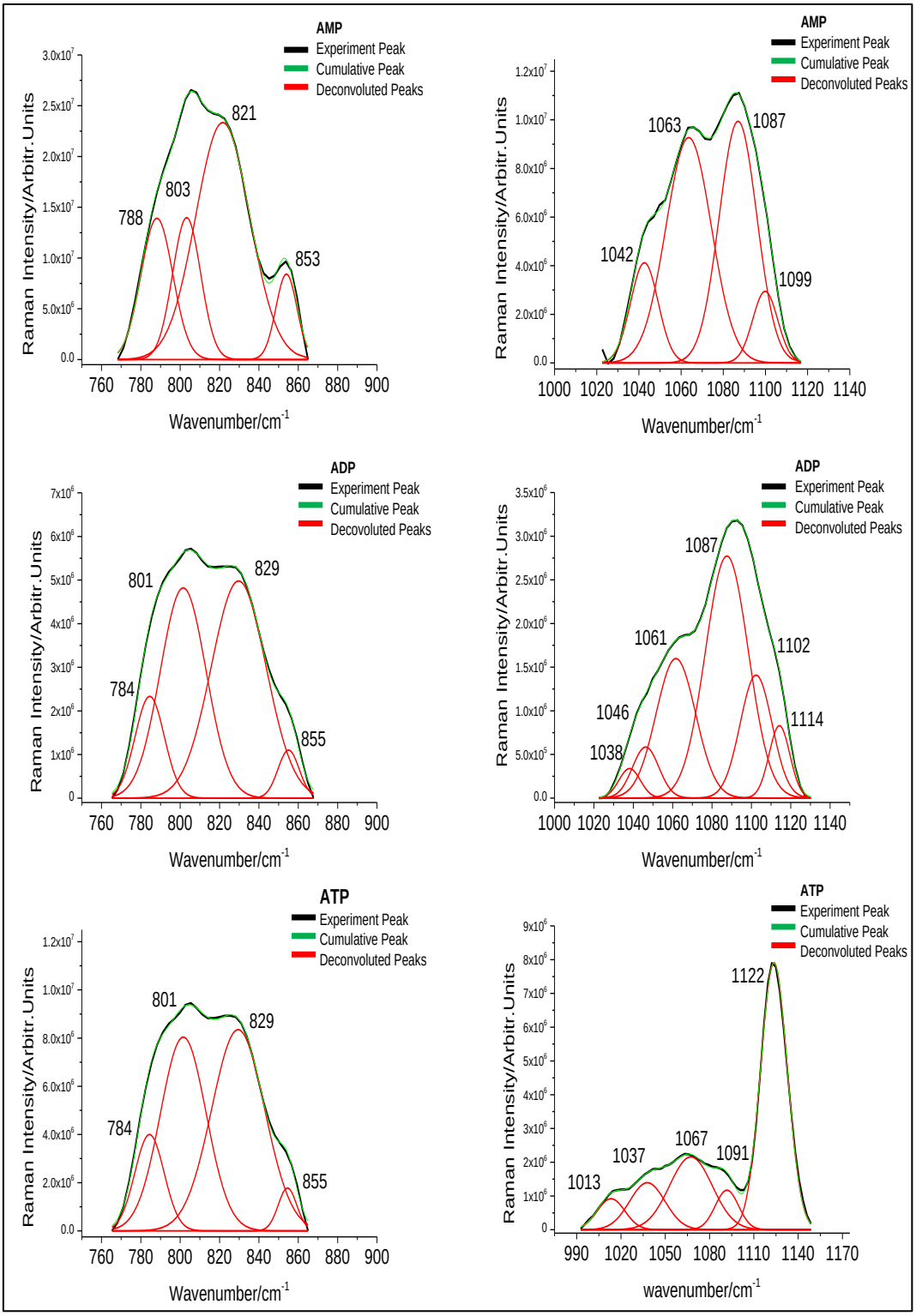

Figure 2-3. Peak deconvolution of the Raman spectrum for 5'- adenosine monophosphate (AMP), 5'- adenosine diphosphate (ADP) and 5'- adenosine triphosphate (ATP) in the regions 760-870 cm^{-1} (left) and 990-1140 cm^{-1} (right) at pH 7.0.

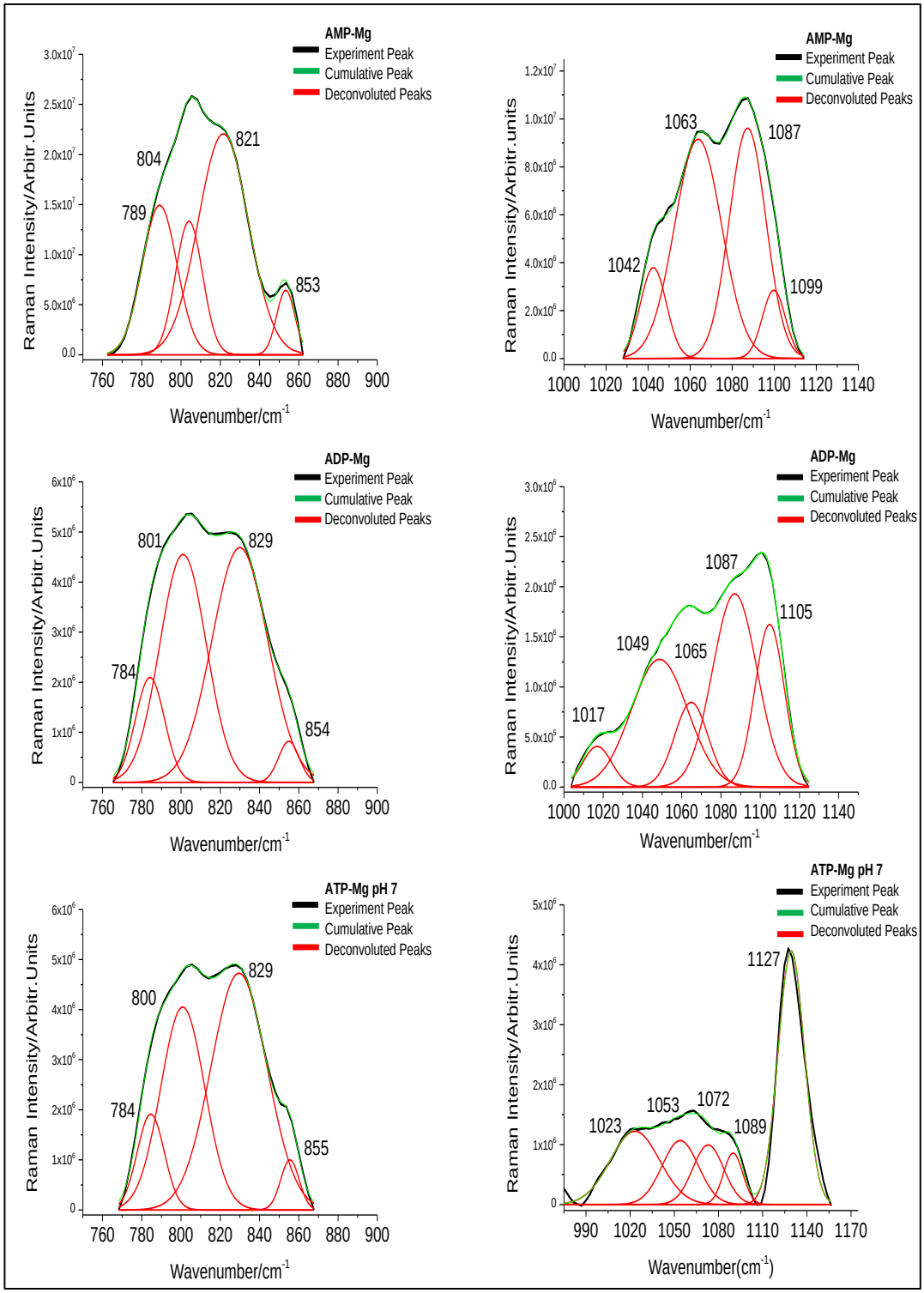

Figure 2-4. Peak deconvolution of the Raman spectra for 5'- adenosine monophosphate-magnesium complex (AMP-Mg), 5'- adenosine diphosphate-magnesium complex (ADP-Mg) and 5'- adenosine triphosphate-magnesium complex (ATP-Mg) in the regions 760-870 and 990-1150 cm^{-1} at pH 7.0.

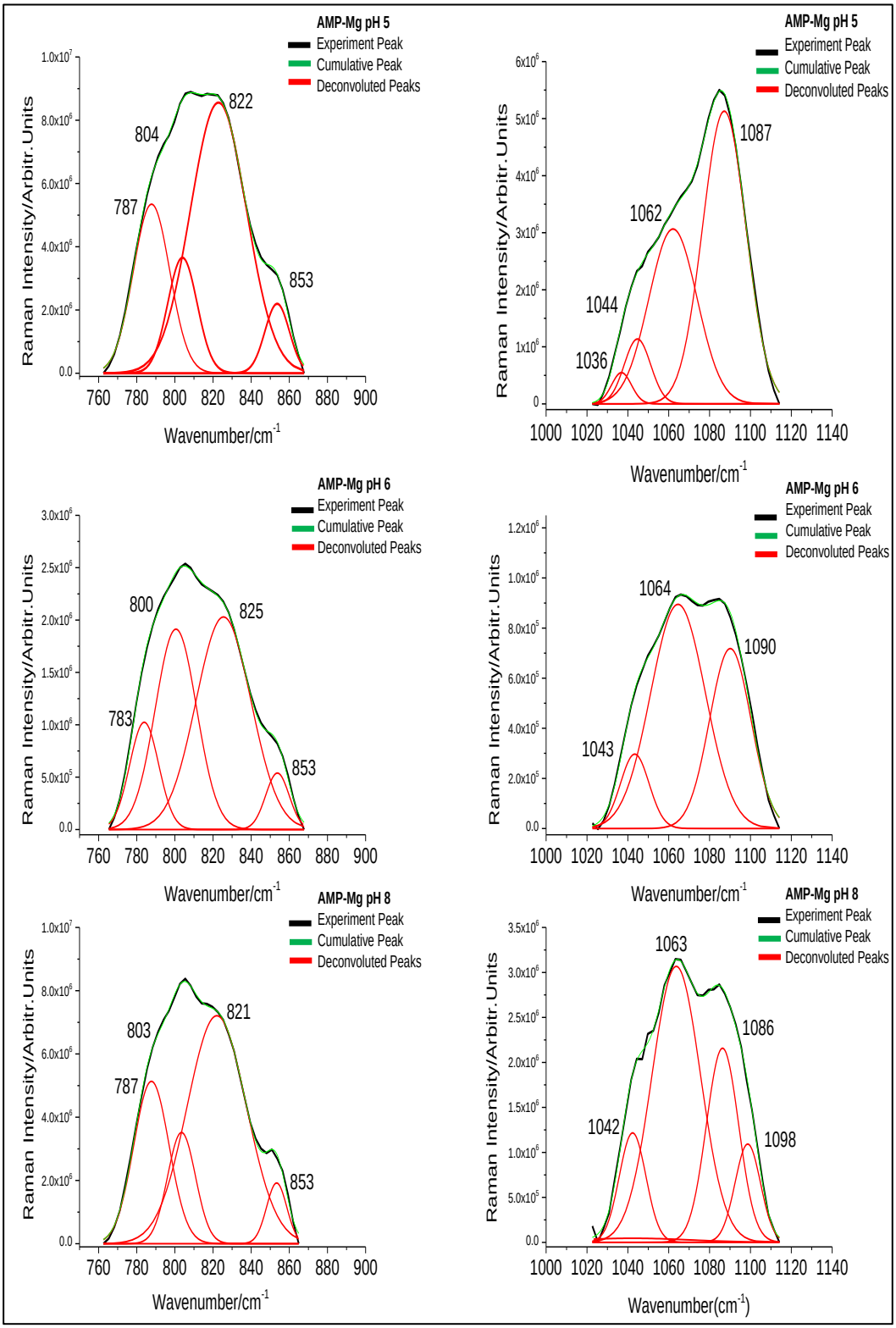

Figure 2-5. Deconvoluted Raman spectra for 5'- adenosine monophosphate-magnesium complex (AMP-Mg) in the regions 760-870 (left) and 1020-1120 cm^{-1} (right) at different pH environments.

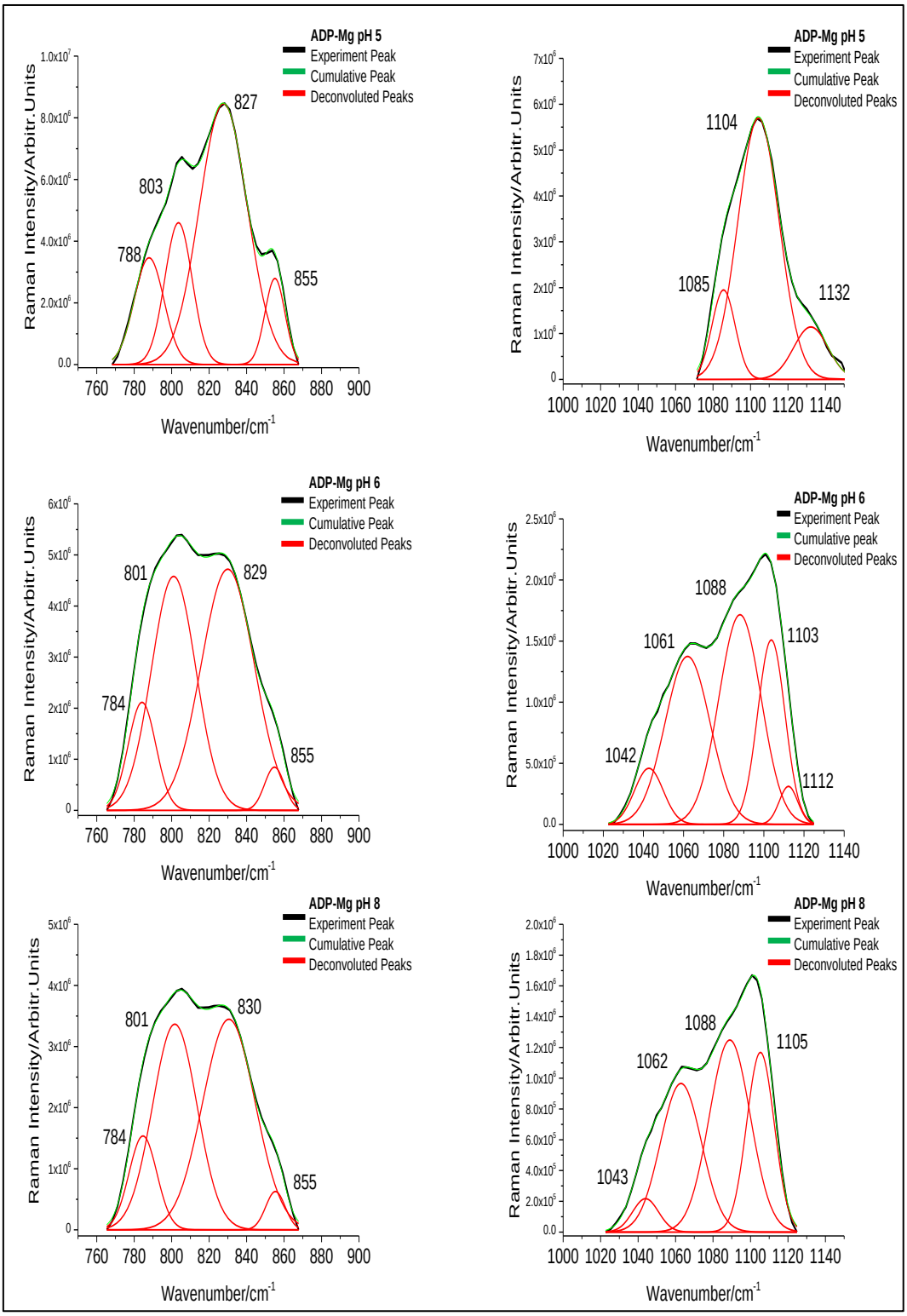

Figure 2-6. Deconvoluted Raman spectra for 5'- adenosine diphosphate-magnesium complex (ADP-Mg**)** in the regions 760-870 cm^{-1} (left) and 1020-1120 cm^{-1} (right) at different pH environments.

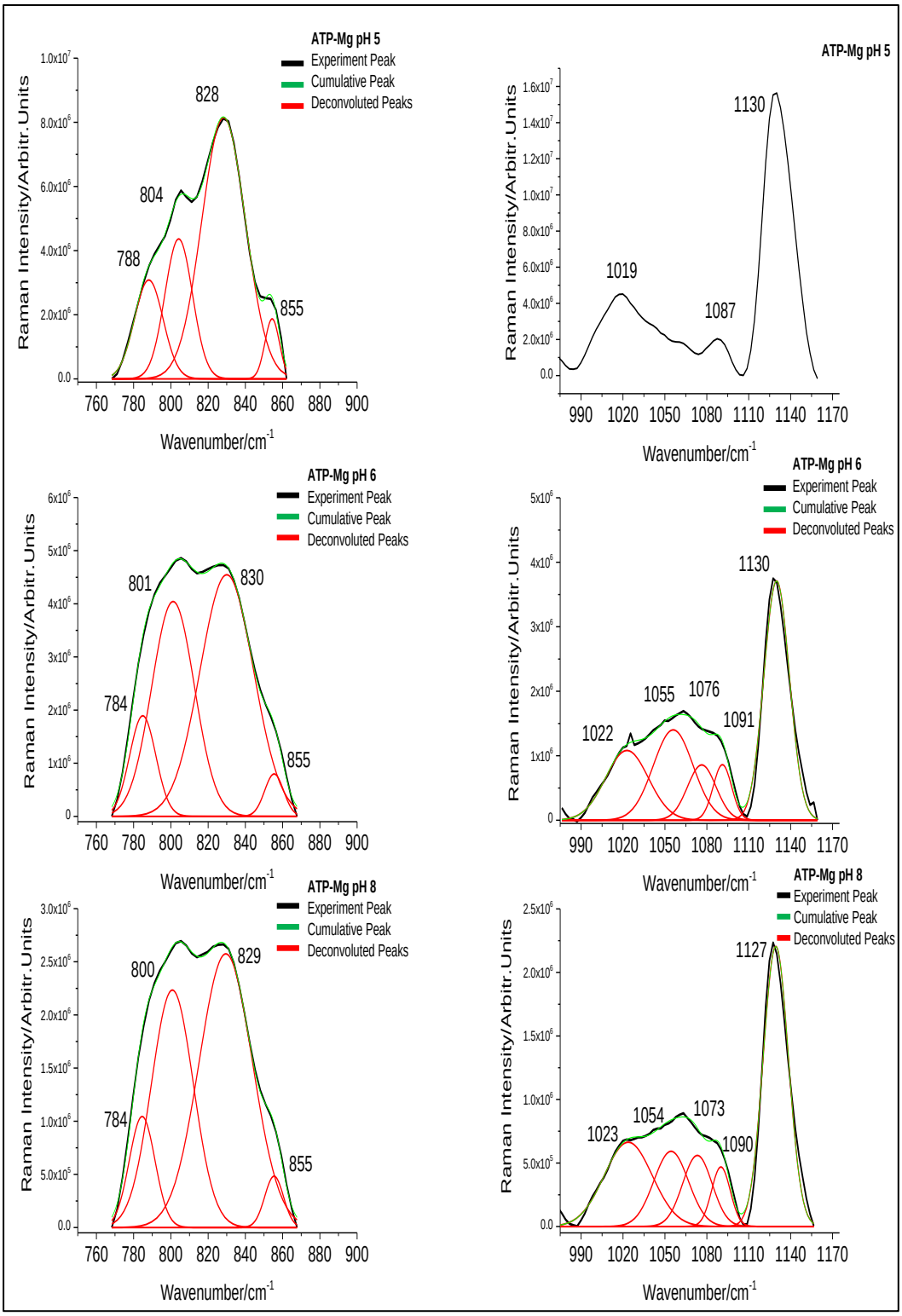

Figure 2-7. Deconvoluted Raman spectra for 5'- adenosine triphosphate-magnesium complex (ATP-Mg) in the regions 760-870 (left) and 990-1150 cm^{-1} (right) at different pH environments.

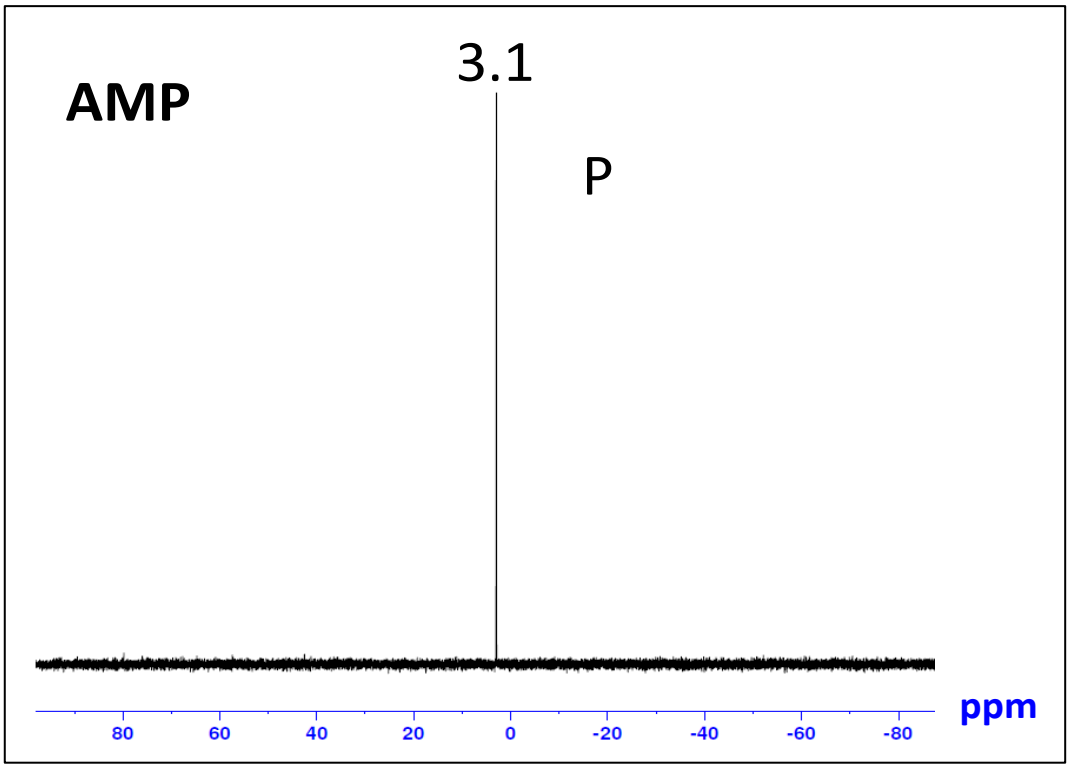

Figure 2-8. ^{31}PNMR for 5'- adenosine monophosphate (AMP) at pH 7.0. (P): phosphate group

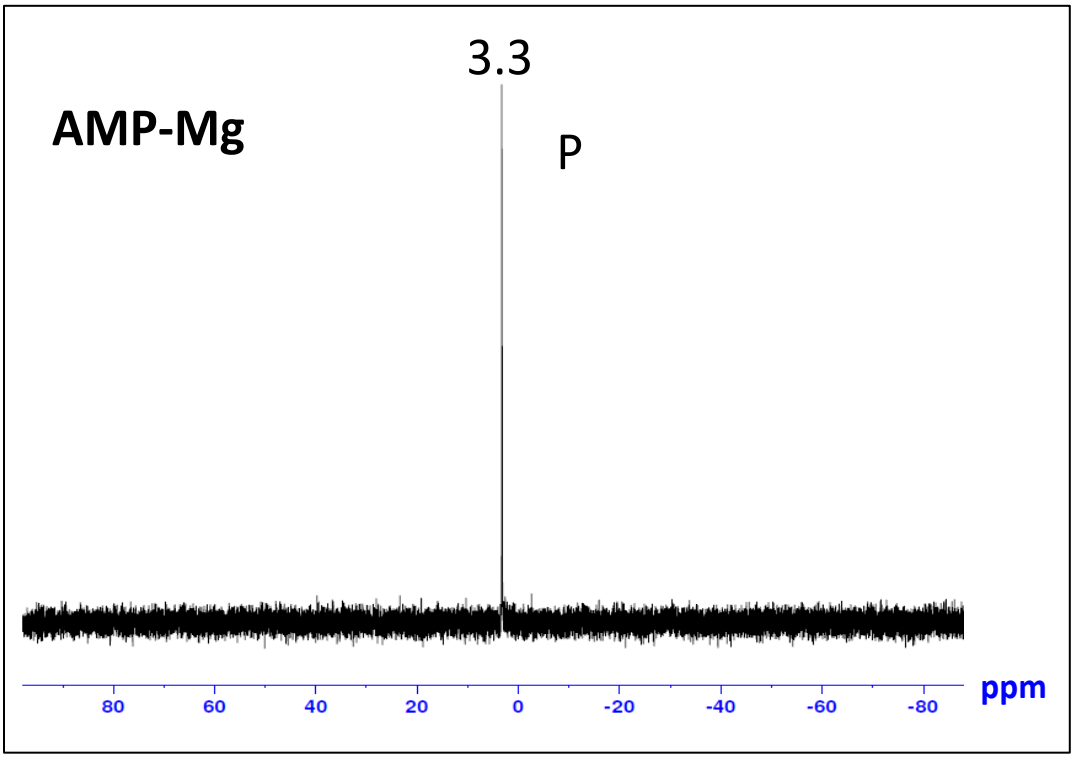

Figure 2-9. ^{31}P NMR for 5'- adenosine monophosphate-magnesium complex (AMP-Mg) at pH 7.0. (P): phosphate group.

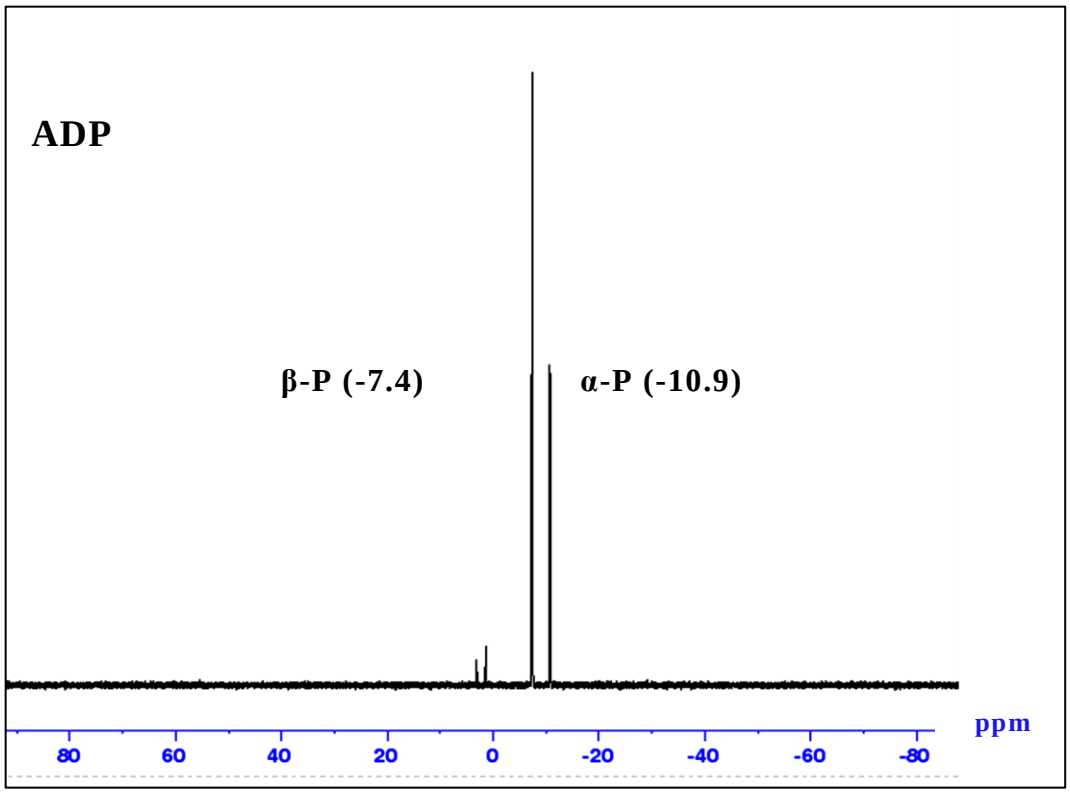

Figure 2-10. ^{31}P NMR for 5'- adenosine diphosphate (ADP) at pH 7 at pH 7.0.

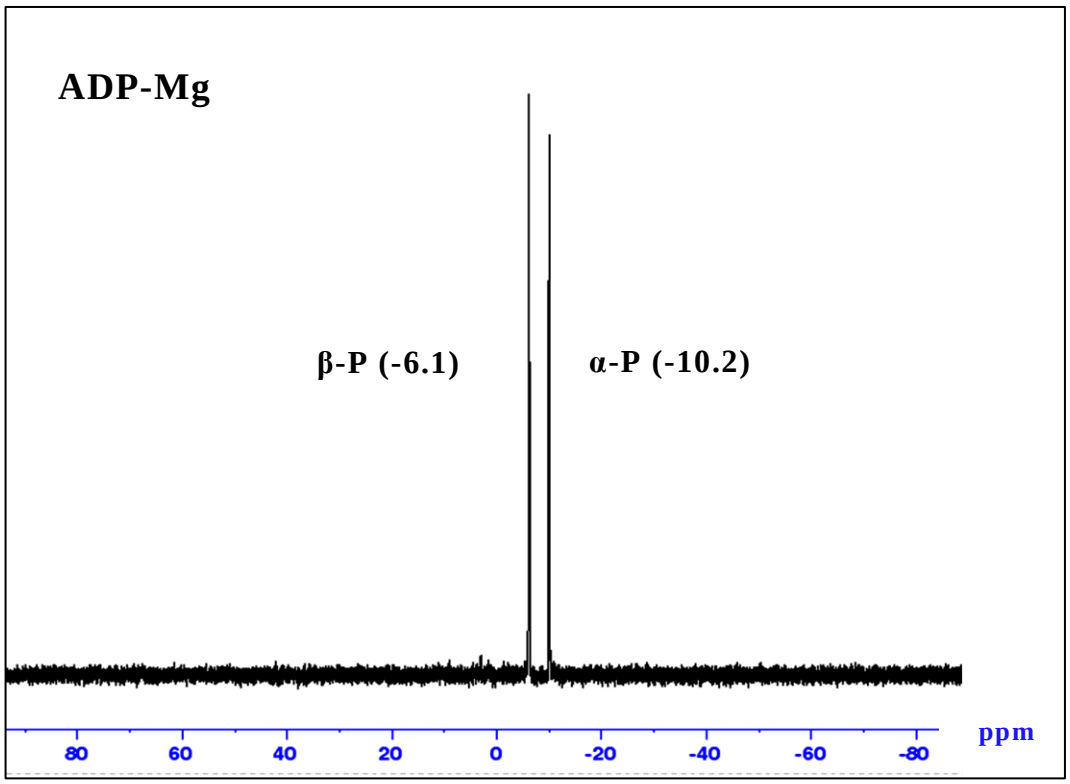

Figure 2-11. ^{31}P NMR for 5'- adenosine diphosphate-magnesium complex (ADP-Mg) at pH 7.0.

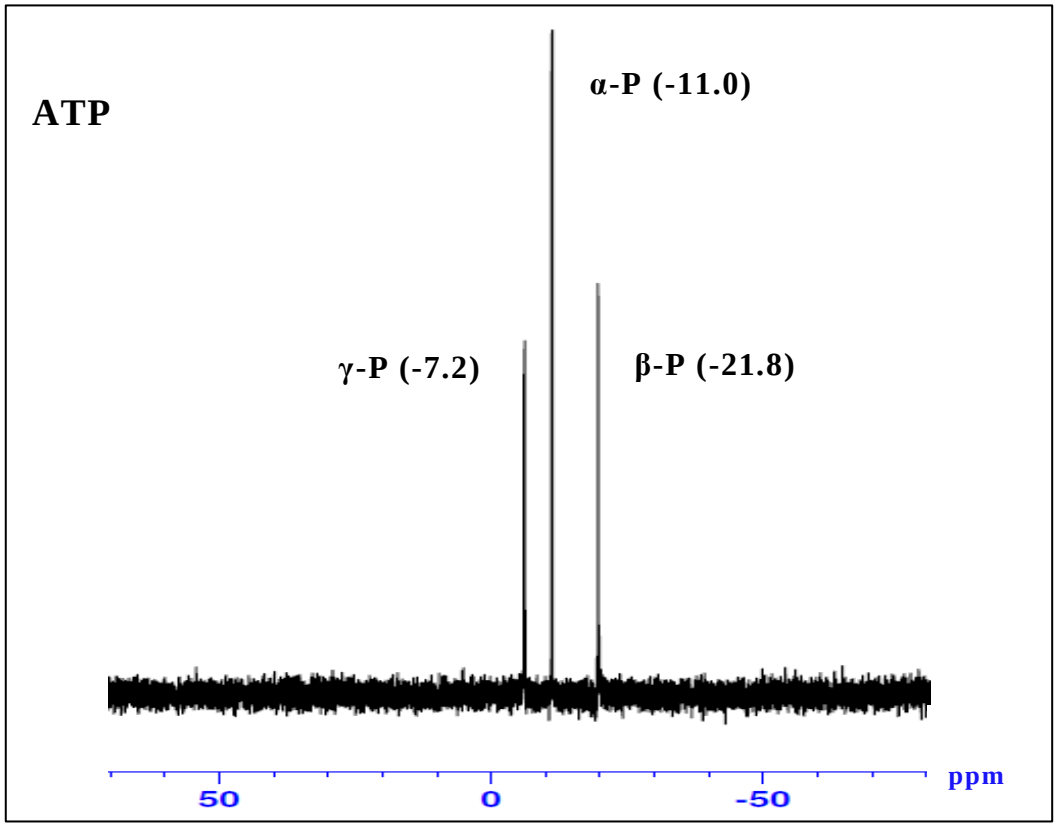

Figure 2-12. ^{31}P NMR for 5'- adenosine triphosphate (ATP) at pH 7.0.

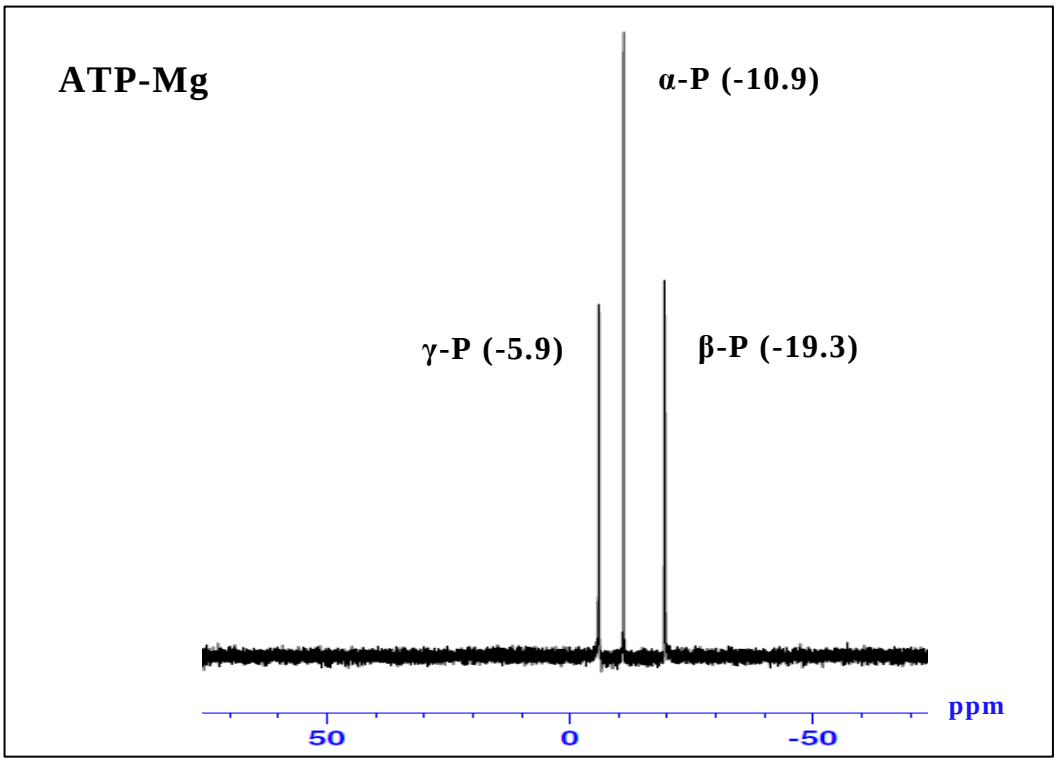

Figure2-13. ^{31}P NMR for 5'- adenosine triphosphate-magnesium complex (ATP-Mg) at pH 7.0.

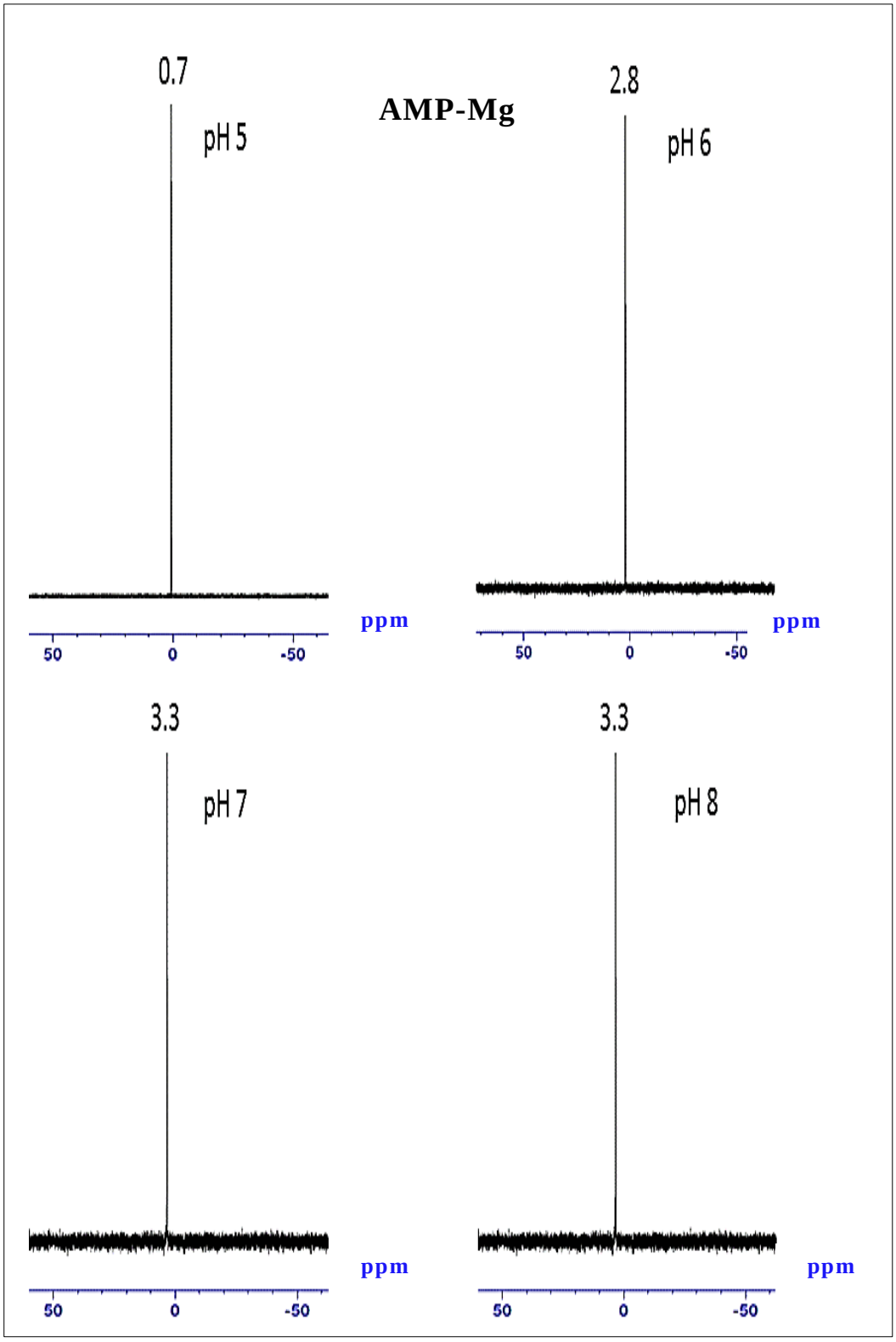

Figure 2-14. ^{31}P NMR for 5'- adenosine monophosphate-magnesium complex (AMP-Mg) at different pH environments.

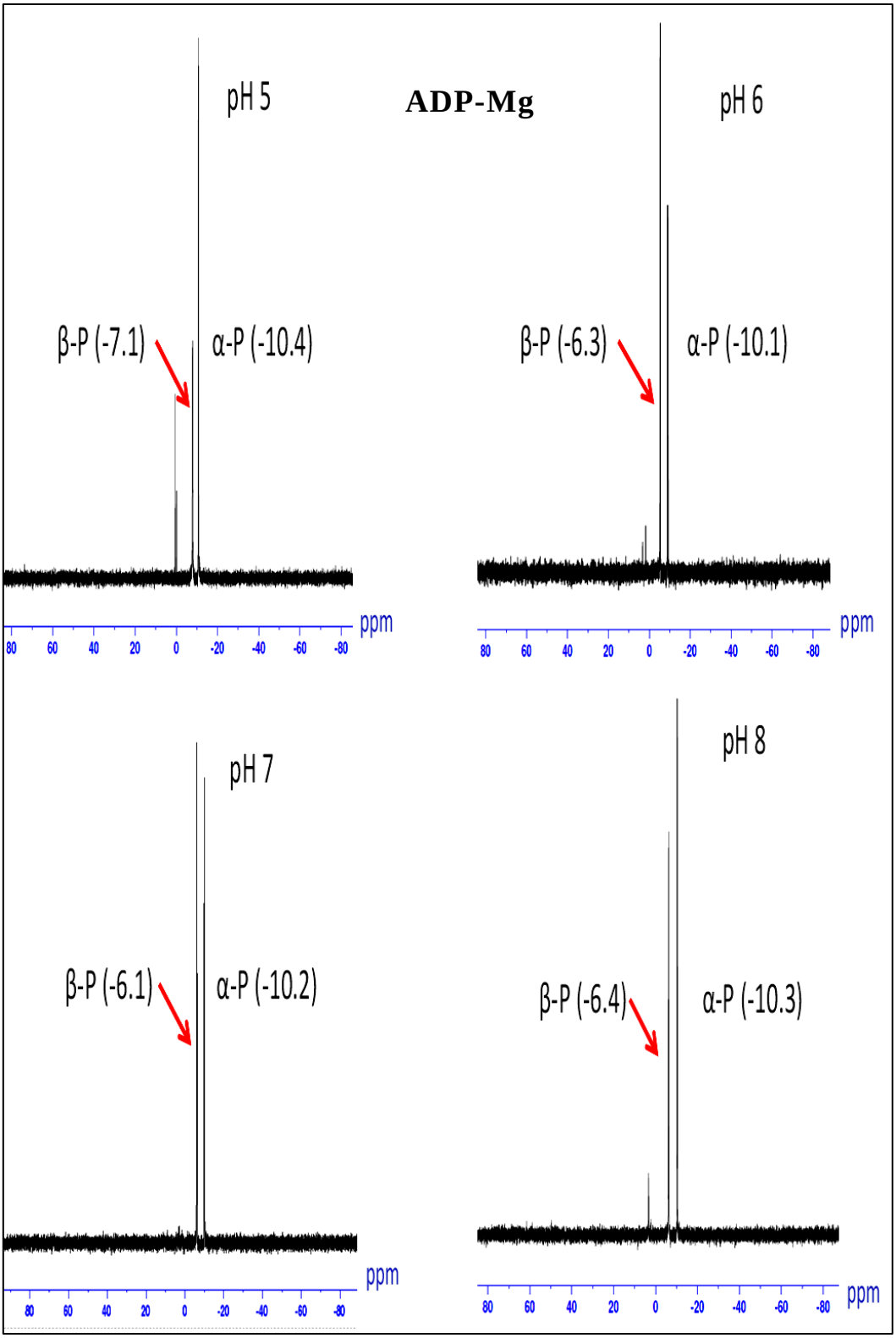

Figure 2-15. ^{31}P NMR for 5'- adenosine diphosphate-magnesium complex (ADP-Mg) at different pH environments.

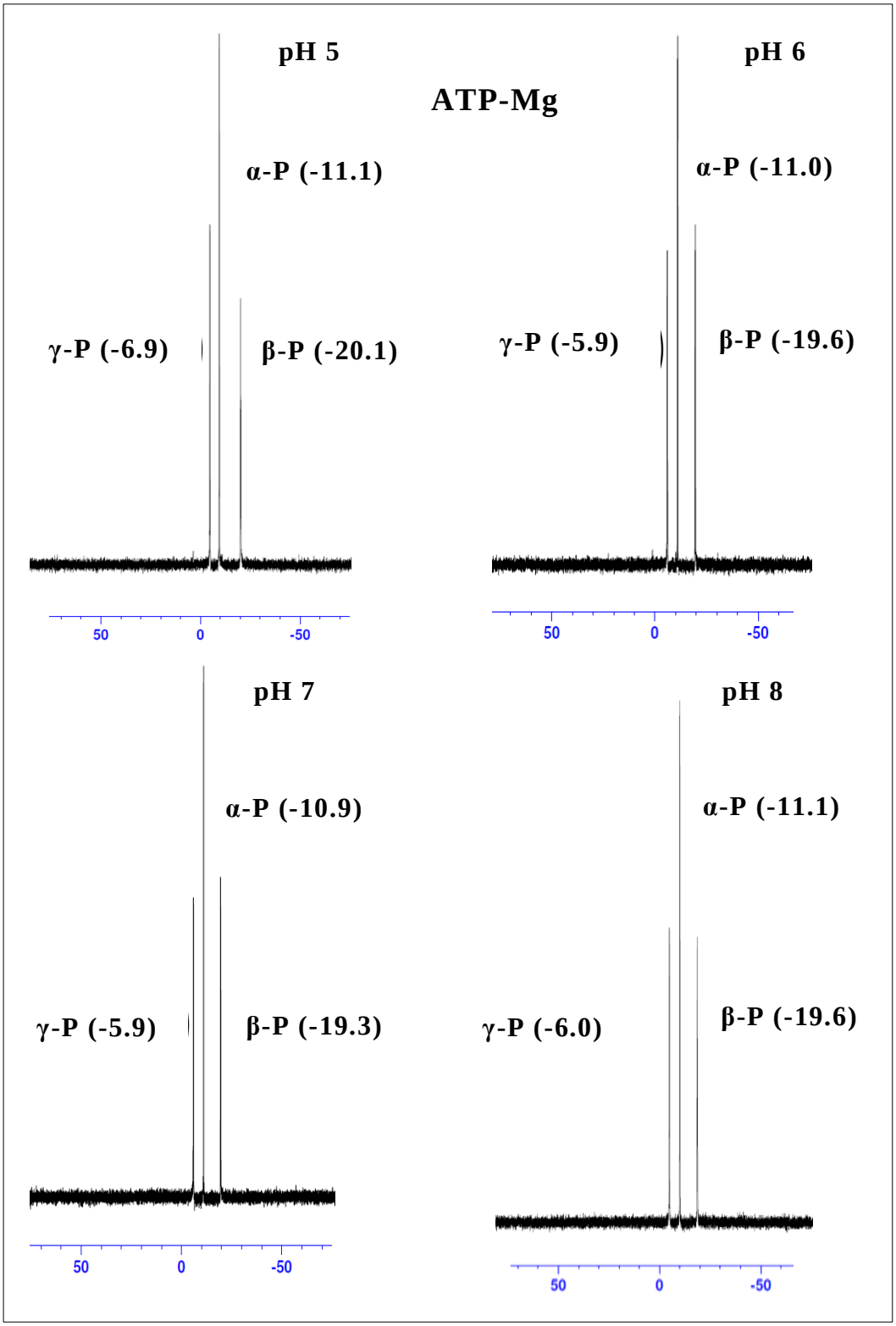

Figure 2-16. ^{31}P NMR for 5'- adenosine triphosphate-magnesium complex (ATP-Mg) at different pH environments.

Appendix 3

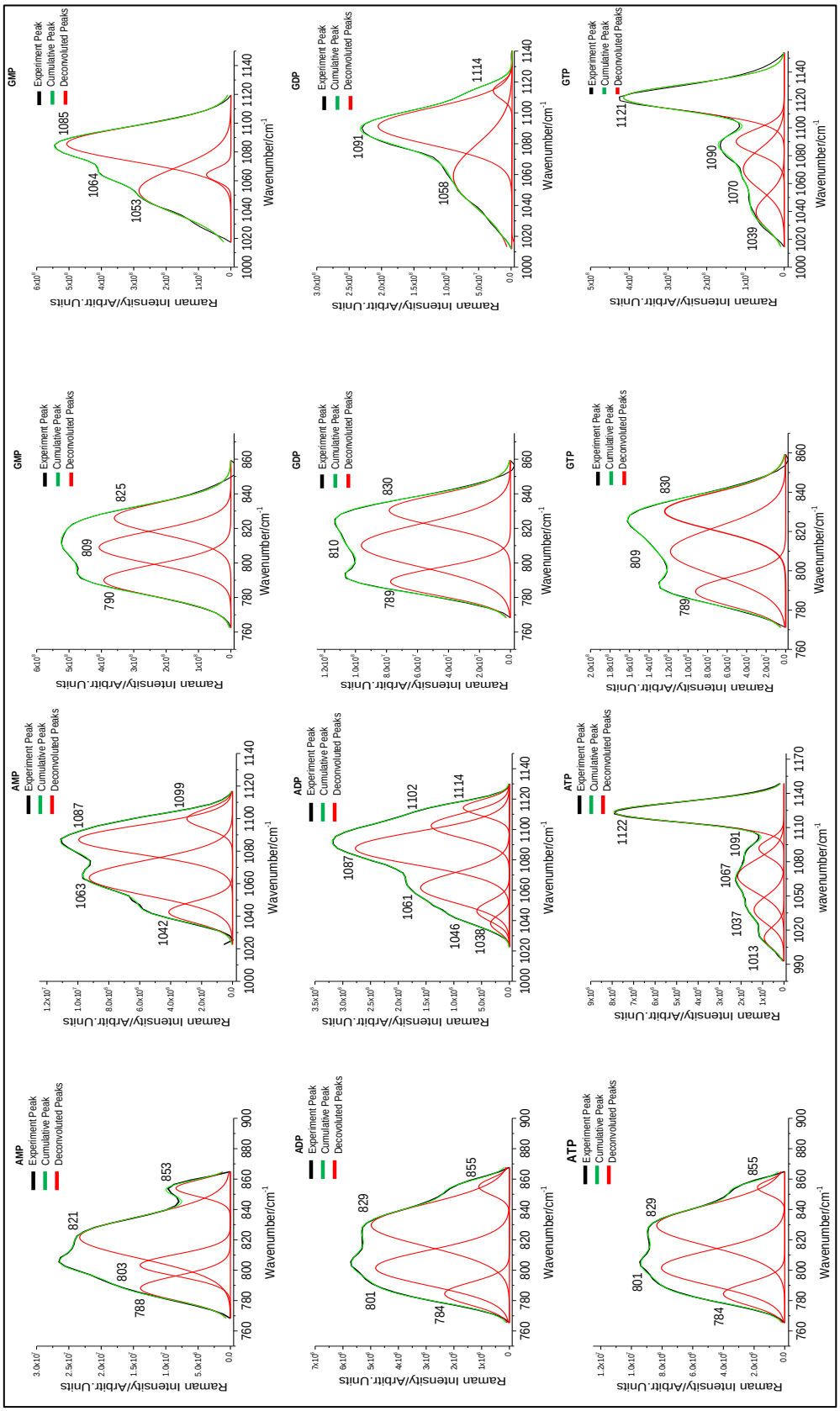

Figure 3-1. The deconvoluted Raman spectra for 5'- adenosine monophosphate (5'-AMP), 5'- adenosine diphosphate (5'-ADP) 5'- adenosine triphosphate (5'-ATP), 5'- guanosine monophosphate (5'-GMP), 5'- guanosine diphosphate (5'-GDP) and 5'- guanosine triphosphate (5'-GTP) at 760-860 and 1020-1120 cm^{-1}.

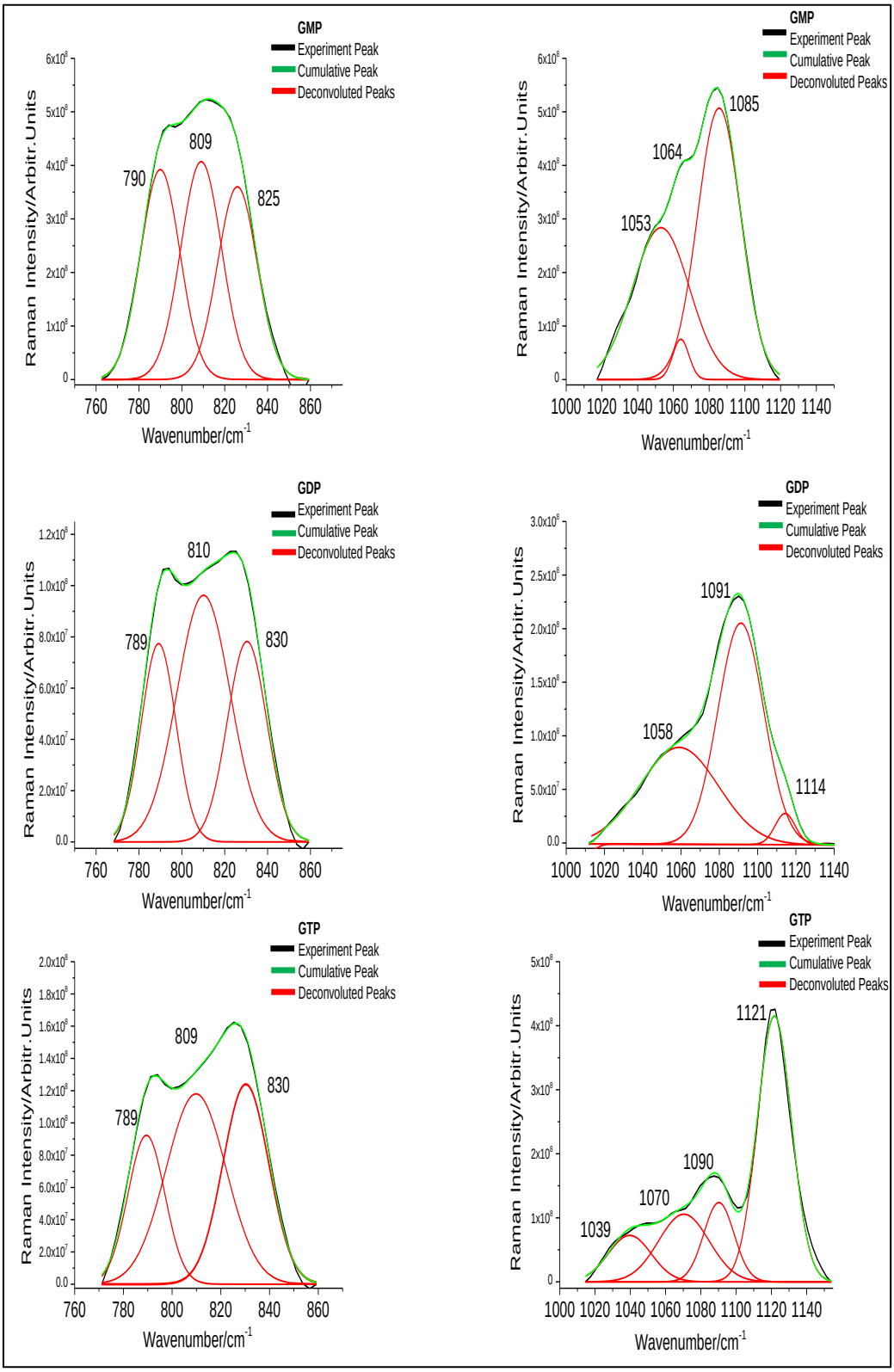

Figure 3-2. Peak deconvolution of the Raman spectrum for 5'-GMP, 5'-GDP and 5'-GTP for the regions 760-860 cm^{-1}.

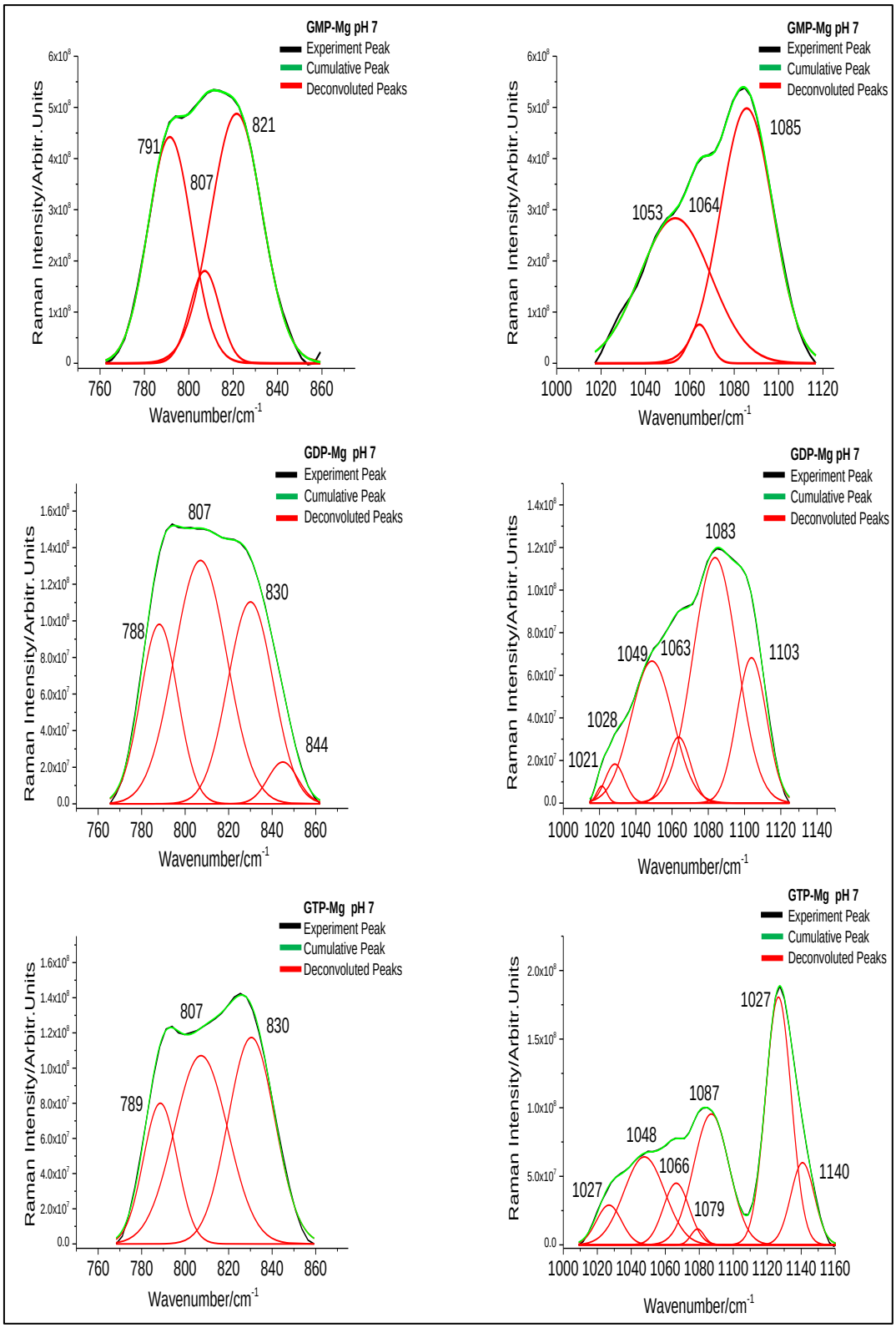

Figure 3-3. Peak deconvolution of the Raman spectrum for 5'-GMP-Mg, 5'-GDP-Mg and 5'-GTP-Mg in the regions 760-870 (left) cm^{-1} and 1020-1120 cm^{-1} (right) at pH 7.0.

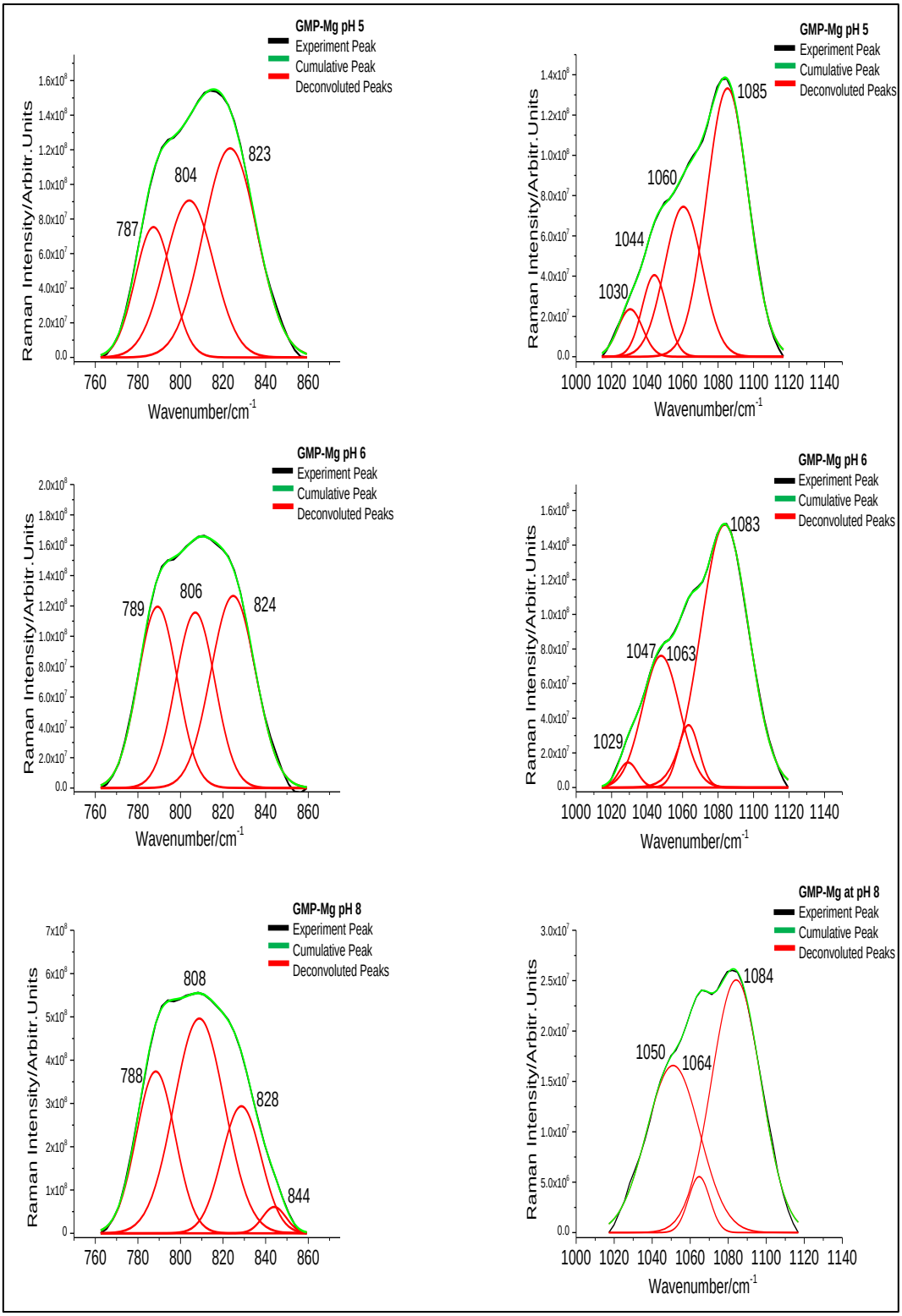

Figure 3-4. Deconvoluted Raman spectra for 5'- guanosine monophosphate-magnesium complex (GMP-Mg) in the regions 760-870 (left) and 1020-1120 cm^{-1} (right) at different pH environments.

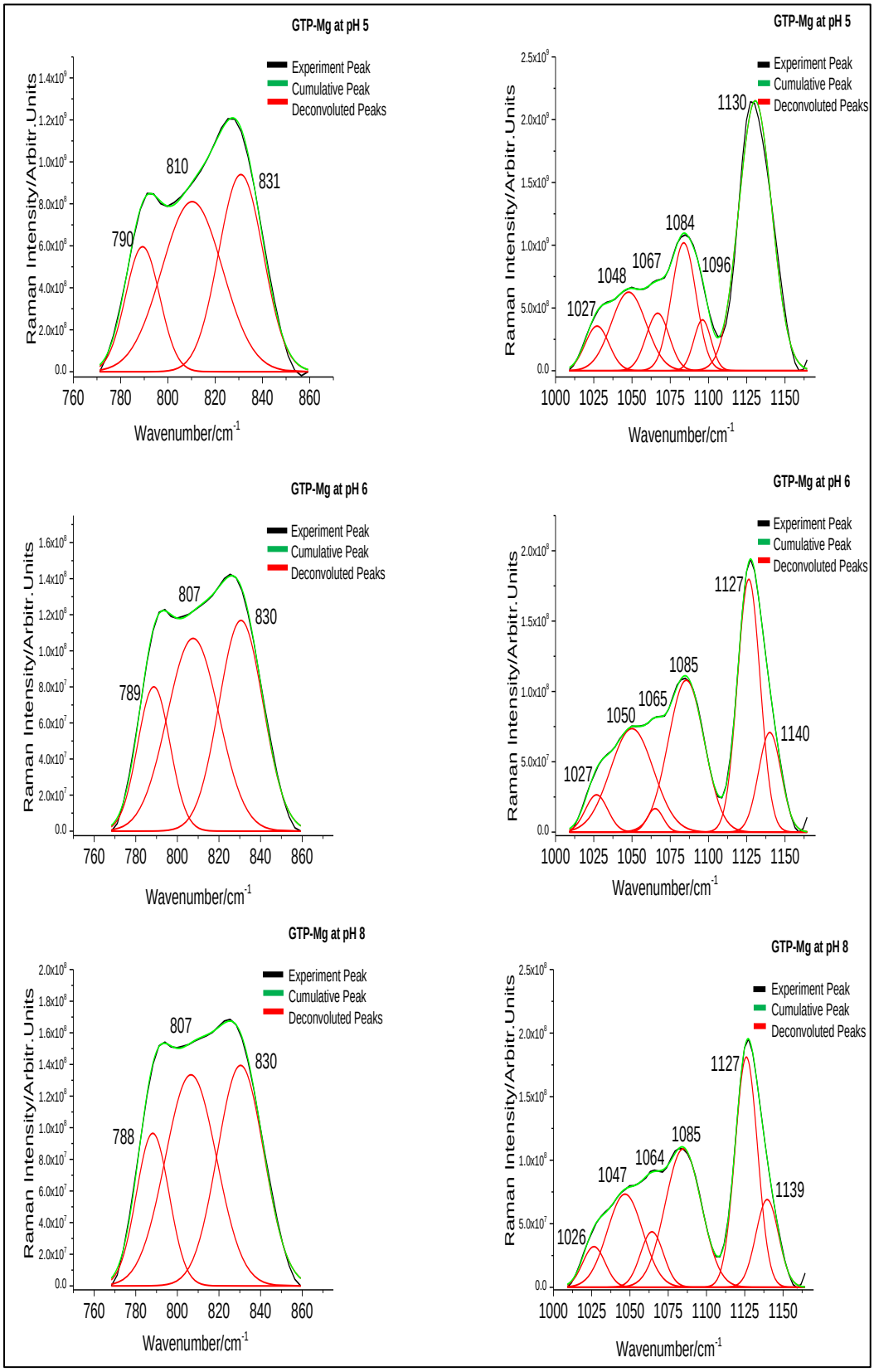

Figure 3-5. Deconvoluted Raman spectra for 5'- guanosine triphosphate-magnesium complex (GTP-Mg) in the regions 760-870 (left) and 990-1150 cm^{-1} (right) at different pH environments.

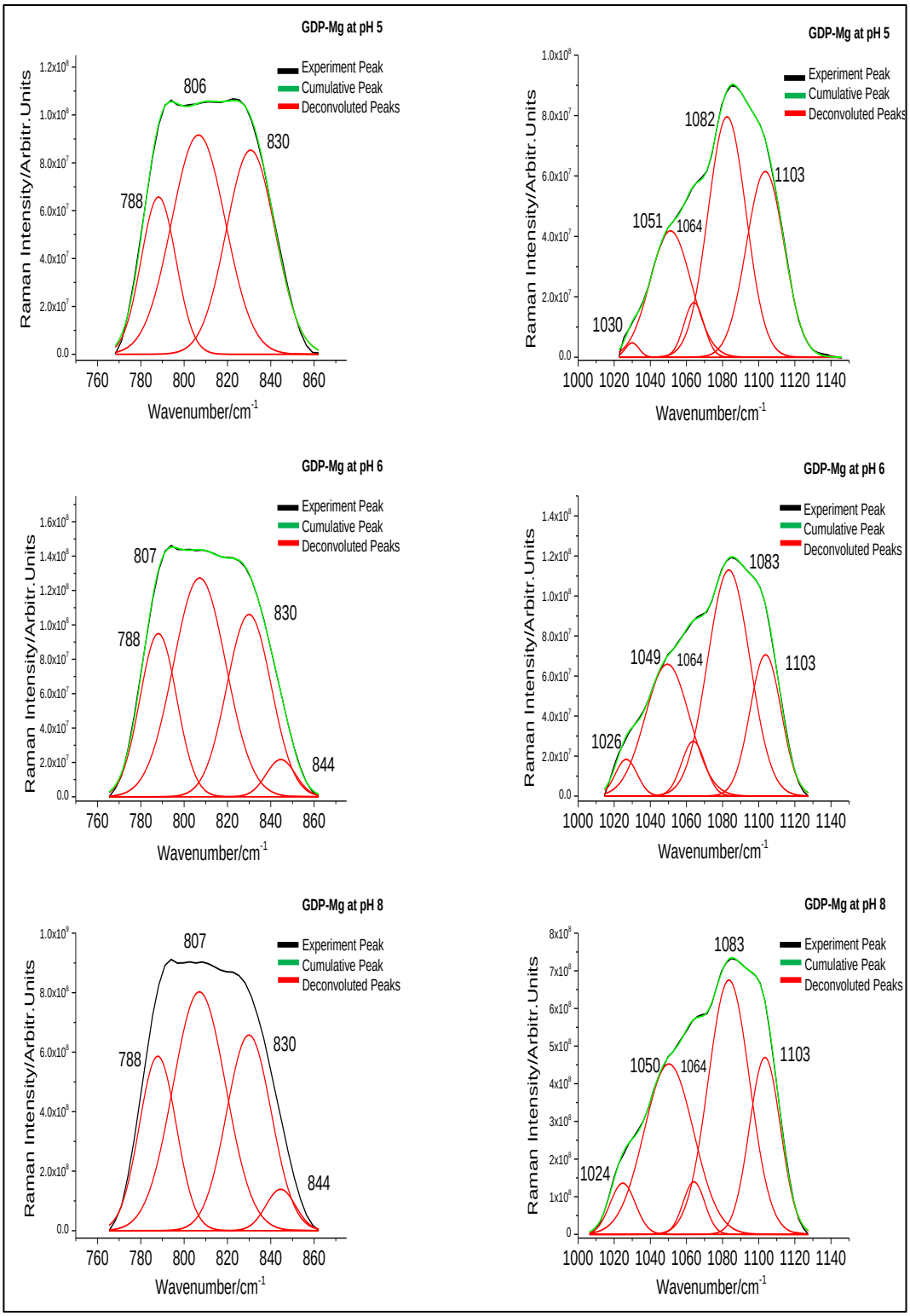

Figure 3-6. Deconvoluted Raman spectra for 5'- guanosine diphosphate-magnesium complex (GDP-Mg) in the regions 760-870 cm^{-1} (left) and 1020-1120 cm^{-1} (right) at different pH environments.

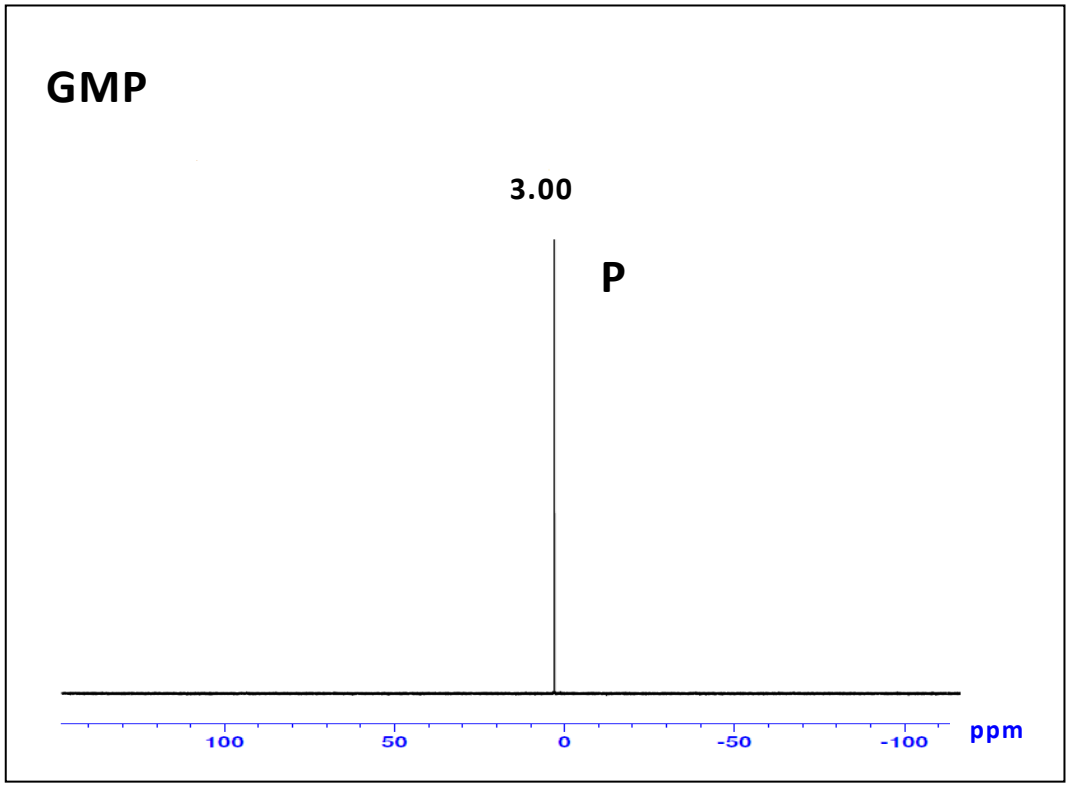

Figure 3-7. ^{31}P NMR for 5'- GMP at pH 7.0. (P): phosphate group

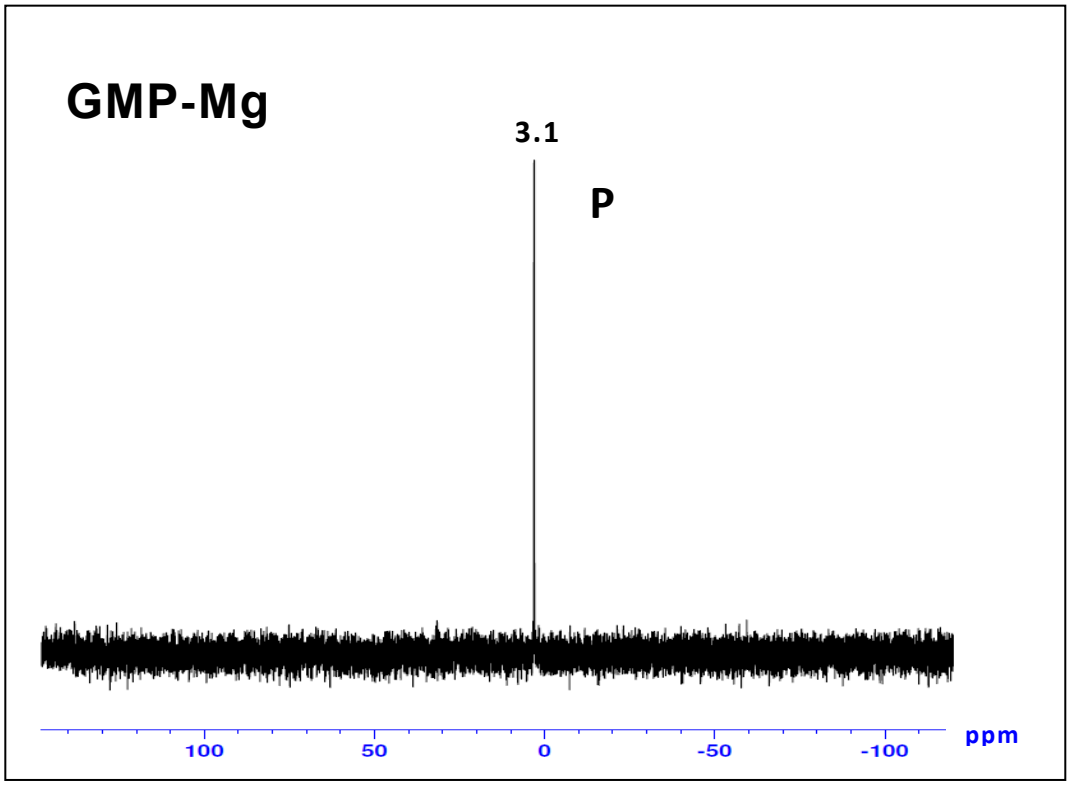

Figure 3-8. ^{31}P NMR for 5'- GMP-Mg complex at pH 7.0. (P): phosphate group.

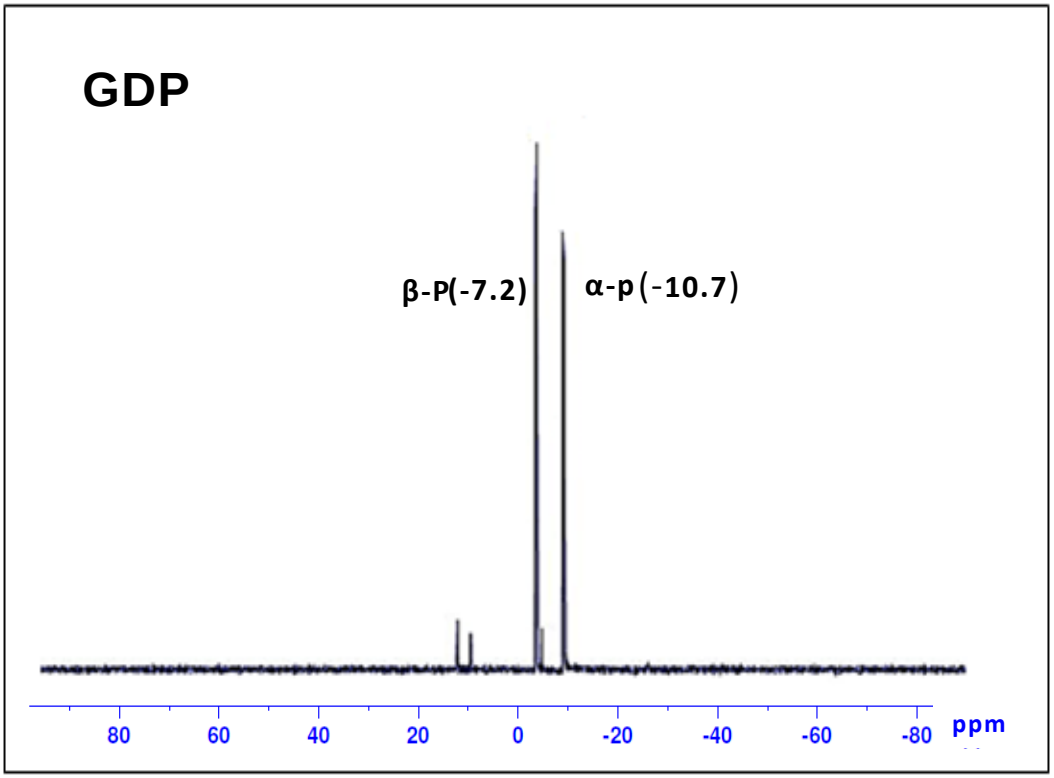

Figure 3-9. ^{31}P NMR for 5'- GMP at pH 7.0. (P): phosphate group

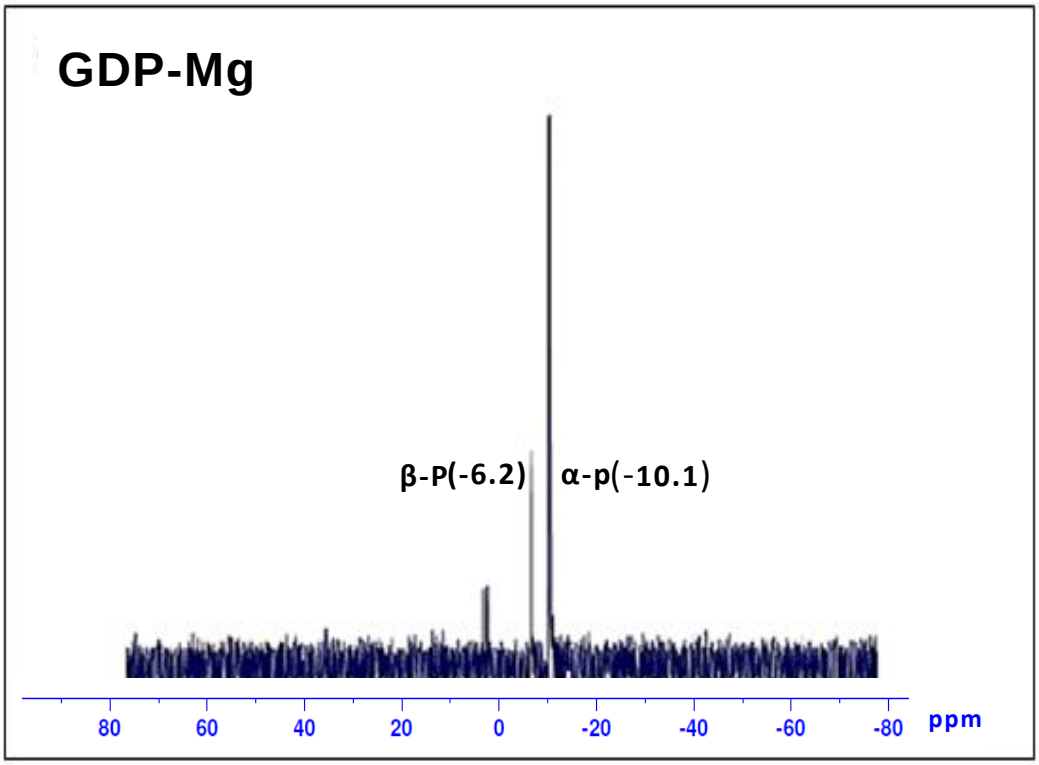

Figure 3-10. ^{31}P NMR for 5'- GDP-Mg complex at pH 7.0. (P): phosphate group.

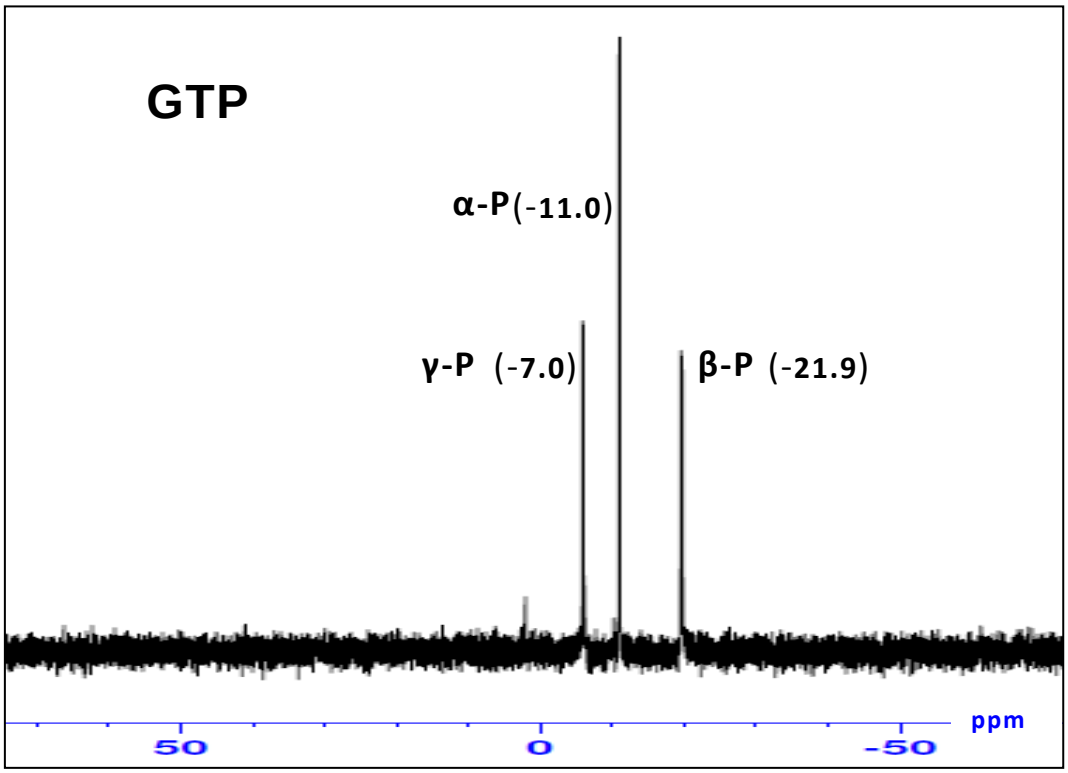

Figure 3-11. ^{31}PNMR for 5'- GTP at pH 7.0. (P): phosphate group.

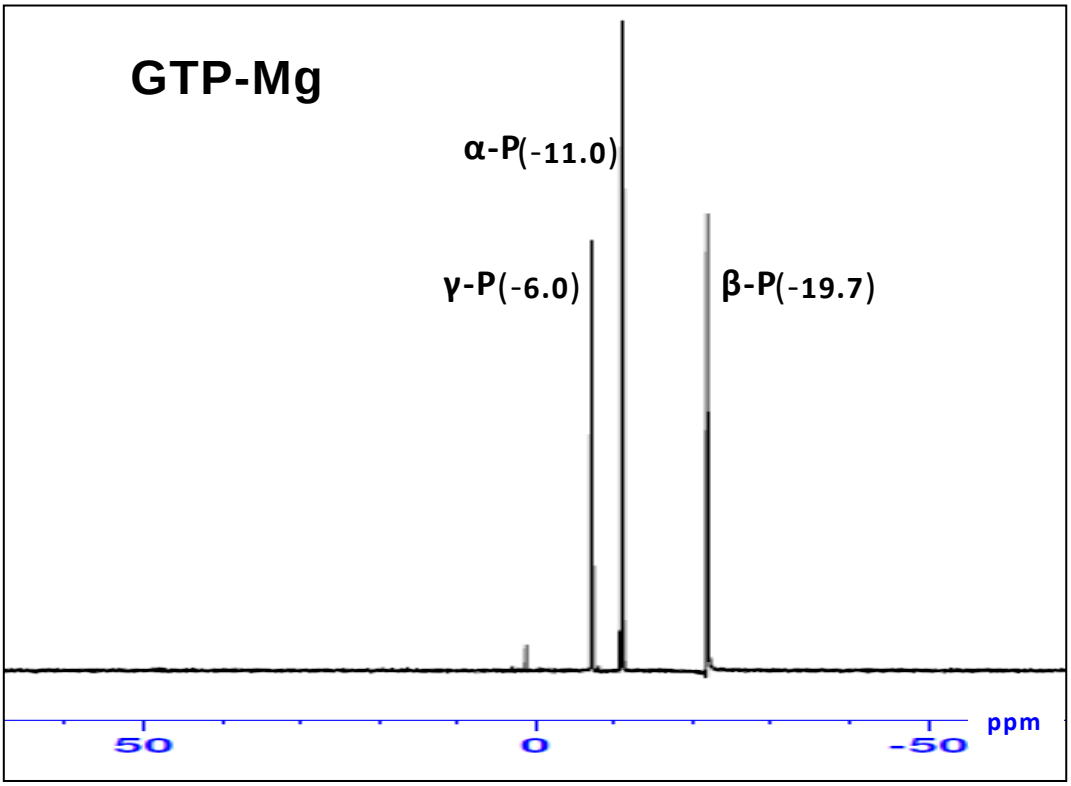

Figure 3-12. ^{31}PNMR for 5'- GTP-Mg complex at pH 7.0. (P): phosphate group.

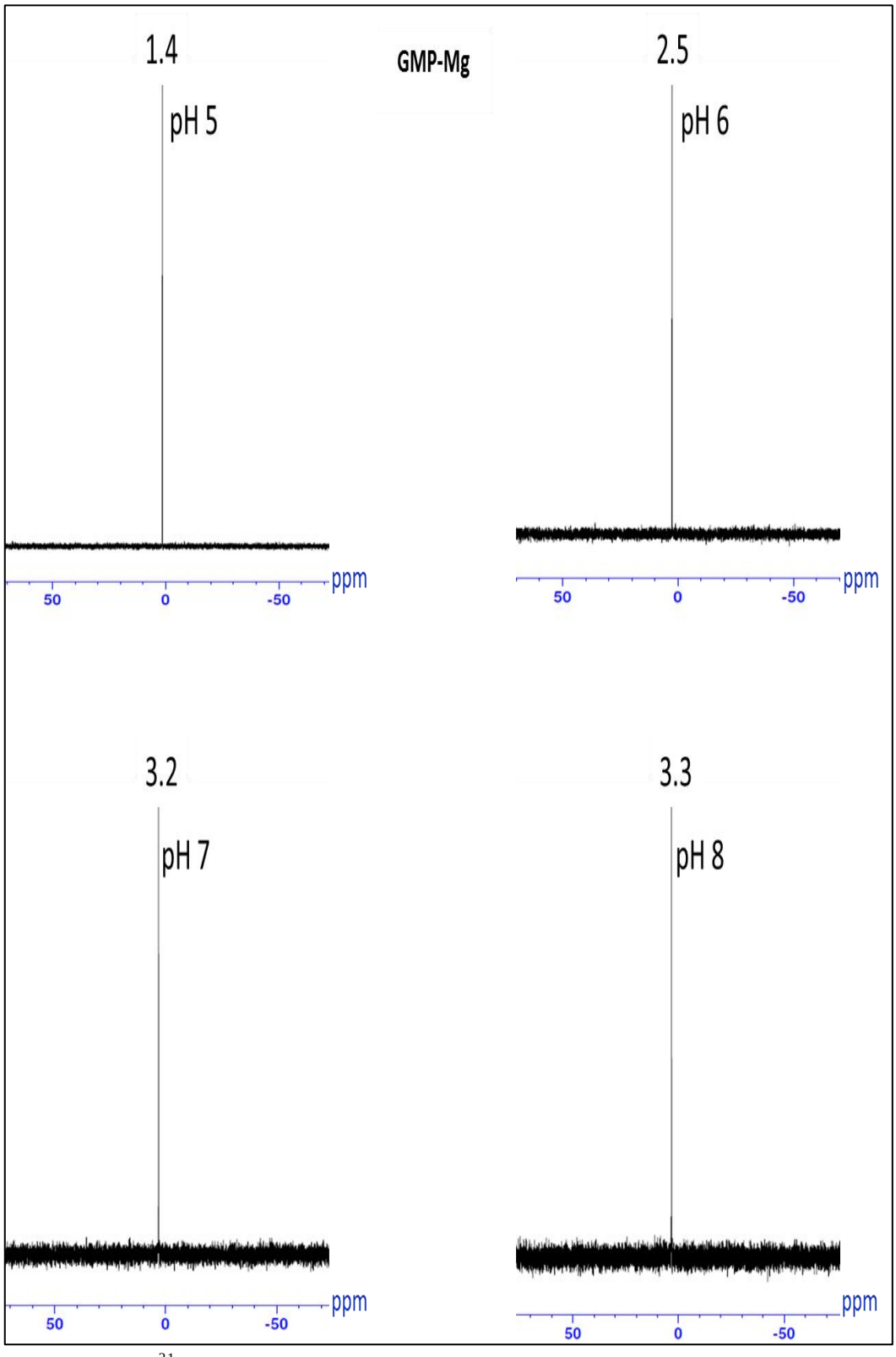

Figure 3-13. ^{31}P NMR for 5'- guanosine monophosphate-magnesium complex (GMP-Mg) at different pH environments.

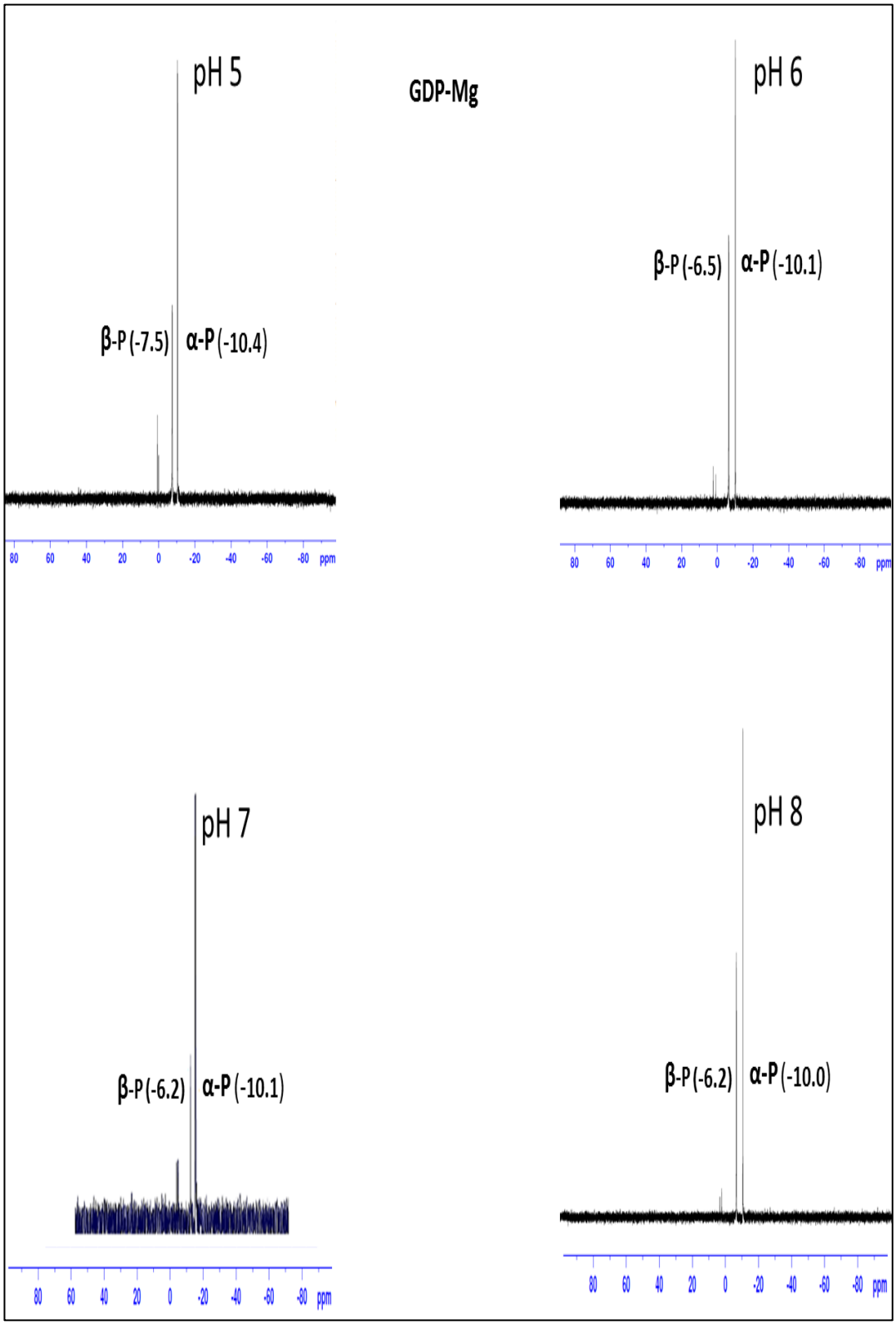

Figure 3-14 . ^{31}P NMR for 5'- guanosine diphosphate-magnesium complex (GDP-Mg) at different pH environments.

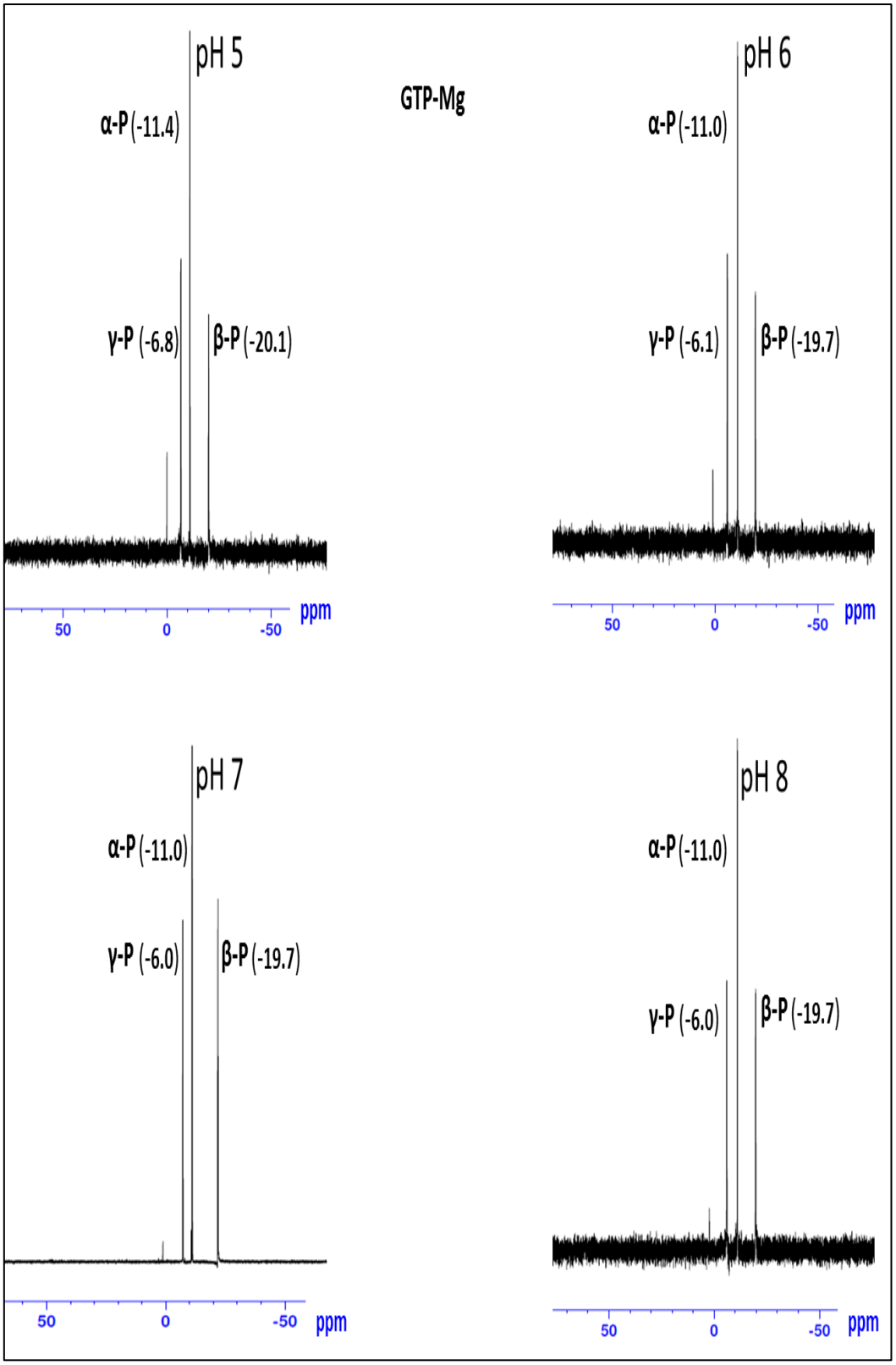

Figure S3-15.[31]P NMR for 5'- guanosine triphosphate-magnesium complex (GTP-Mg) at different pH environments.

Figure 4. 1..Raman (I^R+I^L) spectra of Cytidine, Cytidine 5'-monophosphate (C5-MP), Cytidine 5'-diphosphate (C5-DP) and Cytidine 5'-triphosphate (C5-TP).

Figure 4.2..Raman optical activity ROA(I^R-I^L) spectra of Cytidine, Cytidine 5'-monophosphate (C5-MP), Cytidine 5'-diphosphate (C5-DP) and Cytidine 5'-triphosphate (C5-TP).

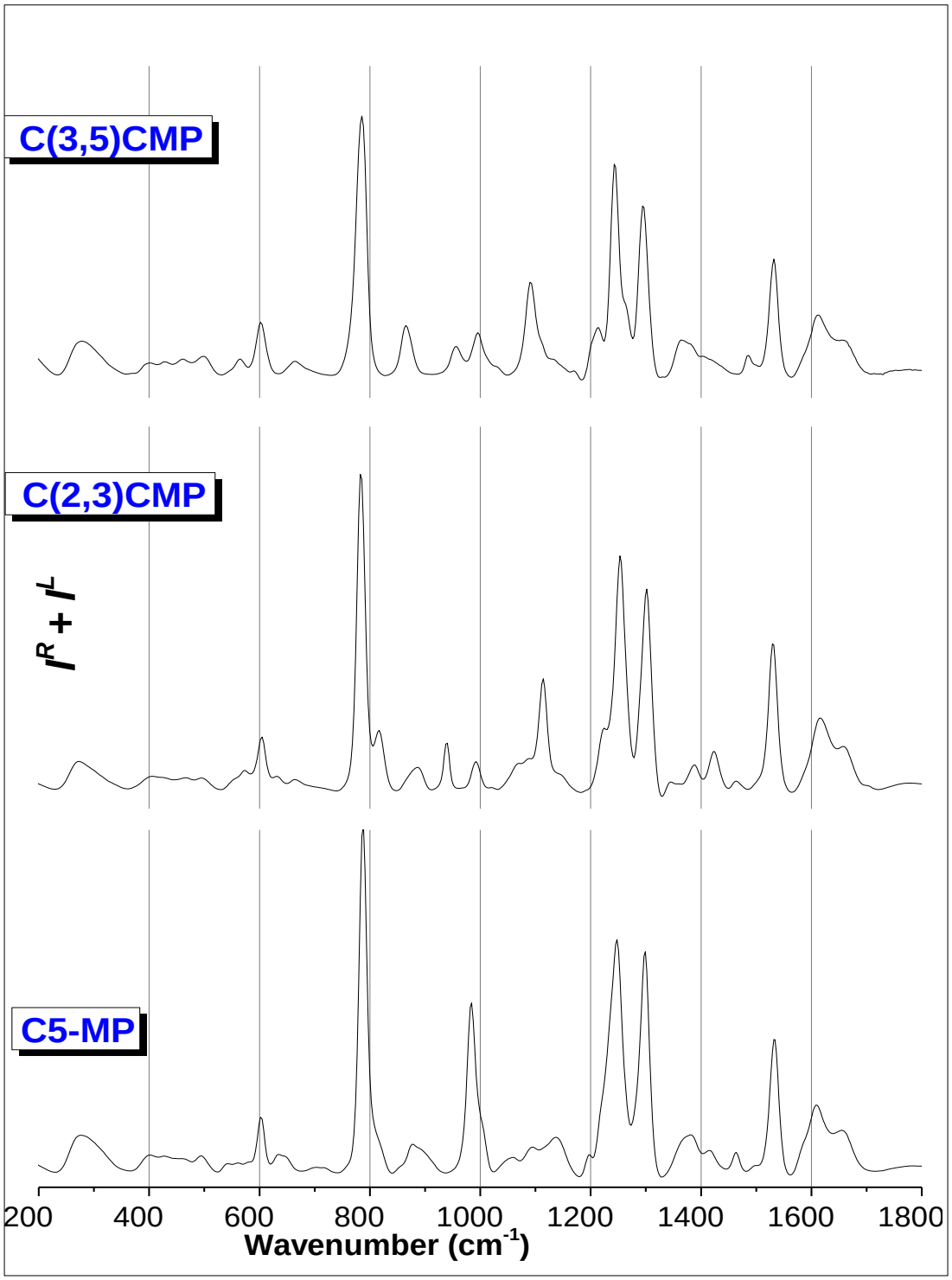

Figure 4.3. Raman (I^R+I^L) spectra of Cytidine 5'-monophosphate (C5-MP), Cytidine 2',3'- cyclic monophosphate (C2,3-CMP) and Cytidine 3',5'-cyclic monophosphate(C3,5-CMP).

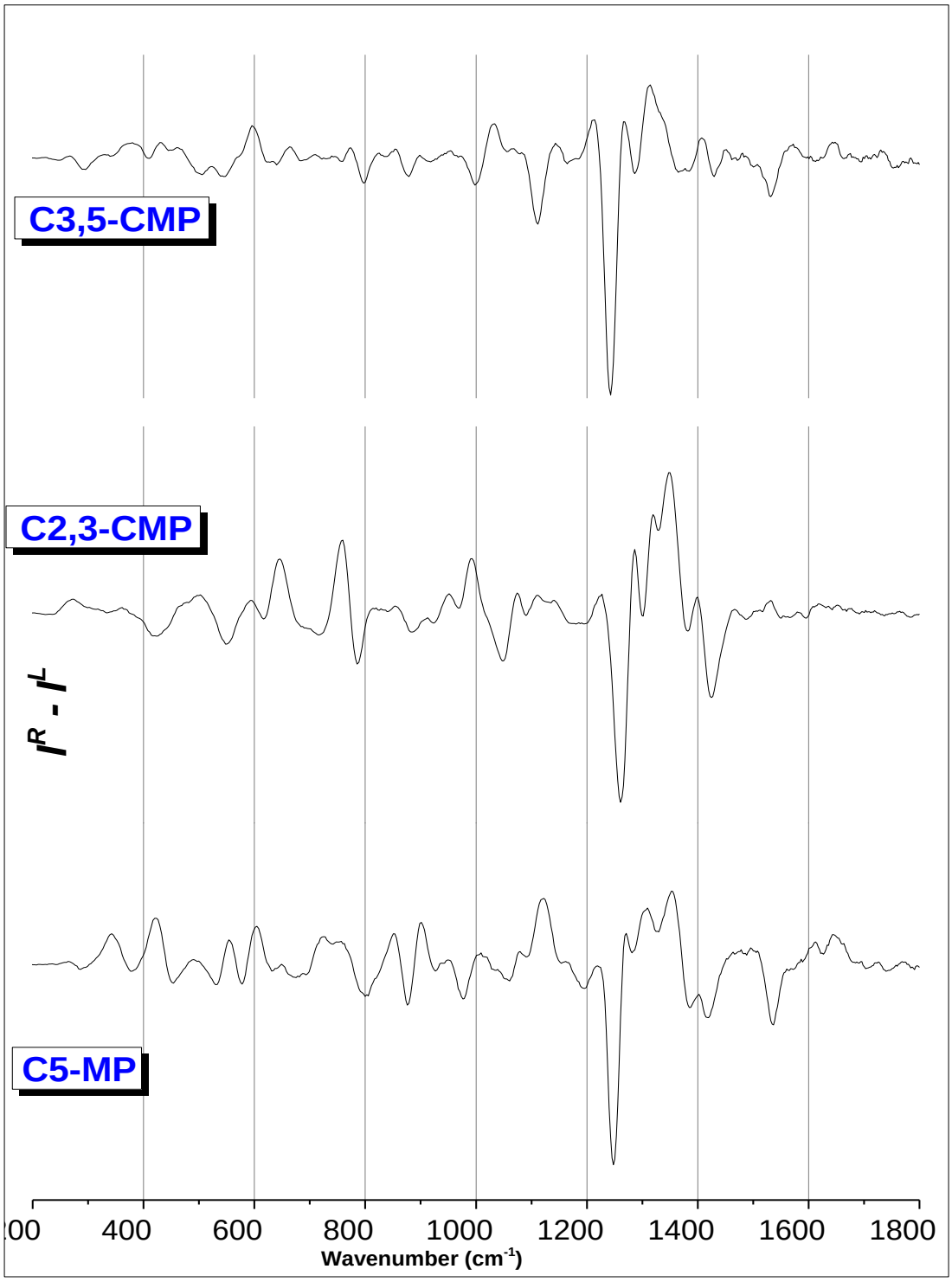

Figure 4.4. Raman optical activity (ROA) (I^R-I^L) spectra of Cytidine 5'-monophosphate (C5-MP), Cytidine 2',3'- cyclic monophosphate (C2,3-CMP) and Cytidine 3',5'-cyclic monophosphate(C3,5-CMP).

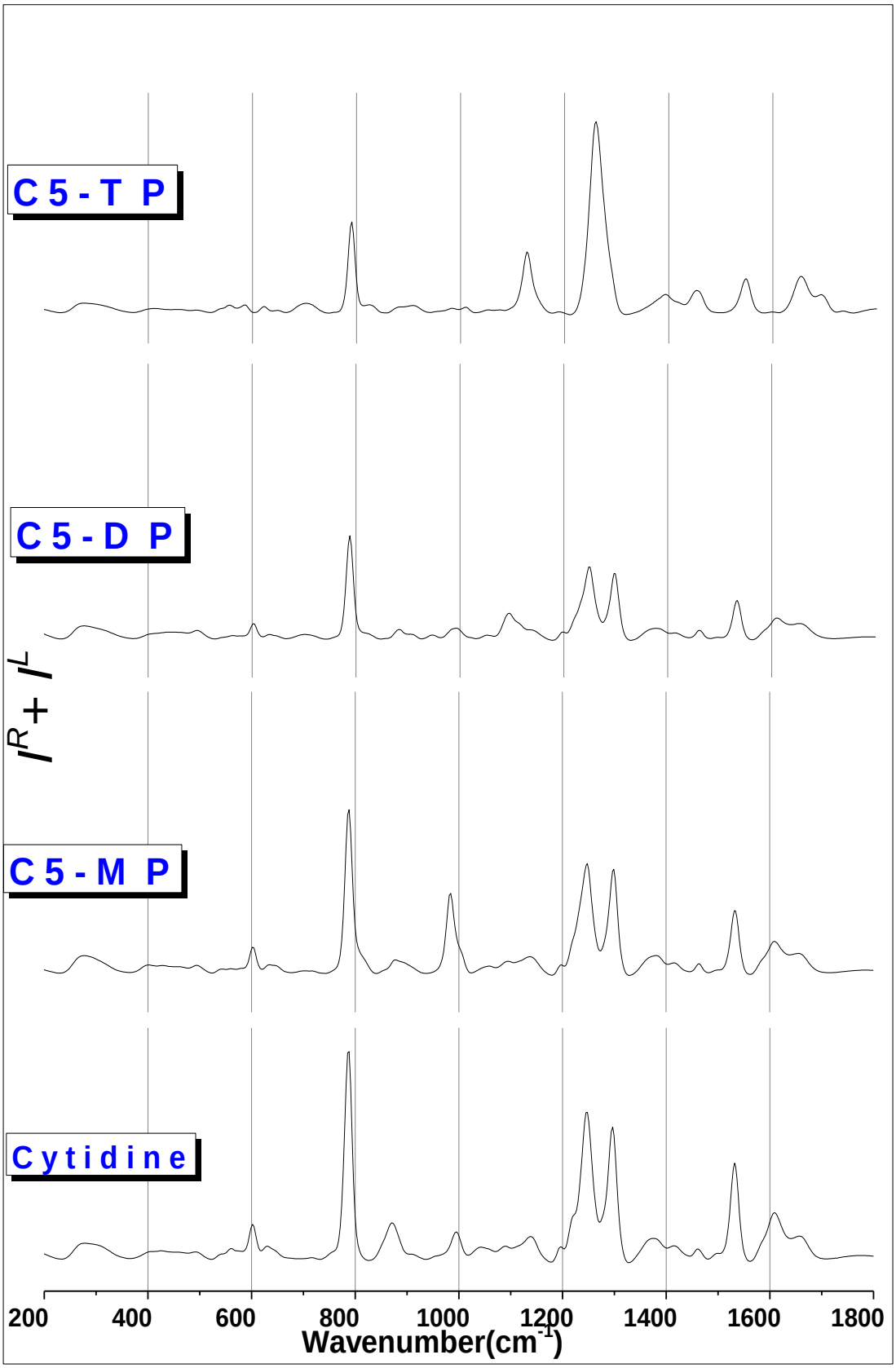

Figure 4.5. Raman (I^R+I^L) spectra of Cytidine, Cytidine 5'-monophosphate (C5-MP), Cytidine 5'-diphosphate (C5-DP) and Cytidine 5'-triphosphate (C5-TP),

Figure 4.6. Raman optical activity (ROA) (I^R-I^L) spectra of Cytidine, Cytidine 5'-monophosphate (C5-MP), Cytidine 5'-diphosphate (C5-DP) and Cytidine 5'-triphosphate (C5-TP).

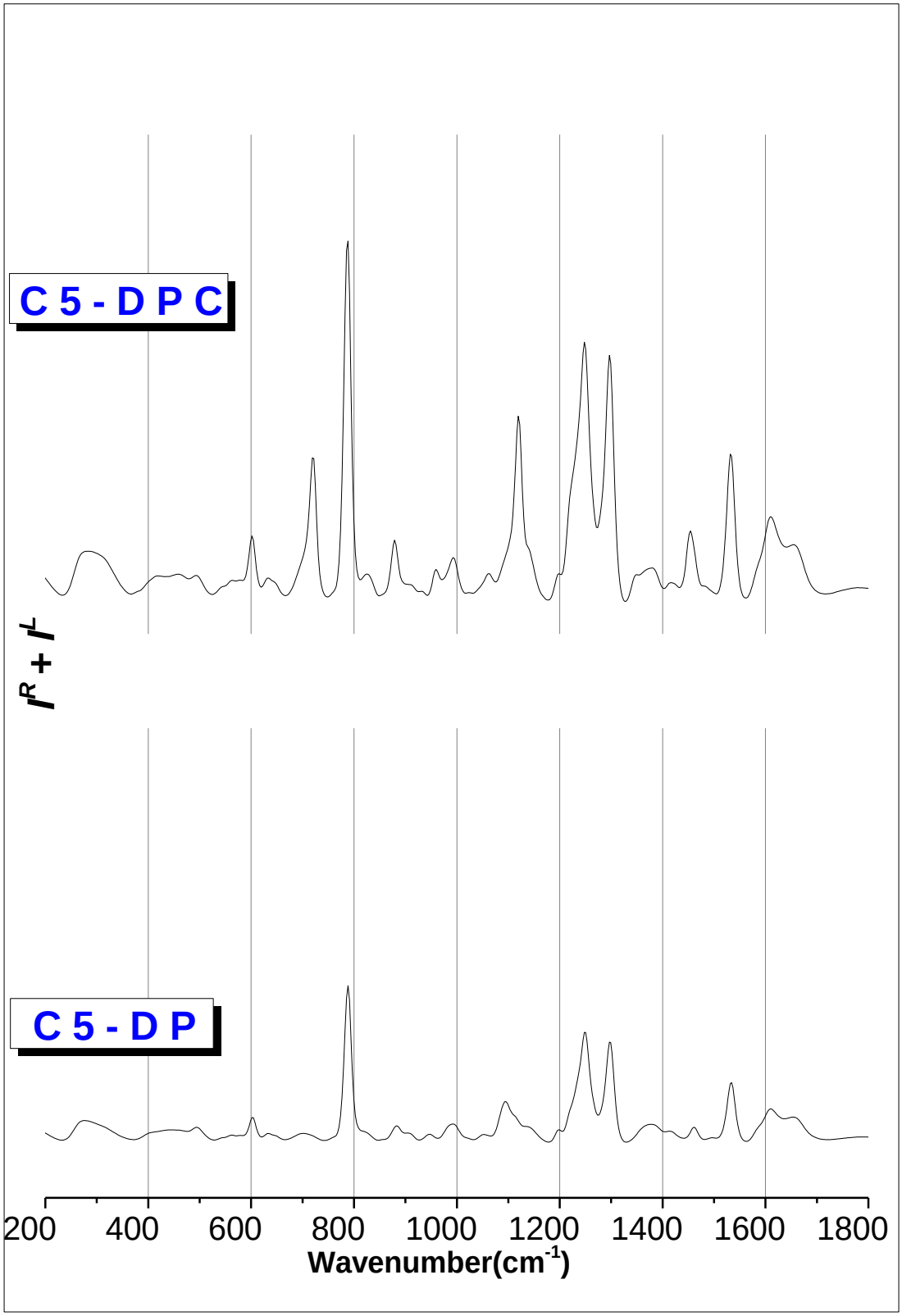

Figure 4.7. Raman (I^R+I^L) spectra of Cytidine 5'-diphosphate (C5-DP) and Cytidine 5'-diphosphocholine (C5-DPC).

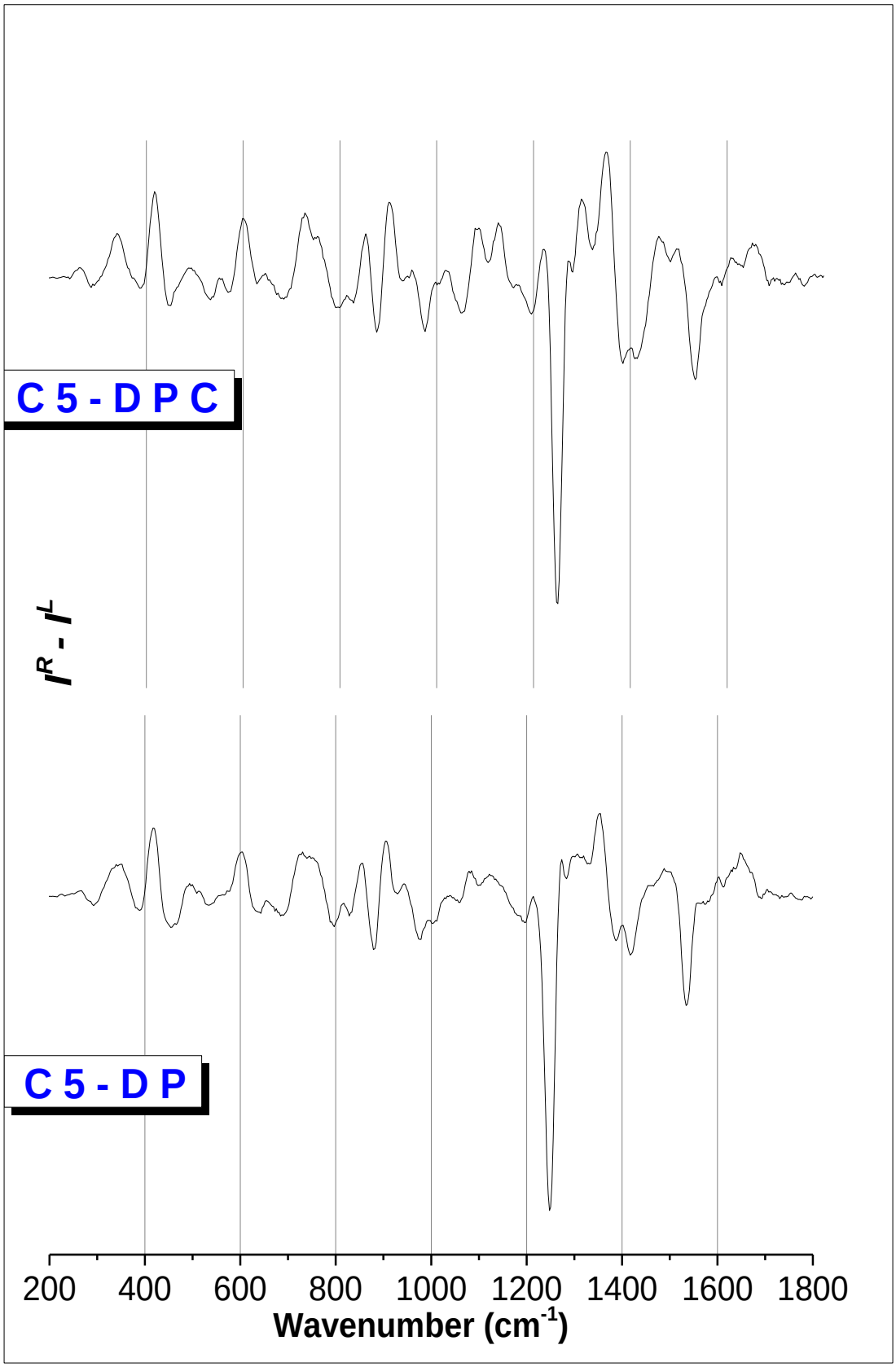

Figure 4.8. Raman optical activity (ROA) (I^R-I^L) spectra of Cytidine 5'-diphosphate (C5-DP) and Cytidine 5'-diphosphocholine (C5-DPC).

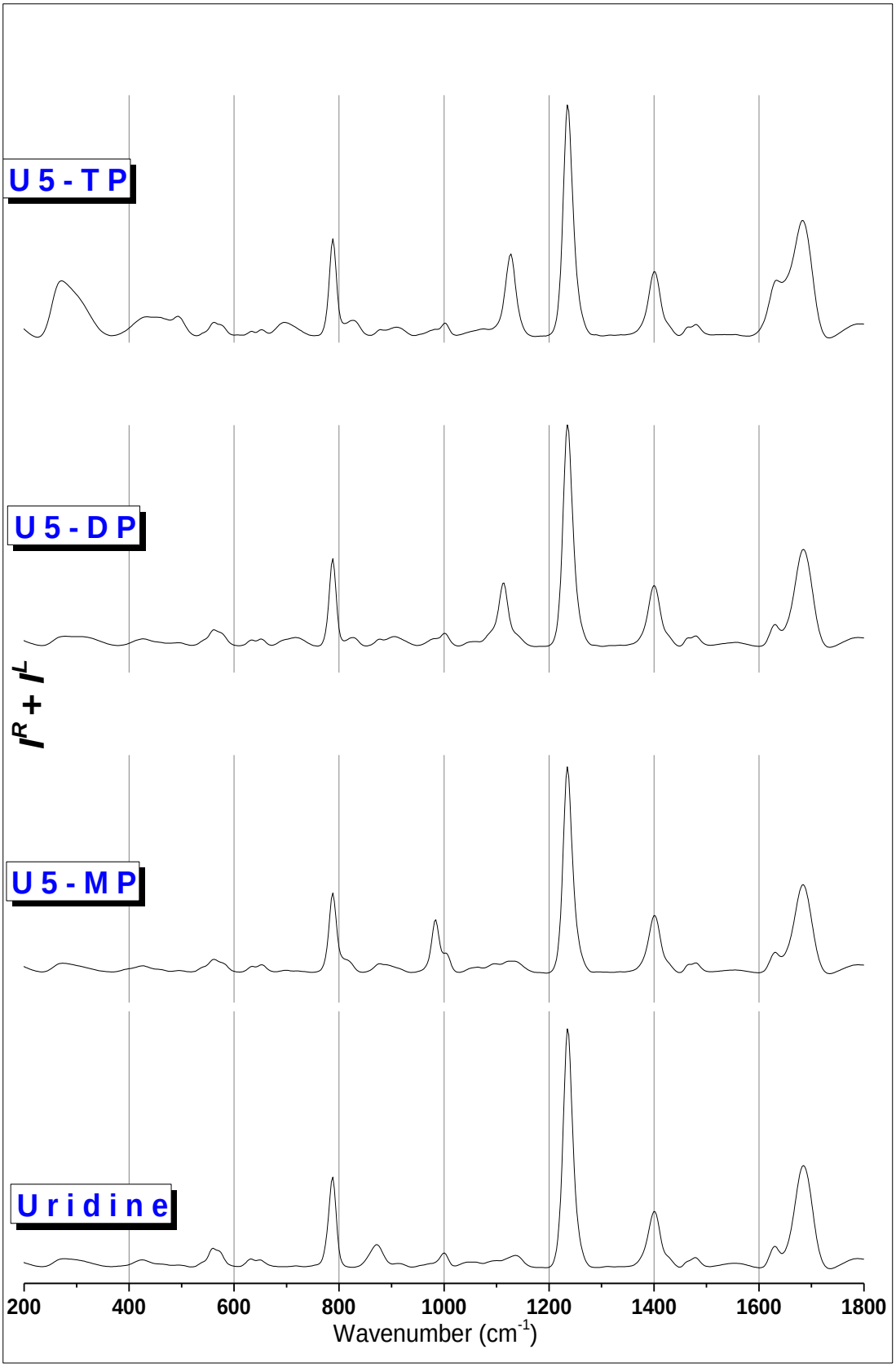

Figure 4.9. Raman (I^R+I^L) spectra of Uridine, Uridine 5'-monophosphate (U5-MP), Uridine 5'-diphosphate (U5-DP) and Uridine 5'-triphosphate (U5-TP).

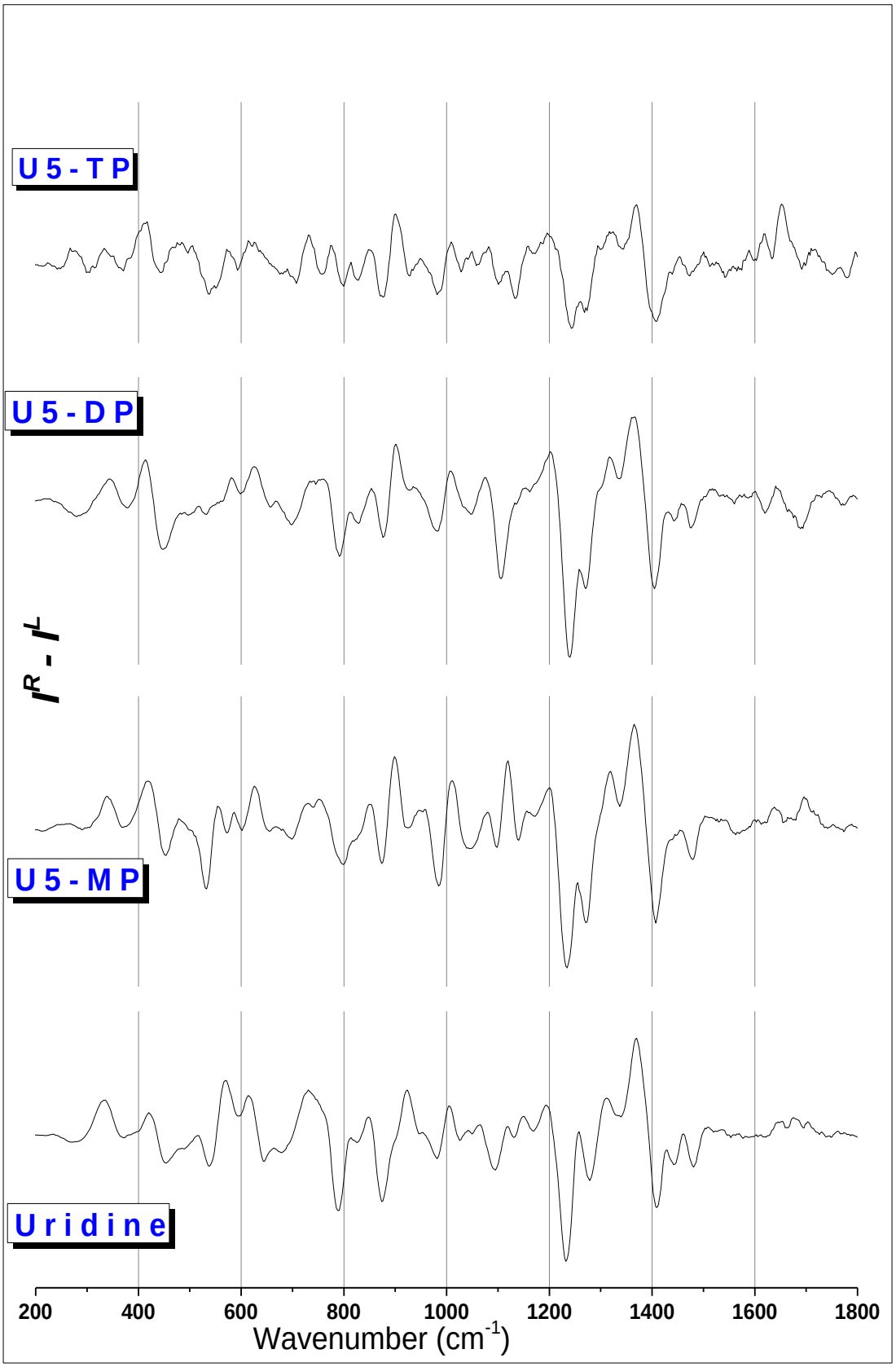

Figure 4.10. Raman optical activity (ROA) (I^R-I^L) of Uridine, Uridine 5'-monophosphate (U5-MP), Uridine 5'-diphosphate (U5-DP) and Uridine 5'-triphosphate (U5-TP).

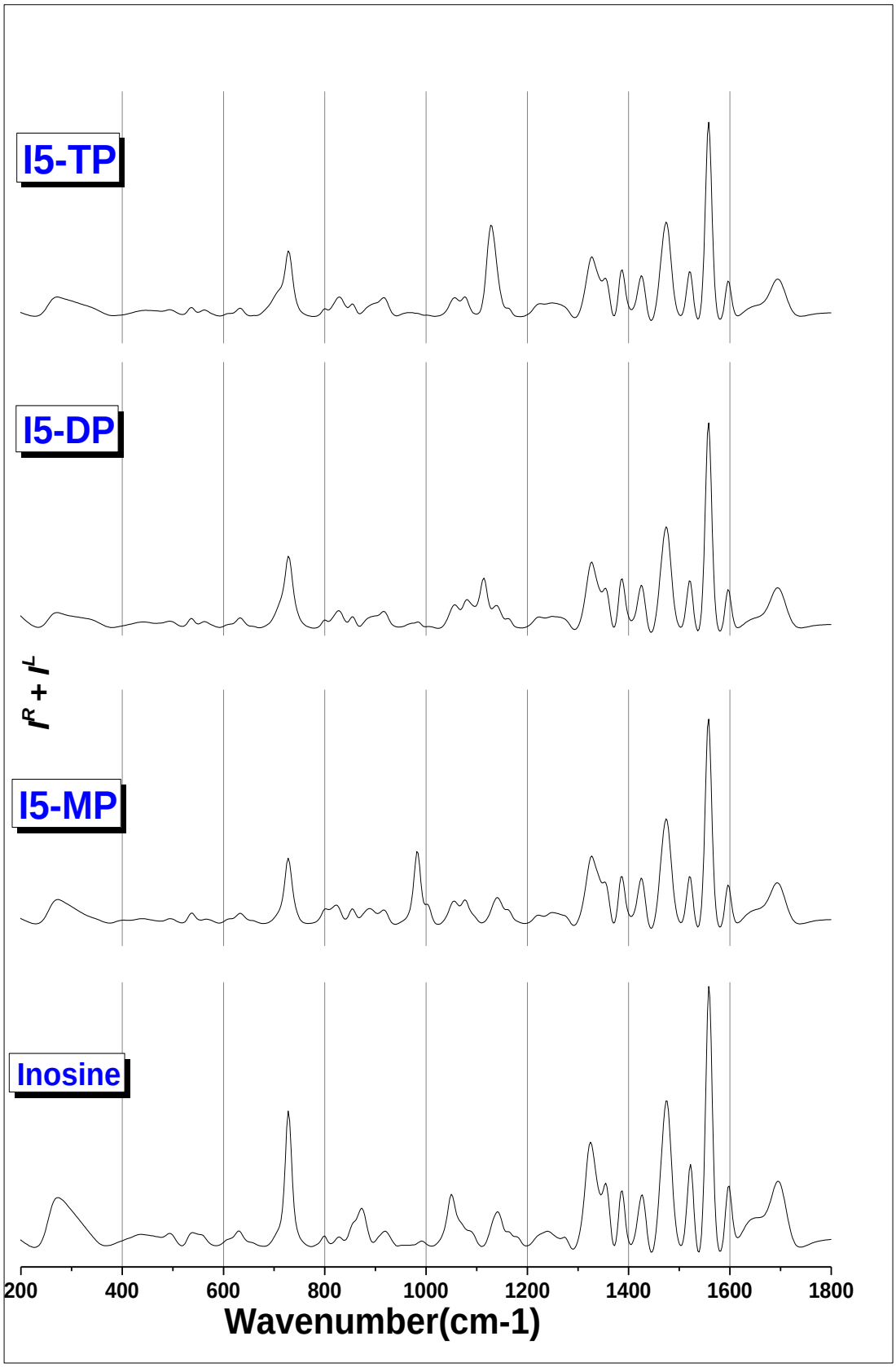

Figure 4.11. Raman (I^R+I^L) spectra of Inosine, Inosine 5'-monophosphate (I5-MP), Inosine 5'-diphosphate (I5-DP) and Inosine 5'-triphosphate (I5-TP).

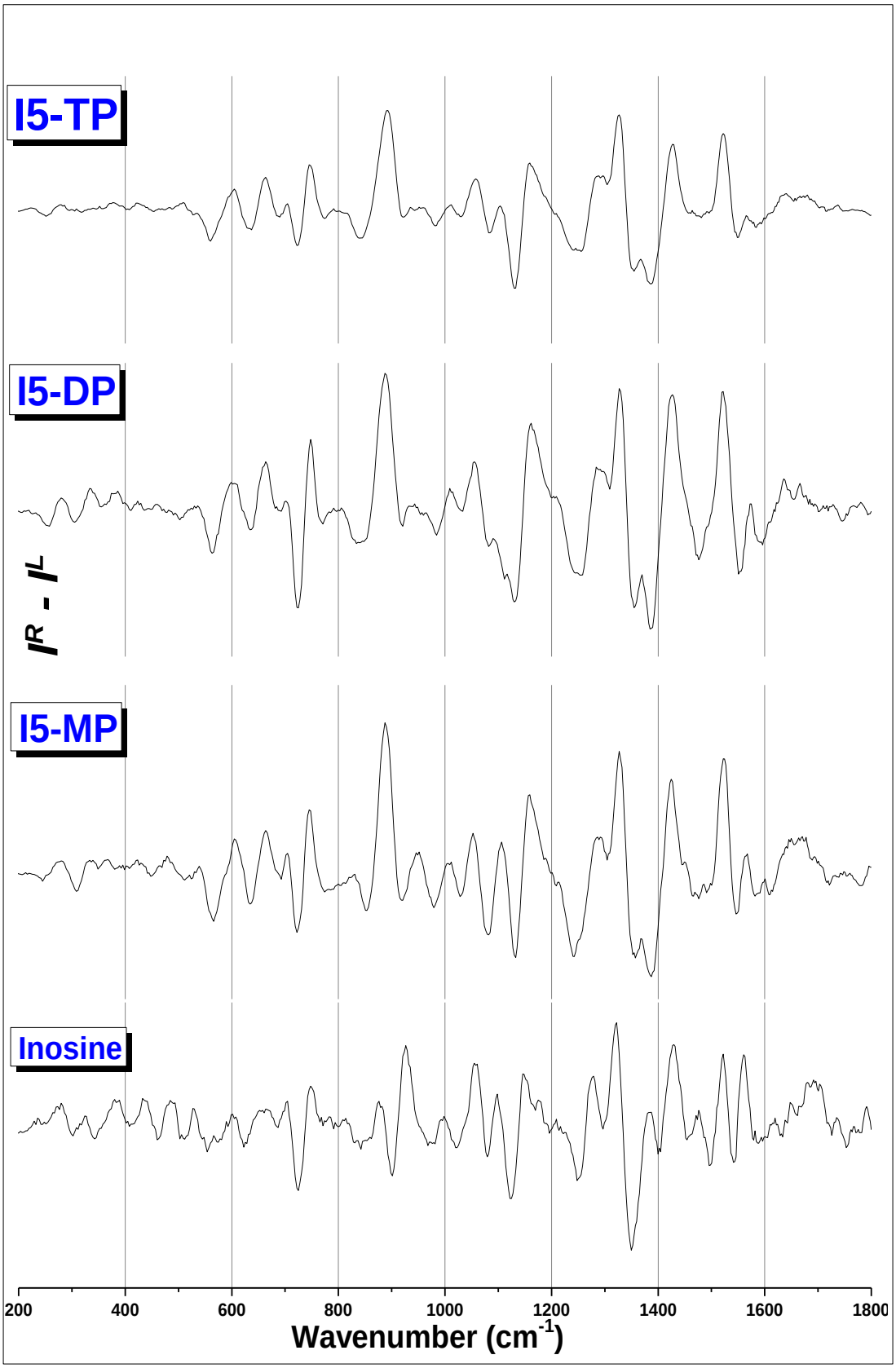

Figure4 .12. Raman optical activity (I^R-I^L) spectra of Inosine, Inosine 5'-monophosphate (I5-MP), Inosine 5'-diphosphate (I5-DP) and Inosine 5'-triphosphate (I5-TP).